Catalytic bio-hybrid polymersomes: towards novel biomedical applications

Inauguraldissertation

zur Erlangung der Würde eines Doktors der Philosophie vorgelegt der Philosophisch-Naturwissenschaftlichen Fakultät der Universität Basel

von

Claire Meyer

Basel, 2021

Genehmigt von der Philosophisch-Naturwissenschaftlichen Fakultät auf Antrag von

Prof. Dr. Cornelia G. Palivan

(Universität Basel, Department Chemie)

Erstbetreuerin

Prof. Dr. Jörg Huwyler

(Universität Basel, Departement Pharmazeutische Wissenschaften)

Zweitbetreuer

Prof. Dr. Corinne Nardin

(Université de Pau et des Pays de l'Adour, Département de Physique)

Expertin

Basel, den 25. Mai 2021

Prof. Dr. Marcel Mayor

Dekan

In memory of my grandmother, Michelle Meyer

Summary

Merging synthetic polymers with potent biomolecules is an effective strategy to build hybrid systems that benefit from the best of both worlds. However, the combination of polymers with biomolecules bearing strong appeal for biomedical applications, e.g., enzymes producing therapeutic compounds or detectable signals as diagnostic indicators, is often compromised due to the properties of the polymers not matching the requirements for the incorporation of the said active biomolecules. Hence, bio-hybrid polymer nanosystems have yet to develop their full potential for biomedical applications.

Chapter 1 introduces the concept of mimicking compartmentalization of biological cells by the means of synthetic polymers able to build nanocompartments with a large potential for accommodating various biomolecules. An overview of polymer properties, self-assembly of amphiphilic block-copolymers and polymersome formation techniques, as well as target applications of bio-hybrid nanocompartments is given. Finally, strategies to overcome drawbacks of such hybrid systems are introduced.

Chapter 2 describes the aim of this work which is to set stage for biomedical applications involving innovative catalytic nanocompartments encapsulating enzymes. The targeted applications and adopted strategies to develop different bio-hybrid systems are presented.

Chapter 3 highlights the development of a theranostic polymersome-based super assembly aimed at providing a novel type of treatment for atherosclerosis. Separate imaging and therapeutic nanocompartments were tethered together via hybridizing surface-exposed, complementary DNA strands, to form dual-functional polymersome clusters with simultaneous therapeutic and imaging properties. On one hand, on-site dopamine production was achieved by therapeutic compartments encapsulating active Dopa Decarboxylase (DDC), which are permeabilized by membrane insertion of OmpF porin. On the other hand, imaging compartments containing fluorescent dyes enabled tracking of the complete super-assemblies in parallel to their attachment to epithelial cells. Special emphasis is placed on the modularity of such polymersome clusters, as

this system represents a novel platform for future dual-functional systems aiming at other biomedical applications.

Chapter 4 presents a polymersome-based bioluminescent system that is able to produce a strong and long-lasting light signal as is desired for pre-clinical imaging applications. The encapsulation of *Gaussia* Luciferase (GLuc) within the cavity of polymersomes enabled efficient light production. The diffusion of GLuc substrate thought the membrane-inserted OmpF was exploited to modulate the enzyme kinetics such that the signal turned long-lasting. The applicability of such a system was investigated *in vitro* in cultured cells and *in vivo* in a mouse model.

Chapter 5 illustrates how mimicking native organelles can be exploited to provide a novel bio-hybrid system showing cell-photoprotective potential. Melanosome mimics were developed via encapsulation of Tyrosinase together with precursors L-DOPA/Dopamine to form macromolecular melanin/polydopamine (PDA) within the cavity of polymersomes. By enclosing the melanin/PDA production, the polymeric membrane prevents the major pitfalls associated with synthetic melanin/PDA nanoparticles and enables a bio-hybrid system with reduced cytotoxicity and enhanced colloidal stability while UV-absorption properties are preserved.

Finally, the mix and match of strategies employed to build the different bio-hybrid systems, the challenge of balancing the polymer/biomolecules selection with the design and optimization possibilities, and the potential of the resulting bio-hybrid systems to evolve into novel biomedical applications are discussed (**chapter 6**). Complementary material including additional experimental details (**chapter 7**), relevant literature (**chapter 8**), contributor and funding acknowledgment (**chapter 9**), and supplementary figures (**chapter 10**) conclude this thesis.

Table of Contents

List of Figures

List of Tables

Abbreviations

Polymers

BA	Butyl acrylate
CMA	4-methyl-[7-methacryloyl) oxyethyloxy] coumarin
DEA	2-(diethylamino)ethyl methacrylate
DEGMA	(diethylene glycol) methyl ether methacrylate
DMAEMA	Dimethylaminoethyl acrylate
OEG	Oligo ethylene glycol
PDTC/DTC	Poly(2,2-dimethyltrimethylene carbonate)
P(ASP)	Poly(α,β-aspartic acid)
P(Asp-AP)	Poly[(5-aminopentyl)-α,β-aspartamide
PAA	Poly(acrylic acid)
PAH	Polyallylamine
PB	Poly(butadiene)
PBMA	Poly(butyl methacrylate)
PCL	Poly(caprolactone)
PCMA	Poly(2-cinnamoylethyl methacrylate)
PDA	Polydopamine
PDPA	Poly(2-(diisopropylamino)ethyl methacrylate)
PDEAEMA	Poly(2-(diethylamino)ethyl methacrylate)
PDMS	Poly(dimethylsiloxane)
PCL	poly(caprolactone)
PEP	Isopropyl ethylene phosphate
PEG/PEO	Poly(ethylene glycol)/Poly(ethylene oxide)
PEOGA	Poly(oligoethylene glycol acrylate)
PGA	Poly(glutamic acid)
PGG	Poly(L-γ-glutamyl-glutamine)
PHPMA	Poly(2-hydroxypropyl methacrylate)
PI	Poly(isoprene)

PIAT	Polyisocyanoalanine(2-thiophene-3-yl-ethyl)amide
PLA	Polylactic acid
PLG	Poly(L-glutamate)
PLGA	Poly(lactic-glycolic acid)
PLL	Poly(l-lysine)
PMA	Poly(methacrylic acid)
PMOXA	Poly(2-methyloxazoline)
PMPC	Poly(2-(methacryloyloxy)ethyl phosphorylcholine)
PNIPAM	Poly(N-isopropylacrylamide)
POEGMA	Poly[2-(2-methoxyethoxy) ethyl methacrylate-co-oligo (ethylene glycol) methyl ether methacrylate]
PS	Polystyrene
PSS	Poly(styrene-4-sulfonic acid)
PTMC/TMC	Poly(trimethylene carbonate)
PVP	Poly(vinylpyrrolidone)
PVPON	Poly(N-vinyl pyrrolidone)

Proteins and peptides

ApoE	Apolipoprotein E
Aqp Z	Aquaporin Z
ASNase	Asparaginase
BR	Bacteriorhodopsin
BSA	Bovine serum albumin
CalB	Lipase B from Candida antarctica
Cat	Catalase
cNGQ	Cyclic NGQ
cRGD	Cyclic RGD
cytC	Cytochrome C
DDC	Dopa decarboxylase
DRD1	Dopamine receptor D1
epCAM	Epithelial cell adhesion molecule
gA	Gramicidin A

GALA	Glutamic acid-alanine-leucine-alanine
GFP	Green fluorescent protein
GLuc	*Gaussia* Luciferase
GOx	Glucose oxidase
GR	Glutathione reductase
HSA	Human Serum Albumin
Hb	Hemoglobin
HRP	Horseradish peroxidase
iNOS	Inducible nitric oxidase synthase
iRGD	InternalizingRGD
LinTT1	Linear TT1
LPO	Lactoperoxidase
Mb	Myoglobin
NLS	Nuclear localization sequence
OmpF	Outer membrane protein F
PGM	Phosphoglucomutase
sCG	Soluble guanylyl cyclase
SEAP	Secreted embryonic alkaline phosphatase
SOD	Superoxide dismutase
Tyr	Tyrosinase
α-HL	α-haemolysin
β-gal	β-galactosidase

Lipids

DOPC	1,2-dioleoyl-sn-glycero-3-phosphocholine
DPPC	1,2-dipalmitoyl-sn-glycero-3-phosphocholine
HSPC	Hydrogenated soybean phosphatidylcholine
POPC	1-palmitoyl-2-oleoyl-sn-glycero-3-phosphocholine

Techniques

CLSM	Confocal Laser Scanning Microscopy

DLS	Dynamic Light Scattering
FCS	Fluorescence Correlation Spectroscopy
HPLC	High Pressure Liquid Chromatography
MRI	Magnetic Resonance Imaging
NTA	Nanoparticle Tracking Analysis
SEC	Size Exclusion Chromatography
SLS	Static Light Scattering
TEM	Transmission Electron Microscopy

Other abbreviations

ATRP	Atom transfer radical polymerization
PBS	Phosphate buffered saline
DBCO	Dibenzocyclooctyne
DNA	Deoxyribonucleic acid
GUV	Giant unilamellar vesicle
Ncomp	Nanocompartment
MW	Molecular weight
LbL	Layer by Layer
OG	N-Octyl-β-D-glucoside
PDB	Protein database
PDI	Polydispersity index
pH	Potential of hydrogen
PIC	Polyion complex
RAFT	Reversible addition-fragmentation chain-transfer polymerization
RNA	Ribonucleic acid
ROS	Reactive oxygen species
RT	Room temperature
siRNA	Small interfering RNA
SPAAC	Strain Promoted azide-alkyne Cycloaddition
ssDNA	Single strand DNA

1. Introduction

This chapter explores the various approaches in which biomolecules can be combined with synthetic polymeric systems to obtain advanced bio-hybrid materials. First, an overview on the polymers used for capsule and vesicle formation, their properties and the methods for self-assembly and capsule preparation is provided. Next, recent advances in the development of nano-sized polymersomes combined with different biomolecules, e.g., peptides, antibodies, proteins/enzymes, nucleic acids, sugars or lipids as biological components are presented, with the focus on catalytic bio-hybrid systems. Finally, targeted biomedical applications of bio-hybrid polymersomes as well as current limitations and possible improvement strategies are addressed. Assemblies of natural polymers like chitosan or alginate, or those primarily composed of polymeric biomolecules like peptides or DNA, are excluded as they are not considered synthetic but nature-derived.

This chapter contains parts adapted with permission from the review[1]

***C. E. Meyer**, S. Abram, I. Craciun, C. G. Palivan, Biomolecule-polymer hybrid compartments: combining the best of both worlds, Physical Chemistry Chemical Physics, **2020**, 22, 11197*

1.1 Compartmentalization: mimicking nature to reach function

1.1.1 Cellular compartmentalization

Compartmentalization is a central characteristic of biological functions as it intervenes at different level of cellular life (**Figure 1.1**): cells are the most prominent example of a biological compartment as their inner aqueous content is separated from the external environment via a thin phospholipidic membrane, forming a micro-meter-sized vesicle.[2] As a result, cell individuality is achieved as specific cellular material is set apart from the extra-cellular environment and neighboring cells. Additionally, an increased level of complexity is achieved for eukaryotic cells, which are individually sub-compartmentalized, e.g., in the form of organelles, to perform multiple functions by isolation of distinct chemical reactions. The compartmentalization strategy is also exploited for cell-cell communication, where membrane-derived sub-micro-meter vesicles that encapsulate relevant biomolecules act as shuttle to deliver signals, highlighting the protective and directive character of these compartments. Thus, compartmentalization is a fundamental principle in biology that is needed for the temporal and spatial separation required for the control of chemical reactions and/or of incompatible biomolecules. For this reason, compartmentalization is placed at the center of numerous studies aiming to mimic or hijack biological functions.

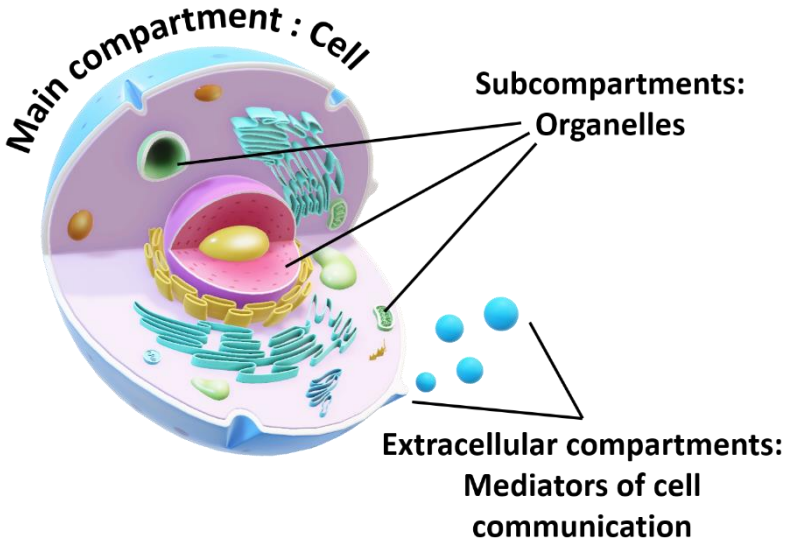

Figure 1.1. *Schematic representation of the compartmentalization of eukaryotic cells.*

1.1.2 Mimicking biological compartments

Synthetic compartments have emerged as a way to mimic biological compartments. Their contents (specific biomolecules) can be controlled in order to reach desired applications ranging from model of study to therapeutic cargos. Liposomes, spherical vesicles made of phospholipids, have been the spearhead for the development of micrometer-sized artificial vesicles used as artificial cells.[3] Beyond that, their nanometer-sized analogues have gained particular interest in drug delivery because therapeutic payloads can be encapsulated inside the vesicles' lumen. At the same time, stealth or targeting agents can be anchored in the vesicle membrane or attached to their surface.[4] Liposomes benefit from great intrinsic biocompatibility and biodegradability, as they consist of phospholipids. Thus they closely resemble biological compartments and easily accommodate a wide variety of biomolecules. However, with regard to applications, their mechanical properties as well as their restricted chemical versatility lessen their potential.[5]

The formation of nano- and micro-sized compartments was also demonstrated for synthetic polymers.[6,7] These polymeric compartments represent an attractive alternative to liposomes as they demonstrate greater chemical versatility and enhanced robustness due to their thicker membrane while, when appropriately selected, they maintain the softness typical for liposomes. Despite their thicker membrane, the flexibility of polymersomes allows for the incorporation of biomolecules which remain functional.[8,9] In addition, the progress in polymer chemistry yielded to a variety of copolymers with tailored properties and excellent biocompatibility that can compete with the intrinsic biocompatibility and biodegradability of natural polymers.[10] The precise chemical tuning, e.g., length, charge, or responsiveness, and the possibility of easy functionalization with reactive moieties for bioconjugation makes synthetic copolymers great building blocks for bio-hybrid compartments.

1.2 Polymer-based bio-hybrid compartments

1.2.1 Biomolecules within polymeric compartments

Polymer-based bio-hybrid compartments integrate biomolecules for their specific functionality into their polymeric scaffold and thus combine the advantages of biological with synthetic systems. The different biological components (nucleic acids, carbohydrates, peptides, proteins)[11–14] can be (I) attached to the compartment's surface, (II) encapsulated inside the cavity or (III) integrated into its membrane (**Figure 1.2**). Thereby, these different classes of biomolecules can be simultaneously exploited for their intrinsic functions at different locations of the compartment. For example, a targeting peptide on the surface can be combined with encapsulated siRNA cargo or a channel protein embedded in the synthetic membrane which allows the access of substrates to an enzyme encapsulated in the cavity. Another interesting way to obtain biohybrids is to encapsulate nano-sized liposomes inside micro-sized polymeric vesicles. Thus, the localization and the type of biomolecules have to be carefully chosen to achieve specific functions.

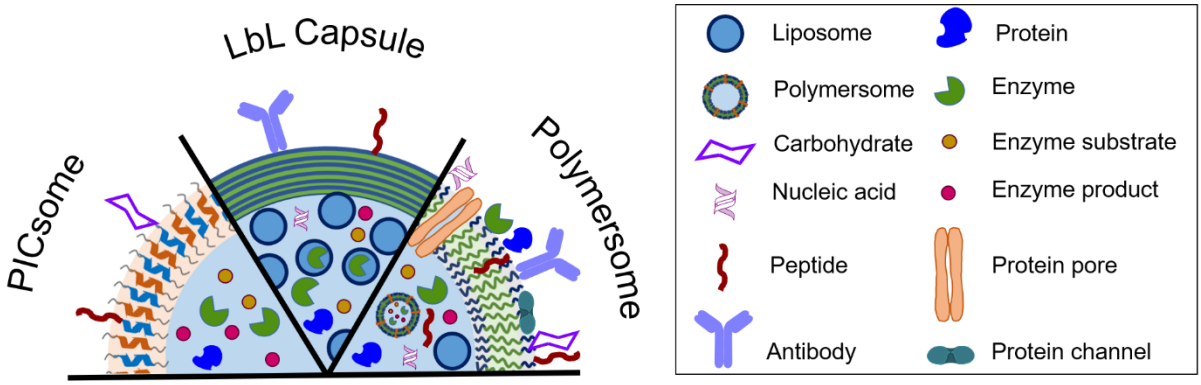

Figure 1.2. *Schematic representation of the different types of biomolecules and their possible locations within the polymeric assemblies.*

1.2.2 Size of bio-hybrid compartments

The size of the polymeric compartment plays an essential role in the applicability of the entire bio-hybrid system. Micro-meter-size bio-hybrid compartments usually serve as cell mimic for studying biological reactions such as enzymatic cascade reactions or actin polymerization.[15–17] These cell-sized polymeric compartments also bear the possibility to be sub-compartmentalized via encapsulation of sub-micro-meter counterparts, resulting in multicompartments that more closely mimic biological cells.[15,16] On the other hand, nano-meter-sized bio-hybrid compartments lean towards more applied goals such as therapeutic/sensing/imaging applications, as their dimensions are compatible with intravenous injection and cell-uptake. However, it has to be noted that the shape and charge of the compartments are also primordial to determine their applicability, e.g., for cell uptake/attachment.

1.2.3 Polymers used to form bio-hybrid compartments

The choice of the polymer is also crucial, as its overall physico-chemical properties, ability to incorporate biomolecules, and associated procedure of compartment formation considerably influence the function of the final bio-hybrid system. The type of compartment differs depending on the kind of synthetic polymers used: polyelectrolytes can self-assemble into a membrane enclosing an aqueous volume, based on the ionic interactions of oppositely charged polymers forming polyion complex (PIC)[18] vesicles called PICsomes (**Figure 1.3**). The two interacting polymers are not covalently linked. Usually, one anionic and one cationic PEG-poly(amino acid)-block copolymer are simply mixed in aqueous solution and assemble into semipermeable unilamellar membranes with PEG units on both sides.[19] PICsomes benefit from a simple preparation procedure in a purely aqueous environment together with intrinsic biocompatibility of the poly(amino acids) part, which are good prerequisites for the encapsulation of active biomolecular cargos. However, mechanical stress and changes in pH/ionic strength can cause the reversible disassembly of the vesicular structure or increase its permeability. Thus, the compromised stability under physiological conditions, as well as the improvement of mechanical properties via crosslinking that can be detrimental to incorporated biomolecules, limit PICsome applications.[20]

Another kind of polymeric compartment, called Layer-by-Layer (LbL) capsules, can also be formed using two different polymers that interact by electrostatic forces or hydrogen bonding (**Figure 1.3**). These polymers are alternately deposited on a sacrificial template (usually silica or $CaCO_3$) which is subsequently dissolved to obtain a polymeric hollow sphere.[21] LbL capsules made of poly(methacrylic acid) (PMA) are biodegradable, nontoxic and semipermeable, thus appear to be well suited for biomedical applications. However, these capsules lose cohesion at physiological pH. This drawback can be solved by crosslinking, but at the cost of the function of associated biomolecules.[22]

In contrast, amphiphilic block-copolymers lend themselves to forming polymeric vesicles (polymersomes) via self-assembly, which feature enhanced mechanical properties while avoiding crosslinking associated drawbacks (**Figure 1.3**). The wide variety of hydrophilic and hydrophobic blocks enable fine tuning of polymersomes properties, thus achieving desired responsiveness, permeability, functionalization, and accommodation of biomolecules. When built from the appropriate block-copolymers, polymersomes are also non-toxic, thus appear to be ideal candidates to develop polymer-based bio-hybrid compartments for biomedical applications.

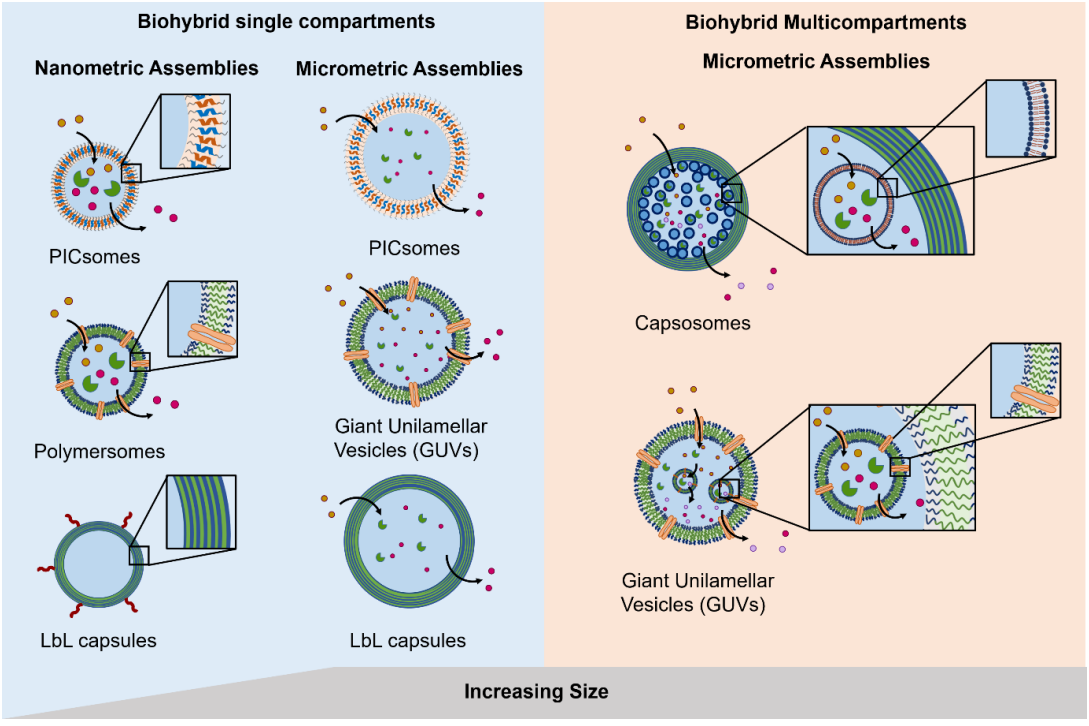

Figure 1.3. *Schematic representation of the different types of hybrid polymer/biomolecule compartments (polymersomes, PICsomes, LbL capsules), showing their diversity in terms of size and arrangement.*

1.3 Polymersome formation: self-assembly of amphiphilic block copolymers

1.3.1 Structure and synthesis of amphiphilic block copolymers

Amphiphilic block-copolymers can consist of two (AB), three (ABA/ABC) or even more (ABABAB…) blocks with one being hydrophilic (A and C) and the other one being hydrophobic (B). Either the two polymeric blocks are prepared separately and then connected by covalent bonding (e.g. by a click reaction) or the first block is functionalized after its polymerization to become a "macroinitiator".[23] The first block can thus be extended just by addition of the second type of monomer.
Commonly used polymerizations include controlled radical polymerization (e.g. ATRP, RAFT) and ionic (ring-opening) polymerizations and their combinations.[24] Popular hydrophilic blocks include PMOXA, PEG, PAA and PIAT and examples for hydrophobic blocks comprise PDMS, PS, PMA, PB, PCL, PHPMA, or PNIPAM. In case one of the blocks used responds to a certain chemical or physical stimulus, the resulting vesicles bear a high potential for applications in triggered drug release or the field of sensors. Thus, the properties of the vesicles can be fine-tuned by the careful selection of the hydrophobic and hydrophilic polymer blocks.

1.3.2 Membranes made of block copolymers

Different types of block copolymers can organize into different types of membranes. For example, diblock copolymers (AB) arrange to form an AB-BA bilayer where the hydrophobic blocks face each other in the core of the membrane and the hydrophilic ones are directied to the aqueous solution outside and inside the vesicle (**Figure 1.4 A**). Such a polymeric architecture closely resembles membranes of biological cells and thus, with appropriate block-length can accommodate membrane protein insertion. Membrane proteins can also insert into triblock copolymer membranes, which can be monolayer (ABA) structures as well as bilayers with a U type configuration of the polymer (**Figure 1.4 A**).[25] In case of immiscible hydrophilic blocks (A and C), they can form domains within the vesicle's membrane.[26] Moreover, a selective orientation of the longer block towards the outside and the shorter one towards the vesicle's interior can be achieved by the careful design of the block length in ABC type

copolymers.[27] Such asymmetric membranes can favor the insertion of a membrane protein in a specific orientation. Depending on the molecular weight of the block-copolymers, the membrane thickness of vesicles can vary in the range of 5-30 nm.[9] The glass-transition temperature T_g of the polymers also needs to be taken into account, especially when aiming for bio-hybrid compartments with membrane insertion or proteins, since T_g determines the flexibility of the membrane as function of temperature.[28] The properties (permeability, mechanical stability, ability to insert membrane proteins) of the resulting polymersomes are directly influenced by the characteristics (type and length) of building blocks used to form the polymeric membrane, which makes up the scaffold for the final bio-hybrid compartment. As an example, polymersomes made of PDMS-PMOXA are typically impermeable, even for small molecules whereas vesicles assembled from PS-PIAT are semipermeable.[29]

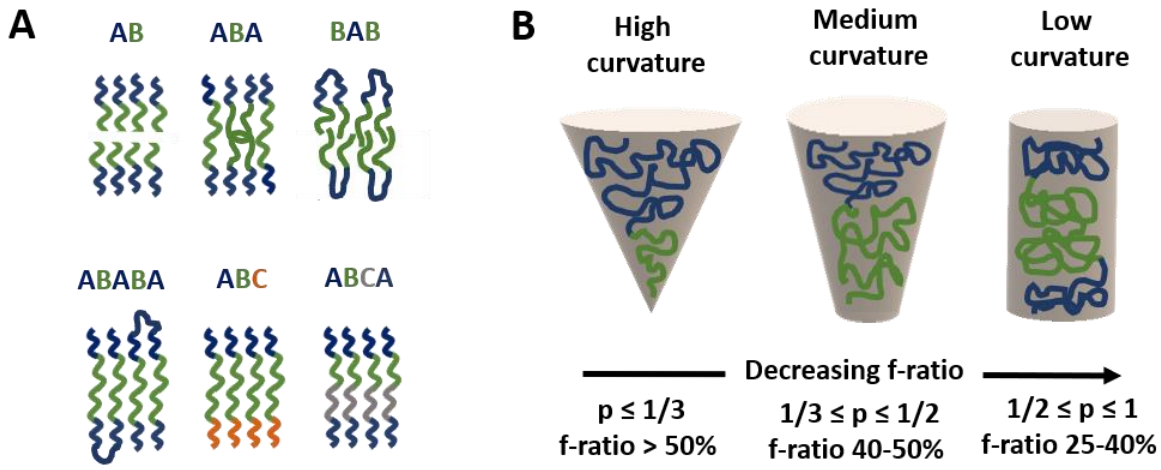

***Figure 1.4**. **(A)** Schematic representation of different membrane architectures resulting from different copolymer structures. **(B)** Influence of the copolymer's f-ratio on the membrane curvature and the morphology of the self-assembly.*

1.3.3 Parameters governing self-assembly

The self-organization of amphiphilic block copolymers does not necessarily result in vesicular structures but in spherical, cylindrical, gyroidal or lamellar ones instead.[23] The influence of the copolymer design on the morphology of self-assembled structures is described by the packing parameter p. It is defined as $p=v/a_O l_c$ with v = volume of the hydrophobic part, a_O = contact area of the head group and l_c length of the hydrophobic part.[30,31] (**Figure 1.4B**) Vesicles are formed for $1/2 \leq p \leq 1$, when $p \leq 1/3$ is typical of spherical micelles and $1/3 < p \leq 1/2$ corresponds to cylindrical micelles.[31,32]

The ratio of the hydrophilic to hydrophobic blocks determines to a great extent the curvature of the membrane structures formed during self-assembly (**Figure 1.4B**).[30,31,33] The f-ratio, i.e. the ratio of the hydrophilic block's molecular weight (MW) to the total MW of the block-copolymer, characterizes the propensity for a specific structure: vesicular structures are generally favored at f-ratios of 35 ± 10%[33] although the specific copolymer also pays a role.[34,35] Higher f-ratios lead to a higher membrane curvature and thus favor the formation of spherical micelles. Finally, the greater stability of assemblies made of block-copolymers compared to their lipidic counterparts is illustrated by the critical aggregation concentration (CAC), which represents the concentration of amphiphilic molecules required to start forming a colloidal system: CAC is 10'000-fold higher for lipids than for block copolymers.[36] Besides the chemical composition, the MW and the dispersity of the block-copolymer, the self-assembly is influenced as well by several external factors like the solvents used, the concentration, the presence of acids, bases or salts, and the method used for the preparation of the vesicles.[30]

1.3.4 Formation techniques

Several techniques are used to support the self-assembly of block copolymers into vesicles. Direct dissolution methods where block-copolymers are dissolved in water or aqueous buffer usually result in the formation or large vesicles with very high dispersity. Film rehydration methods expose an anhydrous copolymer film to a rehydration medium (usually water or an aqueous buffer). Usually combined with stirring, it induces film swelling and self-assembly into vesicular structures. The mutual diffusion between the rehydration solvent and the polymer film determines the formation of the polymersomes: high concentration gradients result in the formation of nano-sized vesicles while mild diffusion conditions lead to micro-sized vesicles.[30,37] If micro-sized vesicles (giant unilamellar vesicles, GUVs) are desired, the rehydration can also be supported by an oscillating electric field (electroformation). As film rehydration does not result in homogeneous size distributions, nano-sized polymersomes can be extruded through a membrane with defined nanopores in order to narrow the size distribution to smaller sizes. Film rehydration is particularly applicable to membrane protein insertion, as it enables the incorporation of membrane proteins during the self-assembly process, by including the protein of

interest in the usually aqueous rehydration solution. In the same manner, using a rehydration buffer containing hydrophilic molecules, e.g., proteins or enzymes, results in the encapsulation of these molecules within the polymersome's cavity. As the organic solvents are evaporated prior to the addition of the aqueous rehydration solution (containing the active molecules), the film rehydration technique is of particular interest for the incorporation of sensitive biomolecules within polymersomes.[38]

Microfluidic tools are needed to achieve homogenous size distributions of micro-sized polymersomes. The copolymers are dissolved in the oil phase of water/oil/water double emulsions produced by the microfluidic device. Removal of the oil phase results in the formation of highly monodisperse GUVs. W/o/w double emulsions are also used in emulsion centrifugation which is the phase transfer of emulsion droplets over an interface. This method has been used for the preparation of lipid-copolymer hybrid GUVs[39] and for the encapsulation of liposomes into GUVs.[40] Microfluidics enable the insertion of membrane proteins and encapsulation of biomolecules within GUVs, with the advantage of controlling the concentration of encapsulated compounds.[17] However, the incorporation of sensitive biomolecules and the formation of nano-sized polymersomes are yet to be achieved, which limits the use of microfluidics to develop bio-hybrid compartments for biomedical applications.

Other methods involving the slow exposure of a copolymer solution in an organic solvent to an aqueous environment (solvent switch, cosolvent and water addition/solvent evaporation methods), also induce self-assembly into polymersomes or GUVs. The copolymer solution can be either added to water or water can be added slowly to the organic copolymer solution. Subsequently, the organic solvent is either removed by evaporation or by dialysis against water. The presence of the organic solvent during self-assembly limits the application of these methods for bio-hybrid vesicle production as it might harm the functionality of the biomolecules. More detailed information on the preparation methods and their comparison are provided by other sources.[5,23,35]

1.4 Bio-hybrid polymersomes as attractive platform for biomedical applications

1.4.1 Surface functionalization of polymersomes with biomolecules

Following the formation of the polymeric nanocompartments, the surface of polymersomes can be decorated via the chemical ligation of biomolecules. Such modifications have been widely exploited in medical applications, especially for targeting and drug delivery purposes.[11,41–45] Cell specific targeting ligands like antibodies can be used to surface-functionalize polymersomes, in order to combine the robustness and loading capacity of the polymeric compartments with the high binding affinity of antibodies.[41,46] However, antibodies are expensive to produce, large in size and often immunogenic which calls for alternatives. Targeting and cell penetrating peptides, less expensive and smaller than antibodies, have been widely exploited to target polymersomes to locations of interest within cells or living organisms. For example, cyclic (RGD and NGQ)[11,12,42,47], pH sensitive fusogenic (GALA)[11] and other targeting (GE11, LinTT1, ApoE, Tet-1, NLS)[43,44,48–51] peptides have been mainly used to deliver smart polymer vehicles to specific cells or organelles and/or to improve their tumour penetration for therapeutic or diagnostic applications. Another approach consist in the coupling of peptides to the block copolymers prior to vesicle formation via mixing of the non-functionalized polymer with a peptide-functionalized counterpart that self-assemble together to form peptide-functionalized polymersomes.[12,47–50] This approach enables the simultaneous use of different types of polymer, e.g., by mixing a triblock co-polymer with a peptide-functionalized diblock copolymer. However, several features like the use of polymers with matching lengths of hydrophilic and hydrophobic parts, are crucial in order to achieve their co-self-assembly into polymersomes.[12] To potentiate the targeting/cell penetrating effect, it is also common to use a peptide-functionalized co-polymer with a slightly longer hydrophilic block to enhance the exposure of the peptide.[50]

Just like their shorter counterparts, proteins like transferrin can be covalently attached to the surface of preformed polymersomes for targeting purposes.[44,52,53] For other applications such as sensors and regulating systems, the surface of polymersomes can be enriched with proteins via electrostatic interactions, and subsequently immobilizied using photo-crosslinking.[54] This way, surface immobilized proteins that exhibit specific binding properties retain their ability to bind and release

their compound of affinity from the external environment, as exemplified by an anti-diabetes system.[54] Furthermore, surface immobilized proteins that are fluorescently labelled are exploited as tags to monitor processes occurring within the membrane. For example the membrane insertion of a non-fluorescent anchor of interest can be detected by linking fluorescent GFP to it.[55]

Nucleic acid-based compounds can also decorate the surface of polymersomes for targeting applications. Of particular interest are aptamers which are DNA or RNA single strands with high binding affinity to specific targets, e.g., certain types of cancer cells.[56,57] For other applications, the specificity of the hybridization of single-stranded DNA (ssDNA) to their complementary strands was exploited to selectively connect distinct polymersomes that are surface-functionalized with complementary ssDNA. This approach enables different spatial organizations of polymersomes into clusters which can serve to mimic the interconnections between natural organelles[58] (**Figure 1.5**).

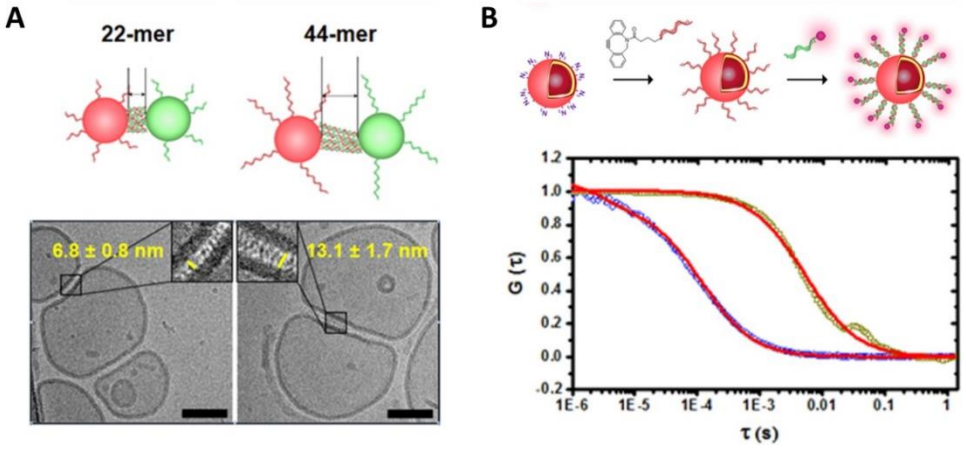

Figure 1.5. (A) *Cryo transmission electron micrograph of DNA functionalized polymersome clusters showing clearly the morphology, the membrane thickness and the gap created by the attached DNA strands.* ***(B)*** *Normalized fluorescence correlation spectroscopy autocorrelation curve of polymersomes functionalized with ssDNA and the hybridized fluorescently labelled complementary strand (dark yellow, red fit) and the free fluorescently labelled ssDNA (blue, red fit). Reprinted with permission from reference [58].*

Besides applications such as sensing, attachment or spatial organization, the main objective of surface functionalization of polymersomes is targeting, which explains the recurrence of selected biomolecules (antibody, peptides, DNA) able to direct polymersomes to a location of choice. However, targeting of polymersomes is

only of interest if they deliver a specific function, which is usually obtained by encapsulation of specific compounds or potent biomolecules inside their cavity.

1.4.2 Encapsulation of biomolecules within the polymersome cavity

Polymersomes are appealing carriers for hydrophilic compounds and biomolecules, especially for catalytic and sensitive molecules like enzymes, as they offer a confined environment inside their aqueous cavity and are thus able to protect the payload from the external milieu. Polymeric vesicles encapsulating nucleic acid cargos (plasmid DNA, siRNA) offer protection from nuclease degradation, which makes them strong candidates for non-viral, potentially safer, gene delivery systems.[46,59,60] Slightly positively charged polymers can support the challenging encapsulation of large nucleic acids like plasmids or entire genes, by binding the negatively charged DNA via electrostatic forces.[59,60] However, such interactions can also destabilize the polymersomes or prevent their self- assembly. Thus, the length of the polymer block containing protonatable groups as well as the pH of the rehydration solution have to be carefully optimized to render DNA encapsulation compatible with self-assembly conditions.[59,60]

Enzymes can be encapsulated inside the polymersomes' cavity to develop catalytic nanocompartments, often called nanoreactors, able to produce or degrade compounds of interest.[61] Depending on the loaded enzymes, such bio-hybrid systems aim at different applications, e.g., as antioxidant by using superoxide dismutase or haemoglobin.[13,62] To cumulate several activities, two kinds of catalytic compartments (encapsulating different enzymes, e.g. uricase and horseradish peroxidase, HRP) that work in tandem have been used, for example to achieve simultaneous detoxification and uric acid degradation for therapeutic applications (**Figure 1.6A**).[63] Also, such systems are interesting models to investigate the effects of distance on the overall cascade reaction efficiency as they mimic the communication within bioassemblies like cells and organelles (**Figure 1.6B**).[63] Indeed, the ratio between the mean intercompartment distance and the diameter of the compartments is about 10, which reflects the order of magnitude of the ratio between cell-cell communication distance (for cells with 1 μm distance typical for autocrine signaling). The compartmentalization of enzymatic cascade reactions is of particular interest as the great majority of biological processes are series of enzyme-mediated cascades. Besides

therapeutic applications, catalytic polymersomes are also used as model for artificial organelles (e.g. chloroplast,[64] peroxisome[65]), and as building blocks of antimicrobial surfaces[66] or biosensors.[67]

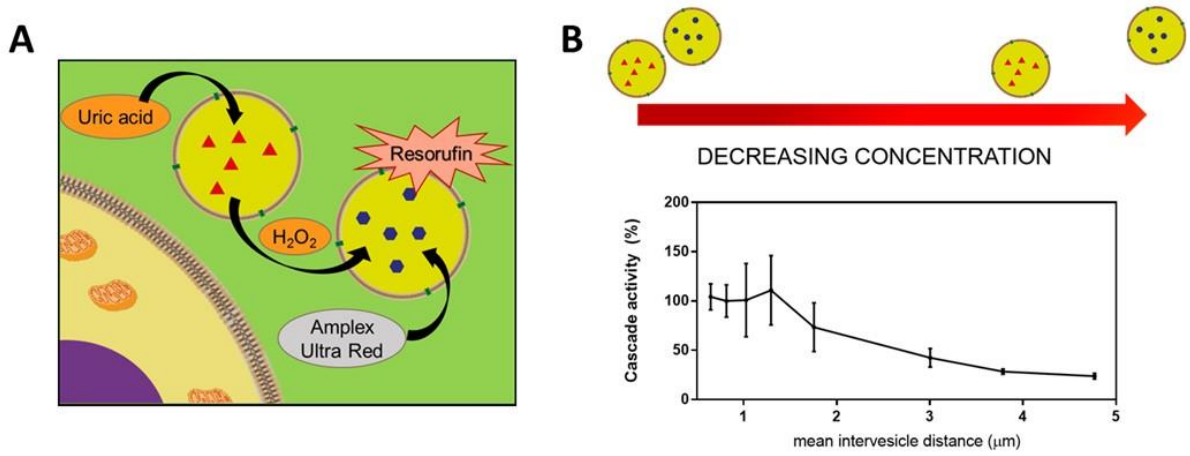

Figure 1.6. ***(A)*** *Scheme of the two catatylic compartments working in tandem.* ***(B)*** *Conversion of substrate Amplex Red by cascade reaction inside the catalytic compartments in tandem representing the cascade reaction efficiency, at different mean intervesicles distances. Reprinted with permission from reference [63].*

The segregation of enzymes within the polymersome cavity primarily aims at shielding them from proteolytic degradation. However, it is essential to maintain the exchange between the encapsulated enzymes and the external environment in order to obtain catalytic activity of nanocompartment. The majority of the polymersomes, e.g., assembled from PS-PIAT[68] or PGG[14], are inherently permeable to small molecules and thus permit a supply of substrate for the encapsulated enzyme and the exit of the resulting product from the compartment. The permeability of polymersomes can be varied depending on different conditions, for example by inserting responsive compounds in the polymeric membrane or by using responsive polymers like PNIMAM that is temperature-responsive. In contrast, polymersomes made of PDMS-PMOXA block copolymers are impermeable to small molecules. Selective permeability has been achieved via incorporation of pores or channels in the polymeric membrane (see next section).[69] To study the permeabilization of the vesicles as well as the diffusion of compounds across their polymeric membrane, catalytic compartments encapsulating stable enzymes has been used for basic research rather than for

biomedical applications: model enzymes as HRP and glucose oxidase (GOx) benefit from the well-established, accessible and convenient monitoring of their reaction kinetics, which makes these enzymes suitable for the development of artificial cells[70], models of molecular crowding[71] or for studying enzyme positioning within the polymersomes.[68] These model enzymes demonstrated that enzyme confinement coupled with a crowded milieu inside polymersomes affects the enzyme kinetics by lowering the Michaelis–Menten constant (K_m) compared to non-encapsulated enzymes (**Figure 1.7**).[71] The co-encapsulation of a substance simulating molecular crowding such as PEG with HRP results in even lower K_m (**Figure 1.7**).[71] When co-encapsulated with their substrate, the decrease of K_m for encapsulated enzymes leads to a greater enzyme-substrate affinity because of the molecular confinement inside the compartment that increases the collision frequencies between the reagents.[71]

In a different system where enzymes are encapsulated inside impermeable PMOXA-PDMS-PMOXA polymersomes and the substrate has to diffuse through the pore to reach the enzymes rather than being co-encapsulated, the diffusion effect is the limiting factor of enzyme efficiency. In fact, if the substrate readily encounters the enzyme once in the compartment (low K_m), the slower efflux of substrate towards the cavity of polymersomes hinders the enzyme activity, according to the decrease of catalytic efficiency (k_{cat}/K_m).[63] These parameters (K_m, k_{cat}/K_m, viscosity) are key factors that need to be optimized when developing efficient catalytic nanocompartments.[71] However, the Michaelis-Menten model cannot be applied to all catalytic nanocompartments systems including catalytic polymersomes working in tandem to support cascade reactions or enzymes with complicated kinetics monitoring.

From therapeutic compounds to catalytic biomolecules (enzymes), encapsulated cargos mainly determine the application of the bio-hybrid nanocompartment. However, the encapsulated payloads can only fulfil their active/therapeutic role in response to environmental conditions, which is usually achieved via tuning of the permeability/responsiveness of the polymeric membrane.

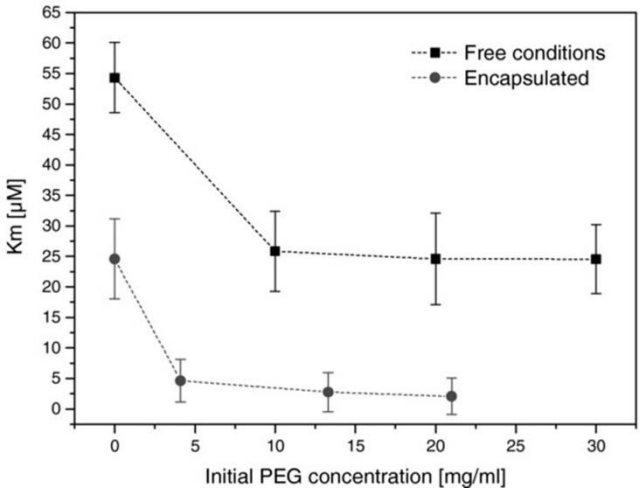

Figure 1.7. *Michaelis-Menten constant of HRP (free in solution and encapsulated in polymersomes) in presence of different concentrations of PEG. Km decreases with increasing concentrations of PEG. Reprinted with permission from reference [71].*

1.4.3 Membrane functionalization of polymersomes with biomolecules

Biomolecules containing a hydrophobic domain can be inserted into the polymeric membrane to add new features such as stimuli-responsiveness, to the bio-hybrid nanocompartments. During self-assembly of polymersomes, peptides can be inserted into the polymeric membrane, to achieve ion-selective membrane permeability[72] or proteinase responsiveness with disruption of the peptide/polymer hybrid assembly.[73] Some peptides, typically derived from the transmembrane domains of membrane proteins from viral, yeast or bacteriophage sources, also spontaneously insert into the polymeric membrane of preformed polymersomes.[55] Their insertion appears to be a concentration-dependent process governed by hydrophobic driving forces. Such ease of insertion has been exploited for the functionalization of polymersomes with other molecules, via the use of peptide/other molecule conjugates that can insert without destabilizing or rupturing the polymersome membranes.[55]

Proteins have been used as a major structural component of bio-hybrid polymersomes, e.g., assemblies of conjugated hydrophilic human serum albumin (BSA) and a hydrophobic polymer block show great potential as drug delivery vehicles.[74,75] Asymmetric conjugates made of ABC triblock copolymers containing

either HRP or myoglobin, have been shown to form vesicles but also other nanoassemblies like micelles or rods.[76] However, only a few examples of such protein-polymer conjugates have been reported to form the desired nanoassemblies as the inherent complexity of these systems impedes the control over their architecture.

Membrane proteins have been reconstituted in polymeric membranes, to permeabilize otherwise impermeable polymersomes via the membrane insertion of protein pores like Outer membrane protein F (OmpF). This porin has a molecular weight cut-off of 600 Da which permits the passage of small molecules into and from the inner space of polymersomes while retaining bigger encapsulated macromolecules like enzymes inside.[71] OmpF can be chemically modified prior to membrane insertion to obtain pores that open in response to a pH change in the environment[77] or function as biovalves with a controllable opening and closing of the pore[78]. The successful incorporation of membrane proteins can be achieved even though polymeric membranes are thicker than cellular membranes. Remarkably, the hydrophobic part of polymeric membranes is thicker than the hydrophobic domain of the membrane proteins, which suggests a conformational adaptation between the polymer and the protein to overcome the hydrophobic mismatch (**Figure 1.8**).[8] However, this phenomenon of adaption requires specific properties of the polymeric membrane: a high flexibility of block-copolymers is essential to achieve membrane fluidity that is similar to natural phospholipidic bilayers.[8] Moreover, the hydrophobic mismatch between the membrane thickness and the size of the protein also influences the insertion process as it should range from 3.5 to 5 times to achieve a successful protein reconstitution (**Figure 1.8**). Finally, block-copolymers with high polydispersity index (PDI) also favor protein insertion as they enhance the ability of the polymer chains to adapt to the dimensions of protein.[8] ABC triblock copolymers have been used to mimic the asymmetry of biological membranes, which is conducive to a preferential orientation of the inserted protein,[79] e.g., to allow for a directional transport across the membrane or to control which domains of the protein are exposed towards the cavity or the surface of vesicles. Recent advances in polymer chemistry moved these synthetic membranes closer to their biological inspiration, thus allowing the successful insertion of a number of proteins (α-hemolysin,[80] Bacteriorhodopsin[81] or AquaporinZ[82]) into polymeric membranes. However, the reconstitution of membrane proteins in polymer membranes remains extremely complex as it requires a high stability of the protein,

adapted surfactant and pH conditions and strategies to deal with the hydrophobic size mismatch between the protein and the synthetic membrane.[83]

Carbohydrates have also been inserted in polymeric membrane, in view of their manifold roles in cellular process, notably in cell-cell and cell-matrix communication. The resulting bio-hybrids have been exploited for applications like cell-surface recognition and cell signalling.[14,84–86] Bio-hybrid vesicles made of block-copolymers containing sugar moieties have been targeted to other applications like detection of pathogenic bacteria[87], glucose regulation,[54] or enzyme prodrug therapy[14].

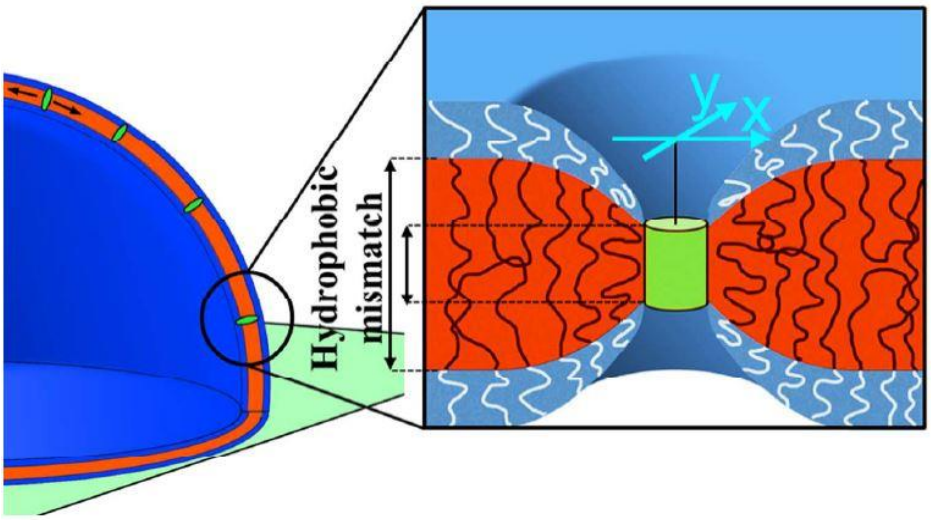

Figure 1.8. *Schematic representation of the structural change of the polymeric membrane required to compensate the hydrophobic mismatch between the hydrophobic membrane thickness and the hydrophobic height of the membrane protein (represented as green cylinder). Adapted with permission from reference [8].*

1.4.4 Polymer-lipid hybrid vesicles

Phospholipids combined with block copolymers have gained interest for the formation of hybrid vesicles with membrane properties closer to biological ones, which have been studied in the context of interaction with cells.[88–90] Both types of macromolecules can also form hybrid vesicles when blended, bringing together the biocompatibility and softness of liposomes and robustness and chemical versatility of polymersomes. The successful assembly of these hybrids closely depends on the amphiphilic building blocks: molar fraction, molecular weight and block size have to be optimized.[90–93] These bio-hybrid vesicles exhibit higher permeability compared to polymersomes and liposomes, which has been further enhanced by the insertion of ionophores or ion channels[94] However, the biggest potential of lipid/polymer hybrid vesicles lies in facilitating reconstitution of membrane proteins as they form a durable environment that lowers the initial enzyme activity but enables a significant extension of the functional lifetime of the protein compared to its reconstitution in liposomes.[95] These hybrids possess a great potential for drug delivery due to their low toxicity and efficacy of payload loading and release that can be modulated by the polymer/lipid ratio.[93,96,97] However, the insertion of a lipid into the polymeric membrane can be a drawback in case of further surface functionalization of the hybrid vesicle: the addition of lipids is diluting the density of polymer brushes on the vesicle's surface that are obstructing targeting ligands due to steric effects.

Taking together, the incorporation of biomolecules in the polymersome membranes mainly enhances the tunability of the membrane, especially permeability and responsiveness. However, the countless combination possibilities of producing bio-hybrid assemblies are greatly limited by the challenges associated with the complex accommodation between polymers and biomolecules.

1.4.5 Principal bio-medical applications of bio-hybrid polymersomes

As illustrated in **Table 1**, most polymer-based bio-hybrid nanocompartments are developed as study models, for example to gain insight on protein reconstitution in polymeric membrane[81,83,95] or to mimic natural organelles[58,64,65,94]. When it comes to therapeutic applications, the vast majority of these bio-hybrids are used as drug delivery systems. Indeed, the encapsulation of therapeutic molecules, e.g., anti-cancer

drugs as 5-fluorouracil[89] or doxorubicin[49], is easily achieved as these compounds are usually small and relatively stable which facilitate the encapsulation process. In such drug delivery systems, the combined biomolecules are mostly peptides that serve to confer targeting properties upon the therapeutic vehicle. More rarely, instead of drugs, similar systems are employed to deliver therapeutic biomolecules such as enzymes[50] or nucleic acids[59,60], for targeted protein therapy and gene therapy, respectively. For example, the toxic enzyme saporin can be delivered to cancer cells to inactivate ribosomes, thus preventing protein synthesis leading to cell death.[50] However, for such delivery applications, the release of the encapsulated drug/therapeutic biomolecule is necessary for a therapeutic effect. In most instances, release has been achieved by using pH or temperature responsive polymers.[88,98]

Other therapeutic applications like detoxification, e.g., of ROS[13,62] or uric acid[63], usually implies the encapsulation of adequate enzymes capable to degrade the harmful compounds. However, in such cases, the release of the enzyme is better avoided: it is preferable to keep the enzymes encapsulated to preserve their activity, e.g., by shielding them from proteolytic degradation. Given appropriate permeabilization of the polymeric membrane, the harmful compounds can enter the polymersome's cavity where they are degraded by the enzyme. On the other hand, larger molecules as proteases, are excluded from the therapeutic compartment. Similar systems have been used for enzyme prodrug therapy, where encapsulated enzymes, e.g., β-galactosidase (β-gal), generate active chemotherapeutics from prodrugs.[14]

In contrast to direct therapeutic purposes, some bio-hybrid systems aim at other biomedical application like imaging. For example, the *in vivo* targeting and imaging of bone metastases have been achieved via encapsulation of MRI agents and surface functionalization of polymersomes with antibodies.[41] Thus, the display and composition of bio-hybrid systems is directly correlated to their applications purposes. Because bio-hybrid systems able to present dual or even multiple activities involve infinitely more complex designs, they are by far more challenging. For example, anti-tumor applications achieved by drug delivery and *in situ* ROS production have been explored by bio-hybrid polymersomes containing drugs (camptothecin) in their membrane and glucose oxidase (GOx) inside their cavity.[99] Triggered by the acid environment of the tumor, the polymersome membrane became permeable to glucose which was subsequently oxidized by encapsulated GOx with a concomitant production of hydrogen peroxide and the release of the drug.[99]

	Polymer	Location of biomolecules	Associated biomolecules	Application	Reference
Polymersome	PDMS-PMOXA-based block copolymers (PMDS-PMOXA-PDMS, PEO-PDMS-PMOXA)	Cavity	Enzyme (SOD)	Antioxidant	13
		Cavity, Membrane	Protein (OmpF), Enzyme (iNOS)	Modification of cell physiology for therapy	100
			Protein (OmpF), Enzyme (sCG)		
			Protein (Hb, OmpF)	ROS detoxification	62
			Protein (OmpF), Enzyme (HRP)	Enzyme kinetic in crowded space	71
				Model of pH-responsive nanocompartment	77
					78
			Protein (OmpF), Enzyme (penicilin acylase)	Model for self-defending surface	66
			Protein (OmpF), Enzyme (LPO, SOD)	Artificial peroxisome	65
			Protein (OmpF), Enzyme (HRP or Uricase)	Detoxification of uric acid	63
			Protein (α-HL, PGM)	Model for glycolysis completion	80
		Membrane	Peptide (gA)	Stimuli-responsive nanocompartment	72
			Protein (proteorhodopsin), Lipid (DOPC)	Model for protein reconstitution study	83
			Protein (Aqp Z)	Model for water treatment/drug delivery	82
			Protein (Aqp)	Model for sensitive bio-device	79
		Membrane, Surface	Peptide (Fusion eGFP-peptides)	Model for surface functionalisation	55
		Surface	Peptide (NLS)	Targeting/delivery	51
			DNA (Single strands)	Interconnected organelles mimicking	58
	PEG/PEO-based block copolymers (PEG-PCL, PEG-PLA, PEG-PTMC, PEG-PTMC-DTC,PEG-PLGA, PEG-PGA, PEG-PDTC-TMC, PEG-PS, PEG-PLC. PEO-PDPA-PAA, PEO-PCMA-DEA, PEO-PDMS-PEO, PEO-PB)	Cavity, Surface	Antibody (Anti-EpCAM), siRNA	Targeting/delivery	46
			Peptide (cRGD, GALA), Protein (cytC)		11
			Peptide (cNGQGEQc), siRNA		12
			Peptide (ApoE), Protein (Saporin)		50
			Peptide (S14G-humanin),Protein (Lactoferrin)		53
		Surface	Peptide (Aptamer AS1411)	Targeting/drug delivery	56
			Peptide (GE11)		49
			Peptide (cell penetrating)		45
			Peptide (Tet-1), Protein (Transferrin)		44
			Peptide (iRG)		42
			Protein (Transferrin)		52
			Peptide (iRGD)		47
			Peptide (LinTT1)		48
			Peptide (NLS)		43
		Membrane	Peptide (MT1)	Enzyme detection	73
			Protein (Mb/HRP)	Model for catalyst development	76
			Lipid (POPC)	Model for drug delivery	96
			Lipid (POPC)		93
			Lipid (HSPC)		101
			Protein (BR), Enzyme (ATP synthase)	Model for protein reconstitution	81
			Protein (Cyt bo3), Lipid (POPC)		95
			Lipid (DOPC)	Model for artificial organelles	94
		Membrane/Surface	Protein (Lectin), Carbohydrate (Glucopyranosyl)	Anti-diabetes therapy	54

Table 1. *Overview on nano-sized biohybrid compartments sorted by their polymeric building blocks.*

Polymersomes	Other block copolymers (PTMC-PGA, PEP, PMPC-PDPA, PS-PAA, PS-PIAT, PCL, PHPMA, PB-PS, DEGMA, PGG, PNIPAM, PNIPAM-CMA-DEA, DMAEMA, PEOGA-PLA)	Cavity	DNA (Plasmid)	Gene delivery	59
			DNA (Plasmid)/siRNA		60
			Enzyme (Trypsin)	Enzyme kinetic in confined space	69
		Cavity, Membrane	Protein (HSA, GFP)	Intracellular delivery	75
			Carbohydrate (matooligosaccharide), Enzyme (β-gal)	Enzyme prodrug therapy	14
		Cavity, Membrane, Surface	Enzyme (GOx,CalB, HRP)	Enzyme positioning in polymersomes	68
		Membrane	Carbohydrate (glucose)	Cell glycocalyx mimicking	85
			Carbohydrate (pyranoside/glucoside)	Model for carbohydrate-protein interaction study	86
			Carbohydrate (hyluronic acid)	Bacteria detection	87
			Carbohydrate (thioglucose)	Drug carrier	84
			Lipid (cholesterol)	Drug delivery	88
			Lipid (cholesterol)	Drug delivery	98
			Protein (cytC), Enzyme (cytC oxidase)	Model for artificial chloroplast	64
			Lipid (HSPC/DPPC)	Model for drug delivery	97
		Membrane, surface	Peptide (aptamer AS1411)	Targeting/drug delivery	55
			Protein (BSA), Antibody (cetuximab)		74
		Surface	Antibody (Trastuzumab)	Targeting/imaging	41
PICsomes	PEG-P(Asp), P(Asp-AP)	Cavity	Enzyme (ASNase)	Therapeutic catalytic nanocarrier	102
			Enzyme (β-gal)	Model for prodrug therapy	103
		Surface	Peptide (cRGD)	Drug delivery, Imaging	104
LbL capsules	PDPA-PEG	Surface	Peptide (GLGYGWS)	Drug delivery	105

Table 1. *Overview on nano-sized biohybrid compartments sorted by their polymeric building blocks. (continued)*

1.4.6 Limitations and possible directions of improvement

Catalytic bio-hybrids involving the encapsulation of enzymes have the potential to improve and extend the bio-medical applications of nano-sized compartments. For example, such systems allow for longer circulation times of the enzymes and thus prolonged activity, while reducing off-target toxicity due to on-site production of drugs.[106,107] Considering the vast range of reactions catalysed by enzymes, such systems could be applied to develop novel pro-drug therapies and go even further to realize unprecedented bio-medical purposes.

However, there is a clear gap between bio-hybrid systems used as models, which depending on the study involve intricate architectures, and bio-hybrids tailored to specific bio-medical applications that usually consist of simpler polymer/biomolecules combinations. To explore the potency of complex model bio-hybrid systems, the same stable and easy to characterise model enzymes (HRP, β-gal, GOx) are often employed because they are rather stable and easy to characterise.[17,69,77,78] Even if these model enzymes were suitable for therapeutic purposes, the range of applications is very limited as the variety of model enzymes is restricted.[14,63,99] In addition, the transfer from model system to applicability is rarely straightforward: a bio-hybrid system that has been developed to accommodate stable model enzymes is not readily adaptable to other enzymes offering greater potential for bio-medical applications.

Difficulties arising from the production/supply of enzymes of interest (low concentration, purity, high costs), as well as from merging enzyme' requirements (temperature, pH, buffer) with polymersome formation/functionalization conditions have to be overcome to build functional systems. To tackle these issues, different strategies could be pursued like, **1)** using polymers that easily self-assemble under a broad range of conditions and at the same time enable the incorporation of membrane proteins, **2)** selecting enzymes (where a good balance between desired activity, stability, cofactors, size, hydrophilicity and encapsulation efficiency is feasible), **3)** choosing efficient reactions/appropriate biomolecules for the functionalization of the polymersomes and **4)** segregating different compounds of interest in different compartments to meet their respective needs and preserve their activity/encapsulation efficiency.

2. Aim of the thesis

The aim of this thesis it to implement the above-mentioned strategies, in the development of polymersome-based enzyme encapsulating compartments as stepping stones towards novel bio-medical applications. The different systems, presented below are all built of di-block PDMS-PMOXA copolymers, while the encapsulated enzymes and other associated biomolecules vary depending on the target application.

To provide a platform for the development of dual-function bio-hybrid systems, e.g., for theranostic applications, we investigated using super-assemblies of nano-size compartments where distinct active compounds are segregated (Chapter 3). To overcome one of the preeminent constraints in achieving dual-function bio-hybrid systems, i.e., the combination of different active compounds without sacrificing their activity, we designed a system comprising two different type of polymersomes: one bearing an imaging function via the encapsulation of fluorescent dye and the other encapsulating recombinant human enzyme Dopa decarboxylase (DDC) to produce dopamine as therapeutic compound. To assure co-localisation of both polymersomes, so both functions in close proximity, and at the same time procure specific cell attachment properties, we explored the surface functionalization of individual polymersomes with complementary DNA strands. To provide evidence of the applicability of such a system, e.g., for the treatment of atherosclerosis, the stability of the assembly as well as the therapeutic and imaging functions have been assessed in cell cultures. Finally, to position this novel system as platform for the developing of future dual-functional bio-hybrid systems, the modularity of the polymersome clusters was evaluated.

To pave the way for a novel kind of pre-clinical imaging application, we developed a polymersome-based bioluminescent system producing a strong and long-lasing light signal (Chapter 4). We exploited bioluminescence to develop a novel imaging system based on nanocompartments to ultimately have available a safer, more convenient and more affordable alternative to nuclear imaging and MRI. Specifically, we encapsulated a light-producing enzyme (*Gaussia* luciferase, GLuc) inside

polymersomes that have been permeabilized via incorporation of OmpF. We investigated the effect of substrate diffusion through OmpF on the enzyme's kinetics and the resulting modulation of the light signal. To gain insight into the applicability of this system, we investigated its activity, cytotoxicity and stability in a cellular environment and carried out preliminary *in vivo* studies using a mouse model.

To offer a cell photoprotective system that sidesteps typical drawbacks associated with melanin/Polydopamine nanoparticles, we developed melanosome mimics (Chapter 5). Melanin nanoparticles and especially their synthetic counterparts made of polydopamine have been extensively used for their great light-absorption properties. However, their compromised long-term colloidal stability and propensity for cytotoxicity restrict their biomedical applications. Inspired by nature, i.e., by native melanosomes, we examined the behavior of confined melanin/polydopamine by means of polymersomes encapsulating Tyrosinase, a key enzyme in melanogenesis, together with melanin/polydopamine precursors L-DOPA or Dopamine, respectively. To assess the applicability of this melanosome mimics, we monitored their colloidal stability upon long-term storage, cytotoxicity, as well as their cell photoprotection properties and compared their effects to non-encapsulated melanin/Polydopamine.

3. Polymersome clusters as nanotheranostic platform

This chapter focus on the development of a nanocompartment-based theranostic system, where nanomaterials and biologically active compounds are merged to achieve diagnosis and treatment at the same time. The current dual-functional nanosystems, e.g., targeted at theranostics, have serious limitations, mainly because there is often a mismatch between the physical properties of the selected nanomaterials and their ease of functionalization, loading ability or overall compatibility with bioactive molecules. Herein we propose a new type of nanotheranostic system based on nanocompartment clusters composed of two different types of polymersomes linked together by DNA. Careful design and procedure optimization were investigated to obtain clusters segregating human Dopa decarboxylase (DDC) as the therapeutic enzyme and fluorescent probes for the detection unit in distinct but colocalized nanocompartments. This dual-functionality polymersome cluster architecture provides a novel type of two-compartment nanotheranostic platform that is expected to provide the basis of a new treatment strategy for atherosclerosis. Also, this system is expected to expand versatility and diversify the types of utilizable active molecules, and thus by extension expand the breadth of attainable applications via dual-functional systems.

Parts of this chapter have been published and reprinted with permission from[108,109]

***C. E. Meyer**, J. Liu, I. Craciun, D. Wu, H. Wang, M. Xie, M. Fussenegger, C. G. Palivan, Segregated nanocompartments containing therapeuthic enzymes and imaging compounds within DNA-zipped polymersome clusters for advanced nanotheranostic platform, Small, **2020,** 16, 1906492*

C. E. Meyer**, C-A Schoenenberger, J. Liu, I. Craciun, C. G. Palivan, DNA-tethered polymersome clusters as nanotheranostic platform, Chimia, **2021

3.1 Introduction

Theranostic approaches provide improved medical solutions by associating therapy with diagnostics, thereby avoiding multi-step procedures and reducing delays in treatment, which may be particularly crucial in the case of rapidly evolving diseases. The therapeutic part of theranostic systems is usually achieved via release of bioactive compounds, hyperthermia or ROS production, while the diagnosis part mostly involves imaging methods like MRI, fluorescence or ultrasound.[110] Theranostic systems are often based on nanomaterials whose small size and interesting intrinsic properties make them particularly suited for such dual applications. For example, inorganic nanoparticles like quantum dots possess the unique advantage of being intrinsic imaging agents but their potential toxicity limits application.[110,111] On the other hand, lipid- or polymer-based micelles are potent support materials as they are non-toxic and can integrate hydrophobic therapeutic/imaging agents within their hydrophobic core.[110,112] However, increasing the range of applications crucially depends on improving the loading capacity for hydrophilic active compounds which cannot be achieved by using micelles. Of particular interest are soft nanocompartments, i.e. liposomes and polymersomes, as they consist of an amphiphilic membrane enclosing an aqueous cavity and therefore allow for integrating hydrophobic compounds within their membrane and loading their cavity with hydrophilic compounds.[1,113,114] In addition, the external surface of nanocompartments can be functionalized to gain targeting properties, especially in the case of polymersomes as they benefit from the sheer endless chemical versatility of polymers.[1] As polymersomes have an increased mechanical stability compared to liposomes, they appear to be ideal materials for building a non-toxic nanotheranostic platform, adaptable to different applications.[1,113]

To date, nanotheranostics based on soft nanocompartments mainly consist of single-assembly architectures containing both therapeutic (e.g., drugs, photosensitizers, enzymes) and imaging compounds (e.g., iron oxide nanoparticles, radioisotopes, fluorescent dyes).[10] However, co-encapsulation can be detrimental for sensitive compounds or negatively affect the encapsulation efficiency of active agents. These serious drawbacks can be overcome by another type of nanotheranostic architecture based on super-assemblies: the combination of distinct nanomaterials

that each are equipped with either the therapeutic or the imaging function. However, most super-assemblies are composed of inorganic nanoparticles and/or held together by weak, non-covalent interactions that compromise their efficacy, especially under physiological conditions where dissociation of the assembly is likely to occur.[115–117]

To overcome such constraints, we developed a super-assembly composed of two different types of polymersomes, one bearing the therapeutic function while the other one enables imaging, tethered together by hybridization of complementary DNA strands exposed on the respective surfaces (**Figure 3.1**).[58,108] In addition, the ssDNA not involved in tethering served to promote attachment to cells expressing scavenger receptors, e.g., epithelial cells.[118] In view of the encapsulated enzyme (Dopa Decarboxylase, DCC) segregated within the therapeutic polymersomes, our system is geared towards applications in the treatment of atherosclerosis in that polymersome clusters could attach to atherosclerotic lesions, produce and deliver on-site a therapeutic compound (dopamine), while at the same time, the imaging compartment filled with fluorescent dye (Dy-633) serves to follow the lesions' dynamics by the imaging modality.[108] The communication between the external environment and the polymersome cavity where enzymes were located, was accomplished by permeabilization of the polymer membrane via incorporation of pore forming proteins (Outer membrane protein F, OmpF).[8,61]

The potency of the theranostic clusters was evaluated with the cell line HEK$_{REWARD}$, which is specifically engineered to express human dopamine receptor 1 (DRD1)[119] and thus is able to respond to dopamine enzymatically produced in the catalytic nanocompartment. The therapeutic activity of the DNA-linked polymersome clusters was determined by evaluating the concentration of the reporter, human secreted embryonic alkaline phosphatase (SEAP), produced by HEK$_{REWARD}$ cells in the presence of dopamine, while their imaging function was established by visualizing their localization and interaction with the cell surface.

The unique advantage of our DNA-linked polymersome clusters over other currently available theranostic systems resides in the segregated location of the imaging and catalytic compounds, which allows them to act independently, without interference that might compromise their specific functionality. As our strategy is based on a modular design, it should be straightforward to expand it from the example presented here to a variety of other bio-medical applications, simply by changing the

functional components, e.g., biomolecules, within the segregated compartments, and then zipping them together in clusters.

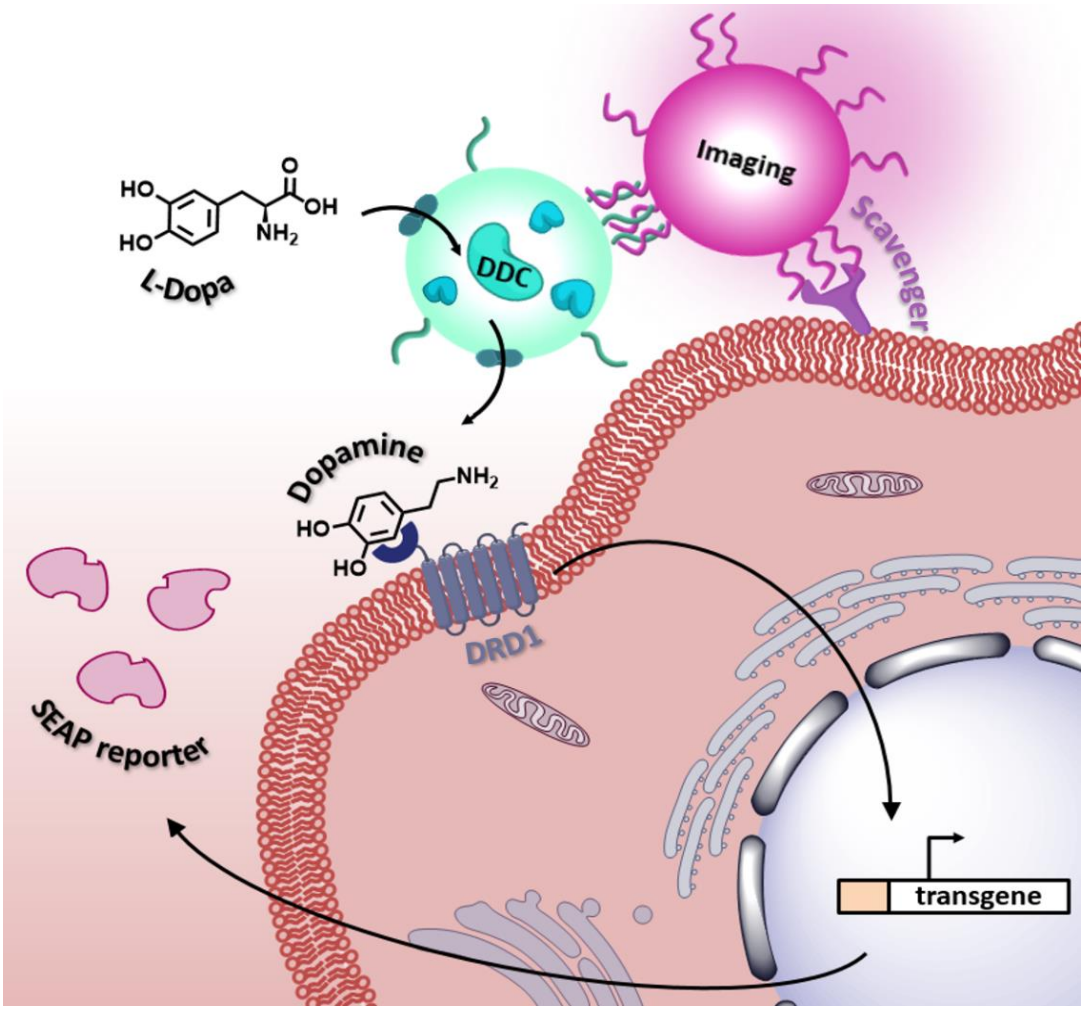

Figure 3.1. *Schematic illustration of cell attachment of DNA-zipped theranostic polymersome clusters composed of two distinct compartments: therapeutic DDC-Ncomp and imaging Dye-Ncomp. While Dye-Ncomp contains fluorescent DY-633 dye, DDC-Ncomp contains DDC, which catalyzes the conversion of L-DOPA into dopamine. This, in turn, triggers gene expression in cells via activation of dopamine receptors D1 (DRD1) resulting in the production of SEAP reporter enzyme. The nanotheranostic platform attaches to the surface of epithelial cells via interaction between DNA strands and scavenger receptors.*

3.2 Design of the nanotheranostic platform

3.2.1 Development strategy of DNA-linked polymersome clusters

Theranostic clusters are formed by self-organization of two types of nanocompartments: the therapeutic polymeric compartment that contains the catalytically active species, and the imaging polymeric compartment that allows the detection and tracking of the whole clusters (**Figure 3.1**). DNA hybridization was used as the driving force to control the construction of nanocompartment clusters with sub-micrometer size.[58] The therapeutic compartment was functionalized with one type of ssDNA (ssDNAa), while the imaging compartment bears the complementary ssDNAb at its surface (see **Table 3** in annex for the details of ssDNA sequences). In order to modulate the DNA attachment to the polymersomes, we also used variants of these ssDNA sequences (called spacer-ssDNAa and spacer-ssDNAb), which contain an additional noncomplementary DNA linker acting as a spacer between the surface of the polymersomes and the complementary DNA sequence. We compared clusters made with ssDNA or spacer-ssDNA and ssDNA, in order to select the most suitable approach to support efficient theranostic application.

We selected amphiphilic diblock copolymers poly(dimethylsiloxane)-*block*-poly(2-methyloxazoline), PDMS-PMOXA for formation of the nanocompartments, because copolymers with a PDMS hydrophobic domain and a PMOXA hydrophilic domain generate polymersomes with flexible membranes,[8] increased mechanical stability and low toxicity, both *in vitro* and *in vivo*.[120] Azide-functionalized poly(dimethylsiloxane)$_{22}$-*block*-poly(2-methyloxazoline)$_8$ ($PDMS_{22}$-$PMOXA_8$-OEG_3-N_3) (**Figure 10.1**) was used to form polymersomes with exposed azide functional groups that do not interfere with other biological processes, as they are bio-orthogonal[121] and promote the attachment of ssDNA. Conjugation was carried out through azide–alkyne cycloaddition (SPAAC) between dibenzocyclooctyne (DBCO) covalently attached to the ssDNA and the azide moieties on the diblock copolymers.[122] We specifically selected short polymer blocks to generate nanocompartments with thin but stable membranes, in order to permit functional insertion of membrane proteins to support the *in situ* enzymatic reaction of the catalytic nanocompartment.[8] Importantly, low-molecular-weight $PDMS_{22}$-$PMOXA_8$ block copolymer is expected to self-assemble rapidly into vesicles, shortening the process of polymersome formation. Indeed, our $PDMS_{22}$-$PMOXA_8$-OEG_3-N_3 is particularly efficient as it self-assemble

into vesicles in less than 1 min when rehydrated in PBS at room temperature (**Figure 3.2**). The vesicular structure of the obtained self-assembled nanocompartments was confirmed by a combination of transmission electron microscopy (TEM) and dynamic

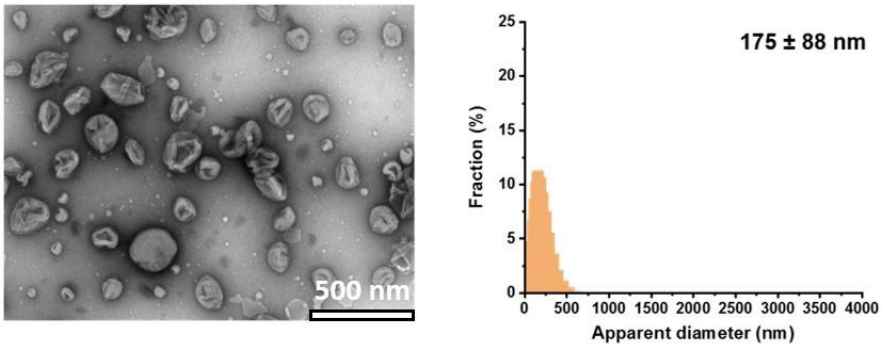

Figure 3.2. *Characterization of empty polymersomes formed in less than 1 min of film rehydration at room temperature via transmission electron microscopy (TEM) and dynamic light scattering (DLS).*

light scattering (DLS) (**Figure 3.2**). This ease of formation of polymersomes, combined with the swiftness of $PDMS_{22}$-$PMOXA_8$-OEG_3-N_3 copolymer formation, also enabled us to increase the initial concentration of copolymer to 10 mg/mL, resulting in a high number of polymersomes ($1.3*10^{12}$ vesicles/mL as determined by nanoparticle tracking analysis, NTA).

3.2.2 Formation of the imaging polymersome

The imaging nanocompartment (Dye-Ncomp) consists of a polymersome loaded with fluorescent dye. We chose to encapsulate DY-633 into polymersomes as a model of the entrapment of small imaging probes in the cavity of the nanocompartments. Like most of the small hydrophilic molecules that have been used to develop imaging nanocompartments, DY-633 is chemically stable, so Dye-Ncomp was formed under normal conditions (room temperature, overnight stirring) by self-assembly through film rehydration of the $PDMS_{22}$-$PMOXA_8$-OEG_3-N_3 polymer (**Figure 3.3A**). The resulting imaging nanocompartments have a hydrodynamic diameter D_H of 218 ± 86 nm as measured by DLS, and their spherical shape was confirmed by TEM (**Figure 3.3B**). As expected, encapsulation of the dye did not affect the self-assembly process, and the resultant imaging nanocompartments appeared similar to empty ones (**Figure 3.3C).** Based on these results with DY-633, the incorporation of other

imaging components consisting of stable small hydrophilic molecules should be relatively straightforward. In contrast, the development of therapeutic catalytic compartments is more complex, as it involves active enzymes.

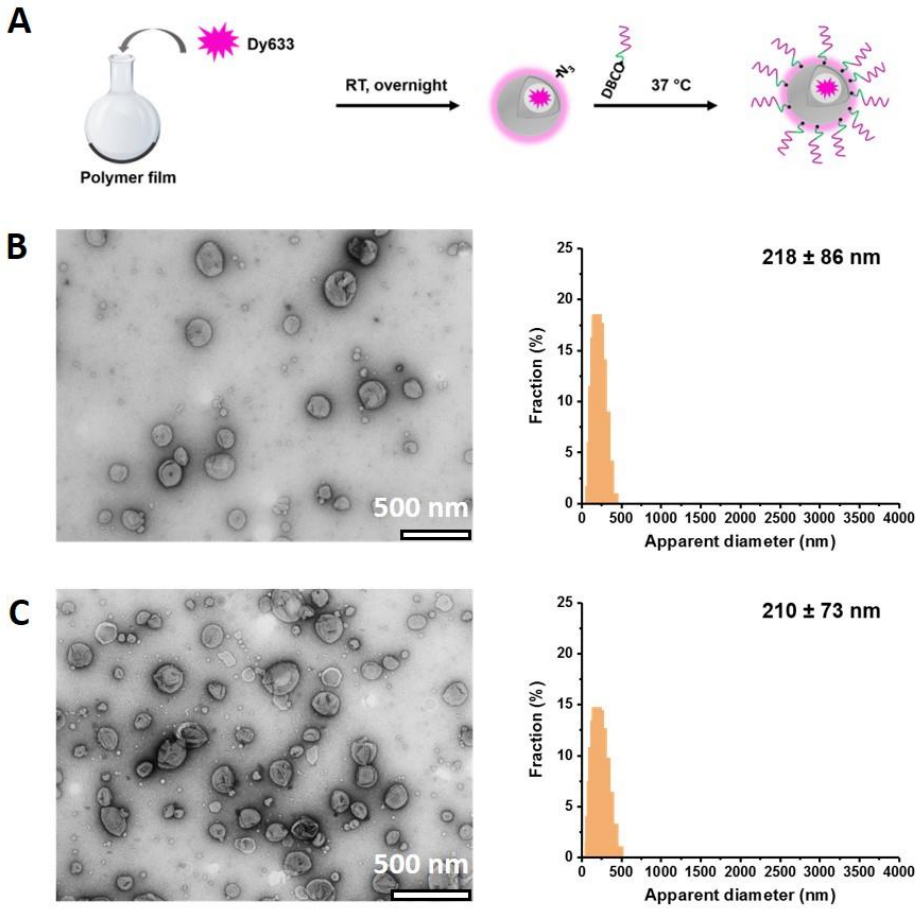

Figure 3.3. *Characterization of Dye-Ncomp and empty polymersomes.* ***(A)*** *Schematic representation of the formation of Dye-Ncomp.* ***(B)*** *Transmission electron microscopy (TEM) micrograph and size obtained by dynamic light scattering (DLS) of Dye-Ncomp and* ***(C)*** *empty polymersomes formed at room temperature overnight.*

3.2.3 Optimized formation of the catalytic therapeutic polymersome

The catalytic nanocompartment (DDC-Ncomp) consists of human DDC encapsulated in the inner cavity of polymersomes equipped with a channel porin, which supports *in situ* enzymatic reactions. We chose the channel porin OmpF as a biological tool for permabilization, as it can be inserted in the membrane of PDMS-PMOXA

polymersomes and has a molecular weight cutoff of 600 Da,[123] thus allowing the passage of small molecules such as the DDC substrate L-DOPA and product dopamine. Compared to other therapeutic nanocompartments reported for theranostic applications, which are based on the entrapment of small and stable therapeutic compounds,[110] we aimed to develop a more versatile and dynamic system involving an active enzyme that produces the desired drug inside the therapeutic compartment. By incorporating an active enzyme, we can produce the needed therapeutic compound on demand at selected locations rather than having a simple one-time delivery system. But, like many enzymes carrying out physiological functions in the human body, DDC is vulnerable to degradation, and loses its activity significantly at 37 °C.[124] Therefore, the formation of DDC-Ncomp requires a complex preparation methodology based on numerous optimization steps.

To preserve DDC activity, it was crucial to conduct polymersome formation (self-assembly and OmpF insertion) as quickly as possible by shortening the time of film rehydration, since at least one day is generally required for the self-assembly of most amphiphilic block copolymers with high molecular weight.[65,125] Our short $PDMS_{22}$-$PMOXA_8$-OEG_3-N_3 copolymer favoured the formation of polymersomes in less than 1 min, thus supporting a rapid generation of DDC-Ncomps (see above). The rapid insertion of OmpF during the such prompt formation of polymersomes was confirmed using model polymersomes encapsulating model enzyme horseradish peroxidase (HRP) that is more stable and easier to work with than DDC (**Figure 3.4**).[126] The production of fluorescent product (resorufin) was only observed for HRP-loaded polymersomes formed in presence of OmpF, while no fluorescent product was observed when polymersomes were formed without OmpF (**Figure 3.4**). This highlights the ease with which membrane proteins can be inserted into $PDMS_{22}$-$PMOXA_8$-OEG_3-N_3, presumably due the thinness of the membrane.[8]

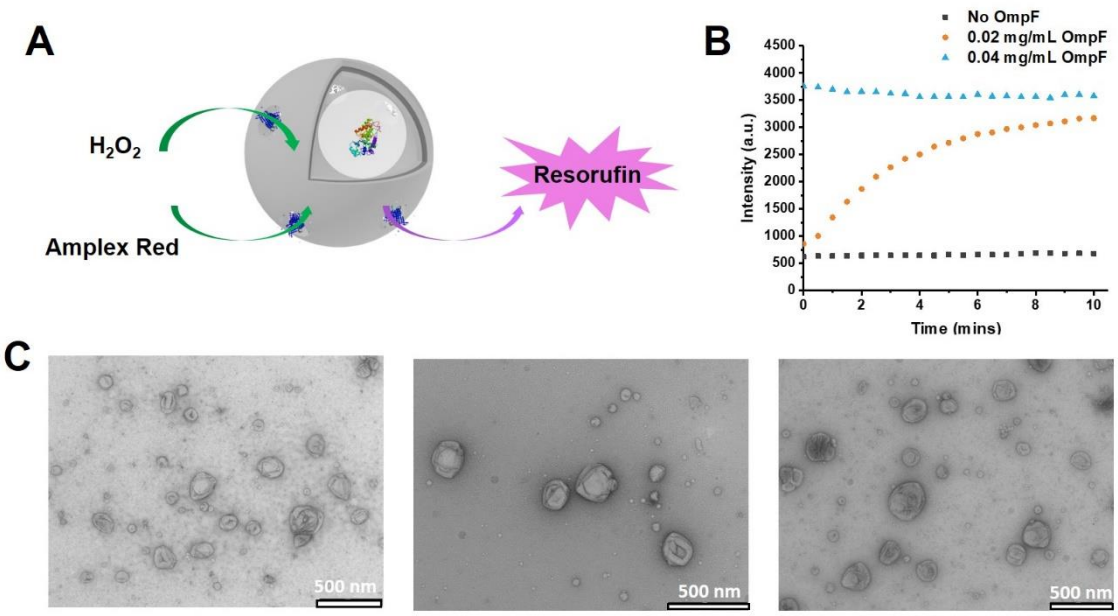

Figure 3.4. *Characterization of instant insertion of Outer membrane protein F (OmpF) in the membrane of polymersomes:* ***A)*** *schematic representation of horseradish peroxidase (HRP encapsulated in OmpF-equipped nanocompartment, which allows the passage of Amplex Red through the membrane and oxidizes it to generate fluorescent resorufin;* ***B)*** *enzymatic kinetics of HRP-encapsulating nanocompartments, prepared at different initial concentrations of OmpF, by monitoring the fluorescent intensity of resorufin as a function of time;* ***C)*** *TEM micrographs of HRP-encapsulating nanocompartments assembled in the presence of 0,0.02 mg/mL and 0.04 mg/mL of OmpF.*

Following these preliminary optimizations using PBS and model enzyme HRP, we proceeded with the encapsulation of our biologically relevant enzyme DDC and optimized the conditions of self-assembly (composition of the rehydration solution, temperature and time). To prevent the degradation of DDC in solution during film rehydration, we added bovine serum albumin (BSA), a commonly used protein stabilizer.[127] We also reconstituted DDC holoenzyme by adding its cofactor pyridoxal phosphate in the rehydration solution. The association of DDC apoenzyme with its cofactor generates the holoenzyme, which is less solvent-accessible, and thus more stable and more compact.[128] As a result, the rehydration solution used to form DDC-Ncomp contained DDC holoenzyme, remaining unbound cofactor pyridoxal phosphate, BSA and OmpF. The obtained DDC-Ncomp formed by rapid film rehydration at room temperature was a mixture of vesicles and worms (**Figure 3.5A**), probably due to the presence of a large number of molecules in the solution, slowing down self-assembly.[129] A rehydration time of 2 h was necessary to obtain only vesicular-shaped DDC-Ncomp at room temperature (**Figure 3.5B**). To avoid the

exposure of DDC to room temperature for 2 h, which can decrease its activity, we investigated the possibility of forming DDC-Ncomp at low temperature (4 °C). After 2 h of rehydration at 4 °C, we obtained a mixture of polymersomes and worms (**Figure 3.5C**), presumably due to the slower kinetics of self-assembly at this temperature.[129]

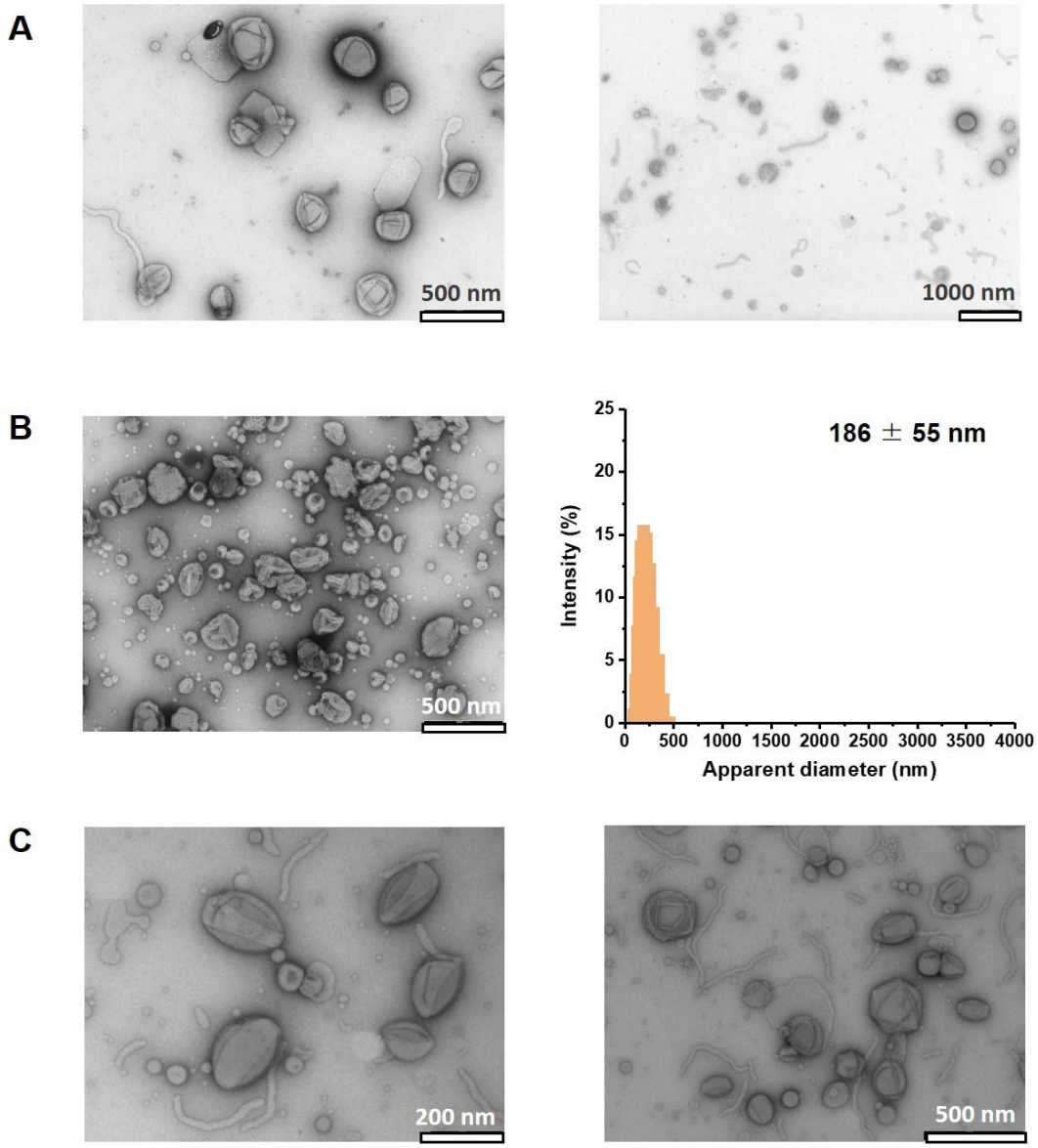

Figure 3.5. *Characterization of DDC-Ncomp.* ***(A)*** *TEM micrographs of DDC-Ncomp instantly formed at RT.* ***(B)*** *TEM micrograph and DLS of DDC-Ncomp formed at RT for 2 h.* ***(C)*** *TEM micrograph of DDC-Ncomp formed at 4 °C for 2 h.*

An extended rehydration time of 3 h was necessary to obtain only vesicular–shaped DDC-Ncomp (**Figure 3.6A**). When DDC-Ncomp was formed under these conditions, the presence of DDC and BSA in the lumen did not influence the polymersome structure, as judged from TEM micrographs, or the size of DDC-Ncomp, since D_H remained constant (184 ± 66 nm) as determined by DLS (**Figure 3.6B**). Systematic investigation of factors affecting the self-assembly process and the enzyme activity (molecular properties of the copolymers and polymersome membrane, self-assembly conditions, stabilizer protein, reconstitution of holoenzyme) led to an optimized procedure to prepare catalytic compartments containing sensitive enzymes, such as DDC-Ncomp.

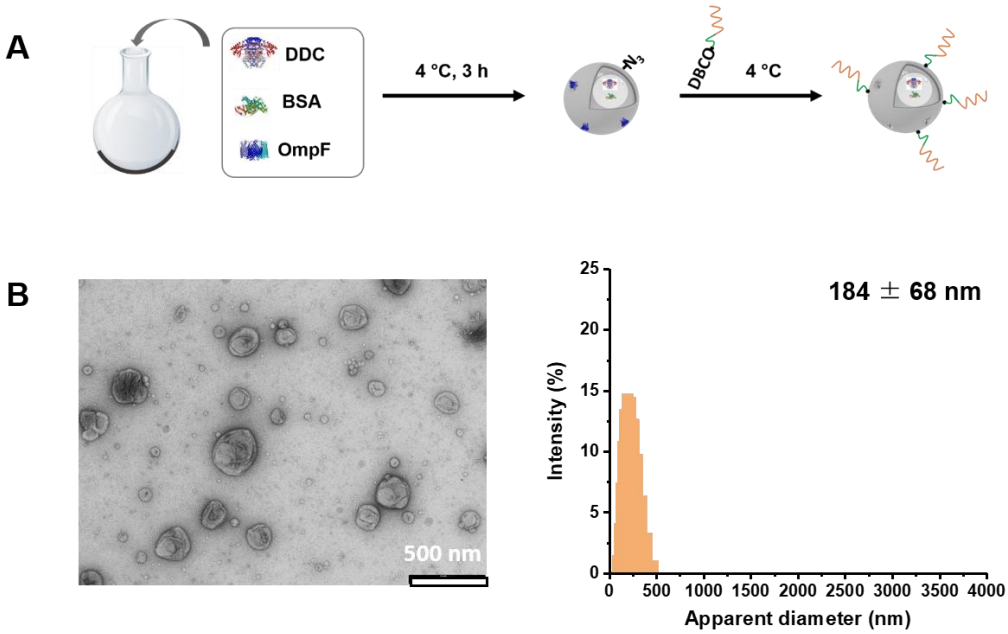

Figure 3.6. *Characterization of DCC-Ncomp.* ***(A)*** *Schematic representation of the formation of DDC-Ncomp.* ***(B)*** *Transmission electron microscopy (TEM) micrograph and size obtained by dynamic light scattering (DLS) of DDC-Ncomp .*

3.2.4 Surface functionalization of polymersomes with ssDNA

With both imaging and therapeutic nanocompartments in hand, the next step consisted of functionalization with ssDNA to assemble them into theranostic clusters. Here again, different strategies had to be adopted to preserve DDC activity during the ssDNA functionalization of DDC-Ncomp and subsequent formation of clusters. The usage of $PDMS_{22}$-$PMOXA_8$-OEG_3-N_3 copolymer, consisting of short polymer chains

less entangled inside the polymersome membrane, promoted the coupling of the ssDNA by increasing the exposure of the azide terminal groups. We used 100 % of this azide-functionalized polymer to obtain the highest density of azide at the surface of polymersomes, thus enabling the attachment of a maximal number of ssDNAs. In addition, we investigated the influence of an additional spacer on the ssDNA sequence in facilitating the formation of dsDNA by hybridization, and thus the clustering of the complementary ssDNA-functionalized polymersomes.

Dye-Ncomp is inherently stable, so its functionalization with ssDNAb or spacer-ssDNAb was accomplished under normal conditions (37 °C, overnight) to obtain maximal reaction efficiency. To quantify the number of ssDNAb attached per polymersome, ssDNAb labelled with a fluorescent dye (Atto-488) were used to enable detection using fluorescence correlation microscopy (FCS). We confirmed that fluorescently labelled ssDNAb (without DBCO) did not interact with polymersomes, so that the count per molecule obtained for ssDNAb-functionalized Dye-Ncomp reflected only covalently attached ssDNA (**Figure 10.2A**) and did not affect the structure of polymersomes (**Figure 10.2B**). The number of ssDNAb attached per Dye-Ncomp can be determined by dividing the counts per molecule of ssDNAb-functionalized polymersomes by the counts per molecule of free ssDNAb (**Figure 10.2C**). We obtained an average value of 163 ± 61 of ssDNAb per Dye-Ncomp (**Figure 3.7A**). Similarly, we determined the density of spacer-ssDNAb as 196 ± 96 spacer-ssDNAb per Dye-Ncomp (**Figure 3.7A, Figure 10.2**).

To avoid loss of the catalytic activity of DDC while performing ssDNA functionalization of DDC-Ncomp, we again had to optimize the reaction conditions. As described for DDC-Ncomp formation, we first investigated the feasibility of conducting ssDNA conjugation at 4 °C by using empty polymersomes (rehydrated with PBS only). DY-633-labelled ssDNAa and spacer-DNAa were used to assess the number of ssDNA covalently attached to polymersomes at 4 °C during overnight reaction (**Figure 10.3A**). The attachment of ssDNAa and spacer-ssDNAa to empty polymersomes was achievable under these conditions (**Figure 10.3B**), but the efficiency of the reaction was drastically reduced compared to the conjugation reactions at 37 °C. Under these conditions (4 °C, overnight) for functionalization of DDC-Ncomp, we obtained an average number of 23 ± 6 for ssDNAa and 22 ± 6 for spacer-ssDNAa attached per polymersome (**Figure 3.7A**). The functionalization of nanocompartments with ssDNA did not affect the architecture of the vesicles or their

size, as determined by TEM and DLS (**Figure 3.7C-F**). Furthermore, the small amount of ssDNAa present at the surface of DDC-Ncomp should be counterbalanced by the large amount of complementary ssDNAb attached to the Dye-Ncomp, allowing the effective formation of theranostic clusters.

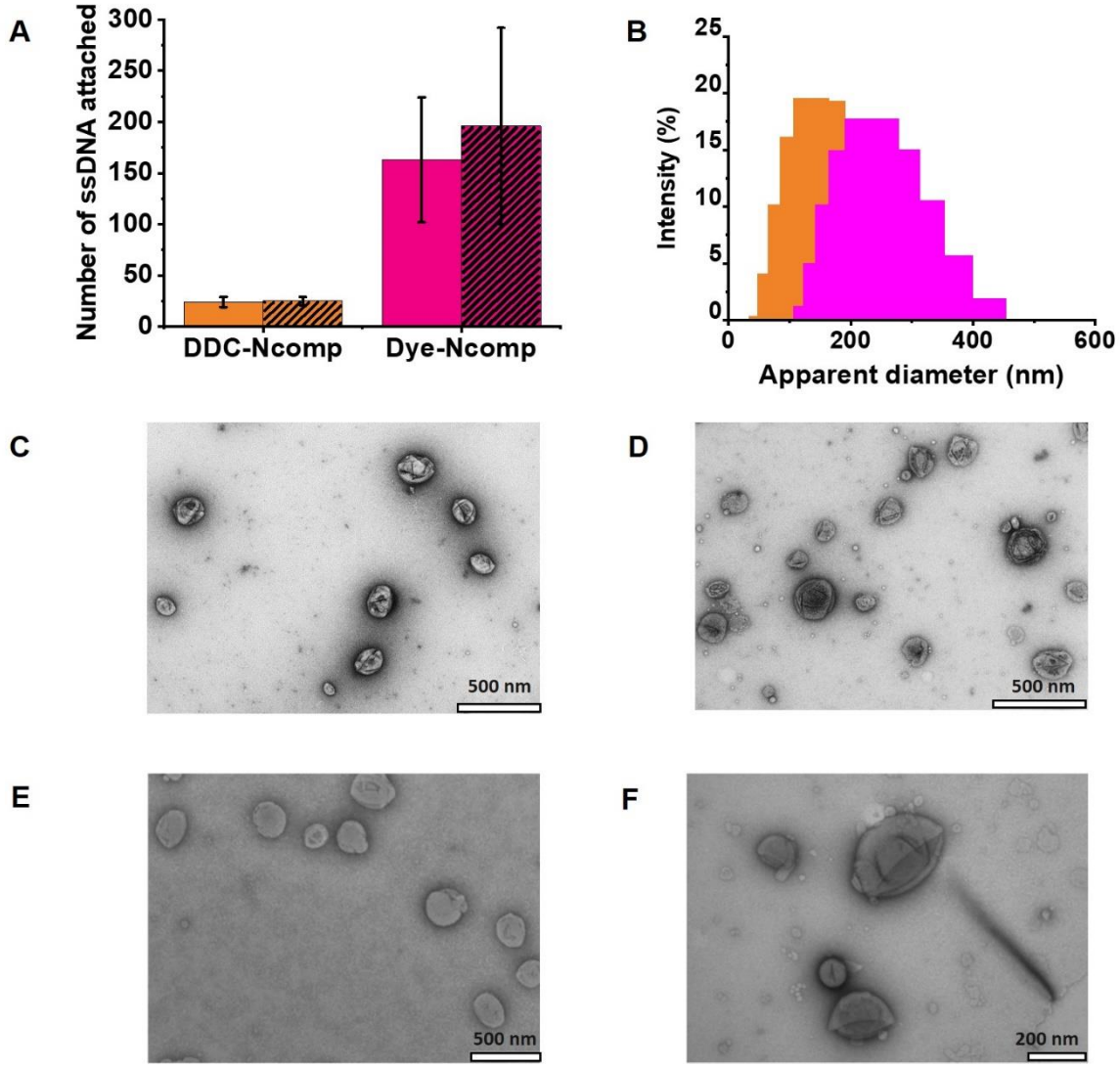

Figure 3.7. *Characterization of the ssDNA and spacer-ssDNA attachment on the surface of DDC-Ncomp and Dye-Ncomp.* ***(A)*** *Average numbers of ssDNA (solid) and spacer–ssDNA (stripped) linked to DDC-Ncomp (orange) and Dye-Ncomp (pink), as determined by FCS (n = 3; each sample was measured 30 times for 10s each).* ***(B)*** *Size of DDC-Ncomp linked with spacer–ssDNAa (orange) and Dye-Ncomp (pink) linked with spacer–ssDNAb as determined by DLS. TEM micrographs of DDC-Ncomp linked with spacer–ssDNAa* ***(C)*** *and Dye-Ncomp linked with spacer–ssDNAb* ***(D)****. TEM micrographs of DDC-Ncomp linked with ssDNAa* ***(E)*** *and Dye-Ncomp linked with ssDNAb* ***(F)****.*

3.2.5 Formation of DNA-linked clusters

We investigated the cluster formation between DDC-Ncomp and Dye-Ncomp under mild conditions at 20 °C (**Figure 3.8.A**). We compared the clusters formed using polymersomes functionalized with ssDNA and those formed using spacer-ssDNA. After overnight incubation at 20 °C, no clusters were observed in the case of ssDNA-functionalized polymersomes (**Figure 3.8B**, green line). In contrast, theranostic clusters formed rapidly when spacer-ssDNA was used (**Figure 3.8B**, blue line). These results support the idea that the spacer enhances the exposure of the complementary ssDNA sequences at the surface of polymersomes, resulting in easier hybridization of complementary strands to trigger the formation of clusters.[122] The theranostic clusters formed using spacer-ssDNA rapidly self-organized into sub-micrometer-sized structures that further aggregated after 4 h (**Figure 3.8**). To slow the ssDNA hybridization process, so that the cluster size could be restricted, as well as to minimize loss of DDC activity, we investigated the formation of clusters at 4 °C using spacer-ssDNA. But, as no clusters were formed after overnight incubation at 4 °C (**Figure 3.8C**), we decided to control the size of the clusters by shortening the clustering time to 20 min at 20°C; this afforded theranostic clusters of around 531 ± 305 nm in size, with a polydispersity index (PDI) of 0.8 from three independent samples (**Figure 3.8D-E**). To maintain the stability, these clusters were stored at 4 °C, where they showed long-term (at least one year) stability as the same size (495 ± 212 nm) was maintained after one year of storage (**Figure 3.8F**).[109]

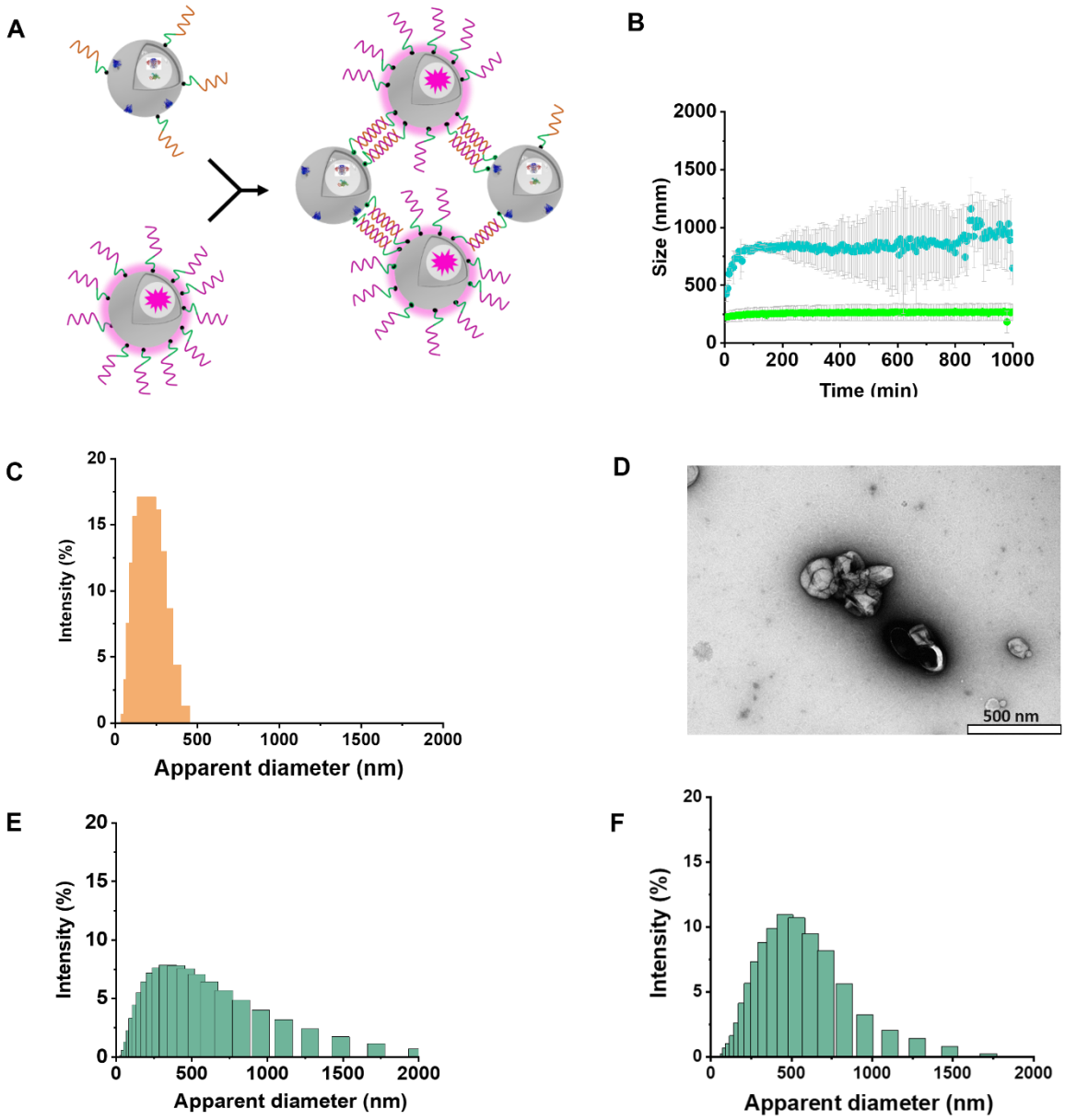

Figure 3.8. *Characterization of theranostic clusters.* ***(A)*** *Schematic representation of the formation of theranostic cluster constituted by DDC-Ncomp and Dye-Ncomp linked together via hybridization of their complementary spacer–ssDNA, the spacer between the reactive DBCO moiety and ssDNA sequences used for hybridization (pink and orange) is represented in green.* ***(B)*** *The change of apparent size of theranostic clusters DDC-linked by ssDNA (green) and spacer–ssDNA (blue) as a function of time. The gray bars represent the standard deviation based on three independent experiments.* ***(C)*** *DLS showing that no clusters were formed using spacer-ssDNA for overnight at 4 °C.* ***(D)*** *TEM micrograph of theranostic cluster.* ***(E)*** *DLS of theranostic clusters.* ***(F)*** *DLS of theranostic clusters after 1 year of storage at 4 °C.*

The analysis of TEM microscopic images indicated that 87% of polymersomes were clustered and 13% remained nonbound. In general, clusters were composed of less than seven polymersomes (79%), with only 8% larger clusters composed of more than seven polymersomes (**Figure 3.9A-B**). These results suggest that the DDC-Ncomp and Dye-Ncomp form non-uniform random clusters with large distribution similarly to a previous observation[122] but only a small fraction of larger clusters (clusters composed of ≥ 7 polymersomes) were formed. Larger clusters or small aggregates can be removed via size exclusion chromatography (SEC) or filtration. Furthermore, using a ratio of 2:1 DDC-Ncomp to Dye-Ncomp also promotes cluster formation at 20 °C (**Figure 3.9C**); however, to achieve a balance between the imaging and therapeutic compartment, we used only a one-to-one ratio for the remained of experiments. The different strategy adopted to obtain a high density of ssDNAb per Dye-Ncomp enabled us to compensate for the low incorporation of ssDNAa per DDC-Ncomp obtained at the low temperature. Overall, the results indicate that incorporation of a spacer within the ssDNA facilitates the hybridization of ssDNA and promotes the formation of nanotheranostic polymersome clusters.

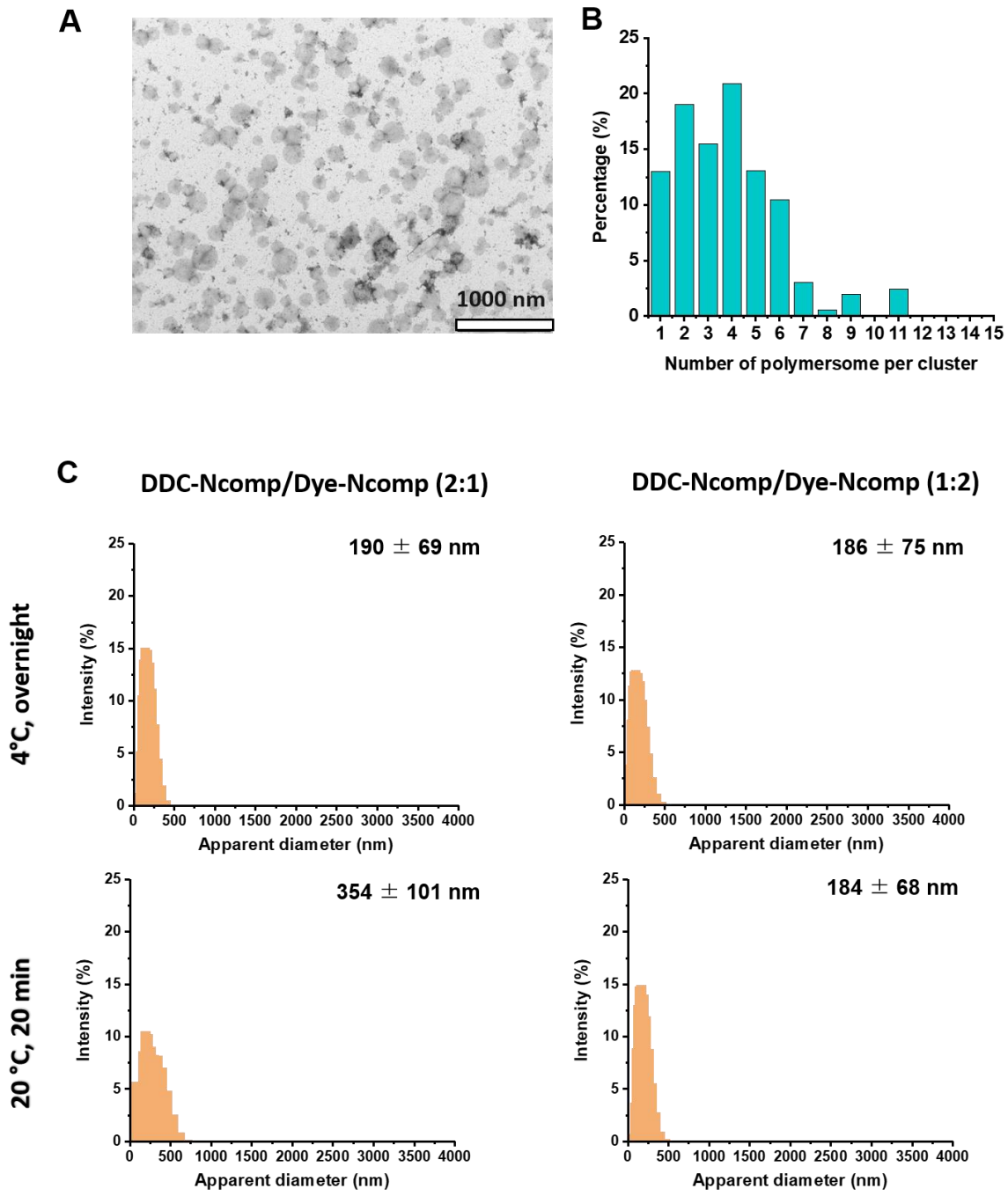

Figure 3.9. *Characterization of polymersome clusters.* ***(A)*** *TEM micrographs showing the size and geometry of polymersome clusters.* ***(B)*** *Histograms showing the distribution of the number of polymersomes per cluster. The data were statistically analyzed using a binomial distribution based on 526 clusters in TEM micrographs.* ***(C)*** *DLS showing the size of clusters formed by mixing spacer-ssDNAb functionalized Dye-Ncomp and spacer-ssDNAa at DDC-Ncomp/Dye-Ncomp ratios of 2:1 and 1:2. Clusters were only obtained in the case of DDC-Ncomp/Dye-Ncomp ratio of 2:1 after 20 min of incubation at 20 °C, as it is the case for 1:1 ratio (Figure 3.8E). For 2:1 and 1:2 ratios, no clusters were formed after overnight incubation at 4° C, as it is also the case for 1:1 ratio (Figure 3.8C).*

3.3 Therapeutic potential of the theranostic clusters

3.3.1 Determination of DDC-triggered production of dopamine

We first estimated the DDC encapsulation efficiency in polymersomes using the model protein BSA, because of its similarity to DDC in size, molecular weight, and solubility (PDB ID: 3V03 and 3RBL); it is also an established model protein for UV-vis absorption measurements[130–132] (see experimental chapter for further details). We obtained a value of 23.01 ± 6.03 DDC molecules per polymersome, representing an encapsulation efficiency of 15.6 ± 4.12 %, which is consistent with the range of encapsulation efficiencies generally obtained for enzymes within PDMS-PMOXA polymersomes.[126] This provides a concentration of encapsulated DDC of 0.054 µg/mL for DDC-Ncomp and the corresponding clusters.

Having determined the amount of encapsulated DDC per polymersome, we proceeded to assess the production rate of dopamine via irreversible decarboxylation of the substrate L-DOPA under physiological conditions.[133] The production of dopamine by DDC was carried out for up to 24 h in PBS at 37 °C; however, both L-DOPA and dopamine spontaneously auto-oxidize *in vivo*,[134] and this also occurs in PBS, affording a dark, insoluble polydopamine precipitate.[135] To overcome this problem, we decided to add a reducing agent during the DDC-triggered conversion reaction of L-DOPA to dopamine in PBS. We chose glutathione, the most abundant free thiol in mammalian cells, and a major antioxidant in the brain, where it is implicated in the prevention of L-DOPA and dopamine oxidation.[136,137] As expected, no dark precipitate was formed in the presence of glutathione (**Figure 10.4**). The assessment of dopamine production by DDC was then possible by HPLC (**Figure 10.5**), allowing us to calculate the percent conversion of L-DOPA to dopamine based on the areas under the corresponding peaks (**Figure 3.10A**). All percentages of conversion recorded correspond to dopamine production in the µM-mM range (the initial concentration of L-DOPA substrate was 0.49 mM).

3.3.2 Catalytic activity of therapeutic polymersomes in situ

Free (non encapsulated) DDC was first assessed to verify the role of BSA as a stabilizer. We compared solutions of free DDC containing only DDC diluted in PBS and

containing DDC in the presence of 0.1 wt% BSA, corresponding to the BSA concentration used in the rehydration solution to form DDC-Ncomp (**Figure 3.10B**, grey and black bars respectively). At all measured time points, the percent conversion of L-DOPA to dopamine in the presence of BSA was higher than in the case of the free DDC alone, confirming that BSA stabilizes DDC.

Considering that the amount of Dopamine produced is closely related to the enzyme concentrations (**Figure 10.6**), to compare the activity of free DCC with that of encapsulated DDC inside DDC-Ncomp, as well as DDC-Ncomp clusters, we ensured that DDC was contained at the same concentration (0.05 μg/mL) in all samples. As shown in **Figure 3.10**, control DDC-Ncomp without OmpF did not show any conversion of L-DOPA since the polymersome membrane is impermeable (**Figure 3.10B**, purple bars). Production of dopamine was observed when DDC was encapsulated in OmpF-equipped DDC-Ncomp, ssDNA functionalized DDC-Ncomp and DDC-Ncomp clusters with the imaging compartment (forming the nanotheranostic system). These results confirm the encapsulation of active DDC inside polymersomes, and the ability of the system to transport and convert L-DOPA and to release therapeutic dopamine (**Figure 3.10B**, orange blue and green bars). The percent conversion of L-DOPA to dopamine by encapsulated DDC is lower than that of free DDC in presence of BSA, presumably due to slow diffusion through the channel porin, resulting in a slower reaction *in situ*. The attachment of ssDNAa and subsequent clustering of DDC-Ncomp together with Dye-Ncomp also decreases the efficacy of conversion of L-DOPA to dopamine (**Figure 310B**, blue and green bars). This decrease in the DDC activity was expected, due to the inherent steric hindrance of OmpF by the ssDNA and ssDNAa-ssDNAb bridges formed during the polymersome clustering process. However, the amount of dopamine (μM) produced by the theranostic clusters is within the range required to induce a cellular response (**Figure 10.7**). With regards to the reaction kinetics at physiological temperature (37 °C), we compared the conversion of L-DOPA to dopamine by free and encapsulated DDC at the beginning of the reaction (up to 2 h) and after 24 h (**Figure 3.10B**). Considering that the L-DOPA substrate is present in excess, the slower conversion rate observed after 24 h is not attributable to a decrease in substrate availability, but should reflect deactivation of the enzyme.

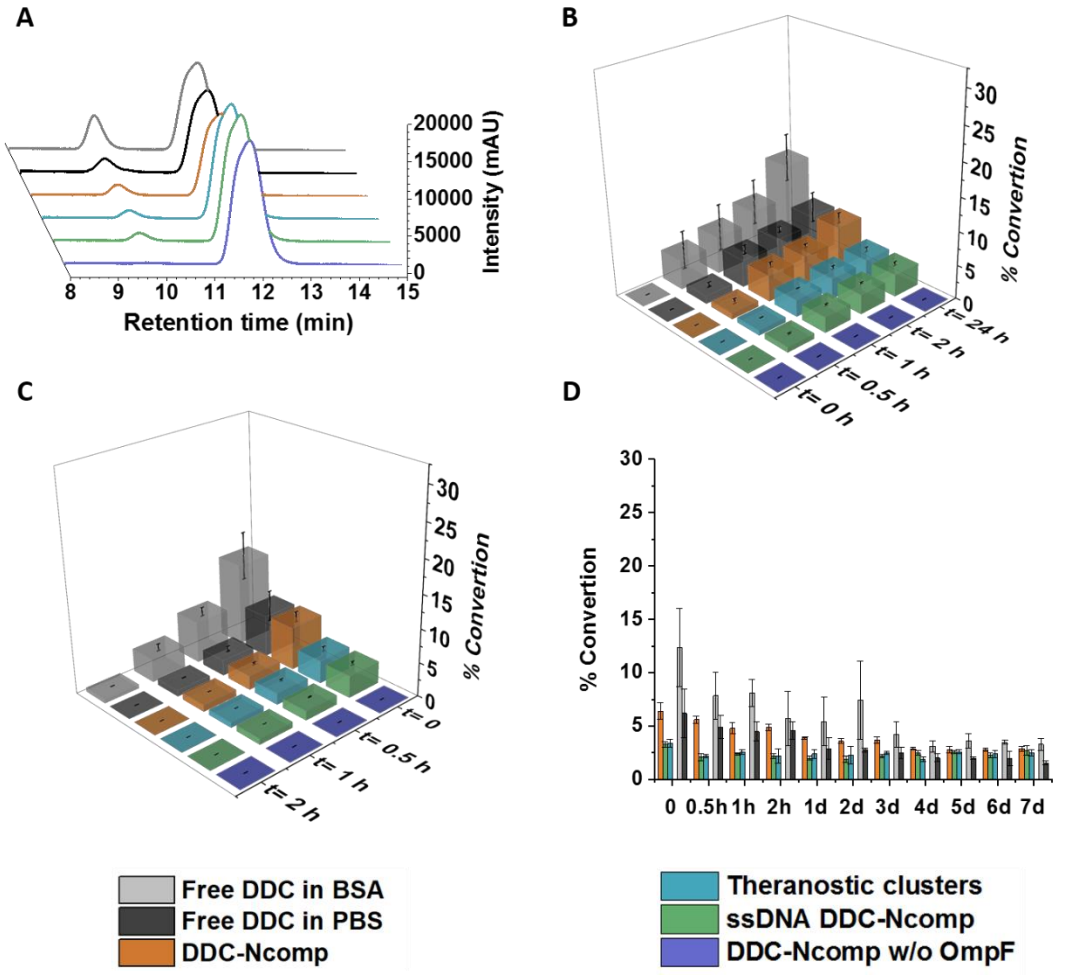

Figure 3.10. *Activity of DDC-Ncomp and theranostic clusters in PBS.* ***(A)*** *HPLC chromatograms showing elution peaks corresponding to dopamine (retention time 10.1 min) and L-DOPA (retention time 11.8 min) for free DDC in PBS (gray), free DDC in the presence of BSA (black), DDC-encapsulating polymersomes (DDC-Ncomp, orange), theranostic clusters (blue), ssDNA-functionalized DDC-Ncomp (green), and control DDC-Ncomp without OmpF (purple), after reaction for 24 h at 37 °C.* ***(B)*** *Processed HPLC data showing the percent conversion of L-DOPA to dopamine by the different DDC-containing samples and assemblies, illustrating the kinetics of these systems up to 24 h at 37 °C in PBS.* ***(C)*** *Processed HPLC data showing the stability of these systems up to 2 h at 37 °C in PBS.* ***(D)*** *Processed HPLC data showing the stability of these systems up to 24 h at 4 °C in PBS. Full conversion (100% conversion) equates to a concentration of 490 × 10−6 m dopamine.*

3.3.3 Stability of therapeutic polymersomes to thermal deactivation

To gain insight into the thermal stability of DDC, we stored free and encapsulated DDC enzyme at 37 °C for different periods of time (0 to 2 h) prior to the addition of L-DOPA, and then measured dopamine production after 24 h (**Figure 3.10C**). Almost no dopamine was produced when free or encapsulated DDC was stored at 37 °C for 2

hours before addition to L-DOPA. These results confirm the rapid thermal inactivation of DDC at 37 °C, and support our explanation of the slower rate of dopamine formation after a longer reaction time at 37°C. To evaluate the stability of free and encapsulated DDC upon storage at a lower temperature, we repeated the same experiment at 4 °C (**Figure 3.10D**). The encapsulated DDC maintained a reasonably consistent percent conversion of dopamine up to one week, while free DDC showed a more pronounced decrease in dopamine formation (9.1% loss of dopamine production for free DDC with BSA, compared to 3.5% loss for DDC-Ncomp after 7 days). This behavior can be attributed to the stabilizing effect of polymersomes on DDC, in accordance with previous findings.[138] Since no activity of encapsulated DDC was retained at 37 °C, we hypothesized that DDC is so sensitive to thermal denaturation that the stabilizing effect of polymersomes is only observable at low temperatures. Thus, even though polymersomes do not extend the active period of encapsulated DDC in PBS at 37°C, they still enhance the stability at 4°C, which may permit longer-term storage – a desirable feature for translational applications.

3.3.4 Cell response to therapeutic polymersomes and theranostic clusters

To investigate the ability of our therapeutic compartments and theranostic clusters to produce dopamine *in vitro*, we monitored the response of dopamine-sensing cells during incubation in the presence of DDC-Ncomp and corresponding DNA-linked polymersome clusters. We selected the HEK$_{REWARD}$ double-transgenic cell line as a dopamine-sensing platform; it was previously used to investigate the reward-based control of hypertension via a synthetic brain-dopamine interface.[119] These cells were engineered to ectopically express human dopamine receptor 1 (DRD1), enabling dopamine-triggered production of the reporter, SEAP. SEAP is induced whenever the cells are exposed to dopamine; other metabolically related small molecules, such as L-DOPA, did not trigger DRD1-driven SEAP expression. This HEK$_{REWARD}$ cell line is sensitive to dopamine in the nanomolar range, positioning it as a very sensitive and selective dopamine sensor. It has also been reported that the cellular expression of SEAP was the highest when the cells were incubated with dopamine for 3 days.[119] The delay presumably reflects the fact that the response to dopamine requires time for the cells to initiate the pathways required for SEAP expression. Therefore we chose an

incubation time of 3 days for incubation of the DDC-Ncomp and theranostic polymersome clusters with cells. It should be noted that even though DDC showed reduced activity after 2 hours at physiological temperature in PBS, the production of dopamine reaches a concentration 31 μM, which is high enough to induce a relevant cell response.

We first investigated the response of HEK_{REWARD} cells when incubated with dopamine alone at various concentrations for 3 days. We observed a linear dependence of cellular expression of SEAP upon dopamine concentration up to 1 μM (**Figure 10.7**). No further increase in SEAP expression was observed at higher concentrations of dopamine, and 12 U/L of SEAP was the highest cellular response achieved in our experiments (**Figure 10.7**). Second, we investigated the cellular response to dopamine produced by free DDC (**Figure 3.11A**). The maximum level of SEAP produced was 3 U/L (**Figure 3.11B**), probably due to the rapid deactivation of DDC as a result of the cumulative effects of physiological temperature and the cellular milieu. In these cellular assays, no change in SEAP production was observed with free DDC in presence of BSA (**Figure 3.11B**) or in PBS buffer only (**Figure 10.8**). This lack of a stabilizing effect of BSA on free DDC in cell assays could be explained by enhanced sensitivity of DDC under cellular conditions, as well as a dilution effect of BSA with other proteins.

Interestingly, we observed higher levels of SEAP production in the presence of DDC-Ncomp in comparison with free DDC (**Figure 3.11C**). Our results clearly indicate the protective role of polymersomes in shielding DDC degradation in the cellular environment (**Figure 3.11C)**: within the nanocompartments, BSA can continue to stabilize DDC and proteolytic degradation is avoided due to the polymeric membrane. DDC-Ncomp functionalized with ssDNAa, and also when present as therapeutic nanocompartments in the theranostic clusters, successfully induced a cellular response, of the same order of magnitude as DDC-Ncomp (**Figure 3.11D, Figure 10.9**). Notably, in the cell-based assay, the presence of ssDNAa and the location of DDC-Ncomp in theranostic clusters appears to compensate for the reduced activity observed in PBS, in agreement with other studies showing that catalytic nanocompartments were more active in cell media than in PBS as compared to free enzymes.[126] This effect is most likely due to the shielding of polymersomes and to the presence of ssDNAa on the surface of the polymersomes, promoting the attachment of single polymersomes and DNA-zipped polymersome clusters to the cell membrane.[118]

Such proximity with the cell membrane eventually leads to a locally increased concentration of dopamine near the DRD1 receptors, resulting in an increase of SEAP expression.

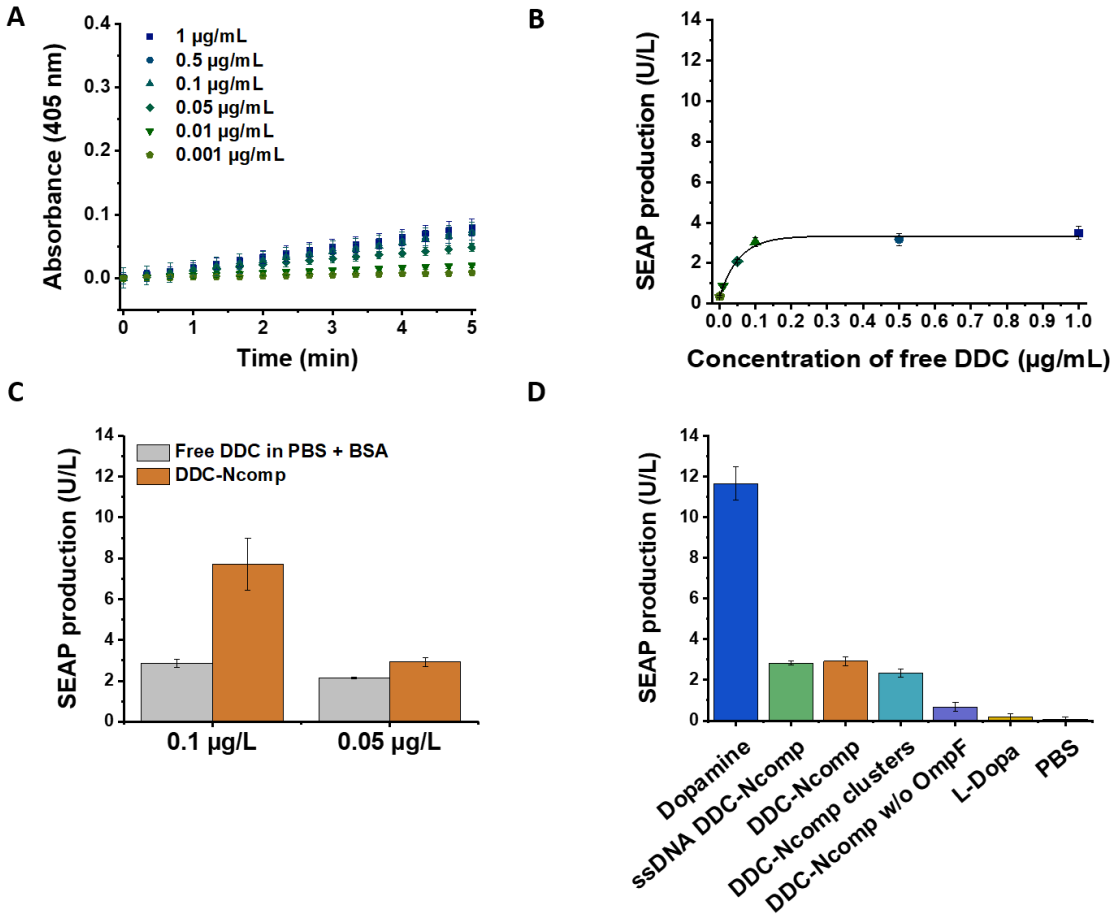

Figure 3.11. *Cell activation by DDC-Ncomp and theranostic clusters.* ***(A)*** *Absorbance monitoring of the enzymatic production of chromogenic p-nitrophenol from SEAP substrate p-nitrophenyl phosphate in the cell supernatant to assess cellular production of SEAP induced by different concentrations of free DDC (0.001–1 µg/mL) in the presence of 0.1 wt% of BSA.* ***(B)*** *Cell expression of SEAP (U/L) induced by different concentrations of free DDC (with BSA) after 3 days.* ***(C)*** *Comparison of cellular production of SEAP (U/L) induced by DDC-encapsulating polymersomes or free DDC in BSA, at 0.1 or 0.05 µg/mL DDC concentration.* ***(D)*** *Cell expression of SEAP (U/L) induced by free dopamine (dark blue), ssDNA functionalized DDC-Ncomp (green), DDC-encapsulating polymersomes (orange), DDCNcomp theranostic clusters (blue), control DDC-Ncomp without OmpF(purple), L-DOPA (gray), and PBS only (black).*

3.4 Imaging potential of the theranostic clusters: cell attachment and tracking

DNA-zipped polymersomes clusters possess interesting surface-binding ability to epithelial cells due to their physical properties[118]: their softness, increased size (unfavourable for endocytosis), and availability of ssDNA on the surface promote their attachment to scavenger receptors present at the surface of epithelial cells. Scavenger receptors are known to bind DNA, RNA and other negatively charged large molecules.[139] Zeta potential measurements of our nanocompartments confirmed that ssDNA-functionalized polymersomes were more negatively charged (- 13.53 ± 2.54 mV for Dye-Ncomp and - 6. 93 ± 3.38 mV for DDC-Ncomp) than non ssDNA-functionalized polymersomes (- 5.24 ± 0.4 mV), thus making them prime candidates for attachment to scavenger receptors. Since the HEK$_{REWARD}$ cell line used for our experiments is of epithelial origin, it should interact with ssDNA-functionalized polymersomes and clusters. To investigate the interaction between polymersome clusters and this new engineered HEK$_{REWARD}$ cell line, we used model systems: ssDNA-functionalized polymersomes or DNA-linked polymersome clusters loaded with fluorescent dyes (DY-633 and Atto-488) as imaging compartments. The binding efficiency of spacer-ssDNA-bearing single polymersomes and DNA-linked polymersome clusters was investigated using confocal laser scanning microscopy (CLSM), at the same concentrations as used for the cellular assay. As expected, the single imaging compartments functionalized with spacer-ssDNA bound to the cell surface of HEK$_{REWARD}$, whereas non-functionalized polymersomes showed lower attachment (**Figure 10.10**).

To investigate whether the clusters also bind to the cell surface, as it was the case for the functionalized polymersomes, we loaded the therapeutic compartment with Atto-488 for visualization purposes and kept the imaging compartment loaded with DY-633 as described above (**Figure 3.12, Figure 10.11**). We incubated these dye-loaded clusters in the presence of the cells for 24 hours, then washed and imaged the cells to assess not only binding to the cell surface, but also whether or not the clusters maintain their bound conformation. For the theranostic system to function, it is imperative that the clustered architecture is maintained and that the two compartments coexist, functioning in unison. After incubation with the cells and

rigorous washing, we could indeed observe the colocalization of the Atto-488 and DY-633 compartments, with a Pearson's colocalization coefficient of 0.77 ± 0.09 (**Figure 3.12**). The co-localisation observed for the two different compartments of the clusters demonstrates clustering of the nanocompartments and the stability of the DNA linkers *in vitro* (**Figure 10.12***)*. Considering the sensitivity and low lifetime of DDC, we wanted to determine how fast cell binding of the clusters occurs, as this would determine the overall efficacy of our system. For this experiment, we incubated the cells in the presence of the dye-loaded clusters and observed their attachment via CLSM live imaging. The results indicate that the cell binding process is fast, as fluorescence was apparent at the cell membrane within 10 min, and continued to increase thereafter (**Figure 10.13**). The fast binding of the DNA-linked polymersome clusters to the cell surface, before thermal deactivation of DDC can occur, is what leads to the locally enhanced production of dopamine, thus resulting in higher SEAP production as compared to that of the free enzyme observed in the cellular assay. This observation also confirms the ability of the dye-Ncomp to track itself and polymersome clusters over time in a biologically relevant milieu, supporting its robustness and potency as an imaging compartment.

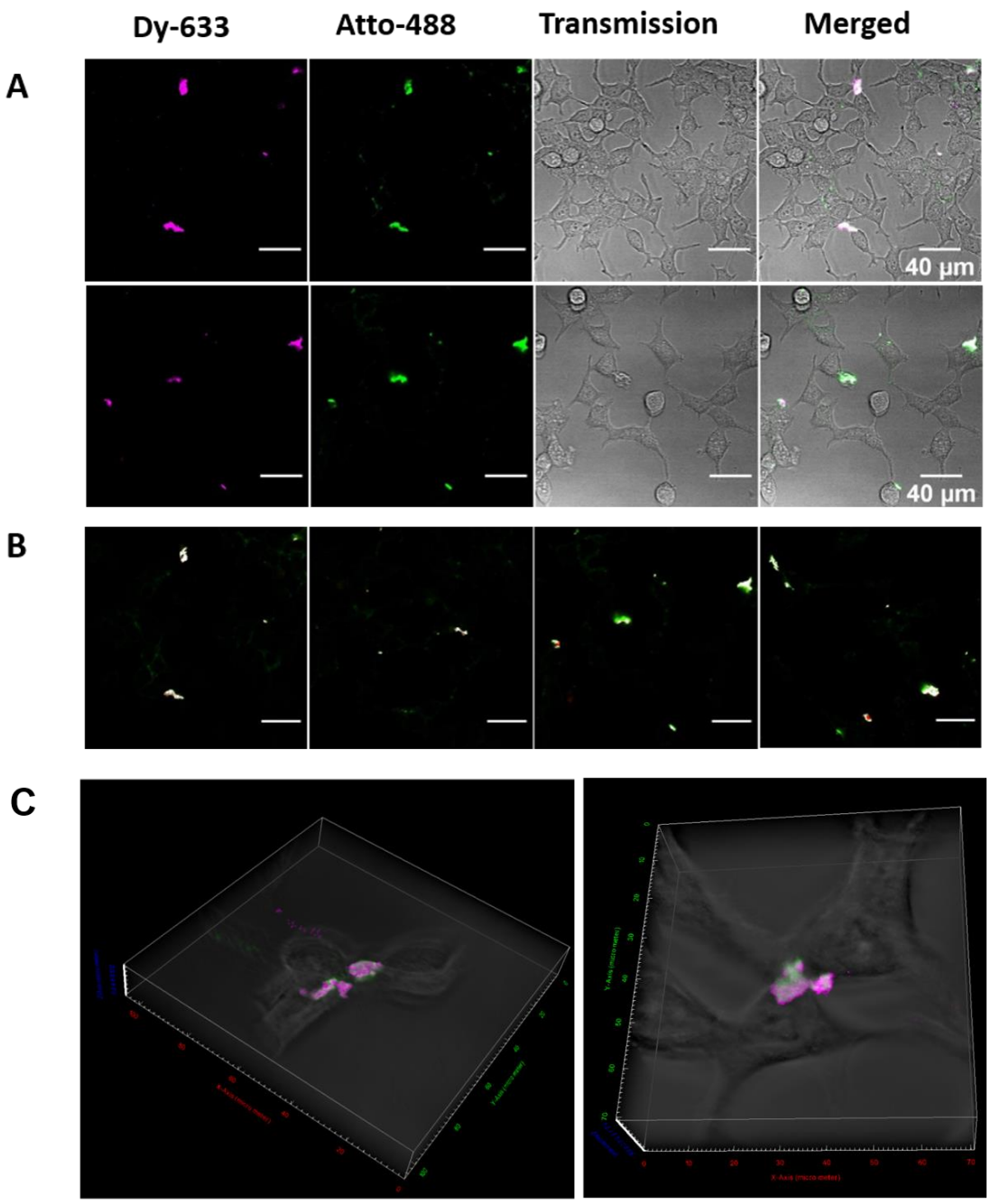

Figure 3.12. *Cell attachment of theranostic clusters.* ***(A)*** *CLSM microscopic images from four different locations of 488-633-Ncomp clusters attached to the surface of HEK*$_{REWARD}$ *cells after incubation for 24 h, showing separate DY-633 and Atto-488 channels, transmission channel and merged images (scale bar = 40 µm).* ***(B)*** *Merged DY-633 and Atto-488 channels of the two locations with colocalized regions appearing in white. Colocalization analysis of the two locations resulted in a Pearson's coefficient of 0.77 ± 0.09. Scale bar = 90 pixels or 37.8 µm.* ***(C)*** *3D rendering of recorded z-stack (left picture: y-axis and x-axis = 100 µm, z axis= 12 µm; right picture: y-axis and x-axis = 70 µm, z-axis= 18 µm).*

3.5 Modularity of polymersome clusters: a novel dual-functional platform

Our strategy to obtain DNA-linked polymersome clusters for theranostics is modular, being based on four steps: 1- thin polymer film formation, 2- polymersome formation by self-assembly, 3- ssDNA coupling to the external surface of polymersomes and 4- clustering of loaded polymersomes into super-assemblies (**Figure 3.13**). Each of these steps had to be optimized in different ways to accommodate a biomolecule of choice (DDC), in a view of a targeted application for atherosclerosis treatment. However, our system is highly modulable as PDMS-PMOXA polymer of different molecular weights and varied types of biomolecules can be selected to match together (**Figure 3.13A**), and the conditions (temperature, time of reaction, concentrations) of each step can be optimized to allow the polymer/biomolecules combination (**Figure 3.13B**).[109] Based on the many possibilities of adaptation, the super-assembly of DNA-linked polymersomes loaded with different active compounds represents a dual-functional platform that can be tailored to specific applications.

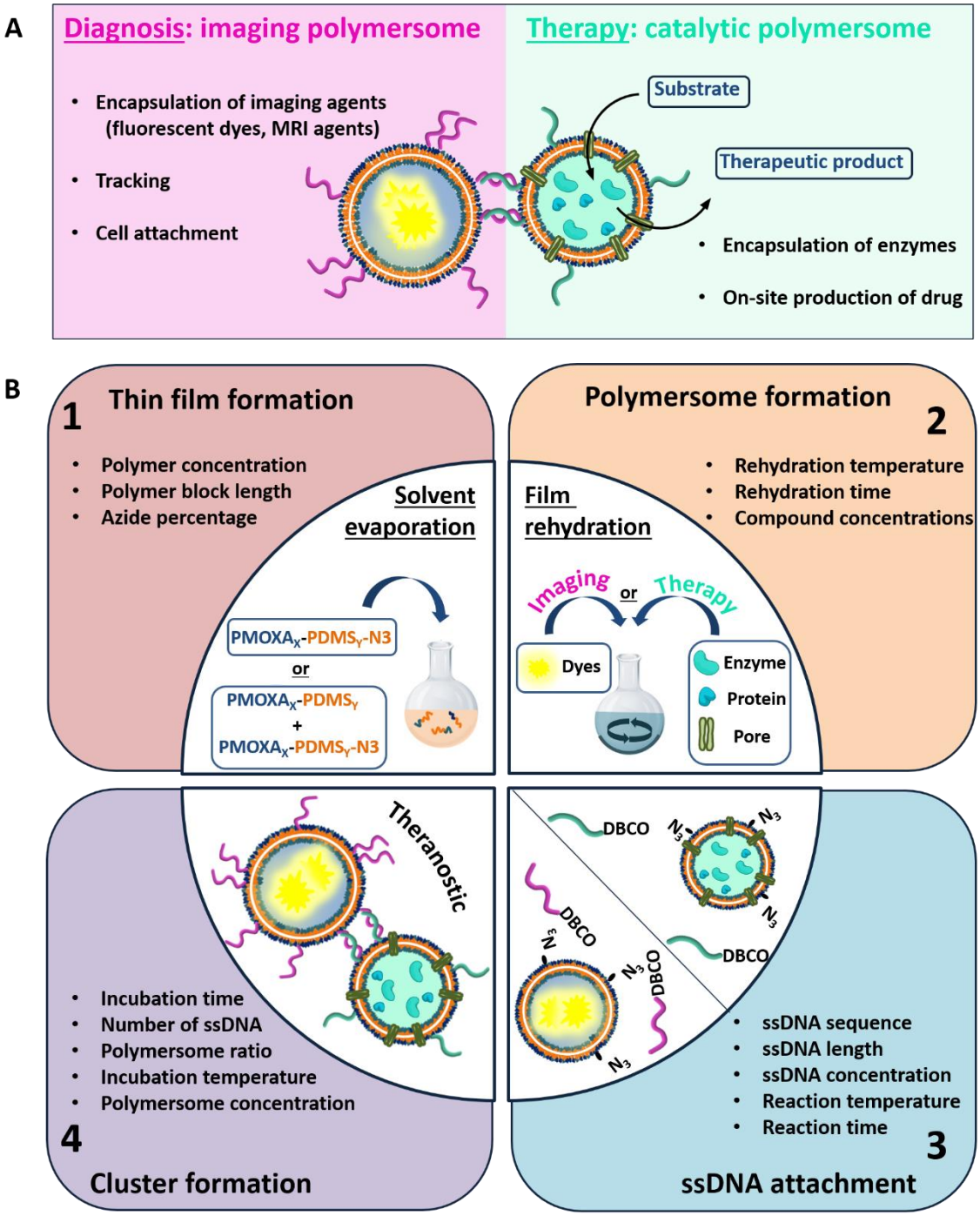

Figure 3.13. *Polymersome clusters as nanotheranostic platform.* ***(A)*** *Architecture providing therapeutic and diagnostic features.* ***(B)*** *The four steps involved in nano-sized clusters formation with corresponding optimization possibilities.*

3.6 Conclusions

We engineered a novel platform composed of segregated catalytic and imaging polymeric compartments linked together via DNA hybridization to form a modular nanotheranostic system. A combination of optimized construction approaches, i.e., high polymer concentration, short block-copolymers, short rehydration time, and low temperature, coupled with mild encapsulation conditions, permits the effective loading of DDC in the cavity of polymersomes, affording an active therapeutic compartment able to produce dopamine. The polymersomes protect DDC activity sufficiently during storage at 4 °C and also in cell media. As a result, active polymersomes encapsulating DCC and corresponding clusters trigger a cellular response via dopamine production and activation of dopamine receptors, with a response that is considerably enhanced compared to the case of free DDC.

By employing a modular system, we were able to assemble the imaging compartment under harsher conditions that permitted a high encapsulation efficiency of the stable DY-633 dye and an increase in amount of attached DNA on the polymersome surface, compared to the therapeutic compartment. This enabled the successful formation of theranostic clusters via DNA-zipping. The presence of DNA on the surface of the therapeutic compartment affects the dopamine production rate by hindering the passage of substrate through the OmpF pore, but interestingly, in cell experiments, this DNA-associated loss of activity is compensated in the case of the theranostic clusters by the focused production of dopamine in close proximity to the dopamine D1 receptor. DNA promotes the attachment of polymersomes and clusters at the surface of epithelial cells, leading to an increased local concentration of dopamine at the cell surface, followed by efficient receptor activation.

From a therapeutic point of view, dopamine activation of cell-surface dopamine D1 receptor molecules present on peripheral arteries has been shown to prevent atherosclerosis.[140–142] Secondly, atherosclerosis can be regarded as a chronic inflammatory state that involves the presence of scavenger receptor-expressing macrophages in locations where atherosclerotic lesions are formed.[143,144] By attaching the nanotheranostic clusters to these macrophages, we may be able to detect the early stages of artherosclerotic plaque formation as well as generate dopamine, preventing progression of the disease. Most current treatments and detection methods for

atherosclerosis are invasive and inadequate[145] and therefore an early detection and prevention system such as our nanotheranostic platform could provide a much-needed alternative.

Being constructed in a modular manner, these clusters offer extensive flexibility by an association of different polymersomes that can be tuned by a straightforward change of the enzymes or active compounds to provide a dual-functional solution for a large variety of pathological conditions. The stable architecture and tunability make these nanosystems a platform particularly suited for implementing this technology with possible additional modalities including targeting, responsiveness to pathological stimuli and synergistic therapies.

4. Polymersomes as bioluminescent system for imaging applications

This chapter introduces an artificial bioluminescent nanocompartment based on the encapsulation of light-producing enzymes, luciferases, inside polymersomes. We exploit nanocompartmentalization to enhance luciferase stability in a cellular environment but also to positively modulate enzyme kinetics to achieve a long-lasting glow-type signal. These features pave the way for expanding bioluminescence to nanotechnology-based applications, for example as tools for pre-clinical imaging.

Parts of this chapter have been published and reprinted with permission from[146]

***C. E. Meyer**, I. Craciun, C-A Schoenenberger, R. Wehr, C. G. Palivan, Catalytic polymersomes to produce strong and long-lasting bioluminescence, Nanoscale, **2021,** 13, 66*

4.1 Introduction

Bioluminescence, described as the production of light resulting from enzyme-catalyzed reactions,[147] is distinguished from other spectroscopy methods that rely on fluorescence or absorbance by superior sensitivity and a lower background. Bioluminescent systems possess unique advantages such as no light excitation requirement (as opposed to fluorophores), particularly strong signal output, and low background due to the lack of endogenous bioluminescent reactions in mammalian cells. Bioluminescence has been extensively exploited to develop *in vitro* and *in vivo* assays based on the real-time detection of light emitting enzymes (luciferases).[148,149] However, because the majority of luciferases have a short half-life or do not produce long-lived light signals, bioluminescence applications are largely restricted to genetically engineered cells with a constant expression of luciferase.[150,151] Although high, but short-lived burst signals, i.e. flash-type kinetics afford high sensitivity, they are extremely complex to implement in an assay format, as special logistics and equipment (e.g. injectors) are required to not miss the signal.[152] Current bioluminescent nanosystems are mainly based on nanoparticles (PLGA, gold, quantum dots) conjugated with luciferases for therapeutic, imaging or sensing applications, where the enzymes are exposed to the surface and subject to proteolytic degradation.[150,151]

Here, we aim to build a cell-free bioluminescent system with a sustained high luminescence output based on functional catalytic nanocompartments. We encapsulated a specific light-producing enzyme (*Gaussia* Luciferase, GLuc) inside the aqueous cavity of nano-sized polymeric vesicles (polymersomes), where the enzyme is protected and preserves its activity (**Figure 4.1**). When an appropriate substrate from the environment penetrates the polymersome, GLuc catalyzes the in situ production of bioluminescence, which represents the core functionality of the catalytic nanocompartments (GLuc Ncomp). Polymersomes have been reported to prolong the stability of encapsulated enzymes and increase the probability of enzyme-substrate interactions within the confined space.[71] The polymeric membrane is equipped with channel proteins (Outer membrane protein F, OmpF) to render the membrane permeable for the passage of substrates and products. However, for channel proteins with low molecular weight cutoffs like OmpF, the diffusion of the substrate towards

the polymersome cavity can decrease the in situ activity of the encapsulated enzymes.[63,153] In our case, exploiting this diffusion process could allow a modulation of the enzyme kinetics to provide a stable bioluminescent system producing a long-lasting, more convenient to work with light signal, aimed to expand the use of bioluminescence.

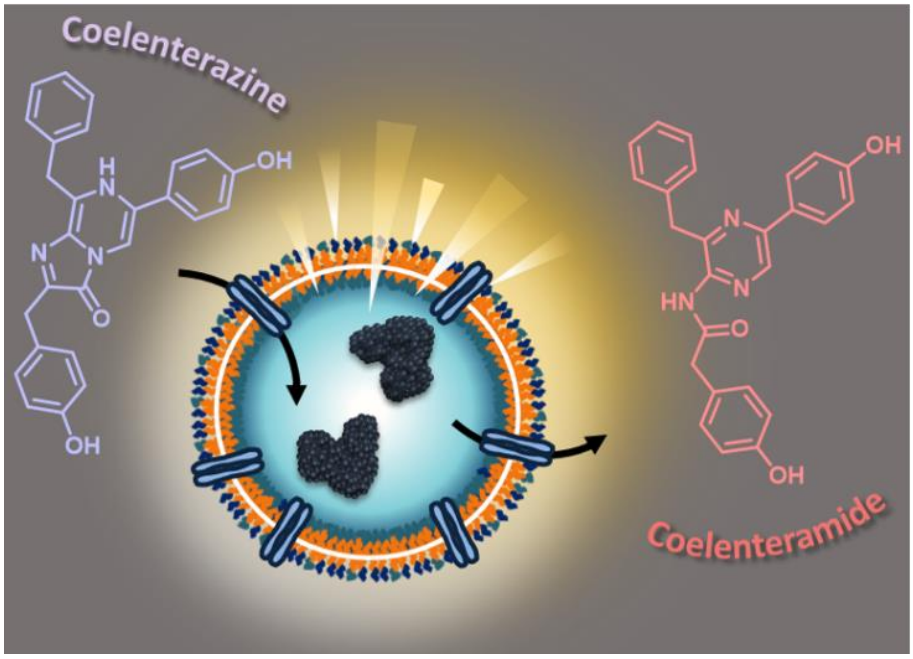

Figure 4.1. *Scheme highlighting the concept of luminescence-producing Gaussia Luciferase nanocompartments (GLuc Ncomp). Light is produced upon addition of coelenterazine (substrate) that reaches the encapsulated enzymes via diffusion through the OmpF channel.*

4.2 Physical characterization of bioluminescent polymersomes

Polymersomes, depending on the properties of the copolymers forming the nanocompartment, offer advantages such as biocompatibility,[67] low protein binding,[154] high blood circulation times[155], and escape from the immune system,[154,156], and have thus proven their suitability for numerous applications (imaging, therapeutic, sensing).[1] Compared to their lipid counterparts (liposomes), polymersomes not only possess greater mechanical stability while maintaining a soft

architecture, but especially benefit from countless tunability possibilities based on associated chemistry.[8,67,118,153,157] Thus, polymersomes are particularly suitable for the development of cell-free bioluminescent systems aiming at expanding the breadth of bioluminescence applications. We selected a poly(dimethyl siloxane)-*block*-poly(2-methyl-2-oxazoline) (PDMS-PMOXA) polymer for its non-toxicity,[67] stealth properties,[154,156] short block length permitting membrane protein reconstitution,[8,153] self-assembly into polymersomes at high polymer concentration (10 mg/mL) and protective effect on enzymes from proteolytic degradation to enhance their half-life.[158]

We synthesized the short-chained $PDMS_{25}$-$PMOXA_{10}$ diblock copolymer via sequential ionic polymerization[34] (**Figure 10.14-15**) and built our functional catalytic compartment via film rehydration. The morphology of the resulting GLuc encapsulating polymersomes (GLuc Ncomp) was first characterized by Dynamic Light Scattering (DLS) (**Figure 4.2A**), from which we obtained an average apparent diameter (D_H) of 189 ± 57 nm, with a polydispersity index (PDI) of 0.167. Their colloidal stability was also demonstrated as no aggregation was observed. Additional characterization was carried out by Static Light Scattering (SLS) to determine the radius of gyration (Rg = 105 nm). The hydrodynamic radius (Rh = 114 ± 17 nm) was obtained from the DLS profile (**Figure 4.2B**), leading to Rg/Rh = 0.92, consistent with a hollow spherical morphology of Gluc Ncomp.[159] Finally, the variation in size of polymersomes as well as their morphology was visualized via Transmission Electron Microscopy (TEM), where we observed the typical collapsed architecture corresponding to soft polymersomes (**Figure 4.2C**). Neither the insertion of OmpF, nor the presence of enzymes inside the cavity of polymersomes affected the morphology or the dispersity of polymersomes, as shown by TEM and light scattering methods (**Figure 10.16-17**). The nanometer size range, high robustness, flexibility and strong colloidal stability of the PDMS-PMOXA polymersomes constitute desirable physico-chemical properties for building a versatile nanotechnology-based bioluminescent system.[67,118,157]

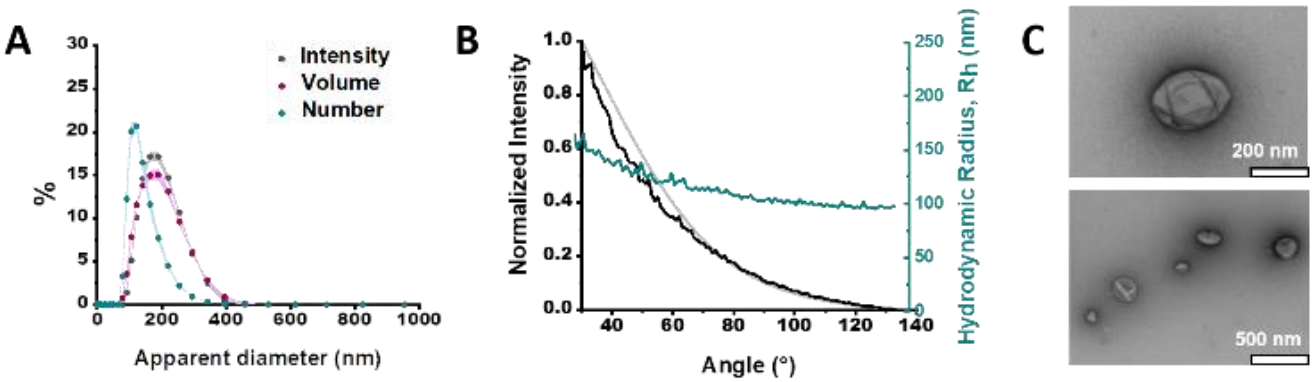

Figure 4.2. *Characterization of GLuc Ncomp.* ***(A)*** *Size determination of GLuc Ncomp measured by DLS.* ***(B)*** *Size determination of GLuc Ncomp measured by SLS: DLS profile showing the hydrodynamic radius (Rh) of GLuc polymersomes at different angles (cyan), the intensity at different angles (black) and the suitable MIE fit (grey) used to determine the radius of gyration (Rg).* ***(C)*** *TEM micrographs of GLuc Ncomp showing the deflated, balloon-like, structure of polymersomes and their variation in size.*

4.3 Catalytic activity of bioluminescent polymersomes

Gluc, the encapsulated enzyme, is a widely used reporter enzyme that we selected for its small size (19.9 kDa), great thermostability, high intensity luminescence output, commercial availability and because it does not require a cofactor.[152,160,161] GLuc produces a recordable light via enzymatic oxidation of its coelenterazine substrate, in the form of a flash-type kinetics that implies a strong albeit very prompt and transitory light signal making the detection difficult.[152] By encapsulating GLuc within polymersomes (12 ± 5 % encapsulation efficiency), we aimed at modulating the flash-kinetics to extend the luminescent signal over long periods of time (1 h) and also increase its stability in a cell environment. To investigate the effects of encapsulation on the enzymatic production of light, we compared the bioluminescence emitted by non-encapsulated (free) enzyme to the one produced by encapsulated enzyme (GLuc Ncomp), at equal final concentration (0.2 μg/mL).[63,153,162] The typical flash-type kinetics of free GLuc was confirmed as after a fast transient burst, the signal quickly faded and was no more detectable after 5 min (**Figure 4.3A**). The advantage of encapsulating GLuc inside polymersomes is immediately observable as the enzyme's kinetics is shifted towards a long-lasting light signal: after 1 min the luminescence signal of GLuc Ncomp overtakes that produced by free enzyme (**Figure 4.3A**). The encapsulation of GLuc enables the production of a signal that slowly increases to plateau at maximum intensity reached after 10 min and that is still readily detectable

even after 1 hour. The permeability of polymersomes exclusively relies on incorporated transmembrane pores (OmpF), as the compactness of the polymeric membrane is not affected by the insertion of such pore-forming proteins. This long-lasting signal arises from the slow diffusion of the substrate coelenterazine through the OmpF pore to reach the encapsulated GLuc. In fact, OmpF has a molecular cutoff of 600 Da allowing smaller molecules such as coelenterazine (423.46 Da) to enter in the cavity of impermeable PDMS-PMOXA polymersomes.[78,163] The resulting diffusion effect is the limiting factor for encapsulated enzyme efficiency, especially in our case as coelenterazine is uncharged and thus, its diffusion does not benefit from the attractive interactions that arise between zwitterionic molecules and charged residues of OmpF.[164] The diffusion of bulky substrates through OmpF pores decreases the activity of encapsulated enzymes, so it is often perceived as a drawback for catalytic compartments, e.g. in applications like the *in situ* production of drugs.[153] Here, this drawback is turned into an advantage as the slow diffusion of coelenterazine though OmpF enables a slow yet steady supply of substrate for the encapsulated enzyme as compared to free enzyme, resulting in the production of a persisting detectable signal (for at least one hour). This can be of particular advantage in applications like bioluminescence imaging as optical imagers equipped with charge-coupled device (CCD) cameras sum the photons detected during the measurement which results in the amplification of signal over the duration of recording.[149] Moreover, in contrast to flash-type signals, such long-lasting luminescence offers greater accuracy as the maximum intensity signal occurs within a plateau. Long-lasting luminescence has already proven its attractiveness as it is akin to the glow-type luminescence of other kinds of luciferases (NanoLuc, Firefly Luciferase), which are particularly sought out for long-term recording in luminescence-based assays.[148,160] While these enzymes have the appropriate glow-type luminescence, they often show poor stability and their expression depends on transfected cells, which again limits potential applications.[148,160]

The same flash-to-glow switch of kinetics of GLuc Ncomp is maintained in cell medium even if the signal intensity is reduced compared to PBS for both free and encapsulated medium that slows down the diffusion of the substate but also from the slightly higher background luminescence obtained due to greater auto-oxidation of coelenterazine in cell medium (**Figure 4.3B-E, Figure 10.18-19**).[165] A similar

background is obtained for GLuc Ncomp without OmpF in the presence of coelenterazine, corroborating the absence of free or exposed enzymes (**Figure 4.3B-E**). However, such backgrounds are negligible compared to the high luminescence signal obtained for free and encapsulated GLuc.

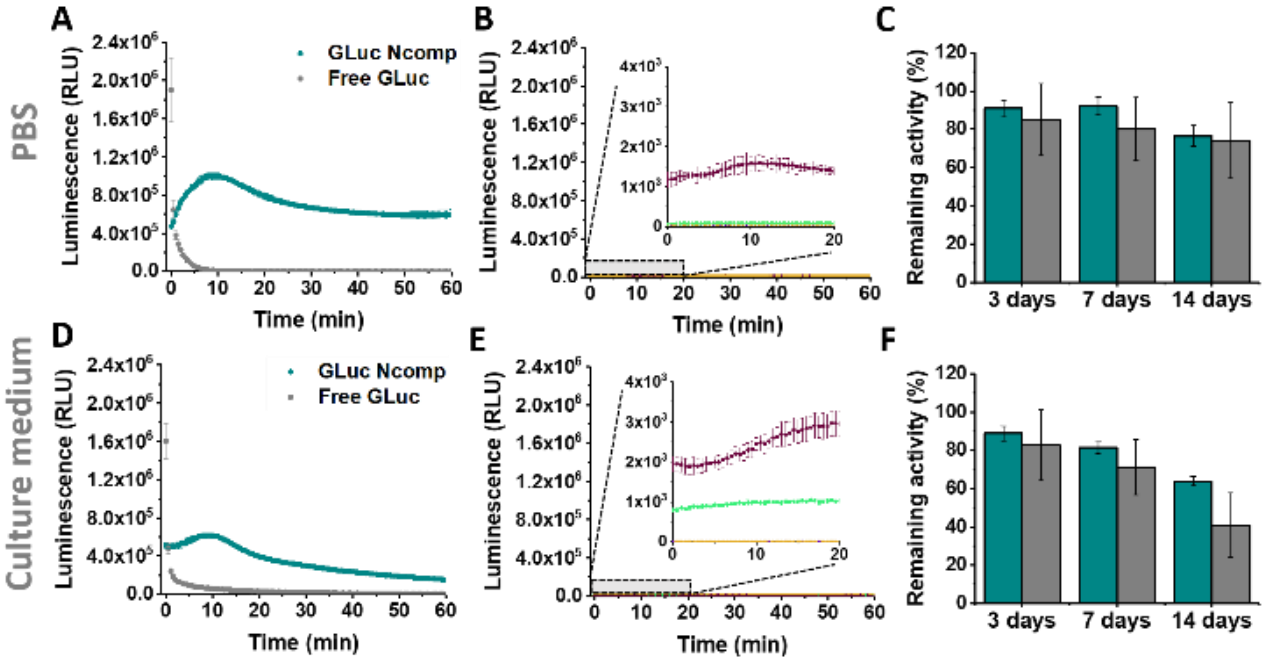

Figure 4.3. *Activity of free and encapsulated Gaussia Luciferase (GLuc Ncomp).* ***(A)*** *Activity of GLuc Ncomp (cyan) and non-encapsulated GLuc enzymes (grey) in PBS and* ***(B)*** *corresponding controls: GLuc Ncomp without OmpF with substrate coelenterazine (purple), PBS alone with coelenterazine (green), GLuc Ncomp with OmpF without coelenterazine (dark blue, hidden by yellow), PBS alone without coelenterazine (yellow).* ***(C)*** *Remaining percentages of activity of free (grey) and encapsulated GLuc (cyan) in PBS, upon storage at 37 °C.* ***(D)*** *Activity of GLuc Ncomp and non-encapsulated GLuc enzymes in culture medium and* ***(E)*** *corresponding controls in culture medium.* ***(F)*** *Remaining percentages of activity of free (grey) and encapsulated GLuc (cyan) in culture medium, upon storage at 37 °C. The remaining percentage of activity were determined using the activity at t= 0 in PBS or culture medium that has been set as 100 % activity.*

4.4 Applicability of bioluminescent polymersomes

Considering the importance of system stability for storage and applicability reasons, we showed activity retention of free and encapsulated GLuc up to 2 weeks of incubation in PBS and cell medium, at 4 °C and 37 °C (**Figure 4.3C-F, Figure 10.20-22**). Furthermore, we demonstrated the protein repellence of our system as GLuc Ncomp did not substantially lose activity after 2 weeks of incubation in culture medium. This indicates that encapsulated enzymes are protected but also well

supplied with substrate, which implies that OmpF is not obstructed as the passage of substrate is maintained. This preservation of activity of GLuc Ncomp reflects that protein adsorption (from the cell medium containing 10% fetal bovine serum) on the surface of polymersomes is predominantly absent and thus confirms the protein repellence of PMOXA based on its non-ionic nature. [154,156] Our system, by means of its stability and protein repellence possesses a certain potency that is essential for developing translational applications.

Enzymatically-triggered coelenterazine oxidation can be exploited to develop redox sensors, as shown for our GLuc Ncomp in presence of ascorbic acid where the light signal is reduced in presence of this antioxidant (**Figure 4.4A**). It should be noticed that our system is scalable as this strong light signal results from a diluted sample of only 50 µL (0.5 mg/mL of GLuc Ncomp resulting in 0.2 µg/mL of GLuc). Therefore, both concentrations and volumes can be easily increased especially using our polymer that self-assembles at high concentrations, to reach even higher signals (2 times higher for twice more concentrated Gluc Ncomp) (**Figure 4.4B, Figure 10.23**).

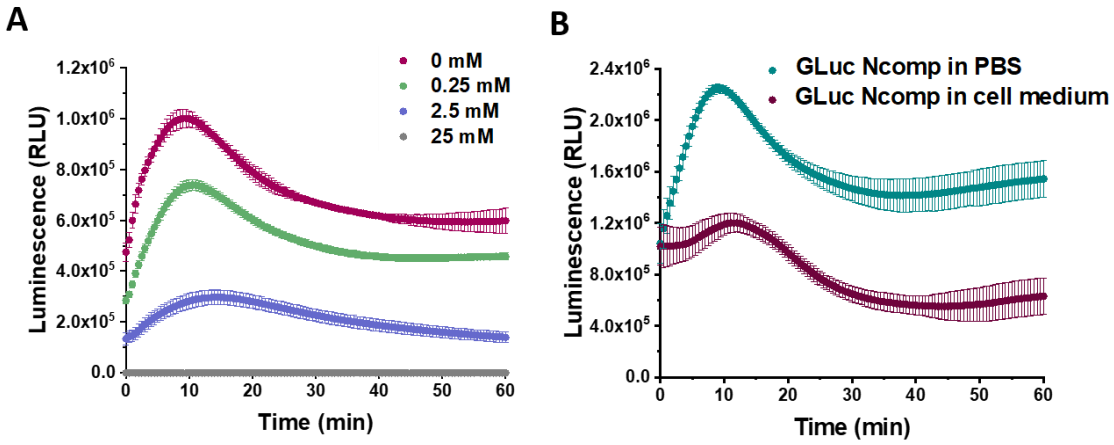

Figure 4.4. *Activity of GLuc Ncomp in different conditions.* ***(A)*** *Activity of GLuc Ncomp in PBS in presence of (0, 0.25, 2.5, 25 mM) ascorbic acid. Ascorbic acid reduce the production of light via prevention of the coelenterazine oxidation in a dose dependent manner.* ***(B)*** *Luminescence production at higher concentration of GLuc Ncomp (50 µL of 2 mg/mL, final concentration = 1 mg/mL), in PBS and cell medium.*

To further probe the applicability of our system in a biological environment, we incubated GLuc Ncomp in the presence of cells (MCF-7) for 3 days and subsequently recorded their activity in the cell supernatant. GLuc Ncomp showed a signal similar to the one obtained in culture medium alone (**Figure 4.5A, Figure 10.24**), indicating that the activity is not affected by the presence of cells. In contrast, free GLuc showed decreased signal intensity in presence of cells compared to culture medium alone **(Figure 4.5A**), corroborating its premature degradation under biological conditions. The encapsulation within polymersomes improves the stability of GLuc by protection from harmful external milieu, e.g. proteolytic degradation (**Figure 10.25**).[63] Such results highlight the advantage of GLuc Ncomp compared to free enzymes that are more likely to be degraded under biological conditions. Thus, by encapsulating the enzyme our polymersome-based system makes do without the cell's continuous supply of luciferase and thereby warrants exploiting bioluminescence entirely cell-free. In addition, inside polymersomes, the shift to an extended, glow-type kinetics of GLuc is maintained under different conditions (with and without cells) which corroborates the integrity of the polymeric membrane, so the robustness of polymersomes even in the environment of cells.[8,63,67,118,153,157] Additionally, GLuc Ncomps are not cytotoxic as the same cell viability is obtained in presence of GLuc Ncomps, free GLuc or PBS (**Figure 4.5B**). Thus, our GLuc Ncomp system is of particular interest for biological applications as it is compatible with cells under physiological conditions and provides enhanced enzyme stability compared to free enzymes.

To provide further indications about the potency of GLuc Ncomps for bioluminescence imaging applications, we carried out a preliminary *in vivo* study using mouse model. GLuc Ncomps (with or without OmpF for the control) were injected in the tail vein of mice, followed by the injection of coelenterazine 30 min later. After anaesthesia, the mice were imaged during 20 min when the photons were summed up to allow for quantification and provide an image indicating the location of the GLuc Ncomps (**Figure 4.5C**). We observed a strong bioluminescent signal in presence of GLuc Ncomps, while for the control, only a small signal was recorded, which probably arise from the background produced by coelenterazine auto-oxidation (**Figure 4.5C**). As we did not functionalized our polymersomes with targeting agents, GLuc Ncomps seemed to be spread in the mouse body, probably circulating in the blood stream. However, the primary goal of this experiment was to demonstrate that the light signal produced by our GLuc Ncomps was strong enough to cross biological

tissue, so had a real potential for being applied in pre-clinical research. In-depth study is still required to optimize the conditions of imaging and investigate the clearance of GLuc Ncomps.

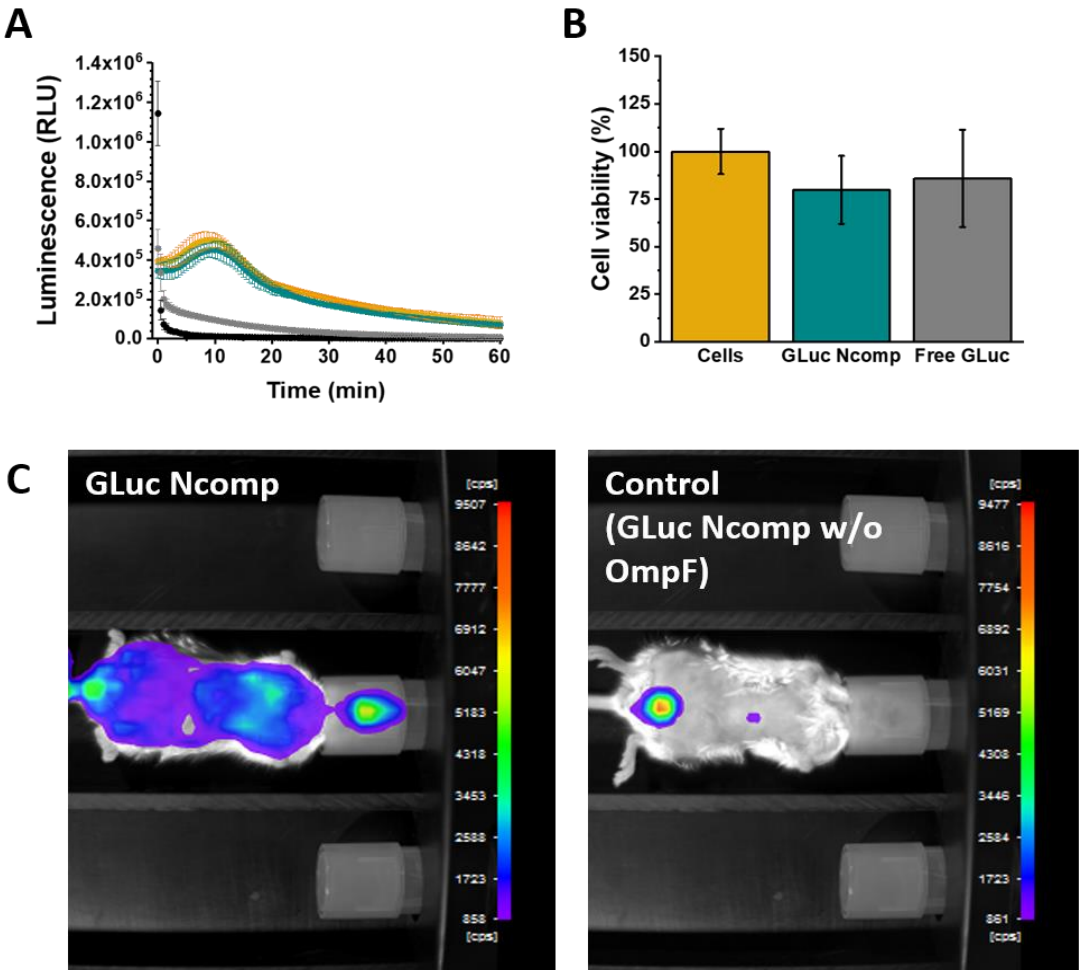

Figure 4.5. *Behavior of GLuc Ncomp in biologically relevant conditions.* ***(A)*** *Activity of GLuc Ncomp in culture medium (orange) or cell supernatant (cyan) compared to kinetics of free GLuc in culture medium (black) and cell supernatant (grey), after 3 days of incubation with cells. (B) Cell viability as percentage of control MCF-7 cells incubated with PBS (yellow), GLuc Ncomp (cyan) and free GLuc (grey). No significant decrease in viability is observed as compared to control cells, indicating the GLuc Ncomp and free GLuc are nontoxic.* ***(C)*** *Preliminary results of Bioluminescence Imaging (BLI). Pictures of BALB/c mice that have been injected with GLuc Ncomp (left) and GLuc Ncomp without OmpF (right). Two intravenous injection (IV) in the tail vein have been performed: 100 µL of nanocompartment solution (2 mg/mL) followed by the injection of 100 µl coelenterazine after 30 min. The luminescence intensity has been recorded for 20 min and summed up.*

4.5 Conclusions

We developed the first artificial bioluminescent nanocompartment with high potential as cell-compatible yet cell-independent bioluminescent system that overcomes the need for using cells transfected with luciferase gene constructs. We also pinpoint that the diffusion of coelenterazine into the nanocompartment, afforded by the membrane insertion of porins, can be exploited to achieve more suitable kinetics. By means of polymersomes confining *Gaussia* Luciferase, our system enables a favorable switch in kinetics towards a glow-type luminescence to reach long-lasting but still powerful light signal. Compartmentalization not only allows for tuning signal output but also stabilizes the encapsulated enzyme in a cell environment. Thus, our system overcomes the restrictions arising from enzyme degradation and those related to quick fading of the signal, which positions these bio-hybrid catalytic nanocompartments as potent, cell-free alternative. In addition, the long-lasting and powerful light signal produced by our system was able to be detected *in vivo* through biological tissues, thus showing its potential for *in vivo* bioluminescence imaging. The intrinsic properties (e.g. robustness, non-toxicity) and tunability of polymersomes could be an attractive extension that could be exploited for developing *in vitro* assays (redox sensing applications)[166] or specific preclinical imaging methods (e.g. detection and targeting of tumours). This new bioluminescent nanosystem, based on an artificial bio-hybrid nanocompartment, is expected to overcome cell-related restrictions and thereby greatly expand the usage of both nanotechnology and bioluminescence in biomedical domains. Further studies are required to assess the biodistribution and clearance of these polymersomes as their application for *in vivo* imaging will greatly depend on these factors.

5. Polymersome-based artificial melanosomes

This chapter describes the development of bio-hybrid polymersomes as melanosome mimics for cell photoprotection applications like in the prevention of skin cancers. Inspired by nature, we built nanocompartments encapsulating melanin or polydopamine to recreate the native architecture of melanosomes. This way, we aimed at exploiting the polymeric membrane to shield the main drawbacks of melanin/polydopamine, i.e., cytotoxicity and compromised colloidal stability, while maintaining the UV-absorption properties. The achievement of such system was possible using a short-chained polymer that self-assembles into polymersomes, encapsulating L-DOPA or dopamine precursors together with melanogenic enzyme Tyrosinase, prior to melanin/polydopamine polymerization. Our system highlights a new strategy to contain melanin/polydopamine drawbacks, thus expanding the possible applications of these macromolecules, and provide a novel system with potential for cell photoprotection.

Manuscript in preparation

5.1 Introduction

Melanin is a natural biopolymer that is spread throughout the body and responsible for hair, eye and skin pigmentation, where its dark color effectively absorbs light. Melanin pigment is synthesized and deposited in specific organelles, termed melanosomes, that protect the outer-most layer of the skin, the epidermis, from UV-related damages.[167] Initially produced in melanocytes residing in the basal layer of the epidermis, mature melanosomes are transported to neighboring keratinocytes where their arrangement into a supranuclear cap around the nucleus protects DNA from UV radiation.[167] Thus, intact melanosomes are essential actors in the prevention of skin cancer. Several diseases are associated with defective melanosomes. In Vitiligo, melanocytes and thus melanosome biogenesis are lost whereas Albinism causes a shortage of tyrosinase, the key enzyme involved in eumelanin synthesis in melanosomes.[168,169] To date, no efficient treatment exists for such diseases. This calls for the development of alternatives such as synthetic melanosomes, in particular as the risk of contracting skin cancer is on the rise.[168,169]

Due to size similarity, melanosomes can be mimicked using various colloidal nanomaterials such as natural melanin, in order to remain close to biological systems. As the extraction of melanin from its natural source remains complex and hardly reproducible, *in vitro* synthesis is usually indicated. For example, the oxidation of substrate L-DOPA is enzymatically-triggered by Tyrosinase to form a heterogenous melanin biopolymer. Synthetic melanin has also been used to coat silica nanoparticles for applications like bone marrow protection upon radiation therapy or as antioxidant.[170,171] Despite considerable efforts, the macromolecular structure of native melanin is poorly understood and its application has been neglected due to the rising popularity of its synthetic counterpart polydopamine (PDA).[172] Despite molecular differences, PDA shares some properties with melanin, e.g., UV-absorption, but has been widely preferred due to easier synthesis.[173] PDA nanoparticles form upon spontaneous oxidation of dopamine under alkaline conditions. Extensive studies have shown the potential of PDA nanoparticles as imaging agents, drug carriers, antioxidants or microparasols for UV-protection.[172,174] Various PDA-based nanoparticle architectures can be developed depending on its association with other nanomaterials. For example, stabilized emulsion droplets made of primary PDA

nanoparticles and polymeric surfactant have led to mesoporous PDA nanoparticles with intrinsic cavities.[175] Different nano objects, e.g., liposomes or polymeric nanospheres, have been used as PDA-coated templates to form shell-like or multicompartment structures.[98,176,177]

However, melanin- or PDA-based nanoparticles barely represent the vesicular architecture of native melanosomes where melanin is enclosed within a phospholipidic membrane rather than being exposed at the surface, as is the case for most melanin- and PDA-based nanoparticles.[167,172] The cytotoxicity of melanin and PDA (under certain conditions) and the often compromised colloidal stability of melanin- and PDA-based nanoparticles prompted us to investigate whether these drawbacks could be solved by biomimicking native-like architectures.[172,176,178–182] In this regard, soft-nanocompartments, i.e., liposomes and polymersomes that are composed of an amphiphilic membrane enclosing an aqueous cavity appear as potent nanomaterials to build melanosome mimics as their architecture resembles biological vesicles. Polymersomes possess the advantage of increased mechanical stability and broad chemical versatility over liposomes.[1] In addition, polymer-based vesicles are frequently non-toxic and enable the integration of a variety of hydrophilic and hydrophobic molecules, be it embedded in their membrane, covalently attached to their external surface or enclosed within their cavity.[1,67] Thus, polymersomes are well suited for many applications including sensing, drug production/delivery, imaging, theranostics and last but not least as artificial organelles.[1,113]

Here, we investigated the potential of biomimicking the vesicular structure of native melanosome for avoiding the main pitfalls of melanin/PDA-based nanoparticles that are cytotoxicity and reduced colloidal stability (**Figure 5.1**). We developed different melanosome mimics composed of polymersomes encapsulating melanin or PDA. L-DOPA or dopamine precursors together with Tyrosinase were encapsulated inside polymersomes and subsequently incubated to induce polymerization into melanin or PDA in the polymersome cavity. We synthesized a short-length diblock co-polymer of poly(dimethylsiloxane)-*block*-poly(2-methyloxazoline) ($PDMS_{24}$-$PMOXA_{12}$) that self-assembles into polymersomes in less than 30 min. This time frame is short enough to encapsulate L-DOPA and dopamine before they polymerize, resulting in intact polymersomes with no aggregation tendency. We investigated the differences between melanin-and PDA-polymersomes in terms of UV-absorption properties, cytotoxicity and colloidal stability. To our knowledge, our system is the first example of melanin

and PDA formation within polymersomes where the confining membrane provides a novel kind of shield against aggregation and cytotoxicity of melanin and PDA while UV-absorption properties are maintained. Our system breaks ground for a new biomimetic strategy based on the encapsulation of melanin/PDA. As proof of principle, we explored biological applications of such melanosome mimics and provide an indication of the potency of our system for cell-photoprotection. Future developments of our basic Melanin/PDA polymersomes should lead to new nanosystems with increased applications.

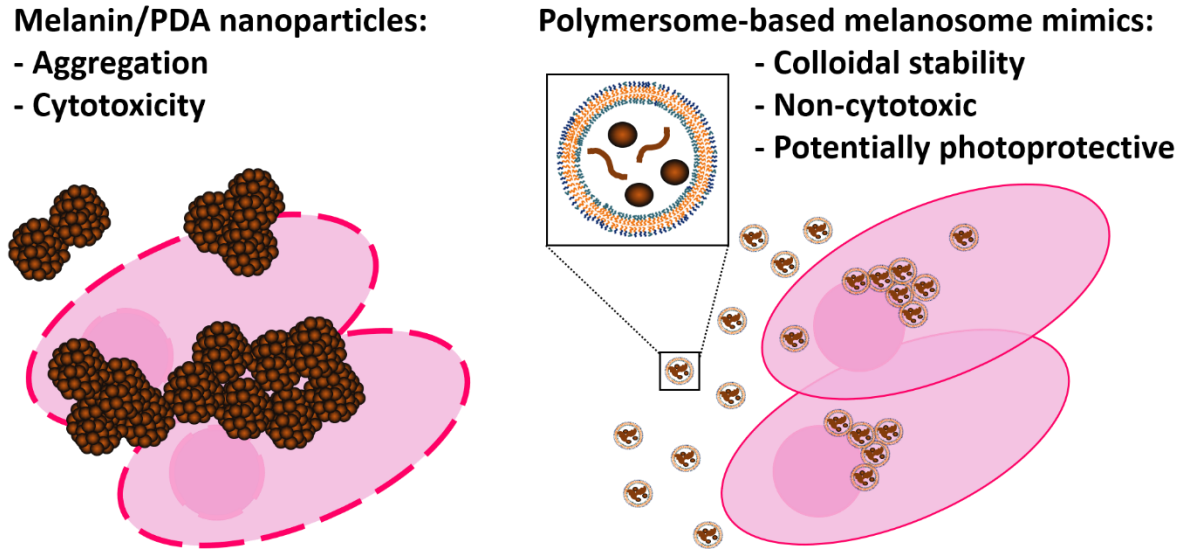

Figure 5.1. *Scheme representating the differences between melanin/PDA nanoparticles and polymersome-based melanosome mimics.*

5.2 Physical characterization of melanosome mimics

Melanin- and PDA-based particles results from a supramolecular buildup involving consecutive protoparticle (10^{-9} m) agglomeration to bigger architectures (10^{-8} - 10^{-7} m). The formation is enigmatic and hardly controllable despite being key to fully exploit the potential of these materials.[183] For these reasons, melanin and PDA have been predominantly used as coating for various materials rather than as nanoparticles. In coating procedures, the deposition on the substrate can be limited by immersion time of the substrate into melanin/PDA solutions.[172] Given the strong tendency of melanin and PDA to randomly accumulate on various materials, the formation of

polymersome-based melanosomes mimics required a strategy for containing aggregation such that the self-assembly of polymersomes is not impeded by aggregation of the polymers with melanin/PDA. For this reason, we investigated the possibility of encapsulating melanin/PDA precursors (L-DOPA/dopamine) together with Tyrosinase inside polymersomes before polymerization occurs.

As base element for our artificial melanosome, we chose a PDMS-PMOXA copolymer for its biological compatibility (stealth, non-toxicity), its mechanical stability and impermeability to small molecules.[67,106,153,154,156] More specifically, we synthesized via sequential ionic polymerization, the short-chained $PDMS_{24}$-$PMOXA_{12}$ to allow for fast self-assembly of polymersomes (**Figure 10.26-27**). To initiate self-assembly into melanin- or PDA-polymersomes, a solution of L-DOPA or dopamine was added to a $PDMS_{24}$-$PMOXA_{12}$ thin film together with Tyrosinase. However, under conditions conducive to polymersome formation (room temperature for 12 h),[58,153,159] no polymersomes were formed but instead, a brown-black sticky material was obtained which obstructed the stirring (data not shown). Thus, the conditions were adapted to achieve encapsulation of L-DOPA/dopamine and Tyrosinase into polymersomes prior to polymerization into melanin/PDA: Polymersome formation was carried out at 4 °C for a short time (30 min), the self-assembled structures were extruded and subsequently purified by size exclusion chromatography (SEC) to remove the unencapsulated L-DOPA/dopamine and Tyrosinase. We previously reported the ability of specific PDMS-PMOXA to rapidly self-assemble into polymersomes at 4 °C.[153] However, it is the first time that polymersome formation was achieved at 4°C in as little as 30 min which is afforded to the short block-length of our polymer and its polydispersity (*Đ = 1.16)* that promote self-assembly. The presence of L-DOPA/dopamine and Tyrosinase affected neither the self-assembly process, nor the architecture of the resulting polymersomes, as shown by transmission electron microscopy (TEM) and dynamic light scattering (DLS) (**Figure 5.2**). A size of 178 ± 70 nm was obtained by DLS for Melanin-polymersomes (**Figure 5.2A**) and 173 ± 68 nm for PDA-polymersomes prepared with Tyrosinase, which is consistent with the size of control polymersomes rehydrated under the same conditions with PBS (172 ± 63 nm) or Tyrosinase only (165 ± 49 nm). Melanin- and PDA-polymersomes prepared without Tyrosinase showed a similar size and morphology (**Figure 10.28**). Importantly, our polymerome-based artificial melanosomes fall within the size range

of the native organelle which greatly varies depending on the ethnicity and skin condition (100 - 800 nm).[167,184,185]

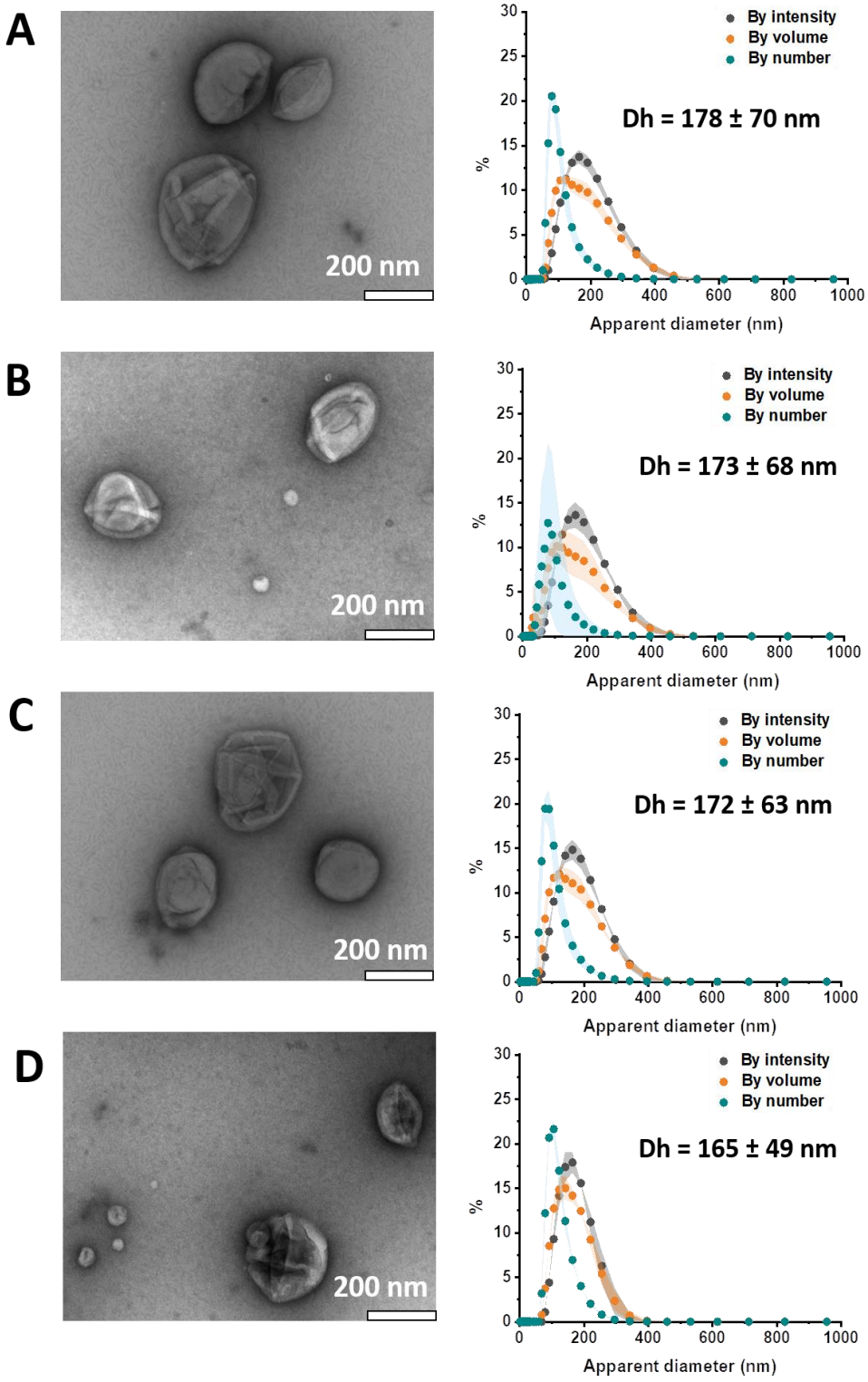

Figure 5.2. *TEM micrographs and corresponding DLS, showing the morphology and size of* ***(A)*** *Melanin-polymersomes (with Tyrosinase),* ***(B)*** *PDA-polymersomes (with Tyrosinase),* ***(C)*** *empty polymersomes rehydrated with PBS only and* ***(D)*** *Tyrosinase-polymersomes.*

Also, the number of Melanin-polymersomes ($2.21*10^{12}$ vesicles/mL), PDA-polymersomes ($2.15*10^{12}$ vesicles/mL) (prepared with Tyrosinase) and Tyrosinase-polymersomes ($2.14*10^{12}$ vesicles/mL) quantified by nanoparticle tracking analysis (NTA) was similar to that of control polymersomes containing only PBS ($2.06*10^{12}$ vesicles/mL), indicating that neither L-DOPA/dopamine, nor Tyrosinase interfered with the polymer self-assembly into polymersomes (**Table 2**). These results were expected as PDMS-PMOXA polymersomes are known for their robustness and ability to encapsulated various active compounds and biomolecules.[100,146,153]

Sample	Concentration (vesicles/mL)
Melanin-polymersomes (w/o Tyrosinase)	$1.94*10^{12} \pm 1.69*10^{11}$
PDA-polymersomes (w/o Tyrosinase)	$1.82*10^{12} \pm 1.97*10^{11}$
Melanin-polymersomes (w/ Tyrosinase)	$2.21*10^{12} \pm 0.79*10^{11}$
PDA-polymersomes (w/ Tyrosinase)	$2.15*10^{12} \pm 2.59*10^{11}$
Empty polymersomes	$2.06*10^{12} \pm 1.09*10^{11}$
Tyrosinase-polymersomes	$2.14*10^{12} \pm 1.24*10^{11}$

Table 2. *Nanoparticle Tracking Analysis (NTA) results showing the concentration of polymersomes (vesicles/mL) for a concentration of 1 mg/mL of polymersomes.*

5.3 Colloidal stability of melanosome mimics

While the supramolecular buildup of melanin from precursors remains unclear, its molecular structure has been identified as an heterogenous macromolecule composed of 5,6-dihydroxyindole (DHI) and 5,6-dihydroxyindole-2-carboxylique acid (DHICA) at variable ratios.[186] Tyrosinase is the key enzyme of melanogenesis, as it is involved in several oxidation steps: from the initial precursor L-Tyrosine to L-DOPA, from L-DOPA to DOPAquinone, and later from DHI to indole-5,6-quinone (**Figure 5.3**).[187] We chose to encapsulate L-DOPA or dopamine together with Tyrosinase inside polymersomes to from our Melanin-polymersomes and PDA-polymersomes,

respectively. We chose L-DOPA as the initial precursor as it is rather stable (compared to highly reactive quinone), has higher solubility than L-Tyrosine, and because the use of downstream precursors is known to decrease the chemical versatility of the melanin produced. For example, DHI and DHICA predispose the resulting melanin structure towards DHI- or DHICA-derived melanin that have distinct properties.[183] The structure of PDA differs from that of melanin as in PDA, monomers interact through π-π stacking and hydrogen bonds rather than covalent bonding.[183,188] Although PDA forms upon autoxidation of dopamine, we also studied the effect of Tyrosinase on PDA formation within polymersomes.[172,189]

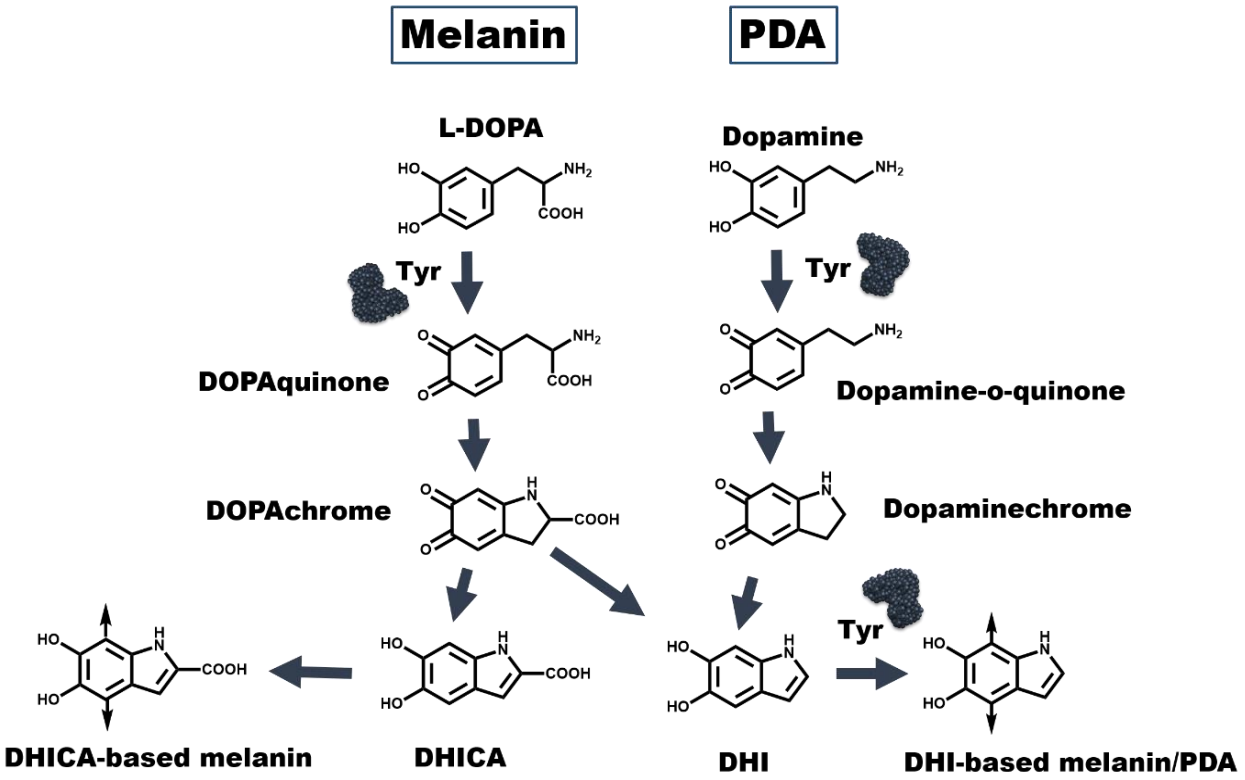

Figure 5.3. *Pathways leading to the synthesis of DHI-based and DHICA-based melanin/PDA, starting from precursors L-DOPA and dopamine, respectively.*

We estimated the concentration of encapsulated L-DOPA (0.13 mM), dopamine (0.11 mM) and Tyrosinase (0.28 μM) for corresponding polymersomes (1 mg/mL) based on the ratio of the starting concentration (used for film rehydration) and the concentration of unencapsulated compounds determined by measuring the absorbance in fractions collected from SEC purification (see Materials and Methods). The resulting encapsulation efficiencies obtained for L-DOPA (13 ± 3 %) and dopamine (11 ± 5 %) were lower than what is usually obtained for encapsulation of small molecules, which probably results from stacking and electrostatic interactions of these respective catecholamines making them tedious to encapsulate. Tyrosinase encapsulation efficiency (9 ± 4 %) was within the range usually obtained for enzyme encapsulation inside polymersomes.[63,146,153,190] We ruled out the presence of L-DOPA, dopamine or Tyrosinase adsorbed to the outer surface of polymersomes as similar zeta potentials were obtained for Melanin-Polymersomes with Tyrosinase (-3.29 ± 0.62 mV), PDA-polymersomes with Tyrosinase (-2.93 ± 1.02 mV), Melanin-polymersomes without Tyrosinase (-2.87 ± 0.54 mV), PDA-polymersomes without Tyrosinase (-2.63 ± 0.36 mV), Tyrosinase-polymersomes (-3.11 ± 0.82 mV) and empty polymersomes (-2.81 ± 0.63 mV). Additionally, we performed a control experiment where empty polymersomes (formed with PBS only) were mixed with 100 times lower of L-DOPA/dopamine (10 μM) and Tyrosinase (30 nM) concentrations than the 1 mM L-DOPA/dopamine and 3 μM Tyrosinase used film rehydration. As shown in **Figure 5.4**, the presence of a small amounts of L-DOPA and dopamine outside polymersomes resulted in the clustering of polymersomes after one week of incubation at 37 °C, followed by extensive aggregation. In contrast, no aggregation or clustering was observed for the melanosome mimics, corroborating the absence of adsorbed compounds at the surface of polymersomes.

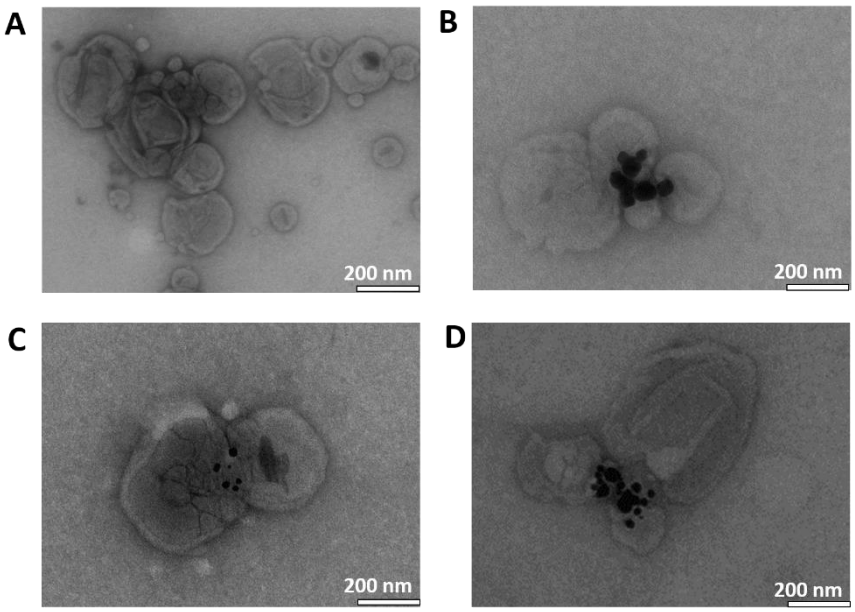

Figure 5.4. *TEM micrographs of polymersome clusters collected in the supernatant of solution containing empty polymersomes in presence of* ***(A)*** *L-DOPA with Tyrosinase,* ***(B)*** *Dopamine with Tyrosinase,* ***(C)*** *L-DOPA,* ***(D)*** *Dopamine, after one week of incubation at 37 °C.*

Indeed, Melanin-polymersomes and PDA-polymersomes showed high colloidal stability as their size was maintained even after 6 months of storage at 37 °C (**Figure 5.5, Figure 10.29**). Hence, by means of encapsulating precursors and Tyrosinase in polymersomes, we introduce a unique approach to preventing melanin and PDA aggregation which could open new avenues for applying these materials. In addition to keeping enclosed light absorbing biopolymers to prevent aggregation, we predict the polymeric membrane to simultaneously confine melanin- and PDA-associated cytotoxicity while their UV-absorption properties are preserved.

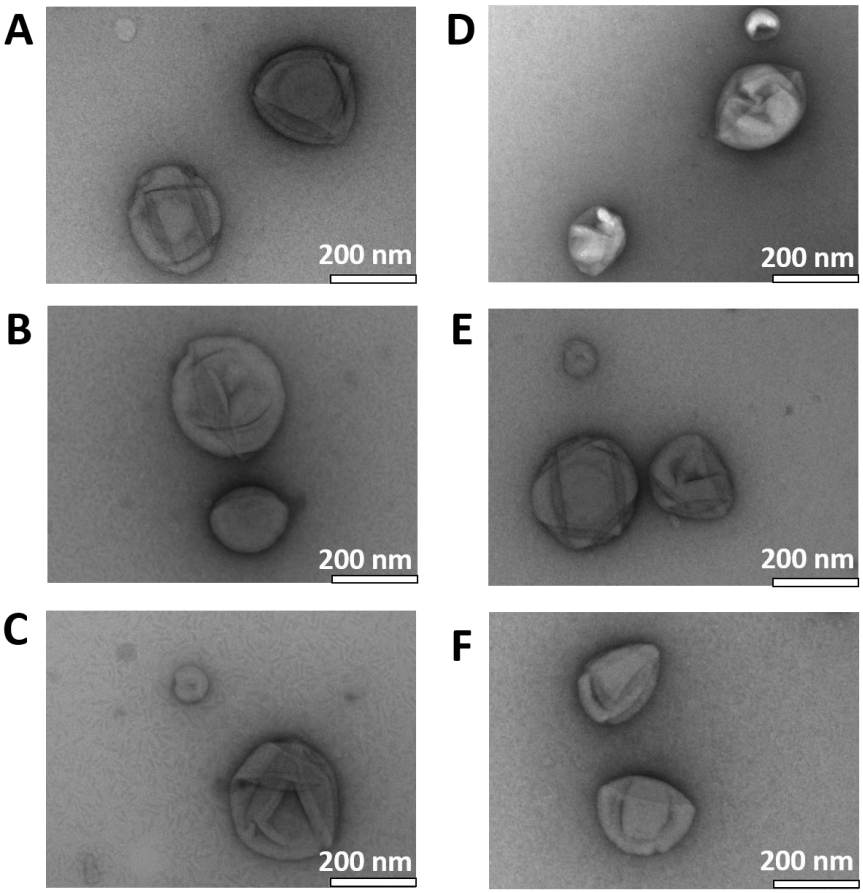

Figure 5.5. *TEM micrographs showing the morphology of* ***(A)*** *Melanin-polymersomes (with tyrosinase),* ***(B)*** *PDA-polymersomes (with tyrosinase),* ***(C)*** *empty polymersomes rehydrated with PBS only,* ***(D)*** *Tyrosinase polymersomes,* ***(E)*** *Melanin-polymersomes (without tyrosinase) and* ***(F)*** *PDA-polymersomes (without tyrosinase), after 6 months of storage at 37 °C.*

5.4 UV-absorption properties of melanosome mimics

Owing to their strong absorption properties, broad-band UV-Vis absorption spectra have been considered the cornerstone for monitoring melanin and PDA polymerization.[171,172,188] Thus, we examined melanin and PDA formation within the polymersome cavity (with and without co-encapsulated Tyrosinase) by measuring absorbance from 250 to 700 nm up to 24 hours (**Figure 5.6**). The absorption spectrum for all polymersomes encapsulating L-DOPA or dopamine (with and without Tyrosinase) showed an upward shift indicative of melanin/PDA compared to control polymersomes (empty polymersomes or polymersomes encapsulating only

Tyrosinase) where no shifts were obtained even after 24 hours (**Figure 5.6).** The presence of Tyrosinase (**Figure 5.6D,F**) led to a higher absorption for L-DOPA- and Dopamine-polymersomes, showing that the enzyme promotes the production of melanin/PDA. In the absence of Tyrosinase (**Figure 5.6C,E**), a plateau occurred around 450 nm, suggesting that a certain amount of DOPAchrome/dopamine-chrome did not spontaneously convert (via decarboxylation) into DHI and thus polymerization did not proceed.[191] Indeed, the intramolecular cyclization of DOPAquinone (via DOPAchrome intermediate) to DHI is known to be very slow.[192] Interestingly, in the presence of Tyrosinase, no unconsumed DOPAchrome/dopamine-chrome was observed, even though Tyrosinase is not directly involved in the Dopa-quinone to DHI conversion (via DOPAchrome intermediate) (**Figure 5.6D-F**).[187] However, Tyrosinase triggers the formation of DOPAchrome precursor (DOPAquinone) and the conversion of DOPAchrome product (DHI) into reactive indole-5,6-quinone.[187] Thus, it is conceivable that Tyrosinase affects the DOPAchrome/dopamine-chrome formation or the conversion to DHI by influencing the equilibrium of intermediates resulting from previous or later reaction steps. This hypothesis is supported by the 500 nm absorption shift obtained for L-DOPA polymersomes in presence of Tyrosinase, indicating the formation of DHI-derived melanin (**Figure 5.6D**).[193] Accordingly, a darker coloration of Melanin-polymersome/PDA-polymersomes was visible by eye, consistent with the fast oxidative polymerization of DHI (**Figure 5.6G**), as opposed to DHICA-derived melanin that is known to be formed slower and result in a color-less solution, even after 24 h of reaction.[194] These results support that Tyrosinase favors the formation of DHI-derived melanin rather than DHICA-derived melanin which is an advantage as DHI-melanin possesses increased visible light absorption properties.[183] Notably, PDA-polymersomes showed stronger absorption compared to Melanin-polymersomes over a broad-range of wavelengths (**Figure 5.6D,E**). It appears reasonable that the formation of PDA occurs more readily because it mainly involves fast occurring non-covalent interactions (charge transfer, π-stacking, hydrogen bonding) rather than covalent linkage among units as it is the case for melanin formation.[188] These data suggest that PDA-polymersomes have an enhanced potency as melanosome mimics (**Figure 5.6**).

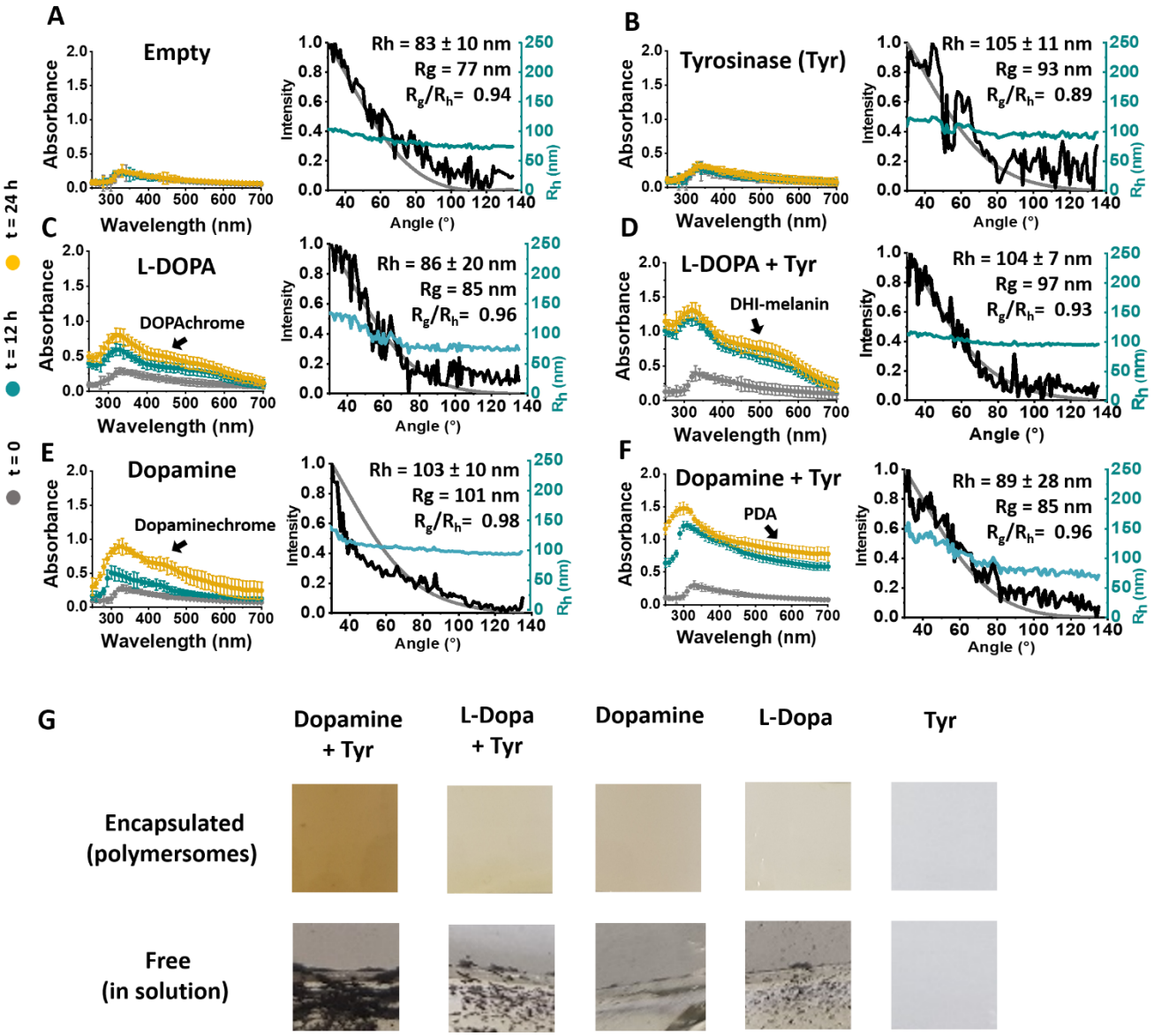

Figure 5.6. *Melanin and PDA formation within polymersomes monitored via UV-vis spectroscopy and SLS. Absorption spectrum (left panels) measured at t = 0 (grey), t=12 h (cyan) and t=24 h (orange) of incubation at 37 °C, and SLS data (right panels) measured at 24 h of* ***(A)*** *Empty polymersomes,* ***(B)*** *Tyrosinase polymersomes,* ***(C)*** *L-DOPA polymersomes,* ***(D)*** *L-DOPA polymersomes (with Tyrosinase),* ***(E)*** *Dopamine polymersomes,* ***(F)*** *Dopamine polymersomes (with Tyrosinase). SLS data are composed of a DLS profile showing the hydrodynamic radius (Rh) at different angles (cyan), the normalized intensity at different angles (black) and a corresponding MIE fit (grey).* ***(G)*** *Snapshots showing the color of the solution of encapsulated (top panels) and free (bottom panels) of L-DOPA or dopamine (with and without Tyrosinase).*

As the concentration of encapsulated L-DOPA/dopamine obtained for our melanin- and PDA-based melanosomes mimics is in the lower range of standard concentrations (25 µM - 100 mM) used for the formation of Melanin and PDA nanoparticles[195,196], we used high concentrations of polymer (10 mg/mL) to obtain concentrated polymersomes solutions (around $2*10^{12}$ vesicles/mL), showing light-

absorption properties (**Table 2, Figure 5.6**). Furthermore, PDMS-PMOXA polymersomes are known to be impermeable to small molecules but allow the diffusion of molecular oxygen.[1,197] Thus, encapsulated L-DOPA/dopamine is unable to diffuse out of the polymersome while oxygen can freely diffuse across the polymer membrane and mediate auto-oxidation or enzyme-catalyzed oxidation of encapsulated compounds, which leads to L-DOPA/dopamine polymerization inside the polymersome cavity. Control experiments with free L-DOPA/Dopamine were performed under corresponding conditions, i.e. solutions of L-DOPA/Dopamine (0.13/0.11 mM) were incubated at 37 °C with or without Tyrosinase (3 μM) (**Figure 5.6G**) to test whether melanin/PDA formation takes place at these concentrations, temperature and time. As shown in Figure 2G (bottom panels), we observed a rapid change in color with subsequent aggregation, indicating that melanin/PDA are formed **(Figure 5.6G, Figure 10.30**). Similar to the Tyrosinase-related color change observed in polymersome samples, the enhancing effect of Tyrosinase was observed with free L-DOPA/dopamine, supporting its contribution to obtaining light-absorbing materials.

In addition, the aggregation of melanin/PDA in solutions provides further evidence for the low colloidal stability of such materials compared to when encapsulated inside polymersomes (**Figure 5.6G, Figure 10.30**). Inside polymersomes, the aggregation process is most likely terminated by the limited amount of L-DOPA/Dopamine available. To gain insight into the buildup of melanin/PDA inside polymersomes, we performed Static Light Scattering (SLS) experiments to determine the radius of gyration (Rg) of polymersomes (**Figure 5.6A-F, right panels**). With the hydrodynamic radii (Rh) derived from the DLS profiles, a ratio 0. 775 < Rg/Rh ≤ 1 was calculated for all Melanin/PDA polymersomes (with and without Tyrosinase) and control polymersomes (empty or encapsulating Tyrosinase alone), which indicates a hollow spherical morphology of polymersomes in the absence of an optically dense core.[159] Thus, the formation of a single, large melanin/PDA nanoparticle in the polymersome's interior can been excluded. Additionally, as an Rg/Rh = 1 indicates an infinitely thin membrane and the Rg/Rh for all polymersomes was closer to 1 than to 0.775, we ruled out the possibility of a thick melanin/PDA coating at the inner membrane surface of the polymersome. We concluded that melanin/PDA within polymersomes was probably present as oligomers and/or lower-nanometer range protoparticles. This notion is consistent published data where

Tyrosinase-mediated formation of melanin in solution lead to melanin protoparticles (6 nm of diameter) when the reaction was induced in a restricted area.[183,198,199] Based on our data showing that by sequestering L-DOPA/dopamine inside polymersomes, melanin/PDA production without large scale aggregation while maintaining interesting light-absorption properties is feasible, and in view of biological applications of such melanin/PDA-polymersomes, we addressed on the interactions of our melanosome mimics with cells.

5.5 Cytotoxicity and potential cell photoprotection activity

Although melanin is a biological pigment and PDA functions in a large variety of bio-applications, both materials can be cytotoxic, as they can promote lipid peroxidation upon UV irradiation, leading to increased cell death.[178,179,182] It has also been reported that a smaller diameter of PDA particles and an increased concentration favor cytotoxicity.[182,200] To test the cytotoxicity of our melanosome mimics, we carried out a cell-proliferation assays with the keratinocyte cell line HaCatT (**Figure 5.7A**). After 1 day of incubation with polymersomes at high concentration (0.25 mg/mL), we did not observe cytotoxicity of our melanin/PDA polymersomes or control polymersomes.

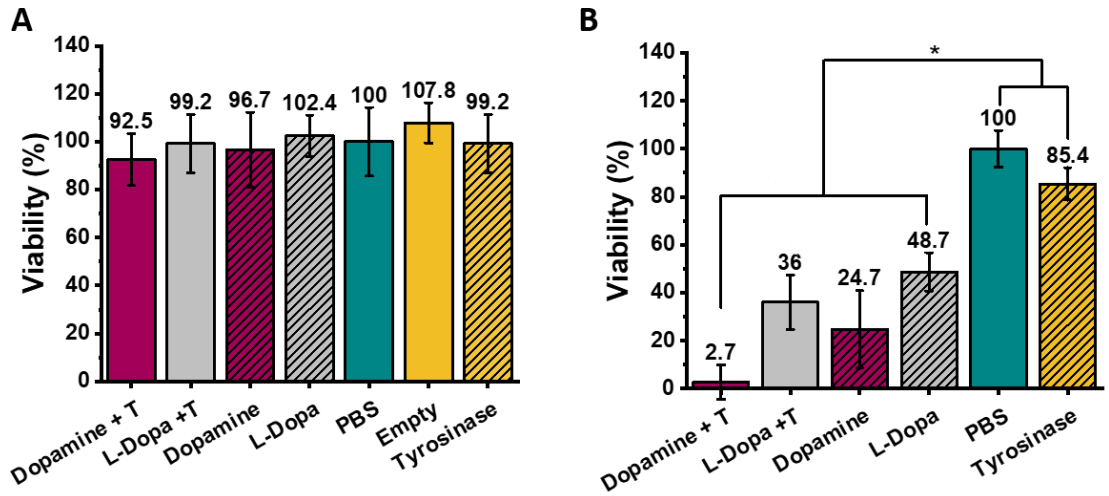

Figure 5.7. *Interaction of polymersome-based melanosome mimics with HaCaT cells.* ***(A)*** *Cell proliferation assay showing the non-toxicity of different kinds of polymersomes compared to PBS.* ***(B)*** *Cell proliferation assay showing the cytotoxicity of free L-DOPA/dopamine (with and without Tyrosinase) as compared to PBS. Statistical significance was shown as p values < 0.02.*

As comparison, we carried out the same experiment with melanin/PDA formed in solution under corresponding conditions and found significant toxicity compared to PBS or a control solution containing only Tyrosinase (**Figure 5.7B, Figure 5.8**).

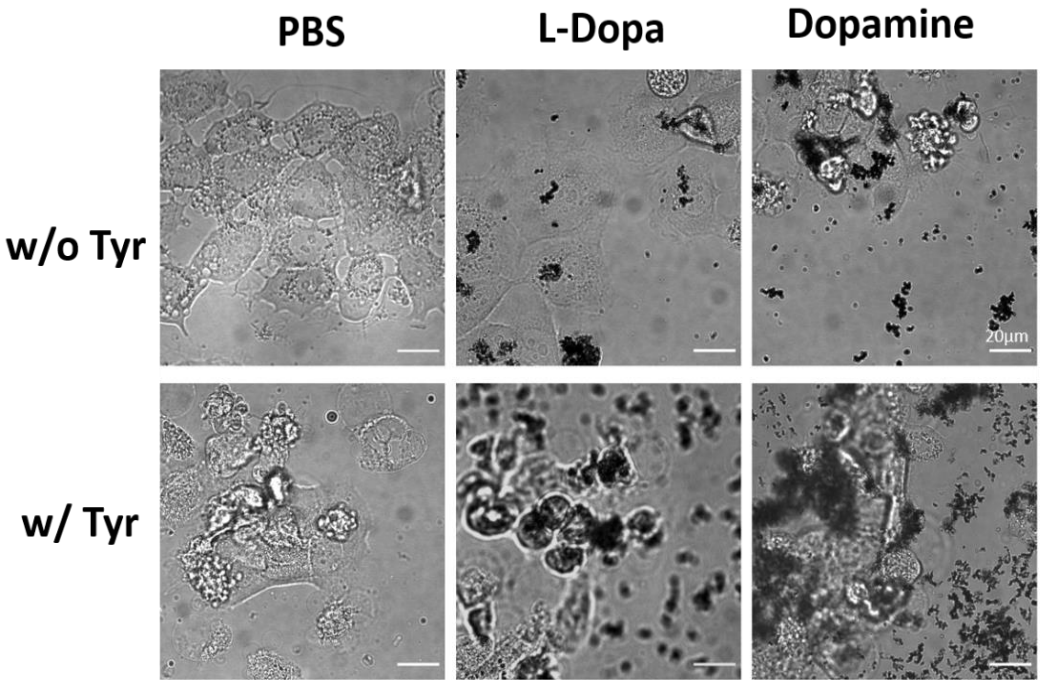

Figure 5.8. *CLSM images showing cell death (round cells) induced by aggregates of melanin/PDA previously formed in presence or absence of Tyrosinase (scale bar = 20 µm).*

The apparent cytotoxicity probably arose from the large melanin/PDA aggregates that hinder cell proliferation when no measures are taken to limit the aggregation of melanin/PDA (**Figure 5.8, Figure 10.31**). Thus, our polymersome-based melanosome mimics, via sequestering of melanin/PDA not only prevent aggregation of melanin/PDA, but elude cytotoxicity which drastically increases their suitability for biological applications.

Additionally, we tested the cytotoxicity of our melanosome mimics after irradiating cells for 40 min with UV and observed no increase in cell death compared to PBS, suggesting the absence of UV-triggered damaging reactions for melanosome mimics and control polymersomes (**Figure 5.9A**). On the contrary, we observed an enhanced cell viability in the presence of PDA-polymersomes (with Tyrosinase),

suggesting protection against UV damage. These data are consistent with the absorbance spectra presented in **Figure 5.9**, where PDA-polymersomes showed the highest absorption, suggesting that UV-protection properties are possibly increased compared to melanin-polymersomes (**Figure 5.9**). However, we deem the amount of polymersomes entering cells is too low for melanin-polymersomes to act as a detectable UV-shield for the nucleus. Confocal laser scanning microscopy images of HaCaT keratinocytes treated with control polymersomes encapsulating Atto-488 fluorescent dye reveal that our polymersomes have the ability to enter cells where they localize around the nucleus albeit to a limited extent (**Figure 5.9B**). In view of possible photoprotection applications, in-depth cell studies are needed to unravel the fate of polymersome-based melanosome mimics inside cells (uptake, endosomal escape and perinuclear accumulation). Moreover, improvements to the melanosome mimics (cell-penetrating/targeting modifications) may be required to achieve optimal photoprotection.

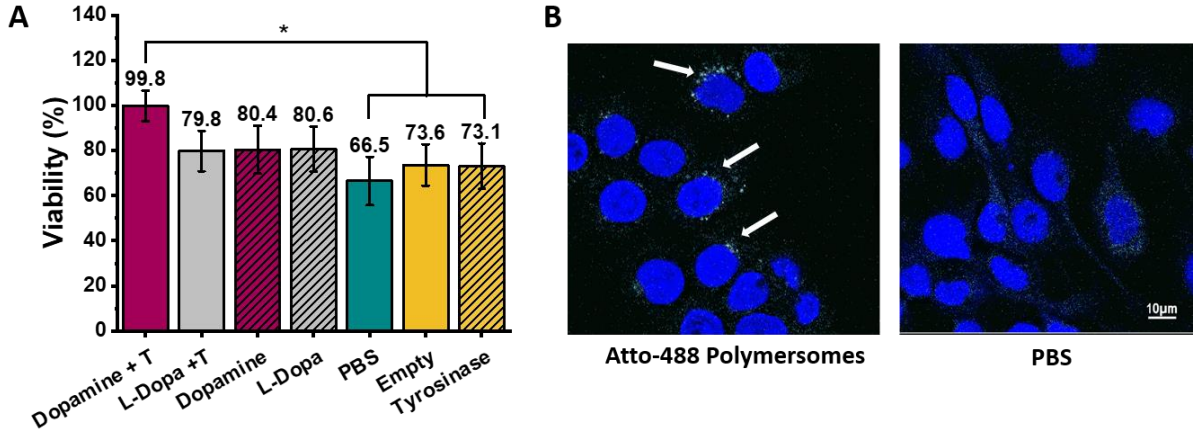

Figure 5.9. *Interaction of polymersome-based melanosome mimics with HaCaT cells.* ***(A)*** *Cell proliferation assay showing the cytotoxicity/cell protection effect of different kinds of polymersomes after 40 min of UV-irradiation of cells.* ***(B)*** *CLSM images showing perinuclear localization of model polymersomes (encapsulating fluorescent Atto-488) in keratinocytes. Statistical significance was shown as p values < 0.02.*

5.6 Conclusions

Biomimetic synthesis of melanin mediated by Tyrosinase is the synthetic route that comes closest to native melanogenesis.[183] By reproducing for the first time this process in the confined environment of a soft nanocompartment, i.e., inside polymersomes, we closely mimic the natural pathway of melanin biosynthesis in melanosomes. For comparison, we produced polydopamine (PDA), which is considered a synthetic melanin, within the cavity of polymersomes in a similar fashion. Being an emerging biopolymer material with interesting coating properties, PDA is gaining increasing attention and might even be more applicable than melanin. By the specific selection of a short-chained PDMS-PMOXA polymer, both polymersome-based systems showed great colloidal stability, UV-absorption properties as well as the absence of cytotoxicity and a potential for cell photoprotection. The sequestering of melanin/PDA inside polymersomes is a new way of avoiding aggregation, even over extended periods of time, that is generally difficult to achieve with melanin/PDA nanoparticles. At the same time, the polymeric membrane enclosing melanin/PDA acts as a barrier preventing cytotoxicity that typically goes hand in hand with non-encapsulated melanin/PDA. Inspired by nature, we provide a new system that side-steps the main drawbacks of melanin and PDA and thus could extend the applicability of these potent macromolecules. Furthermore, the chemical versatility of polymersomes and their numerous possibilities for functionalization greatly extend the range of applications for these biomimetic nanomaterials.

6. Overall conclusions and outlook

Inspired by biological structures and processes, we engineered different synthetic systems hosting relevant biomolecules to obtain superior bio-hybrid nanomaterials with desired functions/interactions with cells or organisms that target specific biomedical applications. In this thesis, combinations of the following four strategies were adopted in producing innovative bio-hybrid compartments: **1)** using polymers that easily self-assemble and enable the incorporation of membrane proteins, **2)** selecting appropriate enzymes with desired activity, **3)** choosing efficient reactions/appropriate biomolecules for the functionalization of the polymersomes and **4)** segregating different active compounds in different compartments.

Short-length PDMS-PMOXA di-block co-polymers were chosen as the synthetic building block of nanocompartments as they rapidly formed polymersomes within a wide range of assembly conditions. Tunability was an important feature, not only to accelerate polymersome production, which is beneficial for translational applications, but also to create conditions necessary for the incorporation and proper function of biomolecules within the polymeric vesicles.

We established a therapeutic nanocompartment encapsulating active Dopa decarboxylase (DDC) which is a relevant enzyme in view of the treatment of atherosclerosis. To go a step further towards theranostic applications, the therapeutic catalytic compartments were coupled to imaging polymersomes by hybridization of complementary DNA strands present on the surface of the respective polymersomes, which also conferred cell attachment properties upon the theranostic polymersome clusters. The resulting dual-functional bio-hybrid system enabled cell imaging and induced relevant cell response via on-site and on-demand production of dopamine. This is the first time that co-localized therapeutic and imaging functions were achieved by clustering two types of nanocompartments. Importantly, the segregation of different modalities enabled to individually adapt the conditions of polymersome formation and surface functionalization to the different active compounds without

abolishing their function. The short lifetime of the encapsulated enzyme (DDC) and the non-specific cell attachment are the main limitations of this system. However, as these clusters are tunable, the incorporated enzymes and targeting agents could be modified to provide a dual-functional system aimed at other applications.

By a similar catalytic compartment layout, we developed an imaging system with a large potential in pre-clinical applications. *Gaussia* Luciferase was encapsulated inside bio-hybrid nanocompartments to deliver a powerful and long-lasting light signal. This is the first example where the modulation of enzyme kinetics by altering the access of substrate to the confined enzyme is beneficial to imaging applications. Our bioluminescent system was able to produce detectable light signals in a cellular environment and was capable to cross biological tissues, corroborating its strong potential for application. The biodistribution and clearance of these polymersomes remain to be assessed to fully appreciate the applicability of such system for *in vivo* imaging. The particular application could be varied via surface functionalization of these polymersomes with targeting agents, e.g., to target and image tumours.

Another kind of catalytic bio-hybrid system was developed to mimic native melanosomes, with the objective of providing a novel treatment approach for Vitiligo, Albinism and for reducing the risk of skin cancer. Melanin and polydopamine (PDA) precursors L-DOPA and dopamine, respectively, were encapsulated in polymersomes together with melanogenic Tyrosinase. The fast self-assembly of a selected polymer into vesicles was exploited to encapsulate the corresponding precursors before their polymerization into melanin/PDA. The polymersome-based system is currently the only example of melanin/PDA encapsulation inside synthetic nanocompartments. The polymeric membrane enabled to overcome the main downsides of conventional melanin/PDA-based nanoparticles: by curbing melanin/PDA production, the melanosome mimics exhibited decreased cytotoxicity and enhanced colloidal stability while maintaining UV-absorption properties, thereby demonstrating their potential for cell photoprotective applications. The relatively low cell uptake and resulting perinuclear aggregation of our polymersomes remain their main limitations, which could be solved with the functionalization of their surface with cell-penetrating agents (e.g., peptides) and nucleus targeting agents.

Taken together, the use of a short length block copolymer was critical parameter in the assembly and adaptability of the synthetic backbone of the bio-hybrid

compartments, which in turn is key to incorporating diverse biomolecules and thus, key to expanding biomedical applicability. The combination of the different strategies resulted in catalytic bio-hybrid systems that lay the grounds for new kinds of biomedical applications, for example a theranostic approach for the treatment of atherosclerosis, bioluminescent imaging systems for pre-clinical studies and photoprotective solutions to prevent skin cancer. In-depth *in vivo* studies are now required to fully appreciate the applicability of such bio-hybrid systems.

7. Experimental

7.1 Chapter 3

7.1.1 Materials

DBCO-ss-DNA sequences were purchased from IBA Lifesciences (Göttingen, Germany). DDC was purchased from Biotechne (Zug, Switwerland). Dulbecco's PBS was purchased from BioConcept (Allschwill, Switzerland). L-DOPA (levodopa), dopamine hydrochloride, pyridoxal 5'-phosphate monohydrate, BSA, reduced L-glutathione, diethanolamine, L-homoarginine, magnesium chloride, and *p*-nitrophenyl phosphate were obtained from Sigma-Aldrich (St. Louis, USA). N-Octyl-β-D-glucoside was purchased from Anatrace (Maumee, USA). The fluorescent probes Atto-488 and DY-633 were purchased from ATTO-TEC GmbH (Siegen, Germany) and Dyomics GmbH (Jena, Germany), respectively. All compounds and solvents were used as received.

7.1.2 Synthesis of $PDMS_{22}$-$PMOXA_8$-OEG_3-N_3

$PDMS_{22}$-$PMOXA_8$ with a hydroxyl functional group ($PDMS_{22}$-$PMOXA_8$-OH) was synthesized accordingly to the well-established protocol of our research group.[34] $PDMS_{22}$-$PMOXA_8$ with azide as the end functional group ($PDMS_{22}$-$PMOXA_8$-N_3) was synthesized accordingly our recently published procedure[122] with slight modifications. Briefly, $PDMS_{22}$-$PMOXA_8$-OH (350 mg) was first dissolved in 10 mL anhydrous chloroform at RT, then succinic anhydride (30 mg,), 4-dimethylaminopyridine (5 mg) and TEA (30 µL) were added successively. The mixture was deoxygenated by means of three vacuum-argon cycles, and then stirred for another 72 h at room temperature under Ar. Ultrafiltration afforded colorless $PDMS_{22}$-$PMOXA_8$ with a carboxylic acid end group ($PDMS_{22}$-$PMOXA_8$-COOH) (yield: 300 mg, 86%). This $PDMS_{22}$-$PMOXA_8$-COOH (300 mg) was dissolved in anhydrous chloroform at room temperature, then 11-azido-3,6,9-trioxaundecan-1-amine (50 mg), N,N'-dicyclohexylcarbodiimide (46 mg) and 4-dimethylaminopyridine (3 mg) were added to the solution. The mixture was

deoxygenated three times, then stirred at 30 rpm for another 48 h at RT. Ultrafiltration afforded colorless $PDMS_{22}$-$PMOXA_8$-N_3 (yield: 220 mg, 73%).

7.1.3 Formation of the different polymersomes

Rapid formation of empty $PDMS_{22}$-$PMOXA_8$-OEG_3-N_3 polymersomes: $PDMS_{22}$-$PMOXA_8$-OEG_3-N_3 block copolymers were dissolved in ethanol to yield a stock solution with a concentration of 10 mg/mL. 400 µL of this solution was transferred into a 5 mL round-bottomed flask, and dried in a rotary evaporator (170 mbar, 40 °C, 75 rpm). 1 mL of PBS was added to the residue, and the flask was gently shaken with stirring bar for less than 1 min at RT. The resulting solution was extruded 15 times through a polycarbonate (PC) membrane with a 200 nm diameter pore size on an Avanti mini-extruder (Avanti Polar Lipids, Alabama, USA) to unify the size of the polymersomes.

Preparation of HRP-Ncomp: $PDMS_{22}$-$PMOXA_8$-OEG_3-N_3 stock solution (200 µL, 10 mg/mL) was transferred into a 5 mL round-bottomed flask, and dried on a rotary evaporator (170 mbar, 40 °C, 75 rpm). HRP solution (100 µL, 0.2 mg/mL) containing 0.1 wt% BSA with either PBS (100 µL) or OmpF (100 µL, 0.1 mg/mL or 0.2 mg/mL) was added to the residue, resulting in a final concentration of 0.16 mg/mL of HRP, 4 mg/mL of $PDMS_{22}$-$PMOXA_8$-OEG_3-N_3 and 0 mg/mL, 0.02 mg/mL, and 0.04 mg/mL of OmpF. The flask was gently shaken with a stirring bar for less than 10 seconds at room temperature. The resultant HRP-Ncomp was extruded the same way as described for the empty polymersomes. Free HRP was removed by means of SEC, eluted with PBS.

Preparation of DDC-Ncomp: A solution of $PDMS_{22}$-$PMOXA_8$-OEG_3-N_3 polymer dissolved in ethanol (600 µL, 10 mg/mL) was transferred into a 5 mL round-bottomed flask, and dried on a rotary evaporator (170 mbar, 40 °C, 75 rpm). In parallel, freshly thawed DDC (20 µg) was dissolved in 0.1 wt% BSA in PBS (1 mL) and pyridoxal phosphate in PBS (50 µL, 5 mM). The mixture was gently stirred at 4°C for 20 min. The thin polymer film was rehydrated with this DDC solution (522 µL) mixed with dialyzed OmpF solution (78 µL, 0.8 mg/mL to give the same polymer/OmpF ratio as used for HRP-Ncomp) (see the SI for further details). The resulting solution was

stirred 3 hours at 4 °C, and then extruded 15 times through a PC membrane with a 200 nm diameter pore size under sterile conditions to unify the size of the polymersomes.

Preparation of Dye-Ncomp: A stock solution of $PDMS_{22}$-$PMOXA_8$-OEG_3-N_3 block copolymer was obtained by dissolution of the polymer in ethanol (600 µL, 10 mg/mL), and transferred to a round-bottomed flask, followed by drying on a rotary evaporator (170 mbar, 40 °C, 75 rpm). The resultant thin polymer film was rehydrated by adding a solution of DY-633 (600 µL, 0.2 mM in PBS). The product was stirred overnight at room temperature before being extruded in the same way as described for DDC-Ncomp.

7.1.4 Conjugation of DNA with empty polymersomes

Empty polymersomes (4 mg/mL) were mixed with 1 eq. per azide group of ssDNAa or spacer-ssDNAa labelled with DY-633 (0.5 mM in water). The reaction was carried out overnight at 4 °C. Free DNA was removed by size exclusion chromatography (SEC) eluted with PBS.

7.1.5 Conjugation of DNA and clusters formation

Extruded DDC-Ncomp and Dye-Ncomp (500 µL each) were mixed with 1 eq. per azide group of ssDNA/spacer-ssDNAa (0.5 mM in water) overnight (4 °C) and ssDNAb/spacer-ssDNAb (0.5 mM in water) overnight (37 °C), respectively. The two solutions were purified by means of SEC to remove free DNA, under sterile conditions, and cold PBS. The volumes of purified polymersomes solutions were adjusted to obtain a polymer concentration of 2 mg/mL. To prepare clusters, the two solutions were mixed (1:1) and incubated at 20 °C for 20 min. The resulting cluster solution was used immediately.

7.1.6 Physical characterization of polymersomes and clusters

Transmission electron microscopy (TEM): A 5 µL aliquot of polymersomes or polymersome clusters (0.1 mg/mL) was absorbed on 400 mesh square copper grids. The grids were further stained with 2% uranyl acetate and the negatively stained image

of nanostructures was obtained with a transmission electron microscope (Philips CM100) at an accelerating voltage of 80 kV.

Dynamic light scattering (DLS): The apparent diameter D_H values of polymersomes and polymersome clusters were obtained on a Zetasizer Nano ZSP (Malvern Instruments Inc., UK) at 25 °C. 400 µL of each sample solution (0.2 mg/mL final concentration) was added to a cuvette and subjected to 11 runs repeated three times. The measured angle was 173° and the data was analyzed by intensity distribution. To examine the kinetics of polymersome cluster formation, measurements were run for 3 min with a 2 min interval.

Zeta potential measurements: The electrophoretic mobility of vesicles in solution was determined by means of laser Doppler velocimetry and phase-analysis light-scattering measurements. A Malvern Zetasizer Nano ZSP (Malvern Instruments Inc, UK) with a 633 nm wavelength laser was used for all measurements. The vesicle samples (0.2 mg/mL) were measured in PBS with five repeat measurements per sample. All experiments were run at 25 °C.

Static light scattering (SLS): Multi-angle dynamic light scattering (DLS) and static light scattering (SLS) were performed on a setup from LS Instruments (Switzerland), equipped with a 21 mW He-Ne laser (λ = 632.8 nm) for scattering angles from 30° to 150° at 25 °C. All samples were diluted in order to suppress multiple scattering. Second-order cumulant analysis for various angles was performed to obtain the hydrodynamic radius (Rh). The radius of gyration (Rg) was obtained from the SLS data using a Guinier plot.

Fluorescence Correlation Spectroscopy (FCS): FCS was performed on a Zeiss LSM 880 microscope (Zeiss LSM 880, inverted microscope ZEISS Axio Observer, Carl Zeiss, Jena, Germany). A 488 nm argon laser was used to excite ssDNA labelled with Atto-488 and the conjugated Ncomp. The laser beam was passed through main beam splitter MBS488 and signals were detected in the range of 500-532 nm. A 633 nm HeNe laser, was used for DY-633 labelled ssDNA and the conjugated Ncomp. The laser beam was passed through MBS488/561/633 filter and the signal was detected in the

range of 650-740 nm, the pinholes were adjusted to maximize the count rate using the corresponding free dye in PBS. The sample volume was 15 µL. Fluorescence fluctuations over time were recorded for 30 x 10 s. The raw data was processed and analyzed using Zeiss software. Autocorrelation curves were fitted to a two-component model (Equation S1).

$$G_{2comp}(\tau) = 1 + \frac{1}{N} \cdot \left(1 + \frac{T_{trip}}{1-T_{trip}} e^{-\frac{\tau}{\tau_{trip}}}\right) \cdot \left[\frac{f_1}{\left(1+\frac{\tau}{\tau_{D_1}}\right)\left(1+\frac{\tau}{S^2\tau_{D_1}}\right)^{1/2}} + \frac{f_2}{\left(1+\frac{\tau}{\tau_{D_2}}\right)\left(1+\frac{\tau}{S^2\tau_{D_2}}\right)^{1/2}}\right] \quad (1)$$

Where $G_{2comp}(\tau)$ is the two-component autocorrelation function, N is the number of particles, S is the structural parameter, T_{trip} is the fraction of fluorophores in the triplet state, τ_{trip} is the corresponding triplet time, f_1 and f_2 are the fractions of the particles of the corresponding component 1 or 2, and τ_{D_1} and τ_{D_2} are the diffusion times of the corresponding component 1 or 2.

7.1.7 Estimation of DDC encapsulation efficiency

Polymersomes encapsulating BSA (BSA-Ncomp) were formed under the same conditions described above, but using BSA in place of DDC and using PBS only (without further 0.1 wt% BSA). The concentration of non-encapsulated BSA was determined from the fraction of free BSA present in the solution after SEC purification of BSA-Ncomp. Polymersomes rehydrated under the same conditions but without BSA were also formed and purified for use as a blank. After UV-vis (280 nm) absorbance measurements using a NanoDrop 2000 spectrophotometer (Thermofisher) in BSA mode, we determined the amount of BSA molecules encapsulated in polymersomes. We calculated the difference between the total amount of BSA used for film rehydration and the amount of non-encapsulated BSA, which gave a number of $1.79*10^{13} \pm 4.71*10^{12}$ molecules of BSA encapsulated. In parallel, the concentration of vesicles ($1.3*10^{12}$ vesicles/mL) was determined via single nanoparticle tracking analysis (NTA) using a NanoSight NS300 instrument from Malvern Panalytical (Malvern, United Kingdom). We divided the number of encapsulated BSA molecules by the number of vesicles in our solution (600 µL), obtaining a value of 23.01 ± 6.03 BSA molecules encapsulated per vesicle. Assuming similar numbers of BSA and DDC, the percentage of DDC encapsulation is calculated to be 15.6 ± 4.12 %.

7.1.8 Expression and extraction of OmpF

Wild-type OmpF was obtained according to a previously reported protocol,[126] with a few modifications: bacteria were grown at 30 °C for 6 h on Terrific Broth (TB) (Difco, U.S.A.), and all ultracentrifugations were performed at room temperature.

7.1.9 Activity determination of catalytic nanocompartments:

Activity of model HRP-Ncomp: HRP-Ncomp (10 μg/mL) was incubated in the presence of H_2O_2 (10 μM) in a 96-well black plate (Thermo Fisher Scientific), before the addition of Amplex Red (1 μM) to give a final volume of 200 μL/well. The change of fluorescence (excitation 570 nm / emission 595 nm) after the addition of Amplex Red was recorded immediately using a Spectramax M5 microplate reader (Molecular Devices, USA).

Activity of DDC-Ncomp: 80 μL of purified 1 mg/mL of DDC-Ncomp, DDC-Ncomp functionalized with ssDNA, theranostic clusters or DDC-Ncomp without OmpF was mixed with 10 μL of L-OPA (5 mM in water), 10 μL of reduced glutathione (20 mM in PBS) and 2 μL of pyridoxal phosphate (5 mM in water), and incubated 24 h at 37 °C. Then, each solution was purified by SEC to remove the polymersomes, and analysed by reverse-phase HPLC to detect the presence of dopamine. The percentage conversion of L-DOPA to dopamine was calculated from the areas of the corresponding peaks: for every sample, the area of the dopamine peak is multiplied by 100 and divided by the sum of the areas of the dopamine and L-DOPA peaks. This approach was chosen to avoid potential errors in the assessment of L-DOPA and dopamine concentrations due to sample dilution during SEC purification, which was required to prevent injection of vesicles into the HPLC. The retention times for dopamine and L-DOPA were determined using a reverse-phase Shimadzu HPLC (Reinach, Switzerland). A 20-min method using water containing 0.1% TFA as a mobile phase at 0.5 mL/min though an analytical Chromolith performance RP-18e column (Merck, Schaffhausen, Switzerland) separated dopamine (10.1 min) and L-DOPA (11.8 min). At equal concentrations, the peaks corresponding to dopamine and L-DOPA showed similar areas. Detection was done at 280 nm.

7.1.10 Cell culture

The stable double-transgenic cell line HEK$_{REWARD}$ was cultured in Dulbecco's modified Eagle's medium GlutaMAX™-I (DMEM-GlutaMAX, Gibco Life Sciences) supplemented with 10% FCS (BioConcept), 100 units/mL penicillin and 100 µg/mL streptomycin (Sigma Aldrich). After 14 days, the polyclonal population was selected according to reported methodology.[119] Cells were maintained at 37 °C in a humidified atmosphere of 5% CO_2 in air.

7.1.11 Cellular attachment and imaging

Freshly trypsinized cells were seeded at a density of 60 000 cells per well, in 8-well ibidi collagen IV-coated plates. After 24 h, the cell culture medium was removed and replaced with 130 µL Opti-MEM (Gibco Life Sciences) live cell imaging medium. Next, cells were dosed with polymersome clusters (70 µL, 2 mg/mL) and imaged by CLSM at intervals for 2 h. CLSM measurements were performed on a laser-scanning microscope ZEISS LSM 880 inverted microscope (ZEISS Axio Observer, Carl Zeiss, Germany).

For visualizing polymersome clusters in the presence of cells, the two Ncomps were loaded with Atto-488 and DY-633, respectively, and two lasers, a 488 nm argon laser and a 633 nm HeNe laser, were used. The beams were passed through MBS488 and MBS488/561/633 filters, respectively, and focused onto the sample through a water immersion objective (C-Apochromate 40x/1.2W korr FCS M27). Detection was done at 505-555 nm and 650-740 nm, respectively. For polymersome clusters formed from DDC-Ncomp and dye-Ncomp, only the 633 nm HeNe laser was utilized.

For the 24 hour time points, freshly trypsinized cells were seeded at a density of 30 000 cells per well in 8-well ibidi collagen IV-coated plates. After 24 h, cells were treated with the polymersome clusters as previously described. After a further 24 h incubation, the cells were washed 3x with Opti-MEM prior to CLSM imaging. Images were processed using Fiji ImageJ and colocalization analysis based on Pearson's coefficient of colocalization was performed using the JACoP plugin. 3D rendering of z-stacks was performed using the Icy Image processing software.[119]

7.1.12 Cell activation by DDC-Ncomp and theranostic clusters

Cells were plated in a 96-well plate (100 µL/well of 10 000 cells) and incubated overnight. The next day, 75 µL of media was removed and 75 µL of free DDC (different concentrations) or 1 mg/mL of DDC-Ncomp w/o OmpF, DDC-Ncomp, ssDNA-functionalized DDC-Ncomp or theranostic clusters was added to the wells. Wells were filled with 100 µL of media containing L-DOPA (10 µM) and pyridoxal phosphate (12.5 µM) and incubated for 3 days. Then, the SEAP level was assayed using a standard *p*-nitrophenyl phosphate–based absorbance method as previously described.[201] In brief, the cell supernatant corresponding to each condition was assayed by recording the rate of production of p-nitrophenol from the SEAP substrate *p*-nitrophenyl phosphate, calculated from the absorbance at 405 nm. The amount of SEAP expressed under each condition was calculated using the slope of the kinetic curve of *p*-nitrophenol production.

7.2 Chapter 4

7.2.1 Materials

Gaussia Luciferase was purchased from Enzo life sciences (Lausen, Switzerland). Water-soluble coelenterazine was purchased from Nanolight technologies (Pinetop, USA). Dulbecco's PBS was purchased from BioConcept (Allschwill, Switzerland). N-Octyl-β-D-glucoside was purchased from Anatrace (Maumee, USA). All compounds and solvents were used as received.

7.2.2 Synthesis of $PDMS_{25}$-$PMOXA_{10}$

Synthesis of monocarbinol-functionalized poly(dimethyl siloxane) ($PDMS_{25}$-OH). All reactions were conducted under argon atmosphere in dried glassware. Hexamethylcyclotrisiloxane (D_3) (100 g, 0.450 mol) was added to a 250 mL one-neck round-bottom flask and dried over calcium hydride at 75 °C. After two days, D_3 was distilled under vacuum into a 250 mL three-neck round bottom flask with a yield of 90.32 g (0.406 mol, 13 eq). Dried cyclohexane (150 mL) was added, followed by dropwise addition of *n*-butyl lithium solution (12 mL, 30 mmol, 2.5 M in hexane, 1 eq).

After stirring for 4 h, dried tetrahydrofuran (15 mL) was added and the reaction was left stirring for 38.5 h at room temperature. The polymerization was quenched by addition of dimethylchlorosilane (9.46 g, 11.1 mL, 100 mmol, 3.2 eq). After 4 h of stirring, the solution was filtered through a glass frit to remove the precipitated lithium chloride salt. Then, the solvents were evaporated using a rotary evaporator and unreacted D_3 was removed via subsequent vacuum distillation. The remaining hydride-terminated $PDMS_{25}$-H (58.35 g, 31.5 mmol) was dissolved in dried toluene (80 mL), followed by the addition of 2-allyloxyethanol (3.76 g, 3.94 mL, 33.1 mmol) and platinum(0)-1,3-divinyl-1,1,3,3-tetramethyldisiloxane complex solution (Pt(dvs), in xylene, 35.9 µL). The flask was equipped with a reflux condenser and the solution stirred at 110 °C overnight. Afterwards, toluene was removed using a rotary evaporator and the crude monocarbinol-functionalized $PDMS_{25}$-OH was dissolved in dichloromethane (100 mL). Activated charcoal was added, the solution stirred for 30 min and filtered through Celite S. Finally, the solvent was evaporated to yield a colorless $PDMS_{25}$-OH oil (55.07 g, M_n = 2000 g/mol, 27.5 mmol). $PDMS_{25}$-H and $PDMS_{25}$-OH were characterized by ^{1}H-NMR.

Synthesis of poly(dimethyl siloxane)-block-poly(2-methyl-2-oxazoline) ($PDMS_{25}$-b-$PMOXA_{10}$). All reactions were conducted under argon atmosphere in dried glassware. $PDMS_{25}$-OH (10 g, 4.89 mmol, 1 eq) was added to a 250 mL three-neck round-bottom flask and dried overnight at 100 °C under vacuum. After addition of dried hexane (85 mL) and dried and distilled trimethylamine (0.643 g, 0.886 mL, 6.36 mmol, 1.3 eq), the solution was cooled with an ice/sodium chloride/acetone bath and stirred for 15 min. Then trifluormethanesulfonic anhydride (triflic anhydride, 1.66 g, 0.987 mL, 5.87 mmol, 1.2 eq) in hexane (15 mL) was added dropwise over 30 min under cooling. After 4 h stirring, the solution was filtered through a glass frit under inert atmosphere in order to remove the precipitated triflate salt. The resulting triflate-activated PDMS ($PDMS_{25}$-OTf) was obtained after evaporation of the solvent. Subsequently, dried ethylacetate (100 mL) and 2-methyl-2-oxazline (4.58 g, 4.56 mL, 53.8 mmol, 11 eq) were added and the solution was heated to 40 °C. After 63 h, the solution was cooled to room temperature and water (5 mL) and trimethylamine (5 mL) were added in parallel to quench the reaction. After 6 h, the solvents were evaporated using a rotary evaporator. For purification, the crude copolymer was dissolved in 300 mL methanol and centrifuged (4000 rpm, 1664 rcf, 10 min) in order to remove the remaining PDMS homopolymer precipitates. After transferring the supernatant to a

round bottom flask, the solvent was evaporated. Subsequently, the copolymer (13.91 g) was dissolved in a 1:1 mixture of ethanol and water and dialysed against ethanol:water (1:1, 2 L in total) with 5 changes over two days, followed by a last dialysis step against water (2 L). The resulting copolymer precipitate was lyophilized. The purified copolymer (11.82 g) was not able to undergo self-assembly into vesicular structures. Therefore, it was extracted in a 1:1 mixture of methanol and hexane (each 200 mL). The solvent from the bottom methanol-enriched phase was evaporated and the purified, $PDMS_{25}$-*b*-$PMOXA_{10}$ was obtained as a slightly yellow gel (10.74 g, M_n = 2850 g/mol, 3.77 mmol). $PDMS_{25}$-OTf and $PDMS_{25}$-*b*-$PMOXA_{10}$ where characterized by ^{1}H-NMR.

7.2.3 Preparation of polymersomes

Preparation of GLuc Ncomp: $PDMS_{25}$-$PMOXA_{10}$ block copolymers were dissolved in ethanol to yield a stock solution with a concentration of 10 mg/mL. 600 µL of this solution was transferred into a 5 mL round-bottom flask and dried in a rotary evaporator (170 mbar, 40 °C, 75 rpm). The resulting thin polymer film was rehydrated with a solution composed of 322 µL PBS, 200 µL *Gaussia* Luciferase (GLuc; 0.1 mg/mL in PBS) and 78 µL dialyzed OmpF solution (0.8 mg/mL) which yields the polymer/OmpF ratio previously used for the preparation of PDMS-PMOXA catalytic polymersomes[153]. The resulting solution was stirred overnight at 4 °C, and then extruded (under sterile conditions) 15 times through a polycarbonate (PC) membrane with a 200 nm diameter pore size using an Avanti mini-extruder (Avanti Polar Lipids, Alabama, USA) to unify the size of the polymersomes. The unencapsulated enzymes were removed by size-exclusion chromatography (SEC) eluted with PBS.

Preparation of control polymersomes: Control polymersomes were prepared as described for GLuc Ncomp (600 µL of 10 mg/mL $PDMS_{25}$-$PMOXA_{10}$ solution; overnight stirring at 4 °C) with the following modifications: empty polymersomes were rehydrated with PBS only and GLuc Ncomp without OmpF were rehydrated with a solution of GLuc and a solution of dialyzed 3 % OG (to match the traces of OG ≃ 0.05 % present after dialysis of OmpF).

7.2.4 Physical characterization of polymersomes

Dynamic light scattering (DLS): The apparent diameter D_H values of polymersomes were determined on a Zetasizer Nano ZSP (Malvern Instruments Inc., UK) at 25 °C at an angle of 173°. Each sample was diluted with PBS to 0.2 mg/mL final concentration. A cuvette was filled with 500 µL sample and subjected to 11 measurement runs with three repetitions.

Static light scattering (SLS): Multi-angle dynamic light scattering (DLS) and static light scattering (SLS) were performed on a setup from LS Instruments (Switzerland), equipped with a 21 mW He-Ne laser (λ = 632.8 nm) for scattering angles from 30° to 150° at 25 °C. All samples were diluted in order to avoid multiple scattering. Second-order cumulant analysis for various angles was performed to obtain the hydrodynamic radius (Rh). The radius of gyration (Rg) was obtained from the SLS data using a MIE fit.[159]

Transmission electron microscopy (TEM): 5 µL aliquots of polymersomes (0.1 mg/mL) were adsorbed to 400 mesh square copper grids. Excess liquid was blotted and grids were negatively stained with 2% uranyl acetate. Micrographs of nanostructures were recorded on a Philips CM100 transmission electron microscope at an accelerating voltage of 80 kV.

7.2.5 Expression and extraction of OmpF

Recombinant wild-type OmpF was produced according to a previously reported protocol,[63] with the following modifications: Transformed *E.coli* were grown for 6 h at 30 °C in Terrific Broth (TB; Difco, U.S.A.), and ultracentrifugation was performed at room temperature.

7.2.6 Estimation of GLuc encapsulation efficiency

The concentration of non-encapsulated GLuc was determined from the fraction of free GLuc present in the solution after SEC purification of GLuc Ncomp. Empty

polymersomes with OmpF formed under the same conditions as GLuc Ncomp (but without GLuc) were used as a blank. After UV-vis (280 nm) absorbance measurements using a NanoDrop 2000 spectrophotometer (Thermofisher), we determined the amount of GLuc molecules encapsulated for 1mL of polymersomes ($1.21*10^{13} \pm 5.52*10^{12}$) by calculating the difference between the total amount of GLuc used for film rehydration and the total amount of enzyme that was not encapsulated. In parallel, the concentration of vesicles ($1.7*10^{12}$ vesicles/mL) was determined via single nanoparticle tracking analysis (NTA) using a NanoSight NS300 instrument from Malvern Analytical (Malvern, United Kingdom). The number of encapsulated GLuc molecules was divided by the number of vesicles, obtaining a value of 7 ± 3 GLuc molecules encapsulated per vesicle. An estimation of the percentage of GLuc encapsulated has been calculated to be 12 ± 5 %. After SEC purification, the concentrated GLuc Ncomp solution (2 mg/mL) was obtained, corresponding to a concentration of GLuc of 0.80 µg/mL.

7.2.7 Activity of GLuc and GLuc Ncomp in PBS

GLuc Ncomp, free GLuc enzyme and control polymersomes were assayed using a spectrophotometer equipped with an injector (SpectraMax ID3 microplate reader, Molecular Devices, U.S.A.) in luminescence mode using black 96-well plates. 50 µL GLuc Ncomp (1 mg/mL), control polymersomes (1 mg/mL), or free GLuc enzyme (0.4 µg/mL, corresponding to 1 mg/mL of GLuc Ncomp) was added to each well. Subsequently, 50 µL/well of a freshly prepared coelenterazine substrate (80 µM in PBS) was added by means of the automatic injector to ensure the direct recording of luminescence. To determine the kinetics, luminescence was measured every 30 seconds for 1 hour.

7.2.8 Activity of GLuc and GLuc Ncomp in cell supernatant

MCF-7 cells were seeded in a 96-well plate (3000 cells in 100 µL /well) and cultured overnight at 37°C. Then, 50 µL of the cell supernatant was removed and replaced by 50 µL of fresh medium and 100 µL of GLuc Ncomp (2 mg/mL), free GLuc (0.8 µg/mL), or control polymersomes (2 mg/mL). After 3 days of culturing at 37°C, 50 µl of cell

supernatant was collected and assayed for luminescence production as described above.

7.2.9 Stability of GLuc and GLuc Ncomp

After storage of GLu Ncomp, GLuc Ncomp without OmpF and free GLuc for 3, 7 and 14 days at 4 °C or 37 °C in PBS or cell medium, samples with a consistent enzyme concentration of 0.40 µg/mL were assayed for luminescence production in the same manner as described above. The activity recorded on the day of polymersome preparation (Day 0) in PBS or cell medium was set to 100%. The activity after different time periods of storage was determined in comparison to the activity of Day 0. Luminescence production at the time point where the luminescence signal is the highest (t = 10 min for GLuc Ncomp and t = 0 for free GLuc enzymes) was used to compare the activity of GLuc over time of storage.

7.2.10 Cell culture

MCF-7 (epithelial breast cancer, human; ATCC, HTB-22) were routinely cultured in Eagle's Minimum Essential Medium (EMEM, Gibco Life Sciences) supplemented with 10% fetal bovine serum (BioConcept), 100 units/mL penicillin and 100 µg/mL Streptomycin (Sigma Aldrich). Cells were maintained in a humidified atmosphere at 37 ^{o}C and 5% CO_2.

7.2.11 Cell viability assay (MTS)

CellTiter 96® AQueous One Solution Cell Proliferation Assay (MTS, Invitrogen) was used to determine cell viability. In accordance with the supplier's protocol, MCF-7 cells were seeded at a concentration of 3000 cells/well in a 96 well plate. After 24 h, 50 µL of medium was removed and replaced by 50 µL of fresh medium and 100 µL of GLuc Ncomp (2 mg/mL), free GLuc, or control PBS. The cells were incubated in the presence of GLuc Ncomp, free GLuc or PBS control for 3 more days in a humidified atmosphere at 37 ^{o}C and 5% CO_2. The MTS reagent (20 µL) was added to each well and absorbance

at 490 nm was measured after 2 h at 37 °C using a Spectramax plate reader. The data was normalized to PBS treated control cells after background absorbance removal.

7.2.12 In vivo Bioluminescence Imaging

BALB/c mice have been intravenously injected (IV) with 100 µL of 2 mg/mL GLuc Ncomp or GLuc Ncomp without OmpF, in the tail vein. After 30min, 100 µl of 1 mg/mL coelenterazine was injected in the tail vein. Mice were anesthetized and placed in the imaging chamber of a IVIS Lumina *In vivo* Imaging system (PerkinElmer) and bioluminescence intensity has been recorded for 20 min and summed up. The number of mice was set to 3 per group, but the difficult technical procedure of double IV injection in the tail vein resulted in only one mice per group with successful double injection. Coelenterazine is usually injected retro-orbitally but animal law protection is Switzerland do no permit this procedure.

7.3 Chapter 5

7.3.1 Materials

All compounds were used as received. Tyrosinase from Mushroom, Dopamine (3,4-dihydroxyphenethylamine) and L-DOPA (3,4-dihydroxy-L-phenylalanine) were purchased from Sigma (Buchs, Switzerland).

7.3.2 Synthesis of $PDMS_{24}$-$PMOXA_{12}$

Poly(dimethyl siloxane)-block-poly(2-methyl-2-oxazoline) ($PDMS_{24}$-*b*-$PMOXA_{12}$) was synthesized following a previously reported protocol.[34] Briefly, hydroxyl-terminated PDMS (PDMS-OH) was obtained after anionic ring-opening polymerization of hexamethylcyclotrisiloxane and end group modification with 2-allyloxyethanol. Subsequently, activation of PDMS-OH with trifluormethanesulfonic anhydride was followed by cationic ring-opening polymerization of MOXA monomer. After quenching the polymerization with water and purification via dialysis, the final block copolymer was obtained. The average composition and molecular weight (Mw =

2400 g/mol) was obtained from 1H NMR spectroscopy, whereas a dispersity of 1.16 was measured via gel permeation chromatography.

7.3.3 Preparation of polymersomes

Preparation of Melanin/PDA polymersomes: $PDMS_{24}$-*b*-$PMOXA_{12}$ block copolymers were dissolved in ethanol to yield a stock solution with a concentration of 10 mg/mL. 600 µL of this solution was transferred into a 5 mL round-bottom flask and dried in a rotary evaporator (170 mbar, 40 °C, 75 rpm). The resulting thin polymer film was rehydrated with a solution composed of 300 µL of Dopamine or L-DOPA (2 mM in PBS) and 300 µL Tyrosinase (6 µM in PBS). The resulting solution was stirred for 30 min at 4 °C, and then extruded (under sterile conditions) 15 times through a polycarbonate (PC) membrane with a 200 nm diameter pore size using an Avanti mini-extruder (Avanti Polar Lipids, Alabama, USA) to unify the size of the polymersomes. The unencapsulated compounds were removed by size-exclusion chromatography (SEC) eluted with cold PBS.

Preparation of control polymersomes: Control polymersomes were prepared as described for Melanin/PDA polymersomes (600 µL of 10 mg/mL $PDMS_{24}$-*b*-$PMOXA_{12}$ solution; 30 min stirring at 4 °C) with the following modifications: empty polymersomes were rehydrated with PBS only; Atto-488 polymersomes were rehydrated with 0.2 mM of Atto-488 in PBS, Dopamine or L-DOPA polymersomes were rehydrated with 300 µL of PBS and 300 µL of Dopamine or L-DOPA (2 mM), respectively.

7.3.4 Physical characterization of polymersomes

Dynamic light scattering (DLS): The apparent diameter D_H values of polymersomes were determined on a Zetasizer Nano ZSP (Malvern Instruments Inc., UK) at 25 °C at an angle of 173°. Each sample was diluted with PBS to 0.1 mg/mL final concentration. A cuvette was filled with 500 µL sample and subjected to 11 measurement runs with three repetitions.

Zeta potential measurements: The electrophoretic mobility of vesicles in solution was determined by means of laser Doppler velocimetry and phase-analysis light-scattering measurements. A Malvern Zetasizer Nano ZSP (Malvern Instruments Inc, UK) with a 633 nm wavelength laser was used for all measurements. The vesicle samples (0.1 mg/mL) were measured in PBS with five repeat measurements per sample. All experiments were run at 25 °C.

Static light scattering (SLS): Multi-angle dynamic light scattering (DLS) and static light scattering (SLS) were performed on a setup from LS Instruments (Switzerland), equipped with a 21 mW He-Ne laser (λ = 632.8 nm) for scattering angles from 30° to 150° at 25 °C. All samples were diluted in order to avoid multiple scattering. Second-order cumulant analysis for various angles was performed to obtain the hydrodynamic radius (Rh). The radius of gyration (Rg) was obtained from the SLS data using a MIE fit.[159]

Transmission electron microscopy (TEM): 5 μL aliquots of polymersomes (0.1 mg/mL) were adsorbed to 400 mesh square copper grids. Excess liquid was blotted and grids were negatively stained with 2% uranyl acetate. Micrographs of nanostructures were recorded on a Philips CM100 transmission electron microscope at an accelerating voltage of 80 kV.

7.3.5 Estimation of Tyrosinase encapsulation efficiency

Tyrosinase polymersomes were produced via film rehydration using 300 μL of PBS and 300 μL of Tyrosinase (6 μM) in the same conditions as for Melanin/PDA polymersomes. The concentration of non-encapsulated Tyrosinase was determined from the fraction of free Tyrosinase present in the solution after SEC purification of Tyrosinase Ncomp. After UV-vis (280 nm) absorbance measurements using a NanoDrop 2000 spectrophotometer (Thermofisher), we determined the amount of Tyrosinase molecules encapsulated for 1 mL of polymersomes ($1.69*10^{13}$) by calculating the difference between the total amount of Tyrosinase used for film

rehydration and the total amount of enzyme that was not encapsulated. In parallel, the concentration of vesicles ($2.1*10^{12}$ vesicles/mL) was determined via single nanoparticle tracking analysis (NTA) using a NanoSight NS300 instrument from Malvern Analytical (Malvern, United Kingdom). The number of encapsulated Tyrosinase molecules was divided by the number of vesicles, obtaining a value of 8 ± 3 Tyrosinase molecules encapsulated per vesicle. An estimation of the percentage of Tyrosinase encapsulated has been calculated to be 9 ± 4 %. After SEC purification, the concentrated Melanin/PDA polymersomes solution (1 mg/mL) was obtained, corresponding to a concentration of Tyrosinase of 0.28 μM.

7.3.6 Estimation of Dopamine and L-DOPA encapsulation efficiency

Control polymersomes enclosing only Dopamine or L-DOPA (see above) were used to assess the number of Dopamine and L-DOPA molecules per polymersome. The concentration of Dopamine of L-DOPA encapsulated in 1 mL of polymersomes (1 mg/mL) was assessed via UV-vis (280 nm) absorbance (SpectraMax ID3 microplate reader, Molecular Devices, U.S.A.), by measuring the unencapsulated Dopamine/L-DOPA obtained after purification of polymersomes. In parallel, the concentration of vesicles (1.9*1012 vesicles/mL for Dopamine polymersomes and 1.9*1012 vesicles/mL for L-DOPA polymersomes) was determined via NTA. The total number of encapsulated molecules was divided by the number of vesicles, obtaining a value of 3.8*104 ± 0.4*104 Dopamine molecules/vesicle and 4.4*104 ± 0.3*104 L-DOPA molecules/vesicle. Considering the initial concentration of Dopamine and L-DOPA used for film rehydration (1 mM), an estimation of the percentage of encapsulation has been calculated to be 13 ± 3 % for Dopamine and 11 ± 5 % for L-DOPA. The concentrated solutions (1 mg/mL) of Dopamine and L-DOPA polymersomes correspond to an estimated concentration of 0.11 mM and of 0.13 mM for Dopamine and L-DOPA, respectively.

7.3.7 Adsorption of L-DOPA/Dopamine on the surface of polymersomes

Empty polymersomes (1 mg/mL) were mixed with L-DOPA/Dopamine (final concentration of 10 μM), with and without tyrosinase (final concentration of 30 nM) and incubated at 37 °C up to 1 week. The concentrations were chosen to correspond to

100 times lower concentrations than what was used form film rehydration of polymersomes. We aimed to reproduce the case figure of if only 1% of compounds was adsorbing on polymersomes' surface or was not eliminated during purification, we would notice because it triggers aggregation of polymersomes.

7.3.8 Melanin/PDA polymerization inside polymersomes

The polydopamine and melanin polymerization within polymersomes was followed up to 24 h days of incubation at 37 °C temperature, via UV-vis (250 – 700 nm) absorbance (SpectraMax ID3 microplate reader, Molecular Devices, U.S.A.). 200 µL of 1 mg/mL polymersomes (directly after their formation) was added in each well of a 96-well microplate (UV-Transparent plates, Corning, USA) and triplicates were measured for each condition. The kinetics of formation of free polydopamine/melanin was not followed with this method as is rapidly led to the sedimentation of aggregates.

7.3.9 Cell culture

HaCatTp5 (keratinocytes) were routinely cultured in Eagle's Minimum Essential Medium (EMEM, Gibco Life Sciences) supplemented with 10% fetal bovine serum (BioConcept), 100 units/mL penicillin and 100 µg/mL Streptomycin (Sigma Aldrich). Cells were maintained in a humidified atmosphere at 37 ^{o}C and 5% CO_2.

7.3.10 Cell viability assay

PrestoBlue cell viability reagent (Invitrogen) was used to determine cell viability. In accordance with the supplier's protocol, HaCatTp5 cells were seeded at a concentration of 7500 cells/well in a 96 well plate. After 24 h, 100 µL of medium was removed and replaced by 75 µL of fresh medium and 25 µL of different polymersomes (2 mg/mL) or PBS. The cells were incubated in the presence of polymersomes or control PBS for 1 more day in a humidified atmosphere at 37 ^{o}C and 5% CO_2. The PrestoBlue reagent (20 µL) was added to each well and fluorescence at 615 nm was measured after 1 h at 37 °C using a Spectramax plate reader. The data was normalized to PBS treated control cells.

7.3.11 Cell viability assay upon UV-irradiation

As described for cell viability assay without UV-irradiation, cells were incubated in presence of polymersomes for 1 day, prior being rinsed with 3 times with 200 µL of PBS to remove non-uptaken polymersomes. Then, 100 µL of PBS was added for UV-irradiation (40 min with UV lamp from the cell hood). After, PBS was removed and 100 µL of fresh media was added and cells incubated overnight. Cell viability was determined using PrestoBlue reagent as previously described for cell viability assay. The data was normalized to cells treated with same kind of polymersomes that have not been irradiated.

7.3.12 Cells imaging

HaCatTp5 cells were seeded and incubated in the same conditions as described for cell viability assay, expect that model polymersomes encapsulating Atto-488 dyes were used. After 24 h of incubation in presence of polymersomes, cells were rinsed 3 times with PBS to get rid of non-uptaken polymersomes before imaging with a Zeiss LSM 880 inverted microscope (Zeiss Axio Observer, Carl Ziss, Germany) with a water immersion objective C-Apochromate 40x/1.2 W korr FCS M27. The beam from 488 nm argon laser was passed through a main beam splitter MBS488 and detection was done at 499-643 nm.

8. References

(1) Meyer, C. E.; Abram, S.-L.; Craciun, I.; Palivan, C. G. Biomolecule–Polymer Hybrid Compartments: Combining the Best of Both Worlds. *Phys. Chem. Chem. Phys.* **2020**, 22, 11197-11218.

(2) Alberts, B.; Johnson, A.; Lewis, J.; Raff, M.; Roberts, K.; Walter, P. The Compartmentalization of Cells. *Mol. Biol. Cell 4th Ed.* **2002**.

(3) Monnard, P. A.; Deamer, D. W. Nutrient Uptake by Protocells: A Liposome Model System. *Orig. Life Evol. Biosphere J. Int. Soc. Study Orig. Life* **2001**, *31*, 147–155.

(4) Riaz, M. K.; Riaz, M. A.; Zhang, X.; Lin, C.; Wong, K. H.; Chen, X.; Zhang, G.; Lu, A.; Yang, Z. Surface Functionalization and Targeting Strategies of Liposomes in Solid Tumor Therapy: A Review. *Int. J. Mol. Sci.* **2018**, *19*.

(5) Rideau, E.; Dimova, R.; Schwille, P.; R. Wurm, F.; Landfester, K. Liposomes and Polymersomes: A Comparative Review towards Cell Mimicking. *Chem. Soc. Rev.* **2018**, *47*, 8572–8610.

(6) Zhang, L.; Eisenberg, A. Multiple Morphologies of "Crew-Cut" Aggregates of Polystyrene-b-Poly(Acrylic Acid) Block Copolymers. *Science* **1995**, *268*, 1728–1731.

(7) Discher, B. M.; Won, Y. Y.; Ege, D. S.; Lee, J. C.; Bates, F. S.; Discher, D. E.; Hammer, D. A. Polymersomes: Tough Vesicles Made from Diblock Copolymers. *Science* **1999**, *284*, 1143–1146.

(8) Itel, F.; Najer, A.; Palivan, C. G.; Meier, W. Dynamics of Membrane Proteins within Synthetic Polymer Membranes with Large Hydrophobic Mismatch. *Nano Lett.* **2015**, *15*, 3871–3878.

(9) Itel, F.; Chami, M.; Najer, A.; Lörcher, S.; Wu, D.; Dinu, I. A.; Meier, W. Molecular Organization and Dynamics in Polymersome Membranes: A Lateral Diffusion Study. *Macromolecules* **2014**, *47*, 7588–7596.

(10) Mohammadi, M.; Ramezani, M.; Abnous, K.; Alibolandi, M. Biocompatible Polymersomes-Based Cancer Theranostics: Towards Multifunctional Nanomedicine. *Int. J. Pharm.* **2017**, *519*, 287–303.

(11) Yao, P.; Zhang, Y.; Meng, H.; Sun, H.; Zhong, Z. Smart Polymersomes Dually Functionalized with CRGD and Fusogenic GALA Peptides Enable Specific and High-Efficiency Cytosolic Delivery of Apoptotic Proteins. *Biomacromolecules* **2019**, *20*, 184–191.

(12) Zou, Y.; Zheng, M.; Yang, W.; Meng, F.; Miyata, K.; Kim, H. J.; Kataoka, K.; Zhong, Z. Virus-Mimicking Chimaeric Polymersomes Boost Targeted Cancer SiRNA Therapy In Vivo. *Adv. Mater.* **2017**, *29*, 1703285.

(13) Axthelm, F.; Casse, O.; Koppenol, W. H.; Nauser, T.; Meier, W.; Palivan, C. G. Antioxidant Nanoreactor Based on Superoxide Dismutase Encapsulated in Superoxide-Permeable Vesicles. *J. Phys. Chem. B* **2008**, *112*, 8211–8217.

(14) Nishimura, T.; Sasaki, Y.; Akiyoshi, K. Biotransporting Self-Assembled Nanofactories Using Polymer Vesicles with Molecular Permeability for Enzyme Prodrug Cancer Therapy. *Adv. Mater.* **2017**, *29*, 1702406.

(15) Thamboo, S.; Najer, A.; Belluati, A.; Planta, C. von; Wu, D.; Craciun, I.; Meier, W.; Palivan, C. G. Mimicking Cellular Signaling Pathways within Synthetic

Multicompartment Vesicles with Triggered Enzyme Activity and Induced Ion Channel Recruitment. *Adv. Funct. Mater.* **2019**, *29*, 1904267.
(16) Belluati, A.; Thamboo, S.; Najer, A.; Maffeis, V.; Planta, C. von; Craciun, I.; Palivan, C. G.; Meier, W. Multicompartment Polymer Vesicles with Artificial Organelles for Signal-Triggered Cascade Reactions Including Cytoskeleton Formation. *Adv. Funct. Mater.* **2020**, *30*, 2002949.
(17) Santos, E. C. dos; Belluati, A.; Necula, D.; Scherrer, D.; Meyer, C. E.; Wehr, R. P.; Lörtscher, E.; Palivan, C. G.; Meier, W. Combinatorial Strategy for Studying Biochemical Pathways in Double Emulsion Templated Cell-Sized Compartments. *Adv. Mater.* **2020**, *32*, 2004804.
(18) Koide, A.; Kishimura, A.; Osada, K.; Jang, W.-D.; Yamasaki, Y.; Kataoka, K. Semipermeable Polymer Vesicle (PICsome) Self-Assembled in Aqueous Medium from a Pair of Oppositely Charged Block Copolymers: Physiologically Stable Micro-/Nanocontainers of Water-Soluble Macromolecules. *J. Am. Chem. Soc.* **2006**, *128*, 5988–5989.
(19) Kishimura, A. Development of Polyion Complex Vesicles (PICsomes) from Block Copolymers for Biomedical Applications. *Polym. J.* **2013**, *45*, 892–897.
(20) Anraku, Y.; Kishimura, A.; Oba, M.; Yamasaki, Y.; Kataoka, K. Spontaneous Formation of Nanosized Unilamellar Polyion Complex Vesicles with Tunable Size and Properties. *J. Am. Chem. Soc.* **2010**, *132*, 1631–1636.
(21) Mercato, L. L. del; Rivera-Gil, P.; Abbasi, A. Z.; Ochs, M.; Ganas, C.; Zins, I.; Sönnichsen, C.; Parak, W. J. LbL Multilayer Capsules: Recent Progress and Future Outlook for Their Use in Life Sciences. *Nanoscale* **2010**, *2*, 458–467.
(22) Kulygin, O.; Price, A. D.; Chong, S.-F.; Städler, B.; Zelikin, A. N.; Caruso, F. Subcompartmentalized Polymer Hydrogel Capsules with Selectively Degradable Carriers and Subunits. *Small* **2010**, *6*, 1558–1564.
(23) Garni, M.; Wehr, R.; Avsar, S. Y.; John, C.; Palivan, C.; Meier, W. Polymer Membranes as Templates for Bio-Applications Ranging from Artificial Cells to Active Surfaces. *Eur. Polym. J.* **2019**, *112*, 346–364.
(24) Feng, H.; Lu, X.; Wang, W.; Kang, N.-G.; Mays, J. W. Block Copolymers: Synthesis, Self-Assembly, and Applications. *Polymers* **2017**, *9*.
(25) LoPresti, C.; Lomas, H.; Massignani, M.; Smart, T.; Battaglia, G. Polymersomes: Nature Inspired Nanometer Sized Compartments. *J. Mater. Chem.* **2009**, *19*, 3576–3590.
(26) LoPresti, C.; Massignani, M.; Fernyhough, C.; Blanazs, A.; Ryan, A. J.; Madsen, J.; Warren, N. J.; Armes, S. P.; Lewis, A. L.; Chirasatitsin, S.; Engler, A. J.; Battaglia, G. Controlling Polymersome Surface Topology at the Nanoscale by Membrane Confined Polymer/Polymer Phase Separation. *ACS Nano* **2011**, *5*, 1775–1784.
(27) Konishcheva, E. V.; Zhumaev, U. E.; Meier, W. P. PEO-b-PCL-b-PMOXA Triblock Copolymers: From Synthesis to Microscale Polymersomes with Asymmetric Membrane. *Macromolecules* **2017**, *50*, 1512–1520.
(28) Austen Angell, C.; Sivarajan, S. Glass Transition☆. In *Reference Module in Materials Science and Materials Engineering*; Elsevier, 2017.
(29) Peters, R. J. R. W.; Marguet, M.; Marais, S.; Fraaije, M. W.; van Hest, J. C. M.; Lecommandoux, S. Cascade Reactions in Multicompartmentalized Polymersomes. *Angew. Chem. Int. Ed Engl.* **2014**, *53*, 146–150.
(30) Mai, Y.; Eisenberg, A. Self-Assembly of Block Copolymers. *Chem. Soc. Rev.* **2012**, *41*, 5969–5985.

(31) Blanazs, A.; Armes, S. P.; Ryan, A. J. Self-Assembled Block Copolymer Aggregates: From Micelles to Vesicles and Their Biological Applications. *Macromol. Rapid Commun.* **2009**, *30*, 267–277.
(32) Smart, T.; Lomas, H.; Massignani, M.; Flores-Merino, M. V.; Perez, L. R.; Battaglia, G. Block Copolymer Nanostructures. *Nano Today* **2008**, *3*, 38–
(33) Discher, D. E.; Ahmed, F. Polymersomes. *Annu. Rev. Biomed. Eng.* **2006**, *8*, 323–341.
(34) Wu, D.; Spulber, M.; Itel, F.; Chami, M.; Pfohl, T.; Palivan, C. G.; Meier, W. Effect of Molecular Parameters on the Architecture and Membrane Properties of 3D Assemblies of Amphiphilic Copolymers. *Macromolecules* **2014**, *47*, 5060–5069.
(35) Dionzou, M.; Morère, A.; Roux, C.; Lonetti, B.; Marty, J.-D.; Mingotaud, C.; Joseph, P.; Goudounèche, D.; Payré, B.; Léonetti, M.; Mingotaud, A.-F. Comparison of Methods for the Fabrication and the Characterization of Polymer Self-Assemblies: What Are the Important Parameters? *Soft Matter* **2016**, *12*, 2166–2176.
(36) Li, F.; Danquah, M.; Mahato, R. I. Synthesis and Characterization of Amphiphilic Lipopolymers for Micellar Drug Delivery. *Biomacromolecules* **2010**, *11*, 2610–2620.
(37) Battaglia, G.; Ryan, A. J. Effect of Amphiphile Size on the Transformation from a Lyotropic Gel to a Vesicular Dispersion. *Macromolecules* **2006**, *39*, 798–805.
(38) O'Neil, C. P.; Suzuki, T.; Demurtas, D.; Finka, A.; Hubbell, J. A. A Novel Method for the Encapsulation of Biomolecules into Polymersomes via Direct Hydration. *Langmuir* **2009**, *25*, 9025–9029.
(39) Peyret, A.; Ibarboure, E.; Meins, J.-F. L.; Lecommandoux, S. Asymmetric Hybrid Polymer–Lipid Giant Vesicles as Cell Membrane Mimics. *Adv. Sci.* **2018**, *5*, 1700453.
(40) Peyret, A.; Ibarboure, E.; Pippa, N.; Lecommandoux, S. Liposomes in Polymersomes: Multicompartment System with Temperature-Triggered Release. *Langmuir ACS J. Surf. Colloids* **2017**, *33*, 7079–7085.
(41) Pourtau, L.; Oliveira, H.; Thevenot, J.; Wan, Y.; Brisson, A. R.; Sandre, O.; Miraux, S.; Thiaudiere, E.; Lecommandoux, S. Antibody-Functionalized Magnetic Polymersomes: In Vivo Targeting and Imaging of Bone Metastases Using High Resolution MRI. *Adv. Healthc. Mater.* **2013**, *2*, 1420–1424.
(42) Karandish, F.; Froberg, J.; Borowicz, P.; Wilkinson, J. C.; Choi, Y.; Mallik, S. Peptide-Targeted, Stimuli-Responsive Polymersomes for Delivering a Cancer Stemness Inhibitor to Cancer Stem Cell Microtumors. *Colloids Surf. B Biointerfaces* **2018**, *163*, 225–235.
(43) Anajafi, T.; Yu, J.; Sedigh, A.; Haldar, M. K.; Muhonen, W. W.; Oberlander, S.; Wasness, H.; Froberg, J.; Molla, M. S.; Katti, K. S.; Choi, Y.; Shabb, J. B.; Srivastava, D. K.; Mallik, S. Nuclear Localizing Peptide-Conjugated, Redox-Sensitive Polymersomes for Delivering Curcumin and Doxorubicin to Pancreatic Cancer Microtumors. *Mol. Pharm.* **2017**, *14*, 1916–1928.
(44) Jia, T.; Sun, Z.; Lu, Y.; Gao, J.; Zou, H.; Xie, F.; Zhang, G.; Xu, H.; Sun, D.; Yu, Y.; Zhong, Y. A Dual Brain-Targeting Curcumin-Loaded Polymersomes Ameliorated Cognitive Dysfunction in Intrahippocampal Amyloid-B1–42-Injected Mice. *Int. J. Nanomedicine* **2016**, *11*, 3765–3775.
(45) Yang, W.; Xia, Y.; Fang, Y.; Meng, F.; Zhang, J.; Cheng, R.; Deng, C.; Zhong, Z. Selective Cell Penetrating Peptide-Functionalized Polymersomes Mediate

Efficient and Targeted Delivery of Methotrexate Disodium to Human Lung Cancer In Vivo. *Adv. Healthc. Mater.* **2018**, *7*, 1701135.
(46) Chen, J.; Liu, Q.; Xiao, J.; Du, J. EpCAM-Antibody-Labeled Noncytotoxic Polymer Vesicles for Cancer Stem Cells-Targeted Delivery of Anticancer Drug and SiRNA. *Biomacromolecules* **2015**, *16*, 1695–1705.
(47) Kulkarni, P.; Haldar, M. K.; Karandish, F.; Confeld, M.; Hossain, R.; Borowicz, P.; Gange, K.; Xia, L.; Sarkar, K.; Mallik, S. Tissue-Penetrating, Hypoxia-Responsive Echogenic Polymersomes For Drug Delivery To Solid Tumors. *Chem. – Eur. J.* **2018**, *24*, 12490–12494.
(48) Simón-Gracia, L.; Scodeller, P.; Fuentes, S. S.; Vallejo, V. G.; Ríos, X.; Sebastián, E. S.; Silvio, D. D.; Suck, M.; Lorenzi, F. D.; Rizzo, L. Y.; Stillfried, S. von; Kilk, K.; Lammers, T.; Moya, S. E.; Teesalu, T. Detection of Small Breast Tumors Using Tumor Penetrating-Polymersomes Engineered to Target P32 Protein. *bioRxiv* **2017**, 187716.
(49) Fang, Y.; Yang, W.; Cheng, L.; Meng, F.; Zhang, J.; Zhong, Z. EGFR-Targeted Multifunctional Polymersomal Doxorubicin Induces Selective and Potent Suppression of Orthotopic Human Liver Cancer in Vivo. *Acta Biomater.* **2017**, *64*, 323–333.
(50) Jiang, Y.; Zhang, J.; Meng, F.; Zhong, Z. Apolipoprotein E Peptide-Directed Chimeric Polymersomes Mediate an Ultrahigh-Efficiency Targeted Protein Therapy for Glioblastoma. *ACS Nano* **2018**, *12*, 11070–11079.
(51) Zelmer, C.; Zweifel, L. P.; Kapinos, L. E.; Craciun, I.; Güven, Z. P.; Palivan, C. G.; Lim, R. Y. H. Organelle-Specific Targeting of Polymersomes into the Cell Nucleus. *Proc. Natl. Acad. Sci.* **2020**, *117*, 2770–2778.
(52) Wei, Y.; Gu, X.; Cheng, L.; Meng, F.; Storm, G.; Zhong, Z. Low-Toxicity Transferrin-Guided Polymersomal Doxorubicin for Potent Chemotherapy of Orthotopic Hepatocellular Carcinoma in Vivo. *Acta Biomater.* **2019**, *92*, 196–204.
(53) Yu, Y.; Jiang, X.; Gong, S.; Feng, L.; Zhong, Y.; Pang, Z. The Proton Permeability of Self-Assembled Polymersomes and Their Neuroprotection by Enhancing a Neuroprotective Peptide across the Blood–Brain Barrier after Modification with Lactoferrin. *Nanoscale* **2014**, *6*, 3250–3258.
(54) Xiao, Y.; Sun, H.; Du, J. Sugar-Breathing Glycopolymersomes for Regulating Glucose Level. *J. Am. Chem. Soc.* **2017**, *139*, 7640–7647.
(55) Klermund, L.; Poschenrieder, S. T.; Castiglione, K. Simple Surface Functionalization of Polymersomes Using Non-Antibacterial Peptide Anchors. *J. Nanobiotechnology* **2016**, *14*, 48.
(56) Alibolandi, M.; Ramezani, M.; Abnous, K.; Hadizadeh, F. AS1411 Aptamer-Decorated Biodegradable Polyethylene Glycol–Poly(Lactic-Co-Glycolic Acid) Nanopolymersomes for the Targeted Delivery of Gemcitabine to Non–Small Cell Lung Cancer In Vitro. *J. Pharm. Sci.* **2016**, *105*, 1741–1750.
(57) Li, X.; Zhu, X.; Qiu, L. Constructing Aptamer Anchored Nanovesicles for Enhanced Tumor Penetration and Cellular Uptake of Water Soluble Chemotherapeutics. *Acta Biomater.* **2016**, *35*, 269–279.
(58) Liu, J.; Postupalenko, V.; Lörcher, S.; Wu, D.; Chami, M.; Meier, W.; Palivan, C. G. DNA-Mediated Self-Organization of Polymeric Nanocompartments Leads to Interconnected Artificial Organelles. *Nano Lett.* **2016**, *16*, 7128–7136.
(59) Lomas, H.; Du, J.; Canton, I.; Madsen, J.; Warren, N.; Armes, S. P.; Lewis, A. L.; Battaglia, G. Efficient Encapsulation of Plasmid DNA in PH-Sensitive PMPC–PDPA Polymersomes: Study of the Effect of PDPA Block Length on Copolymer–DNA Binding Affinity. *Macromol. Biosci.* **2010**, *10* (5), 513–530.

(60) Wang, F.; Gao, J.; Xiao, J.; Du, J. Dually Gated Polymersomes for Gene Delivery. *Nano Lett.* **2018**, *18*, 5562–5568.
(61) Belluati, A.; Craciun, I.; Meyer, C. E.; Rigo, S.; Palivan, C. G. Enzymatic Reactions in Polymeric Compartments: Nanotechnology Meets Nature. *Curr. Opin. Biotechnol.* **2019**, *60*, 53–62.
(62) Dobrunz, D.; Toma, A. C.; Tanner, P.; Pfohl, T.; Palivan, C. G. Polymer Nanoreactors with Dual Functionality: Simultaneous Detoxification of Peroxynitrite and Oxygen Transport. *Langmuir* **2012**, *28*, 15889–15899.
(63) Belluati, A.; Craciun, I.; Liu, J.; Palivan, C. G. Nanoscale Enzymatic Compartments in Tandem Support Cascade Reactions in Vitro. *Biomacromolecules* **2018**, *19*, 4023–4033.
(64) Hvasanov, D.; Peterson, J. R.; Thordarson, P. Self-Assembled Light-Driven Photosynthetic-Respiratory Electron Transport Chain Hybrid Proton Pump. *Chem. Sci.* **2013**, *4*, 3833–3838.
(65) Tanner, P.; Balasubramanian, V.; Palivan, C. G. Aiding Nature's Organelles: Artificial Peroxisomes Play Their Role. *Nano Lett.* **2013**, *13*, 2875–2883.
(66) Langowska, K.; Kowal, J.; Palivan, C. G.; Meier, W. A General Strategy for Creating Self-Defending Surfaces for Controlled Drug Production for Long Periods of Time. *J. Mater. Chem. B* **2014**, *2*, 4684–4693.
(67) Palivan, C. G.; Goers, R.; Najer, A.; Zhang, X.; Car, A.; Meier, W. Bioinspired Polymer Vesicles and Membranes for Biological and Medical Applications. *Chem. Soc. Rev.* **2016**, *45*, 377–411.
(68) van Dongen, S. F. M.; Nallani, M.; Cornelissen, J. J. L. M.; Nolte, R. J. M.; van Hest, J. C. M. A Three-Enzyme Cascade Reaction through Positional Assembly of Enzymes in a Polymersome Nanoreactor. *Chem. – Eur. J.* **2009**, *15*, 1107–1114.
(69) Chen, Q.; Schönherr, H.; Vancso, G. J. Block-Copolymer Vesicles as Nanoreactors for Enzymatic Reactions. *Small Weinh. Bergstr. Ger.* **2009**, *5*, 1436–1445.
(70) Siti, W.; Hoog, H.-P. M. de; Fischer, O.; Yee Shan, W.; Tomczak, N.; Nallani, M.; Liedberg, B. An Intercompartmental Enzymatic Cascade Reaction in Channel-Equipped Polymersome-in-Polymersome Architectures. *J. Mater. Chem. B* **2014**, *2*, 2733–2737.
(71) Baumann, P.; Spulber, M.; Fischer, O.; Car, A.; Meier, W. Investigation of Horseradish Peroxidase Kinetics in an "Organelle-Like" Environment. *Small* **2017**, *13*, 1603943.
(72) Lomora, M.; Garni, M.; Itel, F.; Tanner, P.; Spulber, M.; Palivan, C. G. Polymersomes with Engineered Ion Selective Permeability as Stimuli-Responsive Nanocompartments with Preserved Architecture. *Biomaterials* **2015**, *53*, 406–414.
(73) Kim, H.-O.; Lim, J.-W.; Choi, J.; Lee, H.; Son, H. Y.; Kim, J.; Park, G.; Chun, H.; Song, D.; Huh, Y.-M.; Haam, S. Anchored Protease-Activatable Polymersomes for Molecular Diagnostics of Metastatic Cancer Cells. *J. Mater. Chem. B* **2017**, *5*, 9571–9578.
(74) Liu, Z.; Dong, C.; Wang, X.; Wang, H.; Li, W.; Tan, J.; Chang, J. Self-Assembled Biodegradable Protein–Polymer Vesicle as a Tumor-Targeted Nanocarrier. *ACS Appl. Mater. Interfaces* **2014**, *6*, 2393–2400.
(75) Liu, X.; Gao, W. In Situ Growth of Self-Assembled Protein–Polymer Nanovesicles for Enhanced Intracellular Protein Delivery. *ACS Appl. Mater. Interfaces* **2017**, *9*, 2023–2028.

(76) Reynhout, I. C.; Cornelissen, J. J. L. M.; Nolte, R. J. M. Self-Assembled Architectures from Biohybrid Triblock Copolymers. *J. Am. Chem. Soc.* **2007**, *129*, 2327–2332.
(77) Einfalt, T.; Goers, R.; Dinu, I. A.; Najer, A.; Spulber, M.; Onaca-Fischer, O.; Palivan, C. G. Stimuli-Triggered Activity of Nanoreactors by Biomimetic Engineering Polymer Membranes. *Nano Lett.* **2015**, *15*, 7596–7603.
(78) Edlinger, C.; Einfalt, T.; Spulber, M.; Car, A.; Meier, W.; Palivan, C. G. Biomimetic Strategy To Reversibly Trigger Functionality of Catalytic Nanocompartments by the Insertion of PH-Responsive Biovalves. *Nano Lett.* **2017**, *17*, 5790–5798.
(79) Stoenescu, R.; Graff, A.; Meier, W. Asymmetric ABC-Triblock Copolymer Membranes Induce a Directed Insertion of Membrane Proteins. *Macromol. Biosci.* **2004**, *4*, 930–935.
(80) Lomora, M.; Gunkel-Grabole, G.; Mantri, S.; Palivan, C. G. Bio-Catalytic Nanocompartments for in Situ Production of Glucose-6-Phosphate. *Chem. Commun.* **2017**, *53*, 10148–10151.
(81) Choi, H.-J.; Germain, J.; Montemagno, C. D. Effects of Different Reconstitution Procedures on Membrane Protein Activities in Proteopolymersomes. *Nanotechnology* **2006**, *17*, 1825–1830.
(82) Kumar, M.; Grzelakowski, M.; Zilles, J.; Clark, M.; Meier, W. Highly Permeable Polymeric Membranes Based on the Incorporation of the Functional Water Channel Protein Aquaporin Z. *Proc. Natl. Acad. Sci. U. S. A.* **2007**, *104*, 20719–20724.
(83) Goers, R.; Thoma, J.; Ritzmann, N.; Silvestro, A. D.; Alter, C.; Gunkel-Grabole, G.; Fotiadis, D.; Müller, D. J.; Meier, W. Optimized Reconstitution of Membrane Proteins into Synthetic Membranes. *Commun. Chem.* **2018**, *1*, 35.
(84) You, L.; Schlaad, H. An Easy Way to Sugar-Containing Polymer Vesicles or Glycosomes. *J. Am. Chem. Soc.* **2006**, *128*, 13336–13337.
(85) Pasparakis, G.; Alexander, C. Sweet Talking Double Hydrophilic Block Copolymer Vesicles. *Angew. Chem. Int. Ed.* **2008**, *47*, 4847–4850.
(86) Su, L.; Zhao, Y.; Chen, G.; Jiang, M. Polymeric Vesicles Mimicking Glycocalyx (PV-Gx) for Studying Carbohydrate–Protein Interactions in Solution. *Polym. Chem.* **2012**, *3*, 1560–1566.
(87) Haas, S.; Hain, N.; Raoufi, M.; Handschuh-Wang, S.; Wang, T.; Jiang, X.; Schönherr, H. Enzyme Degradable Polymersomes from Hyaluronic Acid-Block-Poly(ε-Caprolactone) Copolymers for the Detection of Enzymes of Pathogenic Bacteria. *Biomacromolecules* **2015**, *16*, 832–841.
(88) Panneerselvam, K.; Lynge, M. E.; Riber, C. F.; Mena-Hernando, S.; Smith, A. A. A.; Goldie, K. N.; Zelikin, A. N.; Städler, B. Phospholipid—Polymer Amphiphile Hybrid Assemblies and Their Interaction with Macrophages. *Biomicrofluidics* **2015**, *9* 5.
(89) Zong, W.; Thingholm, B.; Itel, F.; Schattling, P. S.; Brodszkij, E.; Mayer, D.; Stenger, S.; Goldie, K. N.; Han, X.; Städler, B. Phospholipid–Block Copolymer Hybrid Vesicles with Lysosomal Escape Ability. *Langmuir* **2018**, *34*, 6874–6886.
(90) Schulz, M.; Binder, W. H. Mixed Hybrid Lipid/Polymer Vesicles as a Novel Membrane Platform. *Macromol. Rapid Commun.* **2015**, *36*, 2031–2041.
(91) Nam, J.; Kyle Vanderlick, T.; A. Beales, P. Formation and Dissolution of Phospholipid Domains with Varying Textures in Hybrid Lipo-Polymersomes. *Soft Matter* **2012**, *8*, 7982–7988.

(92) Chemin, M.; Brun, P.-M.; Lecommandoux, S.; Sandre, O.; Meins, J.-F. L. Hybrid Polymer/Lipid Vesicles: Fine Control of the Lipid and Polymer Distribution in the Binary Membrane. *Soft Matter* **2012**, *8*, 2867–2874.
(93) Lim, S. K.; De Hoog, H.-P.; Parikh, A. N.; Nallani, M.; Liedberg, B. Hybrid, Nanoscale Phospholipid/Block Copolymer Vesicles. *Polymers* **2013**, *5*, 1102–1114.
(94) Paxton, W. F.; McAninch, P. T.; Achyuthan, K. E.; Shin, S. H. R.; Monteith, H. L. Monitoring and Modulating Ion Traffic in Hybrid Lipid/Polymer Vesicles. *Colloids Surf. B Biointerfaces* **2017**, *159*, 268–276.
(95) Khan, S.; Li, M.; Muench, S. P.; Jeuken, L. J. C.; Beales, P. A. Durable Proteo-Hybrid Vesicles for the Extended Functional Lifetime of Membrane Proteins in Bionanotechnology. *Chem. Commun.* **2016**, *52*, 11020–11023.
(96) Khan, S.; McCabe, J.; Hill, K.; Beales, P. A. Biodegradable Hybrid Block Copolymer – Lipid Vesicles as Potential Drug Delivery Systems. *J. Colloid Interface Sci.* **2020**, *562*, 418–428.
(97) Pippa, N.; Stellas, D.; Skandalis, A.; Pispas, S.; Demetzos, C.; Libera, M.; Marcinkowski, A.; Trzebicka, B. Chimeric Lipid/Block Copolymer Nanovesicles: Physico-Chemical and Bio-Compatibility Evaluation. *Eur. J. Pharm. Biopharm.* **2016**, *107*, 295–309.
(98) Zong, W.; Hu, Y.; Su, Y.; Luo, N.; Zhang, X.; Li, Q.; Han, X. Polydopamine-Coated Liposomes as PH-Sensitive Anticancer Drug Carriers. *J. Microencapsul.* **2016**, *33*, 257–262.
(99) Li, J.; Li, Y.; Wang, Y.; Ke, W.; Chen, W.; Wang, W.; Ge, Z. Polymer Prodrug-Based Nanoreactors Activated by Tumor Acidity for Orchestrated Oxidation/Chemotherapy. *Nano Lett.* **2017**, *17*, 6983–6990.
(100) Belluati, A.; Craciun, I.; Palivan, C. G. Bioactive Catalytic Nanocompartments Integrated into Cell Physiology and Their Amplification of a Native Signaling Cascade. *ACS Nano* **2020**, *14*, 12101–12112.
(101) Cheng, Z.; Elias, D. R.; Kamat, N. P.; Johnston, E. D.; Poloukhtine, A.; Popik, V.; Hammer, D. A.; Tsourkas, A. Improved Tumor Targeting of Polymer-Based Nanovesicles Using Polymer–Lipid Blends. *Bioconjug. Chem.* **2011**, *22*, 2021–2029.
(102) Sueyoshi, D.; Anraku, Y.; Komatsu, T.; Urano, Y.; Kataoka, K. Enzyme-Loaded Polyion Complex Vesicles as in Vivo Nanoreactors Working Sustainably under the Blood Circulation: Characterization and Functional Evaluation. *Biomacromolecules* **2017**, *18*, 1189–1196.
(103) Anraku, Y.; Kishimura, A.; Kamiya, M.; Tanaka, S.; Nomoto, T.; Toh, K.; Matsumoto, Y.; Fukushima, S.; Sueyoshi, D.; Kano, M. R.; Urano, Y.; Nishiyama, N.; Kataoka, K. Systemically Injectable Enzyme-Loaded Polyion Complex Vesicles as In Vivo Nanoreactors Functioning in Tumors. *Angew. Chem. Int. Ed Engl.* **2016**, *55*, 560–565.
(104) Kawamura, W.; Miura, Y.; Kokuryo, D.; Toh, K.; Yamada, N.; Nomoto, T.; Matsumoto, Y.; Sueyoshi, D.; Liu, X.; Aoki, I.; Kano, M. R.; Nishiyama, N.; Saga, T.; Kishimura, A.; Kataoka, K. Density-Tunable Conjugation of Cyclic RGD Ligands with Polyion Complex Vesicles for the Neovascular Imaging of Orthotopic Glioblastomas. *Sci. Technol. Adv. Mater.* **2015**, *16*.
(105) Richardson, J. J.; Choy, M. Y.; Guo, J.; Liang, K.; Alt, K.; Ping, Y.; Cui, J.; Law, L. S.; Hagemeyer, C. E.; Caruso, F. Polymer Capsules for Plaque-Targeted In Vivo Delivery. *Adv. Mater.* **2016**, *28*, 7703–7707.
(106) Anajafi, T.; Mallik, S. Polymersome-Based Drug-Delivery Strategies for Cancer Therapeutics. *Ther. Deliv.* **2015**, *6* (4), 521–534.

(107) Matoori, S.; Leroux, J.-C. Twenty-Five Years of Polymersomes: Lost in Translation? *Mater. Horiz.* **2020**, *7*, 1297–1309.
(108) Meyer, C. E.; Liu, J.; Craciun, I.; Wu, D.; Wang, H.; Xie, M.; Fussenegger, M.; Palivan, C. G. Segregated Nanocompartments Containing Therapeutic Enzymes and Imaging Compounds within DNA-Zipped Polymersome Clusters for Advanced Nanotheranostic Platform. *Small* **2020**, *16*, 1906492.
(109) Meyer, C. E.; Schoenenberger, C.-A.; Liu, J.; Craciun, I.; Palivan, C. G. DNA-Tethered Polymersome Clusters as Nanotheranostic Platform. *Chimia* **2021**.
(110) Lim, E.-K.; Kim, T.; Paik, S.; Haam, S.; Huh, Y.-M.; Lee, K. Nanomaterials for Theranostics: Recent Advances and Future Challenges. *Chem. Rev.* **2015**, *115*, 327–394.
(111) Wang, J.; Wang, X.; Song, Y.; Wang, J.; Zhang, C.; Chang, C.; Yan, J.; Qiu, L.; Wu, M.; Guo, Z. A Platinum Anticancer Theranostic Agent with Magnetic Targeting Potential Derived from Maghemite Nanoparticles. *Chem. Sci.* **2013**, *4*, 2605–2612.
(112) Upponi, J. R.; Jerajani, K.; Nagesha, D. K.; Kulkarni, P.; Sridhar, S.; Ferris, C.; Torchilin, V. P. Polymeric Micelles: Theranostic Co-Delivery System for Poorly Water-Soluble Drugs and Contrast Agents. *Biomaterials* **2018**, *170*, 26–36.
(113) Zartner, L.; Muthwill, M. S.; Dinu, I. A.; Schoenenberger, C.-A.; Palivan, C. G. The Rise of Bio-Inspired Polymer Compartments Responding to Pathology-Related Signals. *J. Mater. Chem. B* **2020**, *8*, 6252–6270.
(114) Lee, W.; Im, H.-J. Theranostics Based on Liposome: Looking Back and Forward. *Nucl. Med. Mol. Imaging* **2019**, *53*, 242–246.
(115) Yang, N.; You, T.-T.; Liang, X.; Zhang, C.-M.; Jiang, L.; Yin, P.-G. An Ultrasensitive Near-Infrared Satellite SERS Sensor: DNA Self-Assembled Gold Nanorod/Nanospheres Structure. *RSC Adv.* **2017**, *7*, 9321–9327.
(116) Loh, X. J.; Lee, T.-C.; Dou, Q.; Deen, G. R. Utilising Inorganic Nanocarriers for Gene Delivery. *Biomater. Sci.* **2016**, *4*, 70–86.
(117) Kim, J.-B.; Urban, K.; Cochran, E.; Lee, S.; Ang, A.; Rice, B.; Bata, A.; Campbell, K.; Coffee, R.; Gorodinsky, A.; Lu, Z.; Zhou, H.; Kishimoto, T. K.; Lassota, P. Non-Invasive Detection of a Small Number of Bioluminescent Cancer Cells In Vivo. *PLoS ONE* **2010**, *5*.
(118) Liu, J.; Craciun, I.; Belluati, A.; Wu, D.; Sieber, S.; Einfalt, T.; Witzigmann, D.; Chami, M.; Huwyler, J.; Palivan, C. G. DNA-Directed Arrangement of Soft Synthetic Compartments and Their Behavior in Vitro and in Vivo. *Nanoscale* **2020**, *12*, 9786–9799.
(119) Rössger, K.; Hamri, G. C.-E.; Fussenegger, M. Reward-Based Hypertension Control by a Synthetic Brain–Dopamine Interface. *Proc. Natl. Acad. Sci.* **2013**, *110*, 18150–18155.
(120) Einfalt, T.; Witzigmann, D.; Edlinger, C.; Sieber, S.; Goers, R.; Najer, A.; Spulber, M.; Onaca-Fischer, O.; Huwyler, J.; Palivan, C. G. Biomimetic Artificial Organelles with in Vitro and in Vivo Activity Triggered by Reduction in Microenvironment. *Nat. Commun.* **2018**, *9*, 1–12.
(121) Sletten, E. M.; Bertozzi, C. R. From Mechanism to Mouse: A Tale of Two Bioorthogonal Reactions. *Acc. Chem. Res.* **2011**, *44*, 666–676.
(122) Liu, J.; Postupalenko, V.; Lörcher, S.; Wu, D.; Chami, M.; Meier, W.; Palivan, C. G. DNA-Mediated Self-Organization of Polymeric Nanocompartments Leads to Interconnected Artificial Organelles. *Nano Lett.* **2016**, *16*, 7128–7136.
(123) Kefala, G.; Ahn, C.; Krupa, M.; Esquivies, L.; Maslennikov, I.; Kwiatkowski, W.; Choe, S. Structures of the OmpF Porin Crystallized in the Presence of Foscholine-12. *Protein Sci.* **2010**, *19*, 1117–1125.

(124) Pons, R.; Ford, B.; Chiriboga, C. A.; Clayton, P. T.; Hinton, V.; Hyland, K.; Sharma, R.; Vivo, D. C. D. Aromatic L-Amino Acid Decarboxylase Deficiency: Clinical Features, Treatment, and Prognosis. *Neurology* **2004**, *62*, 1058–1065.
(125) Najer, A.; Wu, D.; Bieri, A.; Brand, F.; Palivan, C. G.; Beck, H.-P.; Meier, W. Nanomimics of Host Cell Membranes Block Invasion and Expose Invasive Malaria Parasites. *ACS Nano* **2014**, *8*, 12560–12571.
(126) Belluati, A.; Craciun, I.; Liu, J.; Palivan, C. G. Nanoscale Enzymatic Compartments in Tandem Support Cascade Reactions in Vitro. *Biomacromolecules* **2018**, *19*, 4023–4033.
(127) Bs, C.; Rr, M. Enzyme Thermostabilization by Bovine Serum Albumin and Other Proteins: Evidence for Hydrophobic Interactions. *Biotechnol. Appl. Biochem.* **1995**, *22*, 203–214.
(128) Giardina, G.; Montioli, R.; Gianni, S.; Cellini, B.; Paiardini, A.; Voltattorni, C. B.; Cutruzzolà, F. Open Conformation of Human DOPA Decarboxylase Reveals the Mechanism of PLP Addition to Group II Decarboxylases. *Proc. Natl. Acad. Sci.* **2011**, *108*, 20514–20519.
(129) Mai, Y.; Eisenberg, A. Self-Assembly of Block Copolymers. *Chem. Soc. Rev.* **2012**, *41*, 5969–5985.
(130) Thakkar, S. V.; Allegre, K. M.; Joshi, S. B.; Volkin, D. B.; Middaugh, C. R. An Application of Ultraviolet Spectroscopy to Study Interactions in Proteins Solutions at High Concentrations. *J. Pharm. Sci.* **2012**, *101*, 3051–3061.
(131) Xu, H.; Yao, N.; Xu, H.; Wang, T.; Li, G.; Li, Z. Characterization of the Interaction between Eupatorin and Bovine Serum Albumin by Spectroscopic and Molecular Modeling Methods. *Int. J. Mol. Sci.* **2013**, *14*, 14185–14203.
(132) Suryawanshi, V. D.; Walekar, L. S.; Gore, A. H.; Anbhule, P. V.; Kolekar, G. B. Spectroscopic Analysis on the Binding Interaction of Biologically Active Pyrimidine Derivative with Bovine Serum Albumin. *J. Pharm. Anal.* **2016**, *6*, 56–63.
(133) Gjedde, A.; Reith, J.; Dyve, S.; Léger, G.; Guttman, M.; Diksic, M.; Evans, A.; Kuwabara, H. Dopa Decarboxylase Activity of the Living Human Brain. *Proc. Natl. Acad. Sci.* **1991**, *88*, 2721–2725.
(134) Asanuma, M.; Miyazaki, I.; Ogawa, N. Dopamine- or L-DOPA-Induced Neurotoxicity: The Role of Dopamine Quinone Formation and Tyrosinase in a Model of Parkinson's Disease. *Neurotox. Res.* **2003**, *5*, 165–176.
(135) Lee, H.; Dellatore, S. M.; Miller, W. M.; Messersmith, P. B. Mussel-Inspired Surface Chemistry for Multifunctional Coatings. *Science* **2007**, *318*, 426–430.
(136) Meister, A.; Anderson, M. E. Glutathione. *Annu. Rev. Biochem.* **1983**, *52*, 711–760.
(137) Zhou, Z. D.; Lim, T. M. Roles of Glutathione (GSH) in Dopamine (DA) Oxidation Studied by Improved Tandem HPLC Plus ESI-MS. *Neurochem. Res.* **2009**, *34*, 316–326.
(138) Chierico, D. C. L.; Tian, X.; Kluthe, K.; Poma, A.; Ruiz-Pérez, L.; LoPresti, C.; Battaglia, G. Protein Structure, Activity and Thermal Stability within Nanoscopic Compartments. *ArXiv160708886 Q-Bio* **2019**.
(139) Platt, N.; Gordon, S. Scavenger Receptors: Diverse Activities and Promiscuous Binding of Polyanionic Ligands. *Chem. Biol.* **1998**, *5*, R193–R203.
(140) Yasunari Kenichi; Kohno Masakazu; Hasuma Tadayoshi; Horio Takeshi; Kano Hiroaki; Yokokawa Koji; Minami Mieko; Yoshikawa Junichi. Dopamine as a Novel Antimigration and Antiproliferative Factor of Vascular Smooth Muscle Cells Through Dopamine D1-Like Receptors. *Arterioscler. Thromb. Vasc. Biol.* **1997**, *17*, 3164–3173.

(141) Zhou, Y.; Shi, W.; Luo, H.; Yue, R.; Wang, Z.; Wang, W.; Liu, L.; Wang, W. E.; Wang, H.; Zeng, C. Inhibitory Effect of D 1 -like Dopamine Receptors on Neuropeptide Y-Induced Proliferation in Vascular Smooth Muscle Cells. *Hypertens. Res.* **2015**, *38*, 807–812.
(142) Yao, Y.; Yang, D.; Han, Y.; Wang, W.; Wang, N.; Yang, J.; Zeng, C. Dopamine D1-Like Receptors Suppress the Proliferation of Macrophages Induced by Ox-LDL. *Cell. Physiol. Biochem.* **2016**, *38* , 415–426.
(143) Bobryshev, Y. V.; Ivanova, E. A.; Chistiakov, D. A.; Nikiforov, N. G.; Orekhov, A. N. Macrophages and Their Role in Atherosclerosis: Pathophysiology and Transcriptome Analysis, **2019**.
(144) Moore Kathryn J.; Freeman Mason W. Scavenger Receptors in Atherosclerosis. *Arterioscler. Thromb. Vasc. Biol.* **2006**, *26*, 1702–1711.
(145) Slijkhuis, W.; Mali, W.; Appelman, Y. A Historical Perspective towards a Non-Invasive Treatment for Patients with Atherosclerosis. *Neth. Heart J.* **2009**, *17*, 140–144.
(146) Meyer, C. E.; Craciun, I.; Schoenenberger, C.-A.; Wehr, R.; Palivan, C. G. Catalytic Polymersomes to Produce Strong and Long-Lasting Bioluminescence. *Nanoscale* **2021**, *13*, 66–70.
(147) Sadikot, R. T.; Blackwell, T. S. Bioluminescence Imaging. *Proc. Am. Thorac. Soc.* **2005**, *2*, 537–540.
(148) Close, D. M.; Xu, T.; Sayler, G. S.; Ripp, S. In Vivo Bioluminescent Imaging (BLI): Noninvasive Visualization and Interrogation of Biological Processes in Living Animals. *Sensors* **2010**, *11*, 180–206.
(149) Coleman, S. M.; McGregor, A. A Bright Future for Bioluminescent Imaging in Viral Research. *Future Virol.* **2015**, *10*, 169–183.
(150) Masser, A. E.; Kandasamy, G.; Kaimal, J. M.; Andréasson, C. Luciferase NanoLuc as a Reporter for Gene Expression and Protein Levels in Saccharomyces Cerevisiae. *Yeast Chichester Engl.* **2016**, *33*, 191–200.
(151) Tannous, B. A. Gaussia Luciferase Reporter Assay for Monitoring of Biological Processes in Culture and in Vivo. *Nat. Protoc.* **2009**, *4*, 582–591.
(152) El-Amouri, S. S.; Cao, P.; Miao, C.; Pan, D. Secreted Luciferase for In Vivo Evaluation of Systemic Protein Delivery in Mice. *Mol. Biotechnol.* **2013**, *53*, 63–73.
(153) Meyer, C. E.; Liu, J.; Craciun, I.; Wu, D.; Wang, H.; Xie, M.; Fussenegger, M.; Palivan, C. G. Segregated Nanocompartments Containing Therapeutic Enzymes and Imaging Compounds within DNA-Zipped Polymersome Clusters for Advanced Nanotheranostic Platform. *Small*, **2020**, 1906492.
(154) Zhang, X.; Zhang, P. Polymersomes in Nanomedicine - A Review. *Curr. Med. Chem.* **2017**, *13*, 124–129.
(155) Anajafi, T.; Mallik, S. Polymersome-Based Drug-Delivery Strategies for Cancer Therapeutics. *Ther. Deliv.* **2015**, *6*, 521.
(156) Najer, A.; Wu, D.; Vasquez, D.; Palivan, C. G.; Meier, W. Polymer Nanocompartments in Broad-Spectrum Medical Applications. *Nanomed.* **2013**, *8*, 425–447.
(157) Kiene, K.; Schenk, S. H.; Porta, F.; Ernst, A.; Witzigmann, D.; Grossen, P.; Huwyler, J. PDMS-b-PMOXA Polymersomes for Hepatocyte Targeting and Assessment of Toxicity. *Eur. J. Pharm. Biopharm.* **2017**, *119*, 322–332.
(158) Tanner, P.; Onaca, O.; Balasubramanian, V.; Meier, W.; Palivan, C. G. Enzymatic Cascade Reactions inside Polymeric Nanocontainers: A Means to Combat Oxidative Stress. *Chem. – Eur. J.* **2011**, *17*, 4552–4560.

(159) Daubian, D.; Gaitzsch, J.; Meier, W. Synthesis and Complex Self-Assembly of Amphiphilic Block Copolymers with a Branched Hydrophobic Poly(2-Oxazoline) into Multicompartment Micelles, Pseudo-Vesicles and Yolk/Shell Nanoparticles. *Polym. Chem.* **2020**, *11*, 1237–1248.
(160) England, C. G.; Ehlerding, E. B.; Cai, W. NanoLuc: A Small Luciferase Is Brightening Up the Field of Bioluminescence. *Bioconjug. Chem.* **2016**, *27*, 1175–1187.
(161) Al-Ani, A. W.; Zhang, L.; Ferreira, L.; Turyanska, L.; Bradshaw, T. D.; Thomas, N. R. Listeria Innocua Dps as a Nanoplatform for Bioluminescence Based Photodynamic Therapy Utilizing Gaussia Princeps Luciferase and Zinc Protoporphyrin IX. *Nanomedicine Nanotechnol. Biol. Med.* **2019**, *20*, 102005.
(162) Yu, T.; Laird, J. R.; Prescher, J. A.; Thorpe, C. Gaussia Princeps Luciferase: A Bioluminescent Substrate for Oxidative Protein Folding. *Protein Sci. Publ. Protein Soc.* **2018**, *27*, 1509–1517.
(163) Kefala, G.; Ahn, C.; Krupa, M.; Esquivies, L.; Maslennikov, I.; Kwiatkowski, W.; Choe, S. Structures of the OmpF Porin Crystallized in the Presence of Foscholine-12. *Protein Sci. Publ. Protein Soc.* **2010**, *19*, 1117–1125.
(164) Nestorovich, E. M.; Danelon, C.; Winterhalter, M.; Bezrukov, S. M. Designed to Penetrate: Time-Resolved Interaction of Single Antibiotic Molecules with Bacterial Pores. *Proc. Natl. Acad. Sci. U. S. A.* **2002**, *99*, 9789–9794.
(165) Zhao, H.; Doyle, T. C.; Wong, R. J.; Cao, Y.; Stevenson, D. K.; Piwnica-Worms, D.; Contag, C. H. Characterization of Coelenterazine Analogs for Measurements of Renilla Luciferase Activity in Live Cells and Living Animals. *Mol. Imaging* **2004**, *3*.
(166) Li, H.-Y.; Zheng, X.-M.; Che, M.-X.; Hu, H.-Y. A Redox-Sensitive Luciferase Assay for Determining the Localization and Topology of Endoplasmic Reticulum Proteins. *PLOS ONE* **2012**, *7*, e35628.
(167) Wasmeier, C.; Hume, A. N.; Bolasco, G.; Seabra, M. C. Melanosomes at a Glance. *J. Cell Sci.* **2008**, *121*, 3995–3999.
(168) Jin, Y.; Birlea, S. A.; Fain, P. R.; Ferrara, T. M.; Ben, S.; Riccardi, S. L.; Cole, J. B.; Gowan, K.; Holland, P. J.; Bennett, D. C.; Luiten, R. M.; Wolkerstorfer, A.; van der Veen, J. P. W.; Hartmann, A.; Eichner, S.; Schuler, G.; van Geel, N.; Lambert, J.; Kemp, E. H.; Gawkrodger, D. J.; Weetman, A. P.; Taïeb, A.; Jouary, T.; Ezzedine, K.; Wallace, M. R.; McCormack, W. T.; Picardo, M.; Leone, G.; Overbeck, A.; Silverberg, N. B.; Spritz, R. A. Genome-Wide Association Analyses Identify 13 New Susceptibility Loci for Generalized Vitiligo. *Nat. Genet.* **2012**, *44*, 676–680.
(169) Alikhan, A.; Felsten, L. M.; Daly, M.; Petronic-Rosic, V. Vitiligo: A Comprehensive Overview: Part I. Introduction, Epidemiology, Quality of Life, Diagnosis, Differential Diagnosis, Associations, Histopathology, Etiology, and Work-Up. *J. Am. Acad. Dermatol.* **2011**, *65*, 473–491.
(170) Silvestri, B.; Vitiello, G.; Luciani, G.; Calcagno, V.; Costantini, A.; Gallo, M.; Parisi, S.; Paladino, S.; Iacomino, M.; D'Errico, G.; Caso, M. F.; Pezzella, A.; d'Ischia, M. Probing the Eumelanin–Silica Interface in Chemically Engineered Bulk Hybrid Nanoparticles for Targeted Subcellular Antioxidant Protection. *ACS Appl. Mater. Interfaces* **2017**, *9*, 37615–37622.
(171) Schweitzer, A. D.; Revskaya, E.; Chu, P.; Pazo, V.; Friedman, M.; Nosanchuk, J. D.; Cahill, S.; Frases, S.; Casadevall, A.; Dadachova, E. Melanin-Covered Nanoparticles for Protection of Bone Marrow during Radiation Therapy of Cancer. *Int. J. Radiat. Oncol. Biol. Phys.* **2010**, *78*, 1494–1502.

(172) Ball, V. Polydopamine Nanomaterials: Recent Advances in Synthesis Methods and Applications. *Front. Bioeng. Biotechnol.* **2018**, *6*.
(173) Caldas, M.; Santos, A. C.; Veiga, F.; Rebelo, R.; Reis, R. L.; Correlo, V. M. Melanin Nanoparticles as a Promising Tool for Biomedical Applications – a Review. *Acta Biomater.* **2020**, *105*, 26–43.
(174) Huang, Y.; Li, Y.; Hu, Z.; Yue, X.; Proetto, M. T.; Jones, Y.; Gianneschi, N. C. Mimicking Melanosomes: Polydopamine Nanoparticles as Artificial Microparasols. *ACS Cent. Sci.* **2017**, *3*, 564–569.
(175) Chen, F.; Xing, Y.; Wang, Z.; Zheng, X.; Zhang, J.; Cai, K. Nanoscale Polydopamine (PDA) Meets π–π Interactions: An Interface-Directed Coassembly Approach for Mesoporous Nanoparticles. *Langmuir* **2016**, *32*, 12119–12128.
(176) Awasthi, A. K.; Gupta, S.; Thakur, J.; Gupta, S.; Pal, S.; Bajaj, A.; Srivastava, A. Polydopamine-on-Liposomes: Stable Nanoformulations, Uniform Coatings and Superior Antifouling Performance. *Nanoscale* **2020**, *12*, 5021–5030.
(177) Mei, S.; Kochovski, Z.; Roa, R.; Gu, S.; Xu, X.; Yu, H.; Dzubiella, J.; Ballauff, M.; Lu, Y. Enhanced Catalytic Activity of Gold@Polydopamine Nanoreactors with Multi-Compartment Structure Under NIR Irradiation. *Nano-Micro Lett.* **2019**, *11*, 83.
(178) Ito, S.; Wakamatsu, K. Chemistry of Mixed Melanogenesis--Pivotal Roles of Dopaquinone. *Photochem. Photobiol.* **2008**, *84*, 582–592.
(179) Simon, J. D.; Peles, D. N. The Red and the Black. *Acc. Chem. Res.* **2010**, *43*, 1452–1460.
(180) Panzella, L.; Gentile, G.; D'Errico, G.; Della Vecchia, N. F.; Errico, M. E.; Napolitano, A.; Carfagna, C.; d'Ischia, M. Atypical Structural and π-Electron Features of a Melanin Polymer That Lead to Superior Free-Radical-Scavenging Properties. *Angew. Chem. Int. Ed Engl.* **2013**, *52*, 12684–12687.
(181) Ju, K.-Y.; Lee, Y.; Lee, S.; Park, S. B.; Lee, J.-K. Bioinspired Polymerization of Dopamine to Generate Melanin-Like Nanoparticles Having an Excellent Free-Radical-Scavenging Property. *Biomacromolecules* **2011**, *12*, 625–632.
(182) Nieto, C.; Vega, M. A.; Enrique, J.; Marcelo, G.; Martín del Valle, E. M. Size Matters in the Cytotoxicity of Polydopamine Nanoparticles in Different Types of Tumors. *Cancers* **2019**, *11*.
(183) Büngeler, A.; Hämisch, B.; Strube, O. I. The Supramolecular Buildup of Eumelanin: Structures, Mechanisms, Controllability. *Int. J. Mol. Sci.* **2017**, *18*.
(184) Konrad, K.; Wolff, K. Hyperpigmentation, Melanosome Size, and Distribution Patterns of Melanosomes. *Arch. Dermatol.* **1973**, *107*, 853–860.
(185) Thong, H.-Y.; Jee, S.-H.; Sun, C.-C.; Boissy, R. E. The Patterns of Melanosome Distribution in Keratinocytes of Human Skin as One Determining Factor of Skin Colour. *Br. J. Dermatol.* **2003**, *149*, 498–505.
(186) Meredith, P.; Sarna, T. The Physical and Chemical Properties of Eumelanin. *Pigment Cell Res.* **2006**, *19*, 572–594.
(187) Ando, H.; Kondoh, H.; Ichihashi, M.; Hearing, V. J. Approaches to Identify Inhibitors of Melanin Biosynthesis via the Quality Control of Tyrosinase. *J. Invest. Dermatol.* **2007**, *127*, 751–761.
(188) Solano, F. Melanin and Melanin-Related Polymers as Materials with Biomedical and Biotechnological Applications-Cuttlefish Ink and Mussel Foot Proteins as Inspired Biomolecules. *Int. J. Mol. Sci.* **2017**, *18* .
(189) Fenoll, L. G.; Rodrı´guez-López, J. N.; Varón, R.; Garcı´a-Ruiz, P. A.; Garcı´a-Cánovas, F.; Tudela, J. Kinetic Characterisation of the Reaction Mechanism of

Mushroom Tyrosinase on Tyramine/Dopamine and l-Tyrosine Methyl Esther/l-Dopa Methyl Esther. *Int. J. Biochem. Cell Biol.* **2002**, *34*, 1594–1607.
(190) Iqbal, S.; Blenner, M.; Alexander-Bryant, A.; Larsen, J. Polymersomes for Therapeutic Delivery of Protein and Nucleic Acid Macromolecules: From Design to Therapeutic Applications. *Biomacromolecules* **2020**, *21*, 1327–1350.
(191) Manandhar, B.; Wagle, A.; Seong, S. H.; Paudel, P.; Kim, H.-R.; Jung, H. A.; Choi, J. S. Phlorotannins with Potential Anti-Tyrosinase and Antioxidant Activity Isolated from the Marine Seaweed Ecklonia Stolonifera. *Antioxidants* **2019**, *8*, 240.
(192) d'Ischia, M.; Napolitano, A.; Ball, V.; Chen, C.-T.; Buehler, M. J. Polydopamine and Eumelanin: From Structure–Property Relationships to a Unified Tailoring Strategy. *Acc. Chem. Res.* **2014**, *47*, 3541–3550.
(193) Ascione, L.; Pezzella, A.; Ambrogi, V.; Carfagna, C.; d'Ischia, M. Intermolecular π-Electron Perturbations Generate Extrinsic Visible Contributions to Eumelanin Black Chromophore in Model Polymers with Interrupted Interring Conjugation. *Photochem. Photobiol.* **2013**, *89*, 314–318.
(194) Sugumaran, M.; Evans, J.; Ito, S.; Wakamatsu, K. Nonenzymatic Spontaneous Oxidative Transformation of 5,6-Dihydroxyindole. *Int. J. Mol. Sci.* **2020**, *21*.
(195) Karan, A.; Khezerlou, E.; Rezaei, F.; Iasemidis, L.; DeCoster, M. A. Morphological Changes in Astrocytes by Self-Oxidation of Dopamine to Polydopamine and Quantification of Dopamine through Multivariate Regression Analysis of Polydopamine Images. *Polymers* **2020**, *12* .
(196) Vega, M. A.; Nieto, C.; Marcelo, G.; Martín del Valle, E. M. Cytotoxicity of Paramagnetic Cations—Loaded Polydopamine Nanoparticles. *Colloids Surf. B Biointerfaces* **2018**, *167*, 284–290.
(197) Lanzilotto, A.; Kyropoulou, M.; Constable, E. C.; Housecroft, C. E.; Meier, W. P.; Palivan, C. G. Porphyrin-Polymer Nanocompartments: Singlet Oxygen Generation and Antimicrobial Activity. *JBIC J. Biol. Inorg. Chem.* **2018**, *23*, 109–122.
(198) Strube, O. I.; Büngeler, A.; Bremser, W. Site-Specific In Situ Synthesis of Eumelanin Nanoparticles by an Enzymatic Autodeposition-Like Process. *Biomacromolecules* **2015**, *16*, 1608–1613.
(199) Strube, O. I.; Büngeler, A.; Bremser, W. Enzyme-Mediated In Situ Synthesis and Deposition of Nonaggregated Melanin Protoparticles. *Macromol. Mater. Eng.* **2016**, *301*, 801–804.
(200) Deng, Y.; Yang, W.-Z.; Shi, D.; Wu, M.; Xiong, X.-L.; Chen, Z.-G.; Wei, S.-C. Bioinspired and Osteopromotive Polydopamine Nanoparticle-Incorporated Fibrous Membranes for Robust Bone Regeneration. *NPG Asia Mater.* **2019**, *11*, 1–13.
(201) Schlatter, S.; Rimann, M.; Kelm, J.; Fussenegger, M. SAMY, a Novel Mammalian Reporter Gene Derived from Bacillus Stearothermophilus α-Amylase. *Gene* **2002**, *282*, 19–31.

9. Acknowledgment

First and foremost I would like to acknowledge my main supervisor **Prof. Cornelia G. Palivan** for giving me the opportunity to pursue my PhD in her group, supervising my work, supporting me during these four years, and trusting me in the development of my own ideas.

I cordially thank the other members of my PhD committee, specifically my second supervisor **Prof. Jörg Huwyler** and **Prof. Corinne Nardin** for taking the time to evaluate my work, and **Prof. Thomas R. Ward** for accepting to chair my PhD exam.

I also wish to thank **Prof. Wolfgang Meier** for his support and helpful discussions during this PhD.

I can never thank **Dr. Ioana Craciun** enough, for all her help and extensive support that goes far beyond this work. She managed to push the little bird out of its nest so it learned to fly on its own. I wish every PhD student would be lucky enough to learn from their PostDocs as much as I did from her.

I am grateful to **Dr. Cora-Ann Schoenenberger** for all her support in my work and beyond. I remember the day I met Cora and she offered me a tea during my interview for this PhD position. The tradition continued as she became my finest tea/coffee-break companion for the next four years. Also, I enjoyed her determination to improve my English and all the fun we had working together.

I thank **Dr. Myrto Kyropoulou** for her valuable support up to the very end of my PhD and for being my most stylish lab companion.

I wish to thank all other collaborators in the projects mentioned in this thesis, especially **Dr. Juan Liu, Dr. Linling Shen** and **Prof. Martin Fussenegger** and his group.

I thank the synthesis team, especially **Riccardo Wehr** and **Dr. Dalin Wu** for providing exquisite polymers, and **Dr. Davy Daubian** for his input and knowledge about SLS.

I am very grateful that I had the chance to work in such a pleasant atmosphere. So, thanks to all of my current and former colleagues, who always made my day brighter, especially: **Dr. Andrea Belluati**, **Dr. Viviana Maffeis**, **Dr. Saziye Yorulmaz Avsar**, **Dr. Sagana Thamboo**, **Dr. Serena Rigo**, **Dr. Samuel Lörcher**, **Dr.**

Pascal Richard, **Dr. Csaba Fodor**, **Dr. Daniel Messmer**, **Dimitri Hürlimann**, **Luisa Zartner**, **Shabnam Tarvirdipour**, **Vittoria Chimisso**, **Maria Korpidou**, **Moritz Muthwill**, **Stefano Di Leone**, **Christoph John**, **Gabriele Persy** and **Sven Kasper**. A special thanks to my compatriot **Alessandro Angelini**, who has always been the nicest person and helped me maintaining my French.

I wish to thank the staff of the Department of Chemistry for being so supportive at all times: **Dr. Michael Devereux**, **Beatrice Erismann**, **Markus Hauri**, **Susanne Foley**, **Mariella Schneiter,** the workshop and particularly **Maya Greuter** for her kindness.

I was lucky to pursue this PhD at the University of Basel as in the PhD Chemistry Community (**PCC**), I met many highly motivated PhD students. They also made sure we had great events, and maintained the cohesion between the different Chemistry buildings.

I am grateful to **Jaicy Vallapurackal**, **Selen Manioglu** and **Olivier Belli** who I met during our NCCR-MSE event at the Locarno Film Festival 2019, as they were funny and supportive mates ever since.

A special thanks goes to **Swiss National Science Foundation**, the **NCCR Molecular Systems Engineering** and the **University of Basel** for the financial support.

I want to thank **Prof. Vincent Ball** and **Dr. Vladimir Torbeev** from the University of Strasbourg, for giving me the best first research experience during my Master. I would probably not have pursued a PhD if I had not done such great internships, with exciting projects and inspiring mentorships.

Finally, I thank my family, especially my father **Denis Meyer**, my sister **Johana Meyer** and my grandparents **Michelle Meyer**, **Bernard Meyer**, **Vera Loda**, **Salvatore Loda** and **Aimé Horn**, and my old friends, **Marion Haag**, **Guillaume Sorg**, **Dominique Naccari** and **Julia Godail**, for the longstanding support and for understanding my lack of availability. I really want to thank my partner **Roberto Vanelli** for always generously putting up with my moods and my non-stop complaints. His continuous support and understanding carried me through this particularly restless period of my life.

10. Appendix

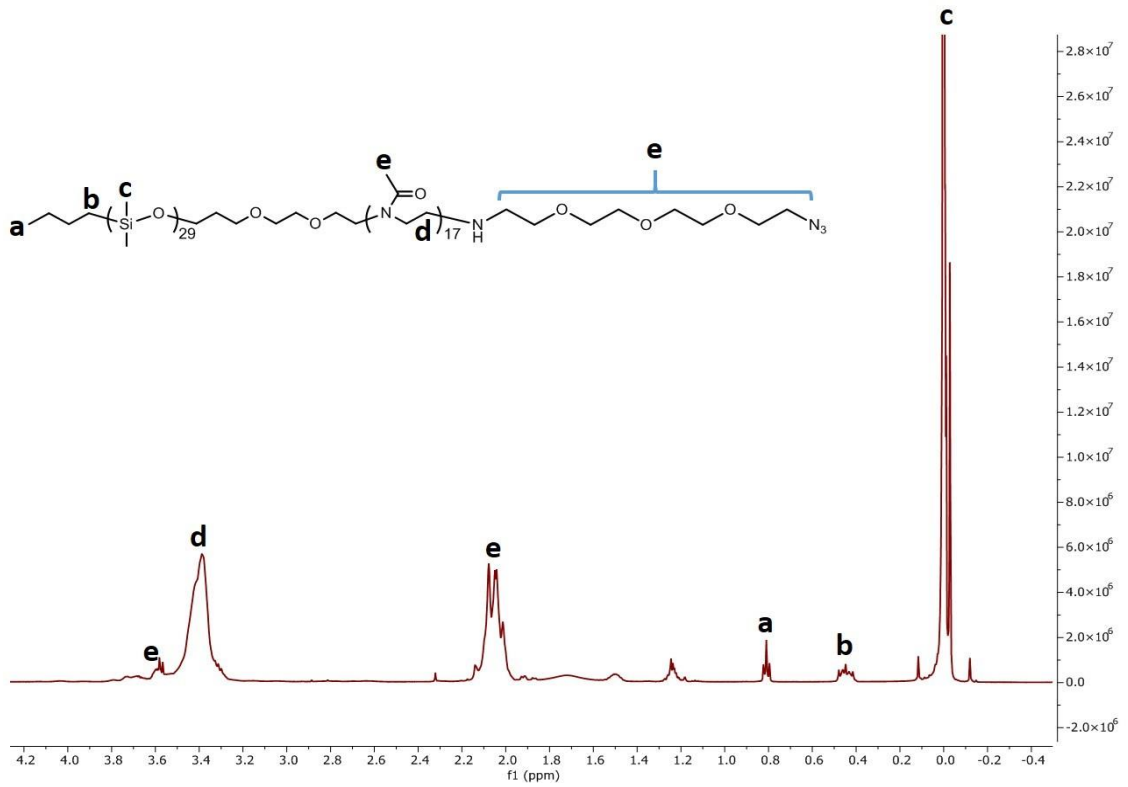

Figure 10.1 *^{1}H NMR of $PDMS_{22}$-$PMOXA_{8}$-OEG_{3}-N_{3}.*

Polymersomes	Name of the ssDNA sequence	ssDNA sequence 5' -> 3'	5' modification	3' modification
DDC-Ncomp	ssDNAa	CCT CGC TCT GCT AAT CCT GTT A	DBCO	DY-633[a)]
	spacer-ssDNAa	TTT TTT TTT TTC CTC GCT CTG CTA ATC CTG TTA		
Dye-Ncomp	ssDNAb	TAA CAG GAT TAG CAG AGC GAG G	DBCO	Atto-488[a)]
	spacer-ssDNAb	TTT TTT TTT TTT AAC AGG ATT AGC AGA GCG AGG		

Table 3. *ssDNA sequences used for the functionalization of polymersomes, enabling the clustering of the different vesicles via hybridization of the single strands.*

[a)] used for FCS measurements only

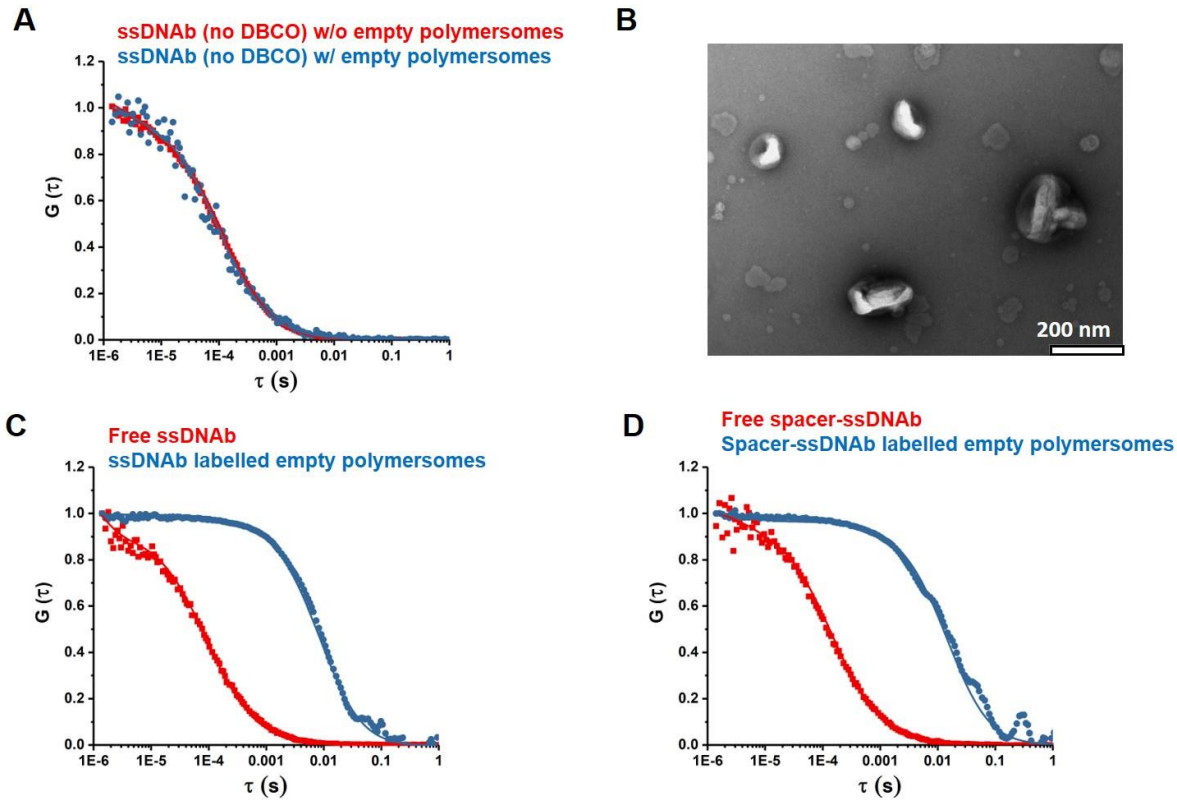

Figure 10.2. (A) *Normalized fluorescence correlation spectroscopy (FCS) autocorrelation curves of control Atto-488 labelled ssDNAb without DBCO group, in presence (blue) or absence (red) of empty polymersomes. Their respective fits are shown by the same-coloured solid lines.* ***(B)*** *TEM micrograph of empty polymersomes in presence of ssDNAb without DBCO.* ***(C)*** *Normalized FCS autocorrelation curves of free Atto-488 labelled ssDNAb (red) and corresponding ssDNAb linked polymersomes (blue).* ***(D)*** *Normalized FCS autocorrelation curves of Atto-488 labelled free spacer-ssDNAb (red) and corresponding spacer-ssDNAb linked polymersomes (blue). Their respective fits were shown by the same-coloured solid lines.*

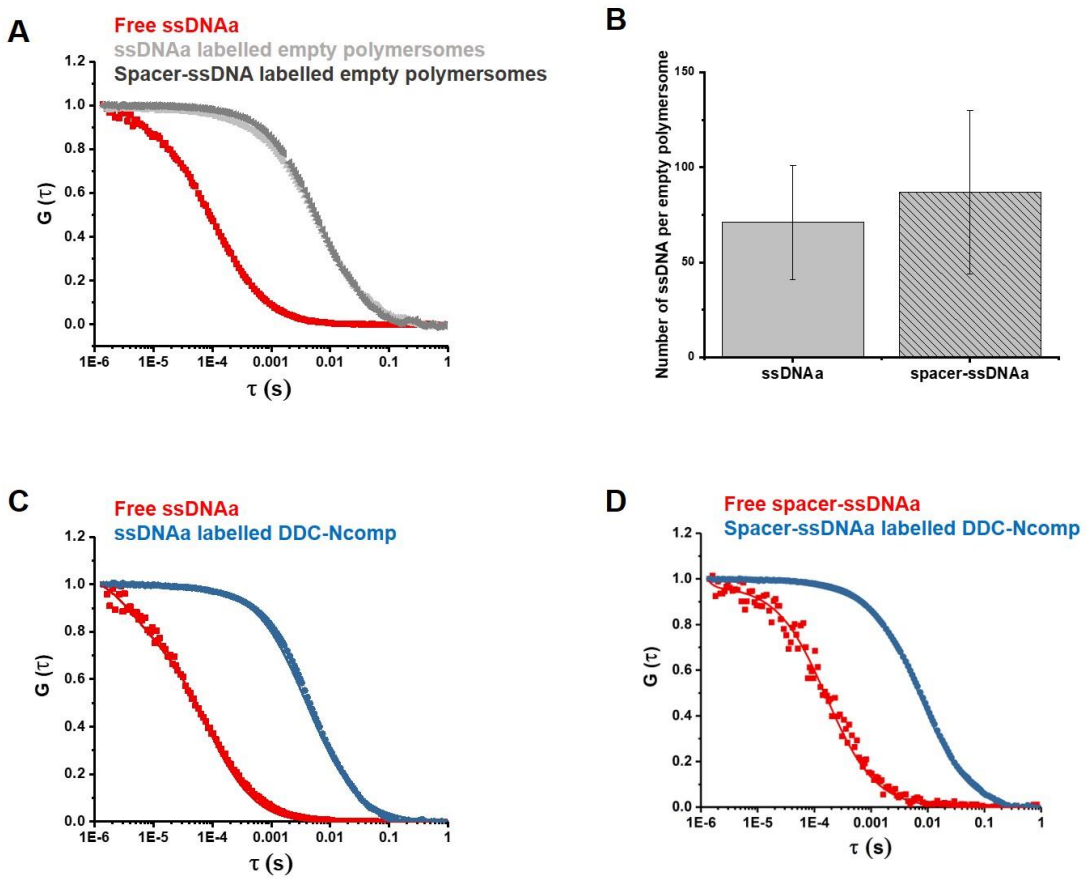

Figure 10.3. *Quantification of ssDNAa per empty polymersome and DDC-Ncomp via FCS.* ***(A)*** *Normalized FCS autocorrelation curves of free DY-633 labelled ssDNAa (red) and empty polymersome conjugated with this labelled ssDNAa or spacer-ssDNAa after an overnight reaction at 4 °C.* ***(B)*** *The corresponding average number of ssDNAa or spacer-ssDNAa linkedon empty polymersome after the reaction. To quantify the amount of ssDNA per polymersome, first we measured the counts per molecule (CPM) for the free ssDNA- DBCO. Next we measured the CPM for the polymersomes with attached ssDNA. By dividing by the CPM of the ssDNA-polymersomes by the CPM for free ssDNA-DBCO, and performing the corresponding error propagation, we obtained the number of attached ssDNA per polymersome ± SD.* ***(C)*** *Normalized FCS autocorrelation curves of free DY-633 labelled ssDNAa (red) and corresponding ssDNAa linked DDC-Ncomp (blue).* ***(D)*** *Normalized FCS autocorrelation curves of free DY-633 labelled spacer-ssDNAa (red) and corresponding spacer-ssDNAa linked DDC-Ncomp (blue). Their respective fits were shown by the same coloured solid lines.*

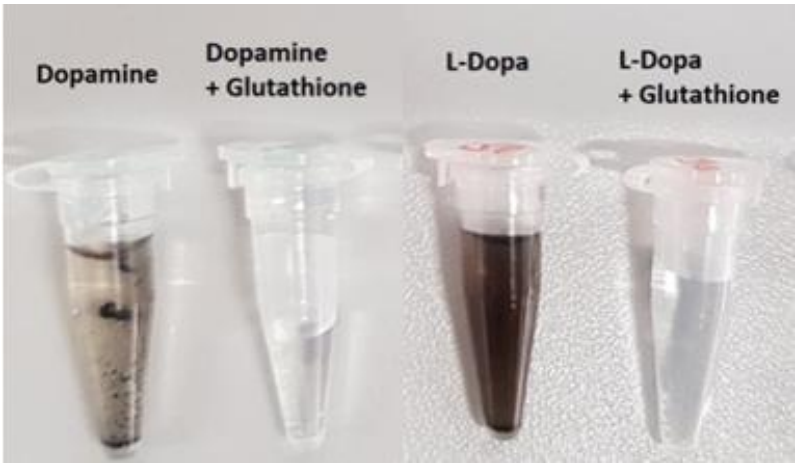

Figure 10.4. *Effect of 2x molar Glutathione on the auto-oxidation process of Dopamine and L-DOPA in solution (1 mM in PBS), after 24 h incubation at 37 °C. Dark brown/black colours of solution correspond to the formation of derivate molecules resulting from auto-oxidation of Dopamine and L-DOPA.*

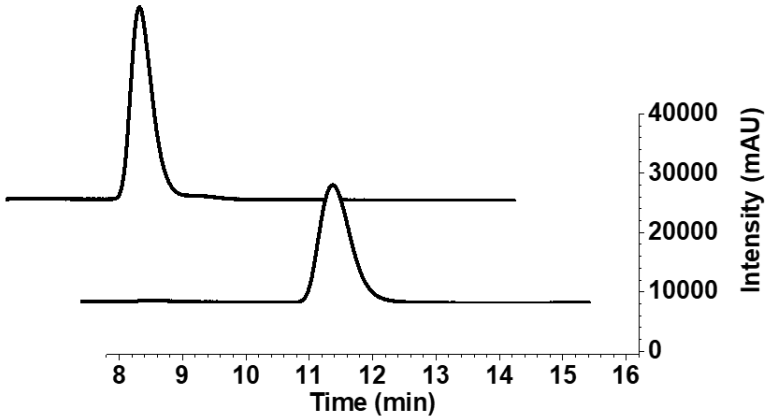

Figure 10.5. *HPLC chromatogram of dopamine and L-DOPA showing their corresponding retention times of 10.1 min and 11.8 min, respectively.*

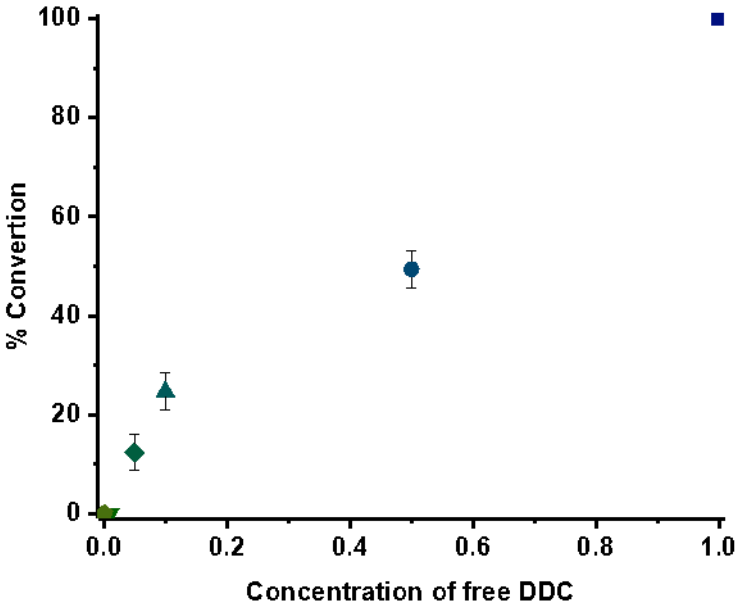

Figure 10.6. *Determination of percent conversion of L-DOPA to dopamine in presence of increasing concentrations of free DDC (with BSA). The percent conversion was determined by HPLC, for DDC enzymes in presence of BSA and after incubation at 37°C for 24 h.*

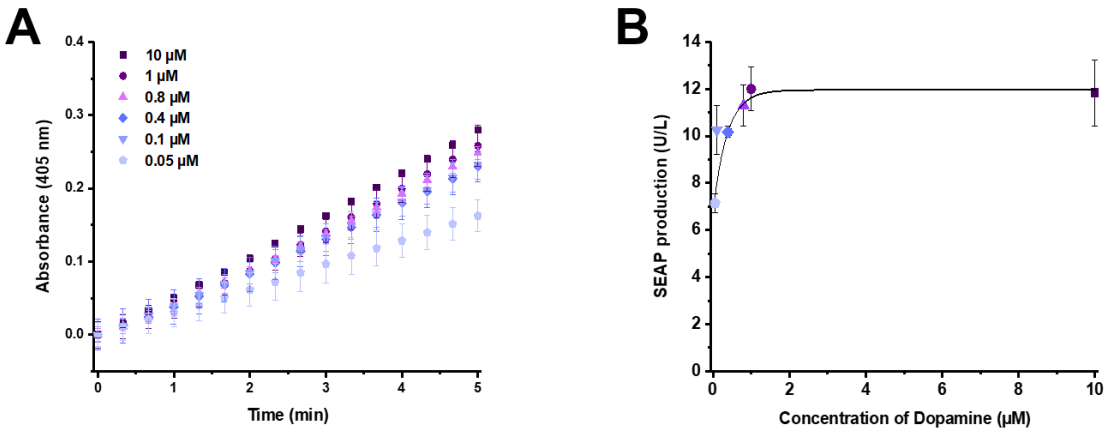

Figure 10.7. *Determination of SEAP production by HEK$_{REWARD}$ cells.* ***(A)*** *Determination of SEAP activity in cell supernatant to assess the concentrations of SEAP expressed by cells in response to increasing concentrations of Dopamine after 72 h of incubation.* ***(B)*** *Processed data showing the expression of SEAP by cells depending on dopamine concentrations.*

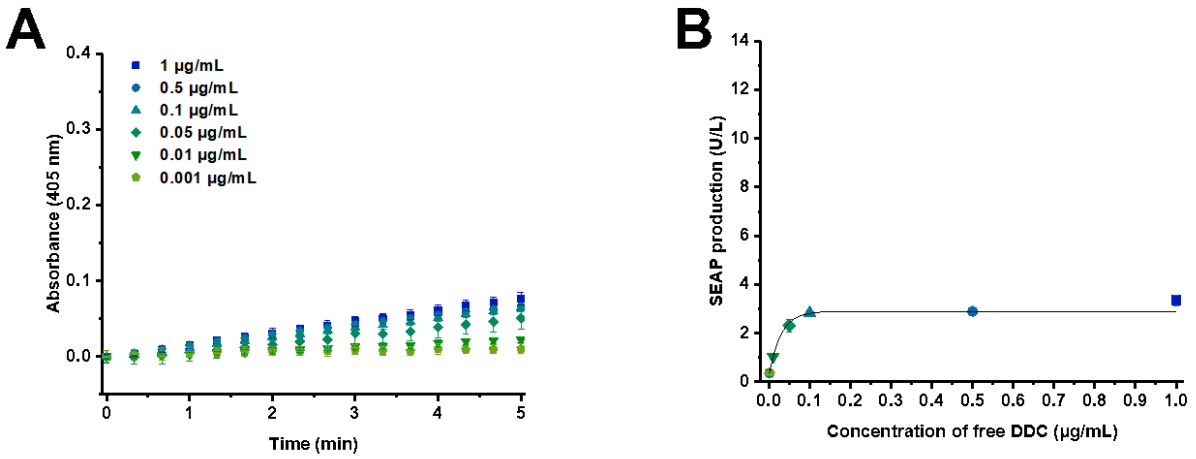

Figure 10.8. *Effect of absence of BSA on SEAP expression.* ***(A)*** *Determination of SEAP activity in cell supernatant in response to increasing concentrations of free DDC (without BSA) in presence of L-DOPA, after 72 h of incubation.* ***(B)*** *Processed data showing SEAP expression by cells as a function of increasing concentrations of free DDC.*

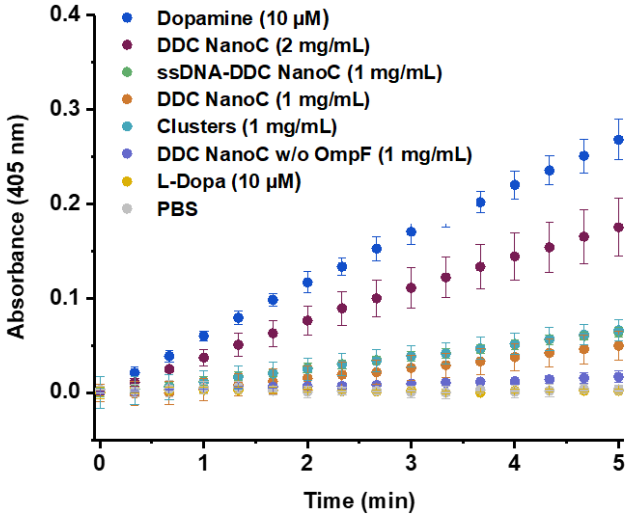

Figure 10.9. *Assessment of SEAP production by cells for different DDC systems.*

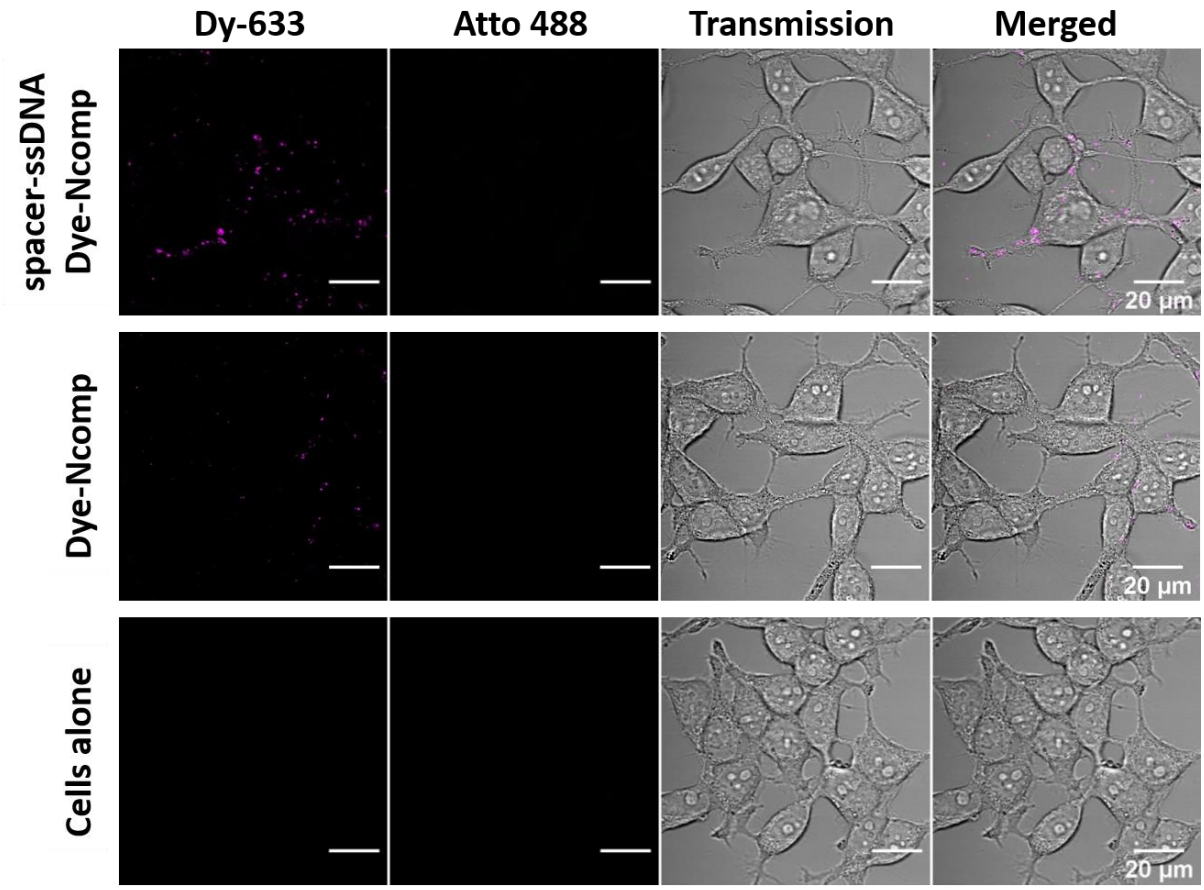

Figure 10.10. *Comparison of the attachment of Dye-Ncomp at the surface of HEK*REWARD *cells, when functionalized or not with spacer-ssDNA, as imaged by CLSM with separated DY-633 and Atto-488 channels, transmission channel and merged images (Scale bar = 20 µm)*

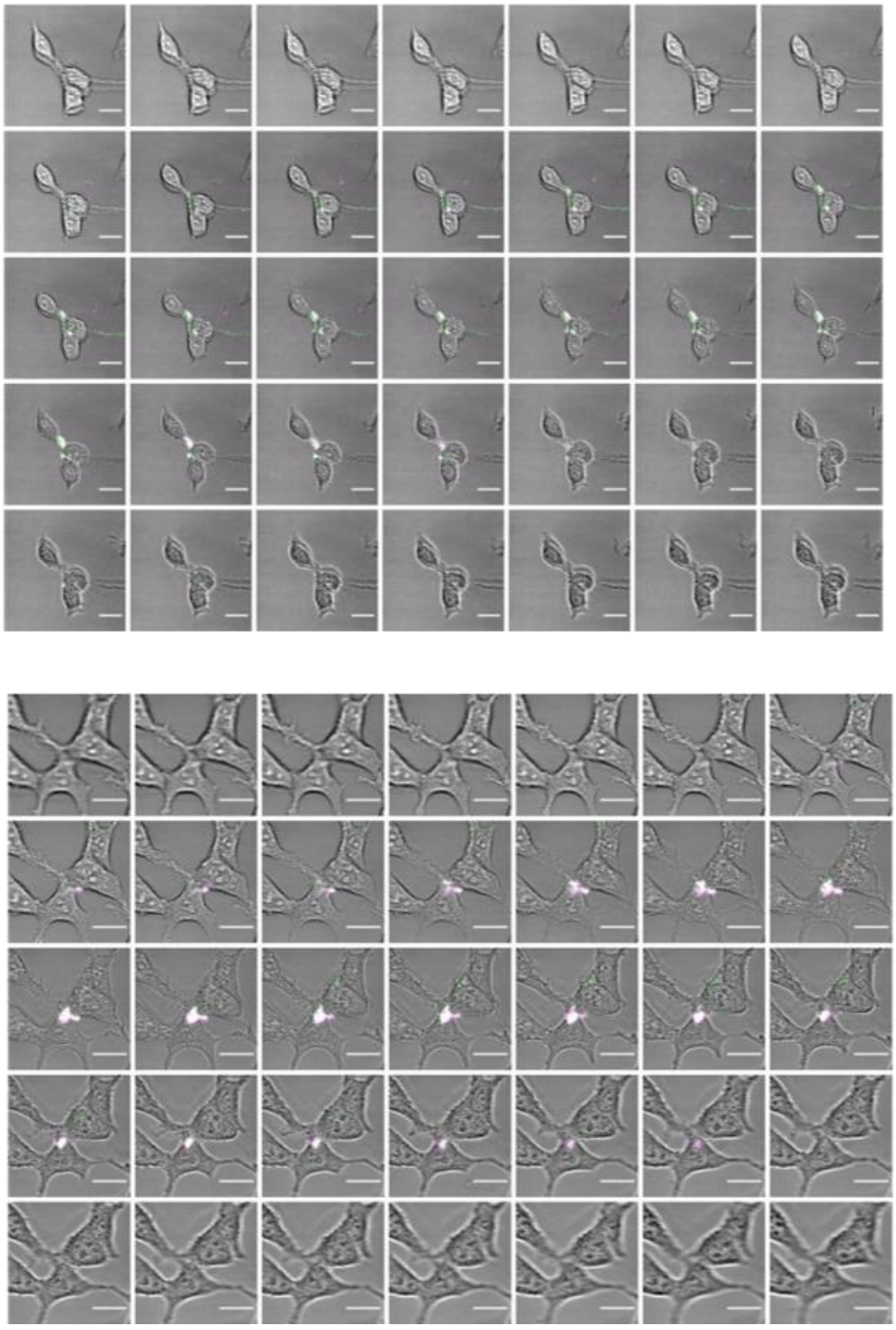

Figure 10.11. *Attachment of polymersome clusters on the surface of HEK*$_{REWARD}$ *cells after 24h, recorded by CLSM. Top panel was used for the left 3D rendering (Figure 3.12) and bottom panel was used for the right 3D rendering (Figure 3.12).*

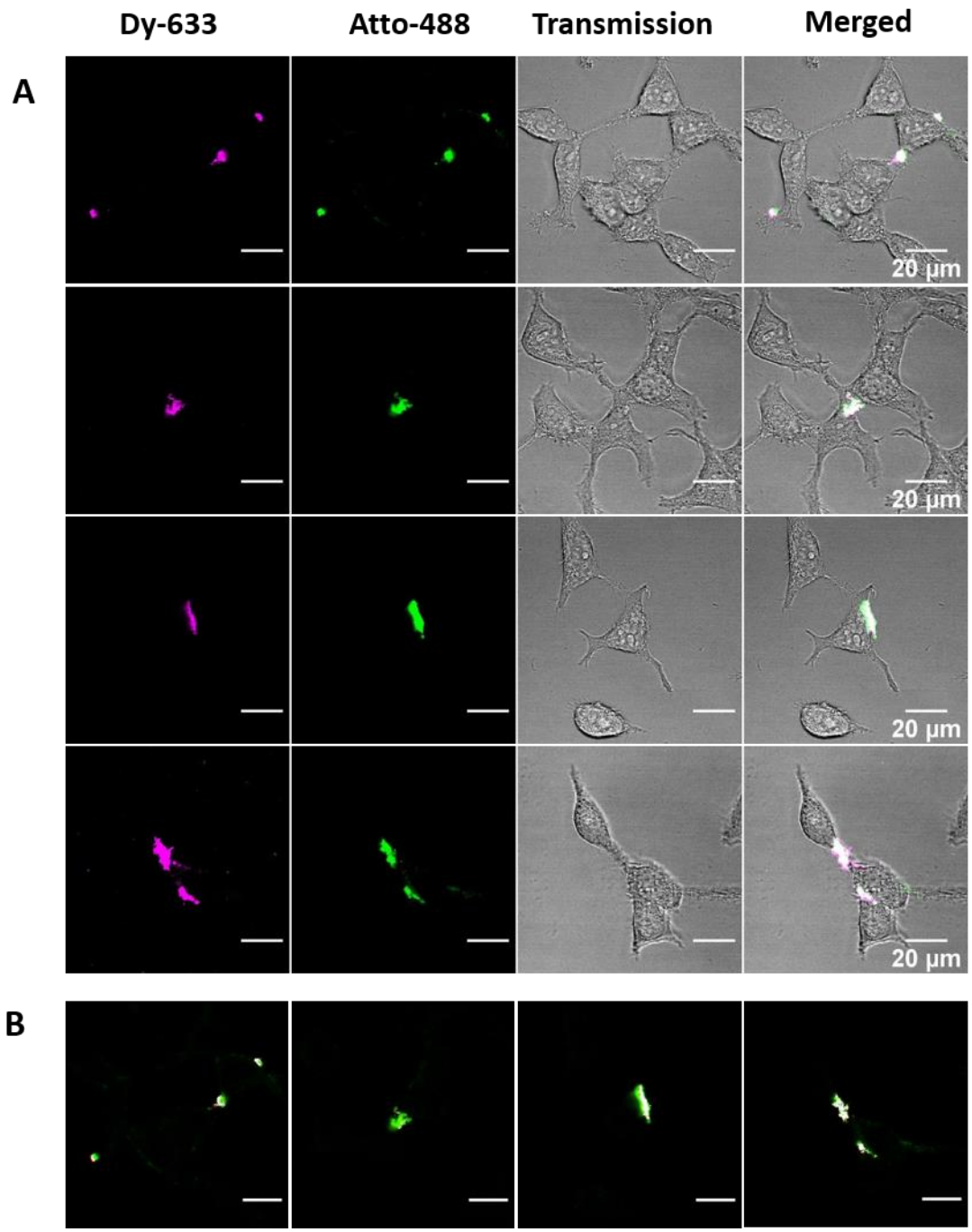

Figure 10.12. *Cell attachment of clusters.* ***(A)*** *CLSM pictures from four different locations of 488-633-Ncomp clusters attached to the surface of HEKREWARD cells after 24 h of incubation, with separated DY-633 and Atto-488 channels, transmission channel and merged images (Scale bar = 20 µm).* ***(B)*** *Merged DY-633 and Atto-488 channels of the four locations with colocalized regions19 appearing in white. Colocalization analysis of the four locations resulted in a Pearson's coefficient of 0.83 ± 0.05. Scale bar = 90 pixels or 18.9 µm.*

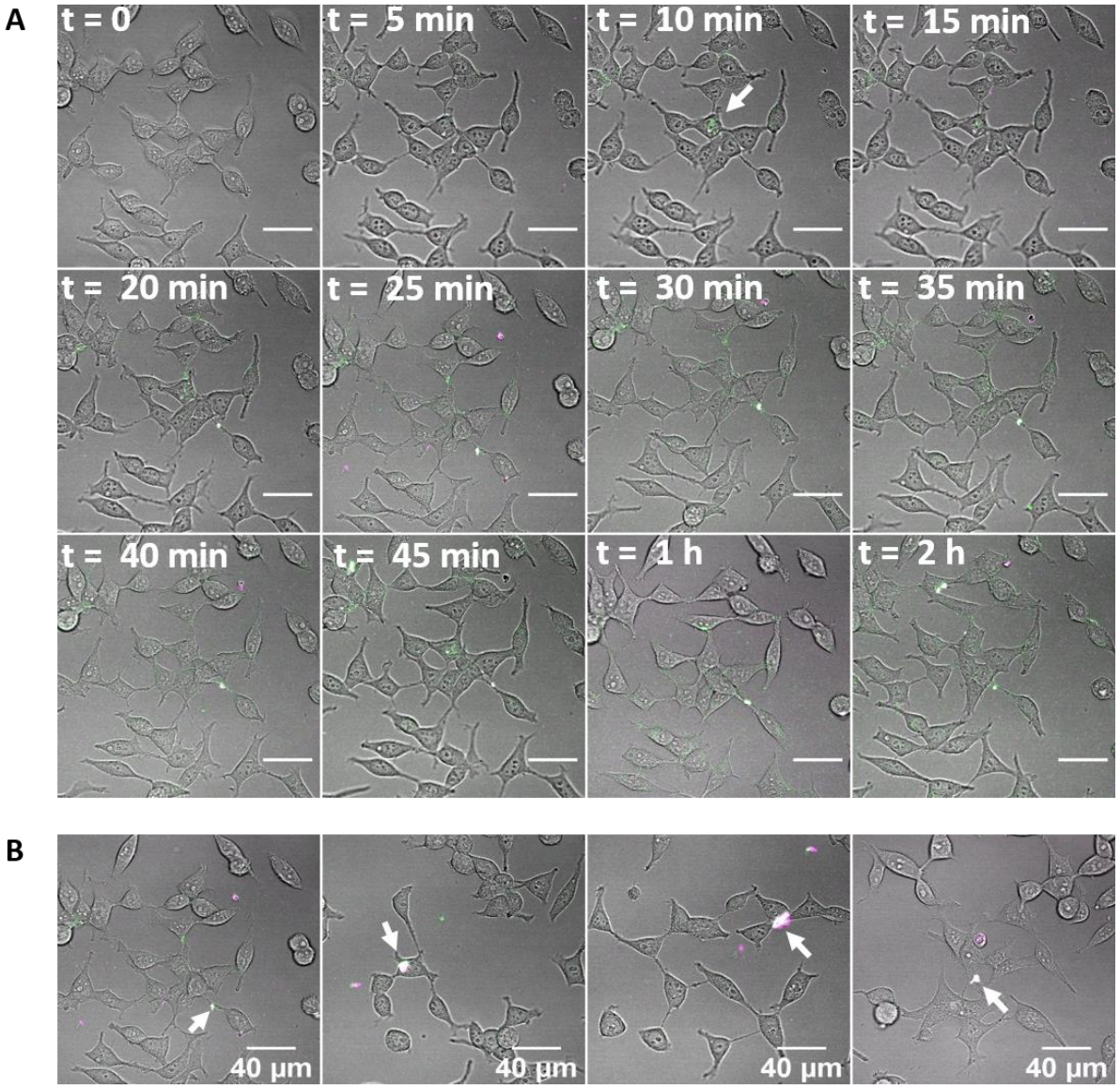

Figure 10.13. *Attachment of polymersome clusters on the surface of HEK$_{REWARD}$ cells, recorded by CLSM,* ***(A)*** *over time,* ***(B)*** *after 30min for four different locations. Scale bars = 40 µm.*

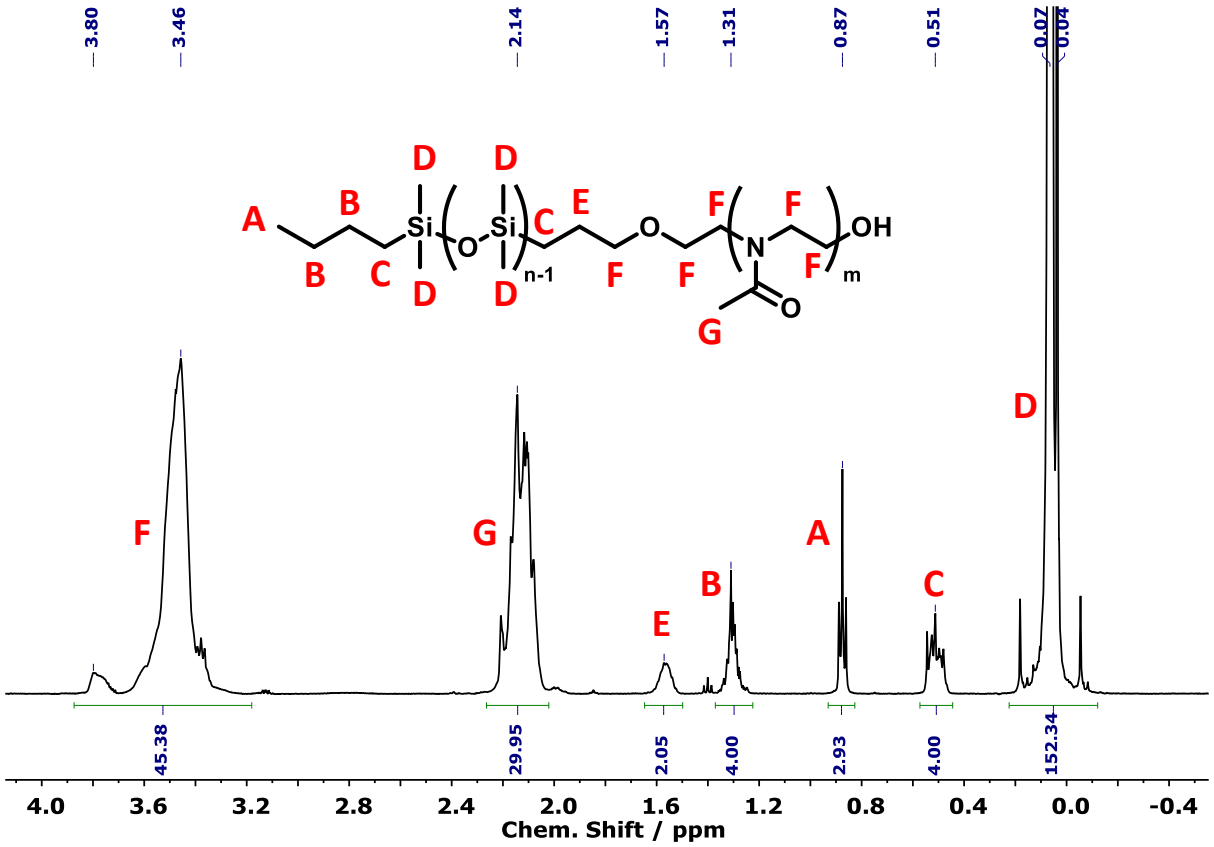

Figure 10.14. *1H-NMR of PDMS25-b-PMOXA10 in CDCl3.*

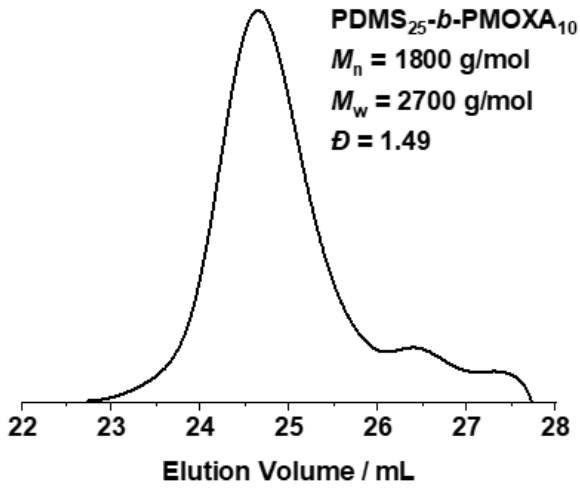

Figure 10.15. *GPC elugram of PDMS25-b-PMOXA10 in tetrahydrofuran, measured via refractive index detector.*

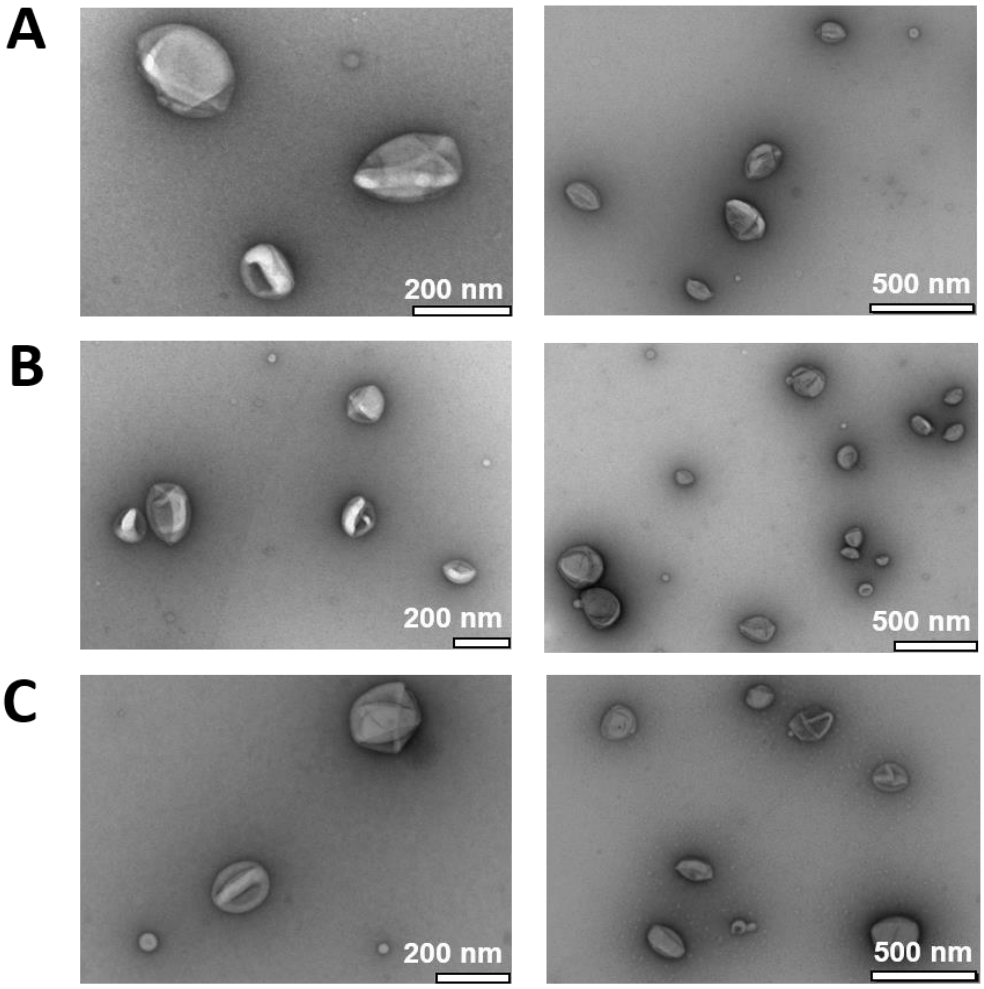

Figure 10.16. *TEM micrographs of* ***(A)*** *empty PMOXA19-PDMS25 polymersomes,* ***(B)*** *empty polymersomes with OmpF,* ***(C)*** *GLuc Ncomp without OmpF.*

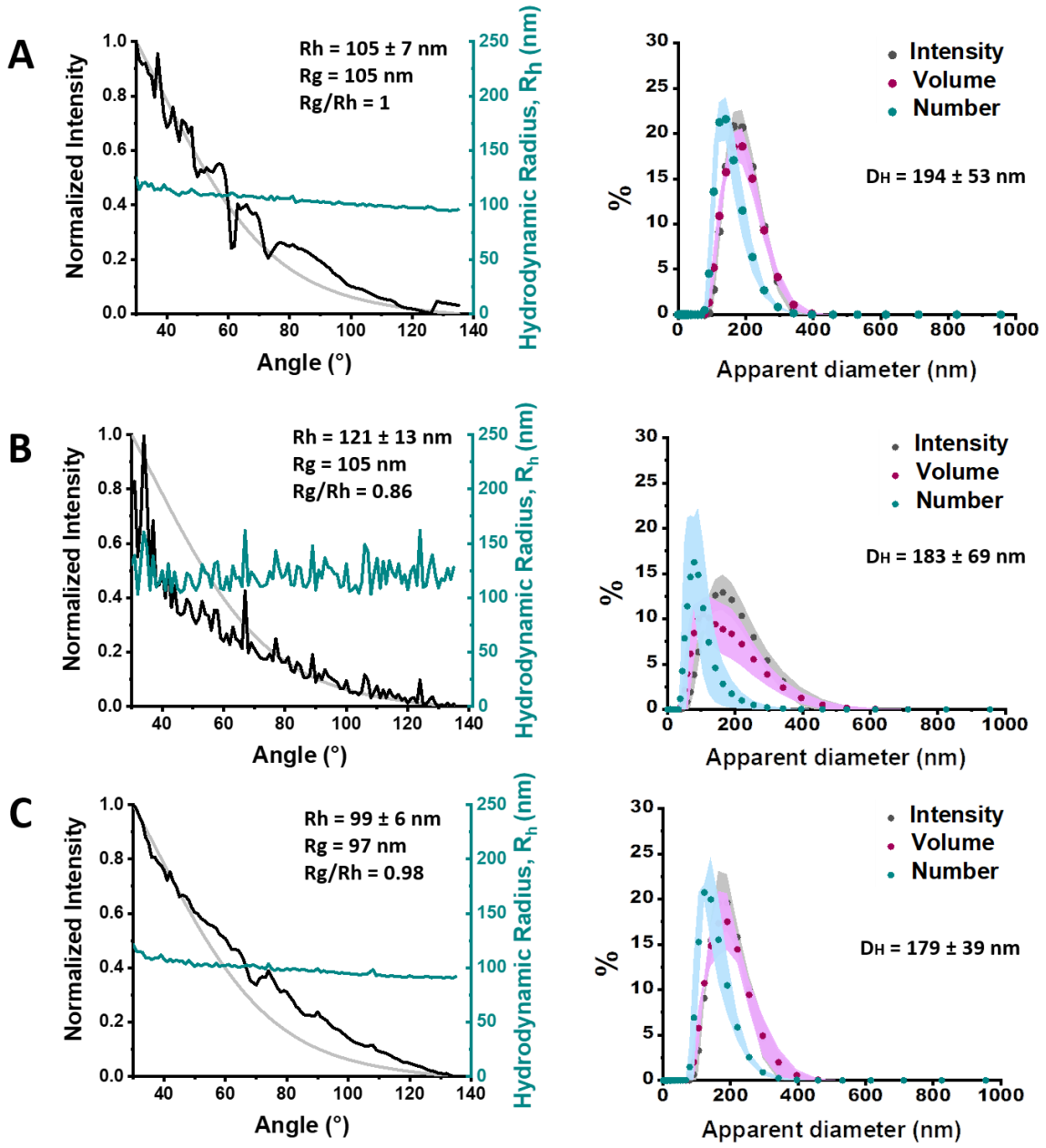

Figure 10.17. *Size determination via SLS (left) and DLS (right) of* ***(A)*** *empty PMOXA19-PDMS25 polymersomes (PDI = 0.163),* ***(B)*** *empty polymersomes with OmpF (PDI = 0.170),* ***(C)*** *GLuc Ncomp without OmpF (PDI = 0.159). SLS measurements show the DLS profile representing the hydrodynamic radius (Rh) of polymersomes at different angles (blue), the intensity at different angles (black) and the suitable MIE fit (grey) used to determine the radius of gyration (Rg). The ratio 0.775 < Rg/Rh ≤ 1 indicates a hollow sphere structure. DLS graphs show the Rh of polymersomes, measured at 173° angle, by percentage of intensity (grey), volume (purple) and number (blue).*

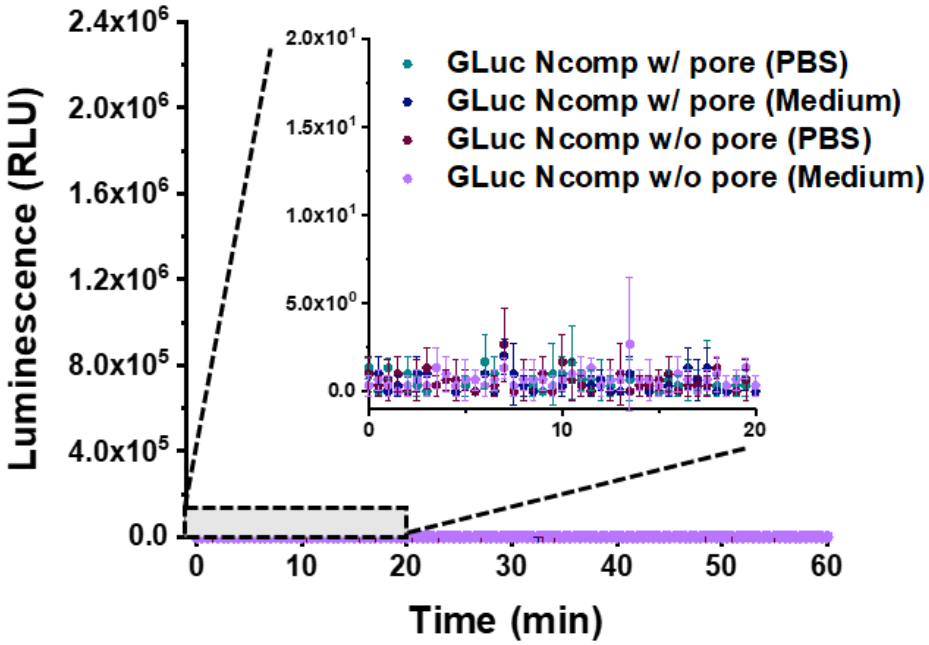

Figure 10.18. *Luminescence production in the absence of coelenterazine substrate: GLuc Ncomp with OmpF in PBS (blue), GLuc Ncomp with OmpF in cell medium (dark blue), GLuc Ncomp without OmpF in PBS (purple), GLuc Ncomp without OmpF in cell medium (light purple).*

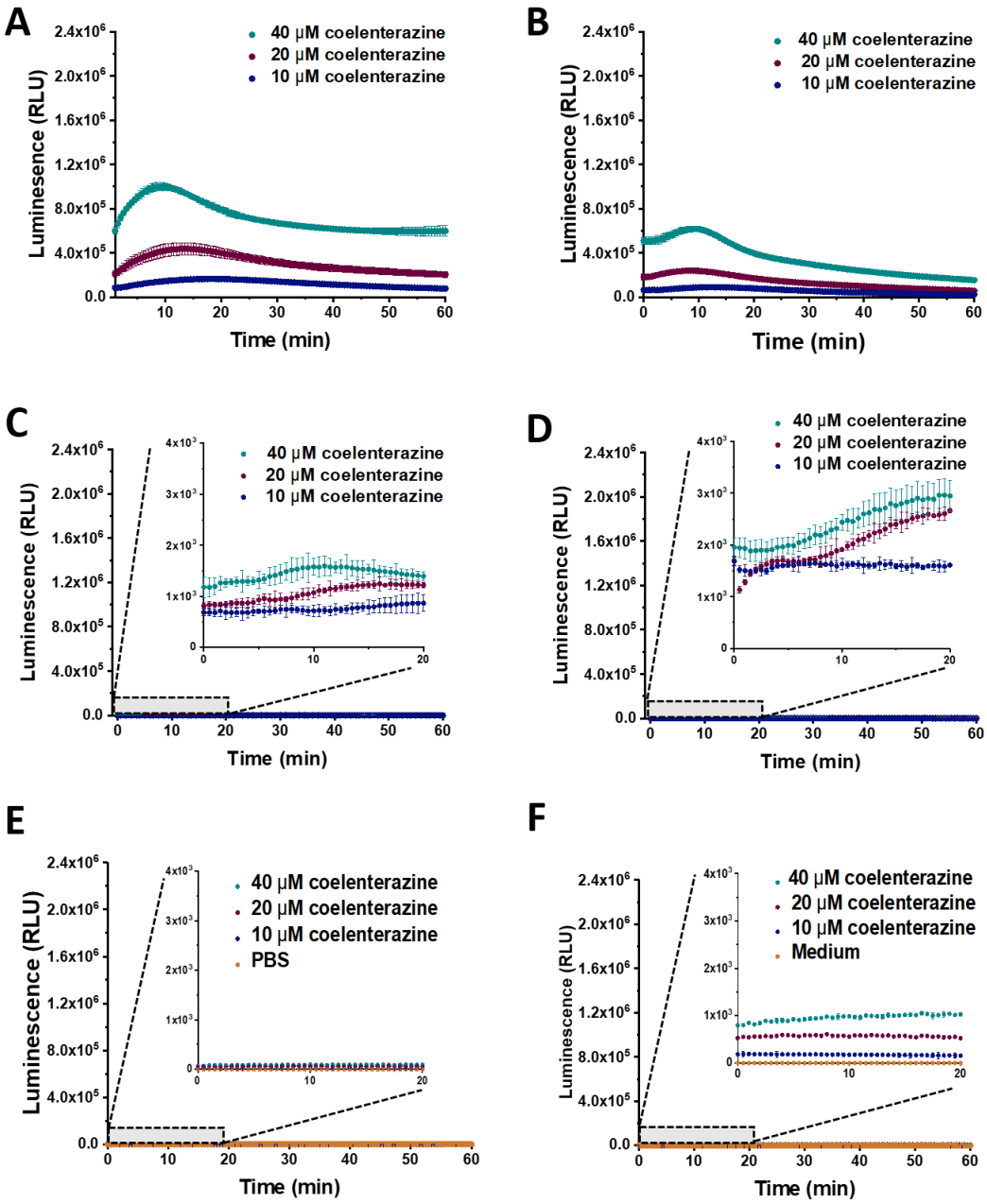

Figure 10.19. *Activity of GLuc Ncomp with and without OmpF in presence of different coelenterazine concentrations in PBS and cell medium.* ***(A)*** *Activity of GLuc Ncomp with OmpF in PBS.* ***(B)*** *Activity of GLuc Ncomp with Ompf in cell medium.* ***(C)*** *Activity of GLuc Ncomp without OmpF in PBS.* ***(D)*** *Activity of GLuc Ncomp without OmpF in cell medium.* ***(E)*** *Luminescence background in PBS alone in presence of different concentrations of coelenterazine.* ***(F)*** *Luminescence background in cell medium alone in presence of different concentrations of coelenterazine.*

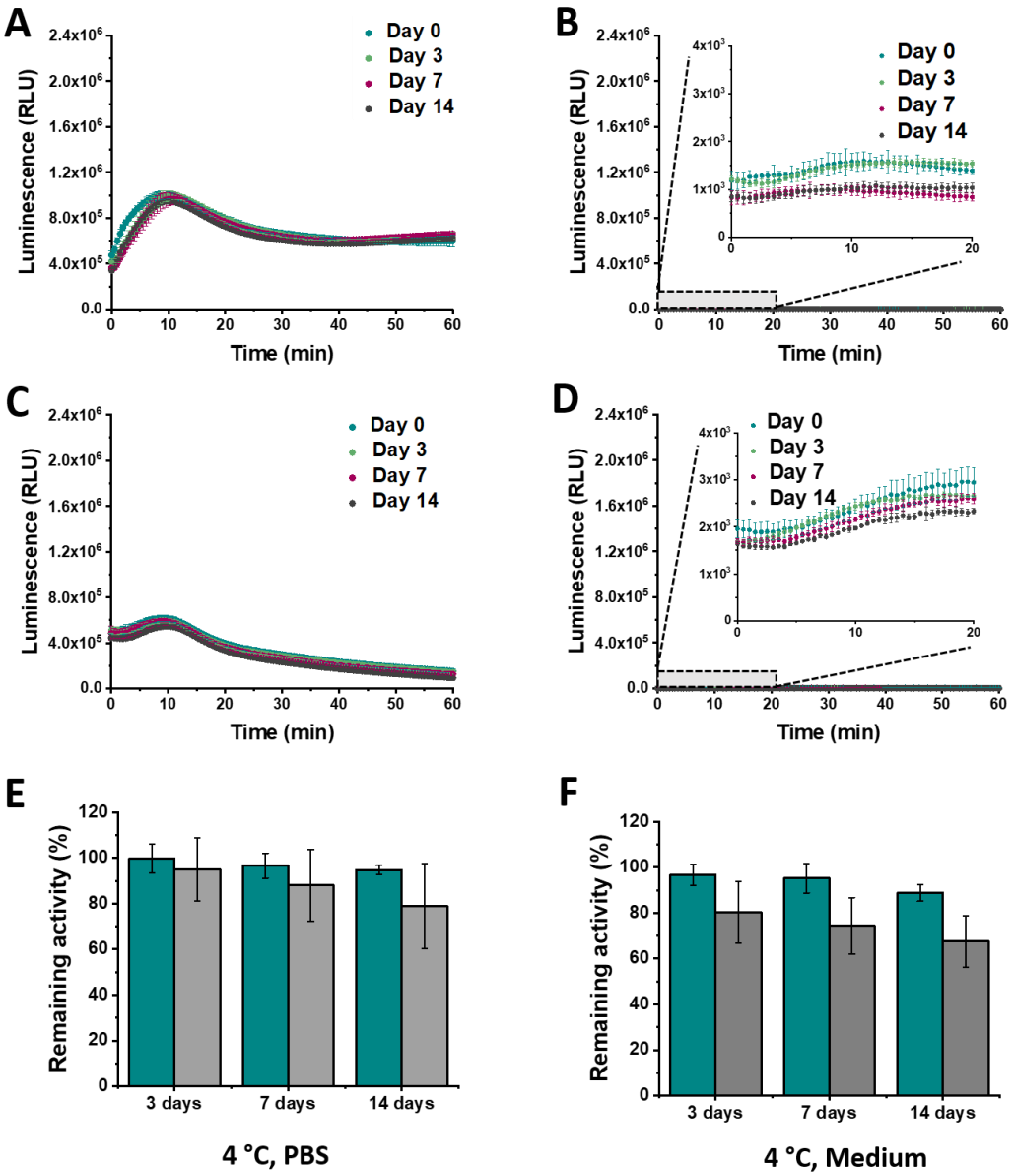

Figure 10.20. *Activity of GLuc Ncomp with and without OmpF after incubation at 4 °C for 3, 7 and 14 days.* ***(A)*** *Activity of GLuc Ncomp with OmpF in PBS.* ***(B)*** *Activity of GLuc Ncomp without OmpF in PBS.* ***(C)*** *Activity of GLuc Ncomp with OmpF in cell medium.* ***(D)*** *Activity of GLuc Ncomp without OmpF in cell medium.* ***(E)*** *Remaining percentages of activity of free (grey) and encapsulated GLuc (cyan) in culture medium, upon storage at 4 °C in PBS.* ***(F)*** *Remaining percentages of activity of free (grey) and encapsulated GLuc (cyan) in culture medium, upon storage at 4 °C in culture medium.*

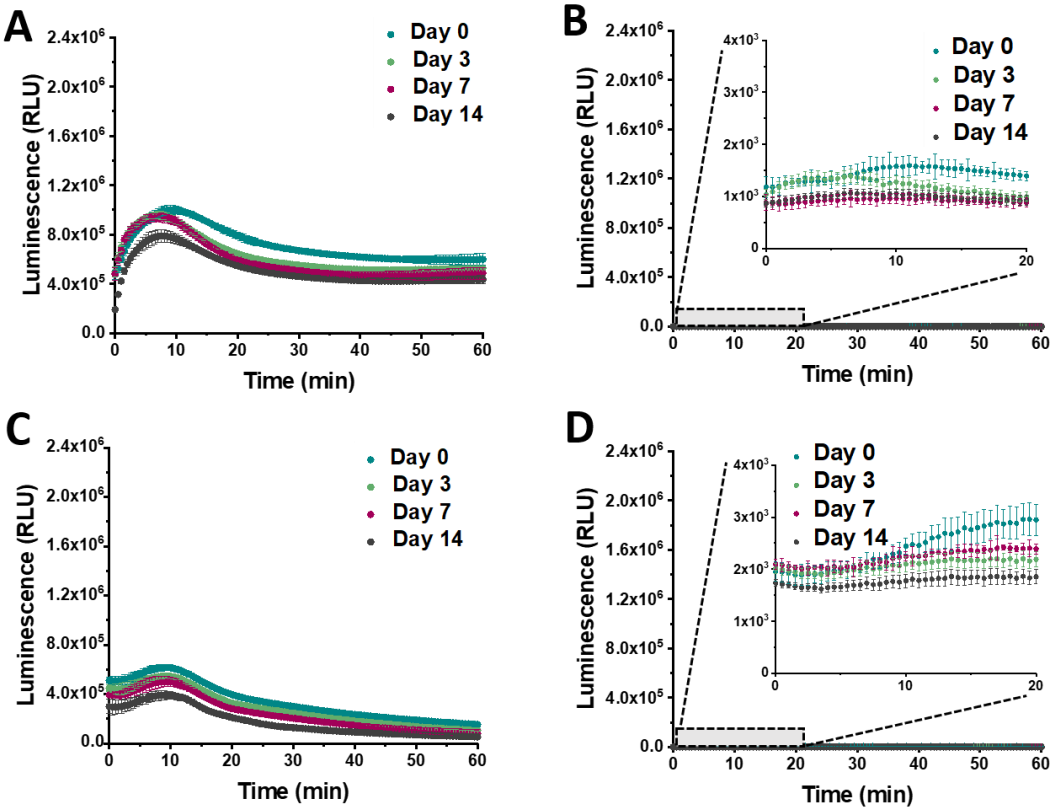

Figure 10.21. *Activity of GLuc Ncomp with and without OmpF after incubation at 37 °C for 3, 7 and 14 days.* ***(A)*** *Activity of GLuc Ncomp with OmpF in PBS.* ***(B)*** *Activity of GLuc Ncomp without OmpF in PBS.* ***(C)*** *Activity of GLuc Ncomp with OmpF in cell medium.* ***(D)*** *Activity of GLuc Ncomp without OmpF in cell medium.*

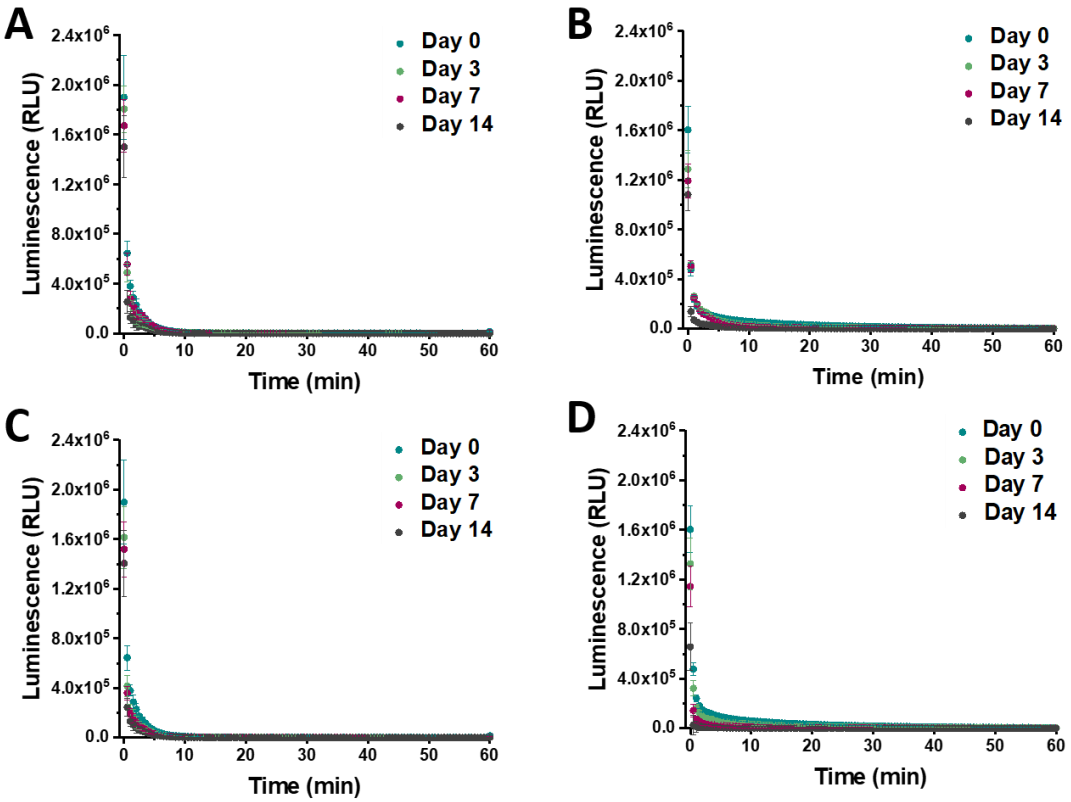

Figure 10.22. *Activity of non-encapsulated (free) GLuc after incubation at 4 °C or 37 °C for 3, 7 and 14 days.* ***(A)*** *Activity of free GLuc at 4 °C PBS.* ***(B)*** *Activity of free GLuc at 4 °C in cell medium.* ***(C)*** *Activity of free GLuc at 37 °C in PBS.* ***(D)*** *Activity of free GLuc at 37 °C in cell medium.*

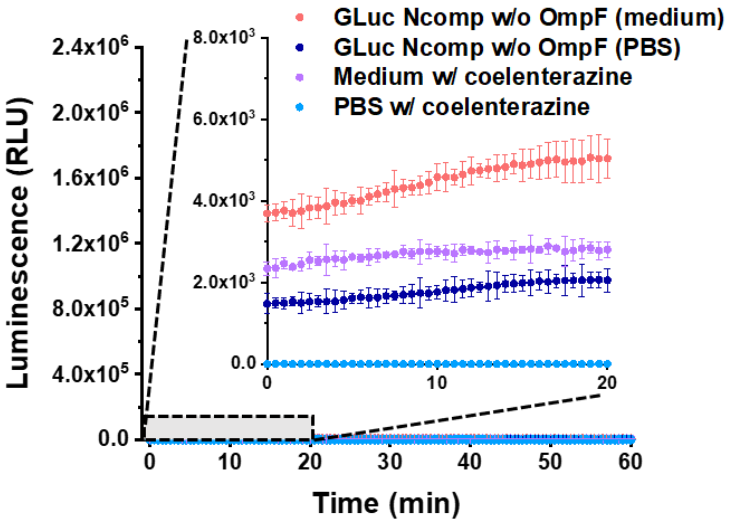

Figure 10.23. *Luminescence production at higher concentration of GLuc Ncomp (50 µL of 2 mg/mL, final concentration = 1 mg/mL). Luminescence background of control samples: GLuc Ncomp without OmpF in PBS and cell medium and coelenterazine in PBS and cell medium. The ratio of the reactants is held constant (50 µL of 160 µM coelenterazine).*

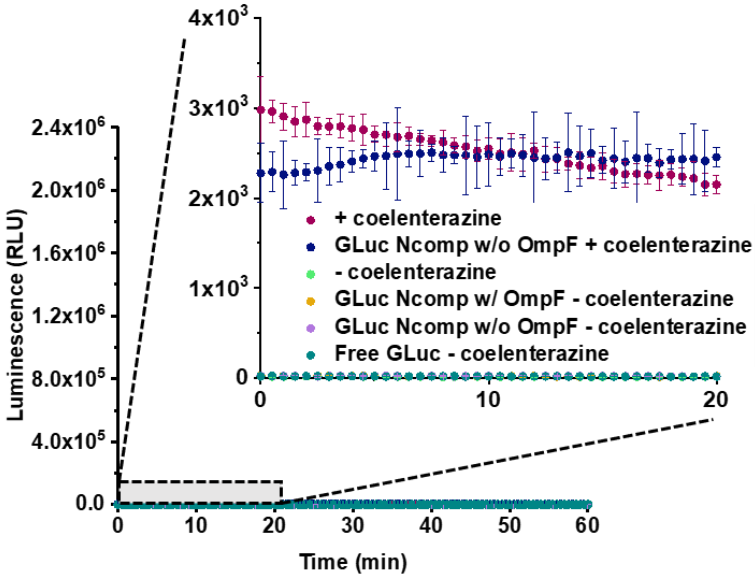

Figure 10.24. *Controls for luminescence production in cell supernatant: Cell supernatant with coelenterazine (pink), GLuc Ncomp without OmpF with coelenterazine (dark blue), cell supernatant without coelenterazine (green), GLuc Ncomp with OmpF without coelenterazine (orange), GLuc Ncomp without OmpF without coelenterazine (light purple), non-encapsulated (free) GLuc without coelenterazine (light blue). In the absence of coelenterazine, the signals remain below 30 RLU.*

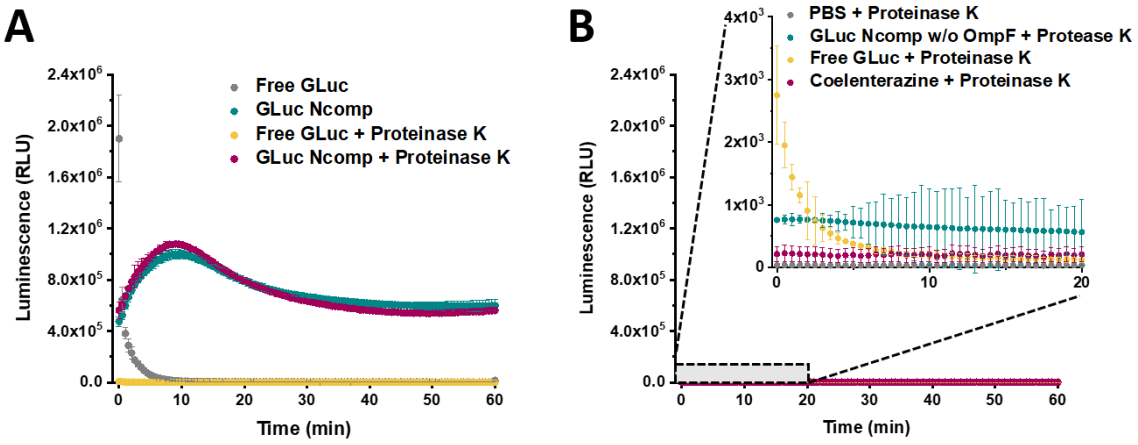

Figure 10.25*. Activity of free and encapsulated GLuc in presence of Proteinase K.* ***(A)*** *Activity of Free GLuc in absence (grey) and in presence (yellow) of Protease K, as compared to encapsulated GLuc in absence (blue) and in presence (purple) of Proteinase K.* ***(B)*** *Activity of free GLuc as compared to controls in presence of Proteinase K: PBS (grey), GLuc Ncomp without OmpF (blue), Free GLuc (yellow) and coelenterazine (purple). The samples have been incubated for 24 h at 37 °C with 0.1 mg/mL of Proteinase K.*

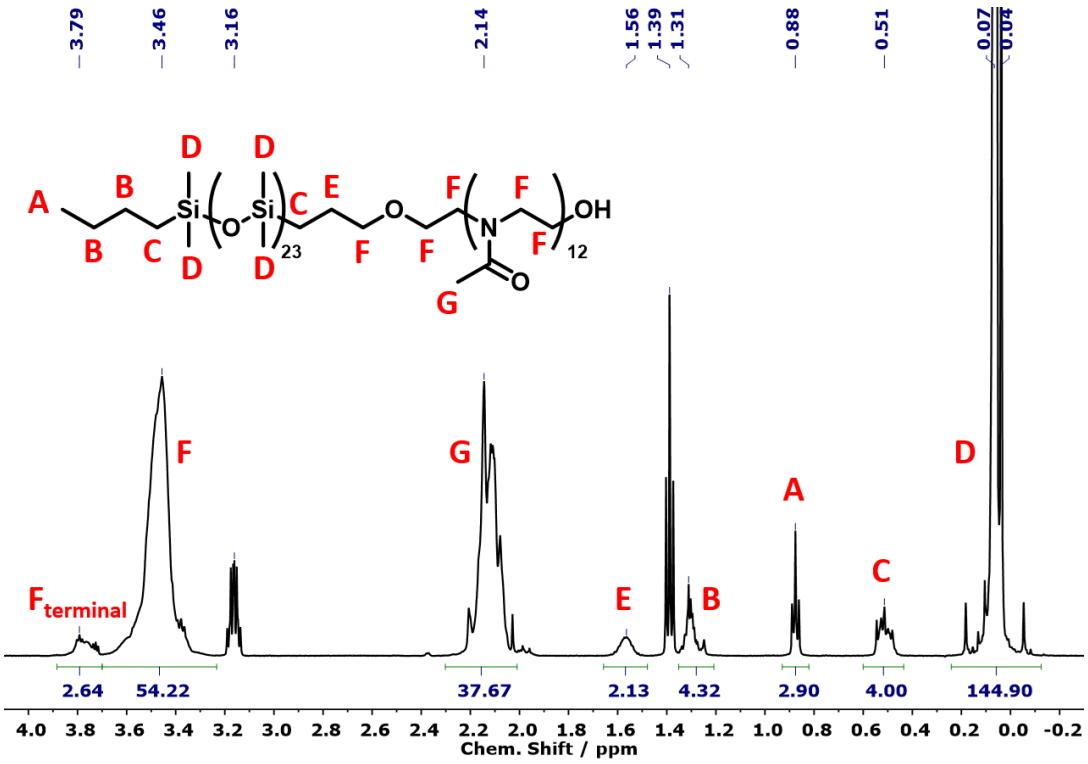

Figure 10.26. *1H-NMR of PDMS24-b-PMOXA12 in CDCl3.*

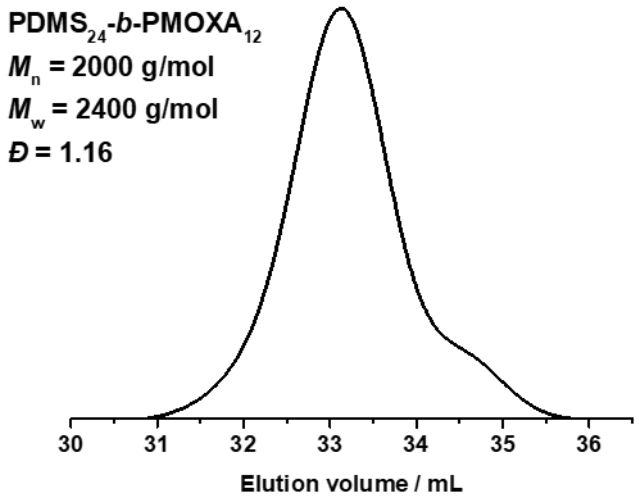

Figure 10.27. *GPC elugram of PDMS24-b-PMOXA12 in dimethylformamide, measured via refractive index detector.*

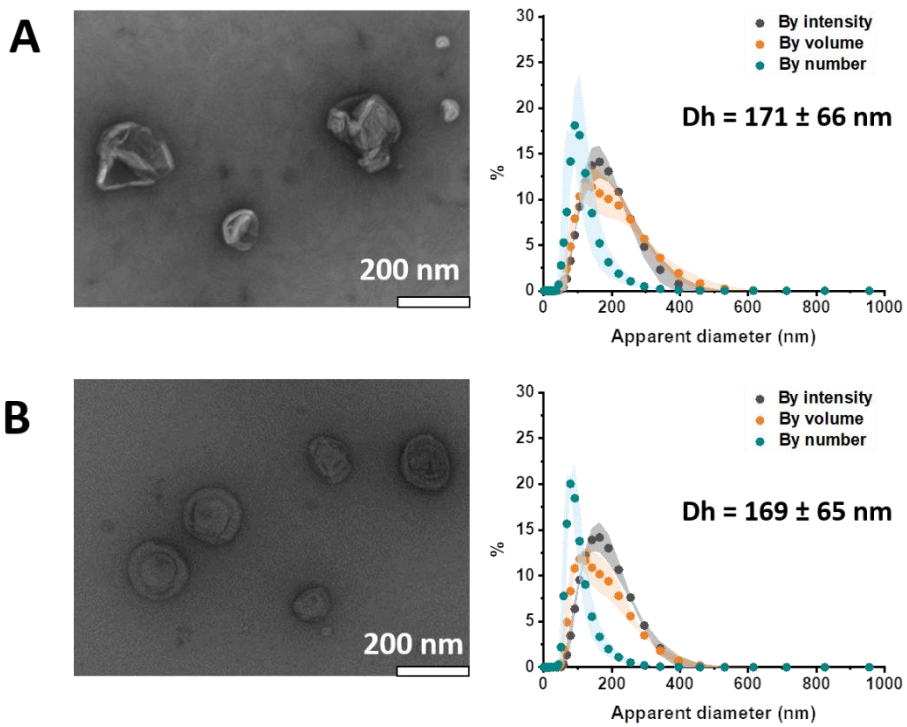

Figure 10.28. *TEM micrographs and corresponding DLS of* ***(A)*** *Melanin-polymersomes (without Tyrosinase) and* ***(B)*** *PDA-polymersomes (without Tyrosinase).*

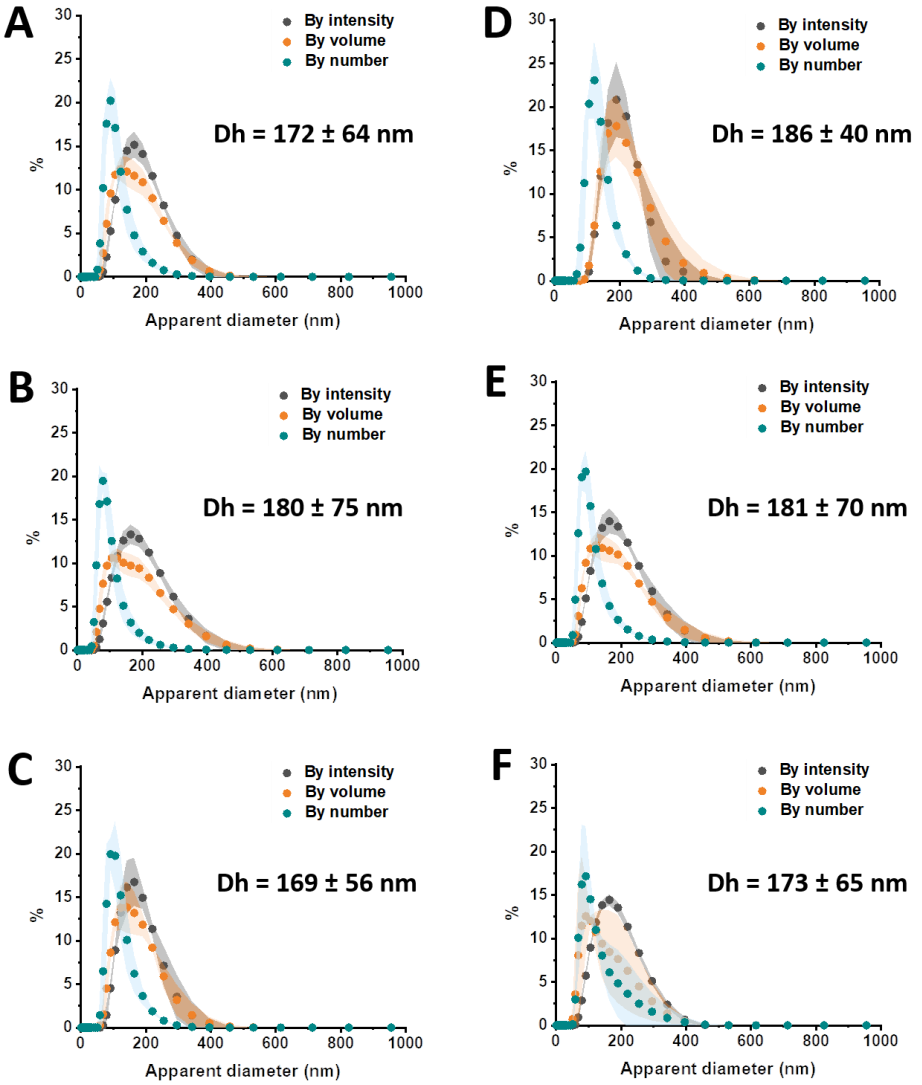

Figure 10.29. *DLS showing the size of* ***(A)*** *Melanin-polymersomes (with tyrosinase),* ***(B)*** *PDA-polymersomes (with tyrosinase),* ***(C)*** *empty polymersomes rehydrated with PBS only,* ***(D)*** *Tyrosinase-polymersomes,* ***(E)*** *Melanin-polymersomes (without tyrosinase) and* ***(F)*** *PDA-polymersomes (without tyrosinase), after 6 months of storage at 37 °C.*

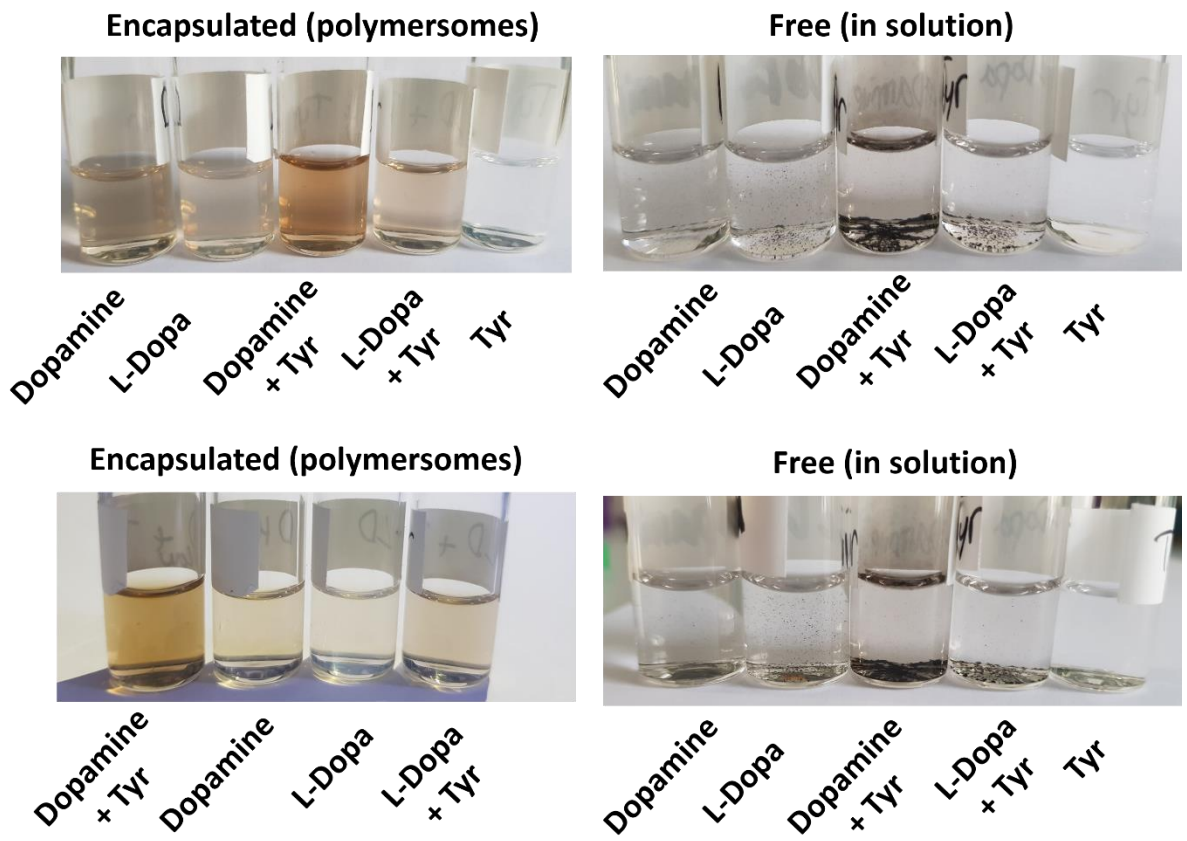

Figure 10.30. *Different photographs of glass vials containing solutions of encapsulated/free dopamine or L-DOPA (with and without tyrosinase), after 24 h of incubation at 37 °C.*

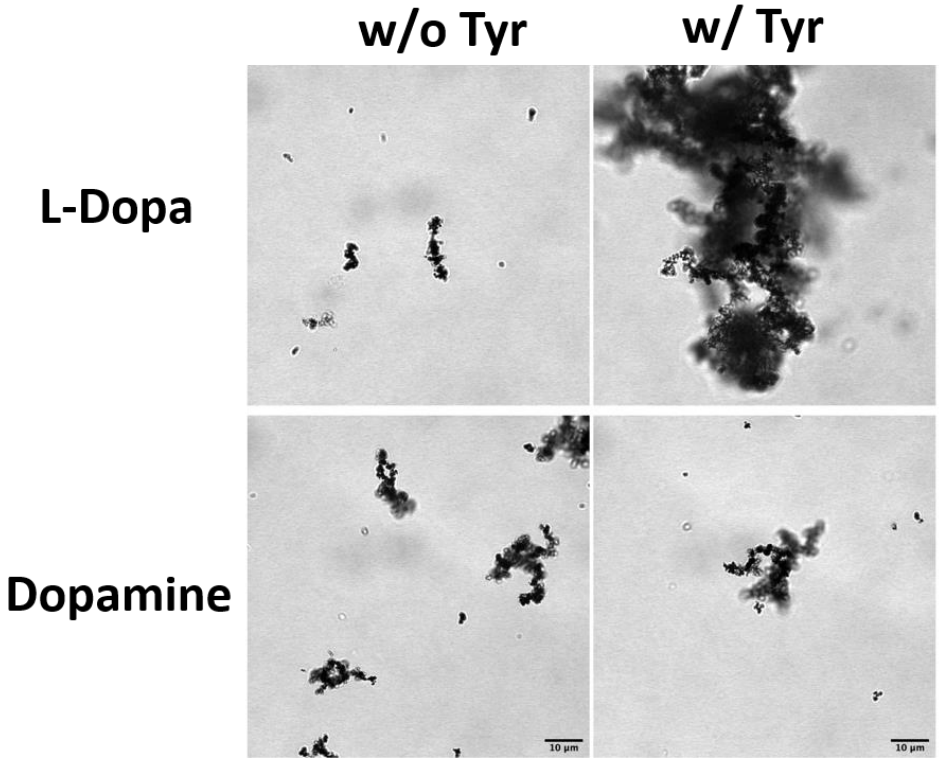

Figure 10.31. *CLSM images showing the morphology of aggregates of melanin/PDA formed in presence or absence of Tyrosinase*

Claire Elsa Meyer

5 rue Alfred Kastler, 68500, Bergholtz, France

claire.meyer@outlook.com

ORCID: 0000-0001-7258-9916

EDUCATION

University of Basel, Basel, Switzerland. Jul 2017 - Jul 2021

PhD candidate in Chemistry

University of Strasbourg, Strasbourg, France. Sept 2015 - Jul 2017

Masters' degree in Chemistry and Biology

University of Strasbourg, Strasbourg, France. Sep 2013 - Jun 2015

Bachelors' degree in Chemistry and Biology

University of Haute-Alsace, Mulhouse, France. Sep 2011 - Jun 2013

2-year Technological degree in Materials Science

University of Strasbourg, Strasbourg, France. Sep 2010 - Jun 2011

1st year of Medical studies

WORK EXPERIENCE

Department of Chemistry, University of Basel, Basel, Switzerland,
Jul 2017 – Jul 2021. PhD candidate in Chemistry.
'Catalytic bio-hybrid polymersomes: towards novel biomedical applications' (Prof. C. G. Palivan)

Institut de Science et d'Ingénierie Supramoléculaire, CNRS, Strasbourg, France,
Feb - Jul 2017. Research intern in Protein Chemistry.
'Peptide-based amyloid inhibitors' (Dr. V. Torbeev)

Institut National de la Santé et de la Recherche Médicale (INSERM),

Strasbourg, France,

Mar - Jun 2016. Research intern in Physical Chemistry.

'Pyrochatecol/metal ions coating for biomedical applications' (Prof. V. Ball)

Trelleborg coated systems, Cernay, France,

Mar - May 2013. R&D intern in coating formulation.

'*Development of a non-adhesive polymer material for advanced printing*' *(Dr. J. Kuczynsky)*

CONTRIBUTION TO CONFERENCES

PCC Christmas Symposium, Basel, Switzerland. Dec 4, 2020. Poster presentation *(online)*

N.I.C.E. International Conference, Nice, France, Oct 12 -14, 2020. Oral presentation *(online)*

SCS Fall Meeting, Switzerland, Aug 25, 2020. Oral presentation *(online)*

Swiss Soft Days (SDD), Basel, Switzerland. Mar 6, 2020. Oral presentation

PCC Christmas Symposium, Basel, Switzerland. Dec 6, 2019. Poster presentation

NCCR MSE fellow retreat, Grindelwald, Switzerland, May 15 -16, 2019. Poster presentation

European Summer School in Physics, Strasbourg, France. Jul 4 - 8, 2016. Poster presentation

PRIZE/AWARDS

SNSF Early Postdoc mobility grant, Sept 2021. *(Paul S. Weiss group, UCLA)*

SCS Award for Best Oral Presentation, SCS Fall Meeting, Aug 25, 2020. *(online)*

Swiss Nanotechnology PhD Award 2020, Jun 2020. *(delivered by SNI and BASF)*

NCCR MSE fellow retreat, Grindelwald, Switzerland, May 15 - 16, 2019. Poster prize winner

PUBLICATIONS

DNA-tethered polymersome clusters as nanotheranostic platform, C .E. Meyer, C-A Schoenenberger, J. Liu, I. Craciun, C. G. Palivan, Chimia**, 2021**

Catalytic polymersomes to produce strong and long-lasting bioluminescence, C. E. Meyer, I. Craciun, C-A Schoenenberger, R. Wehr, C. G. Palivan, Nanoscale, **2020** (DOI:10.1039/D0NR07178A)

Combinatorial strategy of double emulsion templated cell-sized compartments for studying biochemical pathways, E. dos Santos, A. Belluati, D. Necula, D. Scherrer, C. E. Meyer, R. Wehr, E. Loertscher, C. G. Palivan, W. Meier. Advanced Materials, **2020** (DOI:10.1002/adma.202004804)

Biomolecule-polymer hybrid compartments: combining the best of both worlds, C. E. Meyer, S. Abram, I. Craciun, C. G. Palivan, Physical Chemistry Chemical Physics, **2020** (DOI:10.1039/d0cp00693a)

Segregated nanocompartments containing therapeuthic enzymes and imaging compounds within DNA-zipped polymersome clusters for advanced nanotheranostic platform, C. E. Meyer, J. Liu, I. Craciun, D. Wu, H. Wang, M. Xie, M. Fussenegger, C. G. Palivan, Small, **2020** (DOI:10.1002/smll.201906492)

Enzymatic reactions in polymeric compartments: nanotechnology meets nature, A. Belluati, I. Craciun, C. E. Meyer, S. Rigo, C. G. Palivan, Current opinion in Biotechnology, **2019** (DOI:10.1016/j.copbio.2018.12.011)

Nanosensors based of polymer vesicles and planar membranes: a short review, M. El Idrissi, C. E. Meyer, L. Zartner, W. Meier, Nanobiotechnology, **2018** (DOI: 10.1186/s12951-018-0393-7)

Kinetic of deposition and stability of pyrocatechol –FeIII coordinated films, C. Meyer, F. Ponzio, E. Mathieu, V. Ball, Materials Sciences and Engineering: C, **2017** (DOI: 10.1016/j.msec.2016.11.123)